The folded, partially folded, misfolded, and unfolded conformations of cytochrome c probed by optical spectroscopy

A Thesis

Submitted to the Faculty

of

Drexel University

by

Jonathan Barrot Soffer

in partial fulfillment of the

requirements for the degree

of

Doctor of Philosophy

September, 2013

Office of Graduate Studies
Dissertation/Thesis Approval Form

This form is for use by all doctoral and master's students with a dissertation/thesis requirement. Please print clearly as the library will bind a copy of this form with each copy of the dissertation/thesis. All doctoral dissertations must conform to university format requirements, which is the responsibility of the student and supervising professor. Students should obtain a copy of the Thesis Manual located on the library website.

Dissertation/Thesis Title: The folded, partially folded, misfolded, and unfolded unfolded conformations of cytochrome c probed by optical spectroscopy.

Author: Jonathan Barrot Soffer

This dissertation/thesis is hereby accepted and approved.

Signatures:

Examining Committee Chair

Members

Academic Advisor

Department Head

Office of Graduate Studies • 3141 Chestnut Street • Randell Hall 240 • Philadelphia, PA 19104
Tel 215.895.0366 • Fax 215-895-0495 • Email graduate@drexel.edu • Web www.drexel.edu/provost/graduatestudies

Dedication

This thesis is dedicated to my family,

for their unconditional love, support,
and their insistence on my well-being and happiness.

Acknowledgements

There have been many people who supported me and had an influence on my success. Thank you, Reinhard, for being a strong supporter of my project and for your valuable guidance that was offered along the way. The experiences I have had in your lab were both challenging and rewarding. Thank you for all the time and energy that you have invested in my educational process.

In addition to my adviser and members of the Schweitzer-Stenner group, various people have contributed to the research and work presented herein. I would like to thank Prof. Carmichael Wallace for his experienced advice and collaboration in assisting with the cation exchange experiments and for preparing the cytochrome c mutants used in our studies. I would like to thank Dr. Qing Huang for his experienced advice and extending his EPR resources to our group. I would like to thank Dr. Jun Xi for allowing me access to his lab, in particular for the unlimited use of his electrophoresis and stopped flow instruments. I would additionally like to thank Prof. Rousseau for his advice with respect to the peculiar misfolded protein presented in this thesis. And thank all of the colleagues and collaborators I have worked with on projects that are not on the work presented herein, particularly Prof. Papish and Natalie Dixon.

I would additionally like to thank Prof. Tech Kah Lim for our enlightening discussions about science, the university, and life in general. Your door was always open to me, and I found your positive guidance highly encouraging. Additionally, I would like to acknowledge those whom have greatly supported me at Drexel, namely Hon. Ida Chen, Dean David Ruth, and Prof. N. John DiNardo. All of your kind and encouraging words were a source of motivation for me. I would also like to thank all of those with whom I worked in the graduate student association, in particular Kyle Hess and Siobhan Toal.

Finally, part of my research was funded by the Drexel College of Arts and Sciences.

Table of Contents

List of Tables

List of Figures

ABSTRACT

The folded, partially folded, misfolded, and unfolded
conformations of cytochrome c probed by optical spectroscopy

Jonathan Barrot Soffer

Prof. Reinhard Schweitzer-Stenner

Cytochrome c has been a cornerstone of biophysical research since it began.[1-3] Because it is so well characterized,[4] this protein remains an important molecule for ground-truthing new paradigms in protein biophysics.[5] It was one of the first proteins for which a crystal structure was resolved;[6] since then it has served continuously a traditional model system for the fundamentals of electron transfer between proteins[7] and protein folding studies.[8, 9] The work presented here is a spectroscopic study of the folded, partially folded and misfolded states of oxidized cytochrome c, primarily via circular dichroism, absorption and resonance Raman spectroscopies. Here I report the first self-consistent study of the thermal transitions of all protonation states of ferricytochrome c at low anion concentration. UV circular dichroism data indicate only modest unfolding of the protein's helical structure at extreme pH and temperature. Thermally induced conformational changes are assignable to the unfolding of the lowest ranking foldons. Thermodynamic analysis showed a statistically significant enthalpy-entropy compensation, pointing to common physical processes for the unfolding of all protonation states in a similar way, this result suggests that similar physical processes cause all the observed protonation states. Additionally, I report the discovery of a novel (meta)stable, partially unfolded state of cytochrome c, obtained upon incubation under alkaline oxidizing conditions for an extended timed period. This frustrated, misfolded state is reversible; it undergoes an extremely slow transition back to the fully folded state after reintroduction to folding conditions for an extended period of time. Spectroscopic studies of the novel structure suggest a pentacoordinated quantum mixed spin state of the heme, previously found only in ferricytochrome c' and in class-3 peroxidases. Cytochrome c has been shown to acquire peroxidase activity on the surface of liposomes and on the inner membrane of mitochondria, for which a quantum mixed state of the heme iron may be a prerequisite.[10, 11]

(page intentionally left blank)

CHAPTER 1: INTRODUCTION TO PROTEIN FOLDING

Proteins are conformationally dynamic and exhibit functional profligacy giving rise to unique characteristics. It may not be an exaggeration to say that the mysteries of protein folding are key to the mysteries of life itself. The ability of polypeptide chains to fold correctly with sufficient frequency and precision to execute their function has been long investigated as a fundamental and astonishing biological phenomenon. Superficially, the folding process seems straightforward; a linear sequence of amino acids contains all the information that determines the protein's three-dimensional structure. Nevertheless, if one considers the number of possible conformations that a polypeptide chain can sample, the number of folding routes becomes astronomically large. Yet the folding process occurs on a timescale of seconds or less, by a process that is dependent on cooperative actions of many weak nonbonding intra-protein and protein-solvent interactions. Ultimately, folding yields a uniquely compact three-dimensional structure that is usually the biologically functional state. The folded structure depends on the conformational propensities of the amino acid sequence, which has been evolutionarily selected for that protein based on interactions within the protein and with its environment.[12] Under appropriate conditions, the protein spontaneously collapses into a compact globule state and ultimately a fully folded conformation. A recent approach accounting for the existence of complex pathways considers the statistical characterization of the energy landscape of folding proteins as a funnel.[13] In this chapter, we introduce the basic concepts capturing the core physical elements of the protein folding problem that are essential for understanding the further material presented in this thesis.

1.1 Protein Folding

1.1.1 The Protein Folding Problem. The hypothesis that the amino acid sequence (secondary structure) dictates the final structure of a protein (tertiary structure) was based on Anfinsen's famous experiment.[14] Anfinsen showed that the tertiary structure of ribonuclease A could be disrupted in the presence of urea, a chaotropic agent, and mercaptoethanol, a reducing agent. When these reagents were removed via dialysis, the protein spontaneously refolded and fully recovered its activity.[14] Levinthal identified the conceptual difficulty of explaining how a large protein randomly sampling an astronomical number of possible conformations could spontaneously fold on a biologically relevant timescale. This problem is now referred to as "Levinthal's paradox".[15] He argued that if two polypeptide backbone bonds (i.e. N_α -C_α and C_α -C; Figure 1.1) connecting an amino acid residue adopt three isoenergetic conformations with different torsional angles, ϕ (angle across N- C_α) and ψ (angle across C_α-C), then a small protein composed of 104 amino acids, like cytochrome c (cyt c), could have $3^n = 3^{104} \cong 10^{49}$ possible conformations.

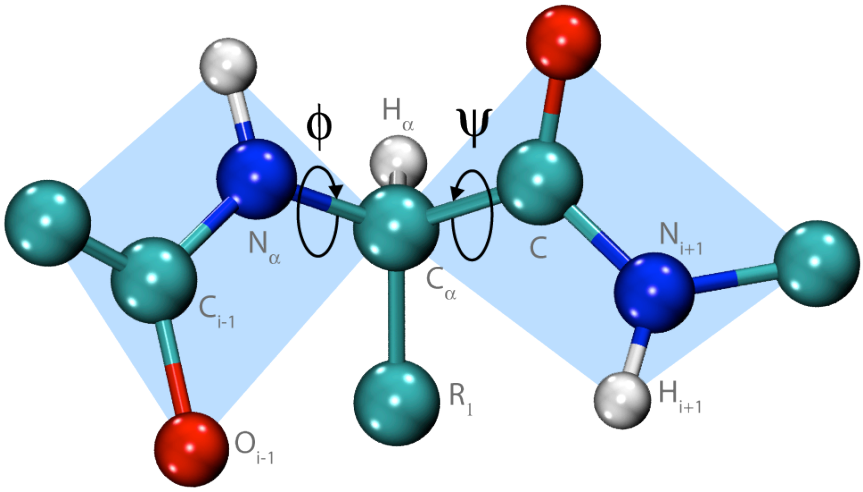

Figure 1.1. Schematic representation of the planar peptide group linking two amino acid residues. Each peptide bond shows some double bond character due to resonance and therefore cannot freely rotate. The two freely rotating bonds on either side of the C_α-carbon define the torsion angles ϕ and ψ. Each atom is represented by a sphere with a radius smaller than its van der Waals radius.[16-18]

Only one of these combinations corresponds to the fully folded state of the protein. By this argument, if the protein was able to sample new conformations at a rate of 10^{13} per second, it would take over 10^{29} years to sample them all, significantly longer then the estimated age of the universe (est. 1.377×10^9 years[19]). In reality, proteins have the ability to fold on a timescale of seconds or less. This led Anfinsen to suggest that the protein itself contained all the information needed to correctly fold, it does not need to explore random conformational space, owing to the existence of a preferred folding pathway, analogous to a chemical reaction scheme.[20]

The observation that ribonuclease A can reversibly fold *in vitro* without any external cellular machinery implies that the folding mechanism can also be studied *in vitro*. This insight led to a whole field dedicated to investigating the underlying mechanism of the folding and unfolding of numerous proteins. Based on these findings, different theoretical models were developed that offer various descriptions of the folding process and predictions of the final folded structure of proteins.[20]

1.1.2 Folding Pathways. To circumvent Levinthal's paradox, Anfinsen hypothesized a sequential folding model in which proteins fold following a well-defined pathway as the rationale for the capabilities of proteins to adopt fully folded three-dimensional structures. In its simplest form the folding process of a monomeric protein is describable as an equilibrium between two states, the fully folded state, F, and the unfolded state, U. The most simple representation for these states is shown in Figure 1.2.[21-23] Cyt c was used primarily for illustrative purposes in Figure 1.2, since it is the topic of this thesis. Under physiological conditions, the fully folded protein almost always represents the most stable conformation. It is

often referred to as its "native" conformation in reference to its three-dimensional structure and biological function. However, progress in the heavily investigated heme proteins, including cyt c, cytochrome b5, myoglobin, neuroglobin, cytochrome P450, and heme-based sensor proteins such as CO sensor CooA, has shown that various native functions are closely associated with so-called "non-native" states.[24-26] Since a number of proteins perform certain functions while adopting an incompletely folded, or non-native state, the term "fully folded state" will be used in place of "native" state throughout this thesis.

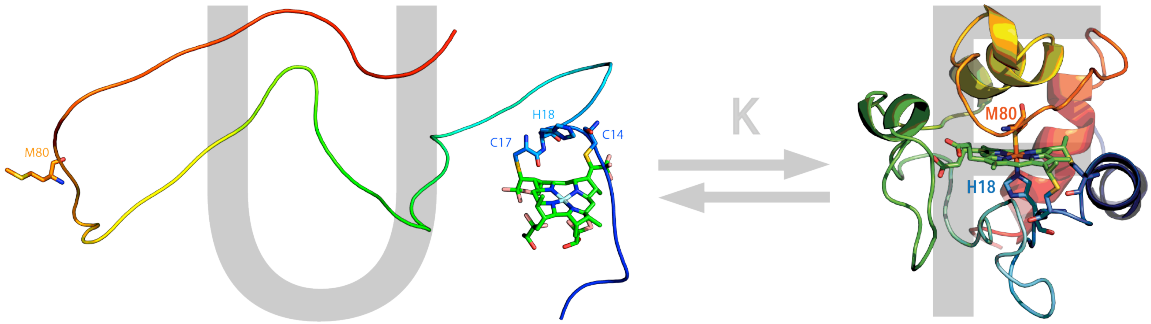

Figure 1.2. A small monomeric protein cytochrome c illustrating the equilibrium unfolding transitions between an extended unfolded conformation (unpublished) and the fully folded state (PDB: 1AKK).[17, 18, 27, 28]

The rapid equilibration between different unfolded conformations prior to complete folding can be explained through a two state model. One reason for protein folding being frequently describable by a two-state model is the cooperativity of the underlying folding process. Privalov and coworkers applied the van't-Hoff criterion to evaluate the cooperativity of denaturational transitions for several proteins.[29] The van't Hoff criterion is based on spectroscopic, calorimetric, or other measurements to determine the equilibrium constant, K. [25] The van't Hoff equation for the standard enthaply change relies on the two-state folding transition and can be considered as all-or-none, with the unfolded state sampling a much larger conformational space. If folding is highly cooperative, disrupting one interaction in the protein will affect all other interactions, meaning that the protein can never be partially folded, only

fully folded (F) or fully unfolded (U). In this view the U state is a distribution of many rapidly exchanging unfolded or partially folded conformational states. Proteins that deviate from this two-state behavior are usually either large (>100 residues) and fold via one or more intermediates, or small and fold extremely rapidly. Some proteins, such as apomyoglobin, barnase, and the λ-repressor fragment have been shown to fold in a stepwise manner[30-34] by forming a rapidly distinct nuclei comprising of nascent secondary structure elements, followed by their collision and consolidation.

1.1.3 The two-state to multi-state models of protein folding. If a protein's folding involves only two states, the corresponding reversible two-state reaction can be written as

$$U \underset{k_U}{\overset{k_F}{\rightleftharpoons}} F \qquad [1.1]$$

where k_U and k_F are unfolding and folding reaction rate constants. The equilibrium constant, K_{eq}, and the Gibbs free energy of folding within the transition region can be determined by:

$$K_{eq} = \frac{\chi_F}{\chi_U} \qquad [1.2]$$

Changes are dependent only upon the fraction of molecules that are unfolded (χ_U) or folded (χ_F) and conditions of the system and not dependent upon the path. Partially folded states, i.e. thermodynamic intermediates, are not significantly populated in this model. This thermodynamic model does not rule out kinetic intermediates, so the rate constants must be considered as effective rate constants, k_{eff}.

To clarify, a kinetic intermediate reflects the transient accumulation of non-native conformations preceding the formation of the native structure.[35] Kinetic intermediates exist only briefly (<*seconds*) and cannot be isolated for structural studies, and most spectroscopic methods do not sample fast enough to measure kinetic folding and unfolding. However, neither equilibrium nor kinetic data alone can define a kinetic sequence.[36, 37] What is needed instead is the order to the steps of the protein path.[38] Kinetic methods also do not describe the structure of the intermediates that they show. The thermodynamic intermediate state represents a partially unfolded state that is distinctly structured. Unlike kinetic intermediates, this compact conformational state has mostly intact secondary structure.[23, 29] Transition from one thermodynamic state to another is preceded by a change in the enthalpy, entropy, volume, etc.[23, 29] Stable intermediates may be studied by general spectroscopic methods, whereas the properties of transition states and transient intermediates must be inferred from kinetics.

When both F and U are populated, the free energy difference of folding, δG^0_F, can be expressed as:

$$\delta G^\circ_F = G^\circ_F - G^\circ_U = -RT \ln k_{eff} \qquad [1.3]$$

In contrast to the rapid folding/unfolding equilibrium of proteins in native conditions, it is common for additional intermediate conformations to accumulate under more destabilizing solution conditions. These are less folded than the native state but more folded than the denatured state, yet not fully stabilizing of the denatured state. Generally, the two-state model is deceptively simple, implying that the folding reaction does not involve the rapid collision and isomerization of thousands of atoms and bonds concurrently, thus neglecting a large portion of folding.[39]

While many small proteins often follow the two-state unfolding equilibrium, most proteins are not small, and a two-state mechanisms should not be taken for granted.[39, 40] Certain intermediate structures must be populated between the native and denatured states, since no covalent bonds are broken during folding. Experimental evidence suggests that a protein folds through a series of temporarily populated yet obligatory kinetic intermediate states, termed I.[8, 41]

To account for the fraction of partially unfolded states a more complex model must be used to explain and characterize partially folded intermediate conformations. This can be accomplished through an extension of the classical two-state view to allow for the possibility of transiently populated metastable states, i.e., partially folded on-pathway, off-pathway, or misfolded intermediates.[8, 42-44] The reaction scheme found in eq. 1.1 can be extended to include these partially folded intermediate state(s) in thermodynamic equilibrium by the following:

$$U \underset{k_{IU}}{\overset{k_{UI}}{\rightleftharpoons}} \left(I \ldots I_n\right) \underset{k_{FI_n}}{\overset{k_{I_nF}}{\rightleftharpoons}} F \qquad [1.5]$$

Each intermediate state, I_n, represents an additionally observed metastable state. Kinetic studies can potentially offer additional insight into the thermodynamic properties of intermediate states even in cases where the whole process of folding occurs in a single step, which is the case for many small globular proteins.

Kinetic approaches commonly rely on rapid mixing techniques to initiate folding as a result of sudden changes in solvent conditions. These changes are typically studied with optical spectroscopy, i.e. absorbance, fluorescence, circular dichroism. These techniques have been used to detect and characterize transient kinetic folding intermediates on subsecond to sub millisecond time scales.[8, 45-49] Nonetheless, these experimental approaches are limited as well,

often indicating a change of signal during the dead time of the kinetic measurement (conventional instruments are often limited to a few milliseconds), often referred to as the "burst" phase. This observation has been attributed to a rapid hydrophobic collapse, producing a molten globule with a high degree of secondary structure, while the tertiary structure is still rather disordered.[50] Here non-polar regions of the extended polypeptide chain reorient themselves to minimize the disruption of the hydrogen bonding in the solvent network, thus creating a hydrophobic core (Figure 1.3). Molten globule states have a radius of gyration that is larger than that of the native protein by 10-30%.[51] Classification of this equilibrium of compact states is usually not based on studies of their conformations but on indirect measurements of hydrophobicity and the averaged ensemble properties using fluorescence and circular dichroism spectroscopy. Kinetic measurements during refolding of several proteins (i.e. interleukin-1β, staphylococcal nuclease, and apomyoglobin) have provided firm evidence for the molten globule state to be an on-pathway folding intermediate in most cases.[52-54]

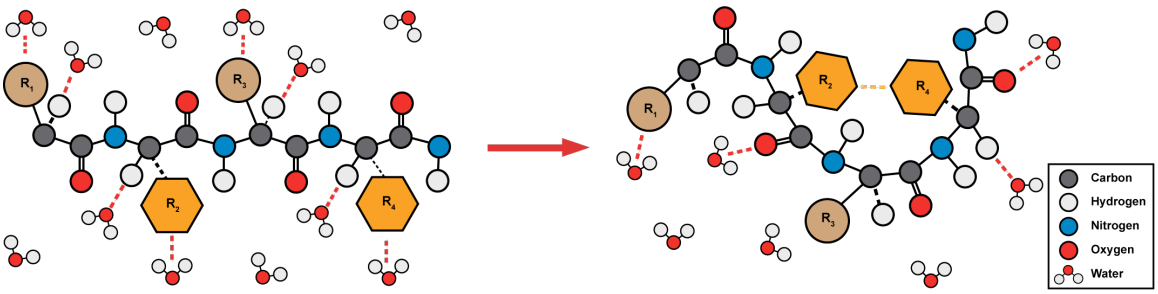

Figure 1.3. Simplified illustration of hydrophobic collapse, where an extended polypeptide chain (left) interacts with the solvent, even if these interactions are unfavorable, to rapidly bury the hydrophobic residues, R_2 and R_4, into the interior of the structure (right), enabling them to interact with each other, shown in orange, leaving the more polar groups exposed to the solution, a more energetically favorable conformation. R_2 and R_4 represent hydrophobic a.a. A, V, L, F, W, or M.[17]

After this initial hydrophobic collapse, or "burst phase", there is an intermediate folding phase, in which the folded tertiary structure begins to appear over a timescale of 5 ms to 1 s. Here the secondary structure is further stabilized and the tertiary structure starts to form, while the side-chains of the amino acid residues are still mobile. This is followed by the final folding

phase in which the native structure is achieved over a period of several seconds for small single-domain proteins but takes longer for more complex proteins. In this phase, relatively rigid core packing occurs, involving the expulsion of any residual water present in the hydrophobic core.

1.1.4 The foldon cooperative structural unit. Folding is a dynamic process; under native conditions a protein having reached the fully folded state will repeatedly fluctuate to the unfolded state and refold again, cycling through all of its higher energy forms.[55] Thus, a protein molecule repeatedly revisits the same intermediate forms that carried it to its fully folded state, according to its Boltzman factor.[56, 57] This behavior is normally spectroscopically silent, with the higher energy forms never becoming predominantly populated under folded conditions. For hydrogen exchange (HX) methods, this sampling can be used to exploit the transient unfolding reaction (high energy forms) that govern the slowest hydrogen exchange in many proteins, under folding conditions.[58, 59] HX experiments rely on the fact that the main chain amide group (-C(O)-NH-) exchanges hydrogens naturally with water, providing non-perturbing structure-sensitive probes to allow study of every amino acid in a protein (except proline). The HX folding process begins with a denaturant-unfolded protein (pH 5) that is fully deuterated at amide sites (in D_2O). This denaturant is then diluted by stopped flow techniques into the folding buffer (H_2O) where the D-to-H back exchange is very slow. If the refolding protein encounters a large on-pathway barrier, a folding intermediate transiently accumulates. The intermediate is then exposed to a short intense burst of mixing briefly at high pH (pH 10) that labels the exposed amides of the intermediate. This technique is called HX pulse labeling. The amide at the exposed positions will appear unprotected and exchange with H. As the protein folds, any labeled amide position switches from fully unprotected (i.e. exchange a H when it is unfolded) to almost fully protected (i.e. remain D labeled). The gain of HX protection is associated with the formation of H-bonded secondary or tertiary structure.

[60-62] This technique revealed that some proteins are composed of cooperative structural units of the fully folded protein, called foldons.[63]

This technique allows the relative stabilities of different parts of a protein to be determined and mapped onto the overall structure. The foldon formation and their ordered sequence of assembly systematically puts native-like foldon building blocks into place, guiding the protein through sequential stabilization mechanisms, constituting a cooperative stepwise protein folding pathway.[55, 64] These foldons are ranked by a code for order of increasing unfolding free energy (at native conditions) in proportion to the size of the unfolding structure $\delta(\Delta G°)/\delta[\text{Den}]$:[65, 66] infrared (I), red (R), yellow (Y), green (G) and blue (B).[66]

It should be emphasized that even though foldon formation is related to lower free energy on the folding pathway, foldons are often extremely difficult to detect in a thermodynamic experiment. Although they could appear as kinetic intermediates in some techniques, they are still very difficult to observe them. Luckily, due to the vast structural knowledge of cyt c, its foldon units have been correlated to some of its conformational arrangements.[67] The stablity of some protein foldons seems to provide the supporting scaffolding to tertiary structure, while regions with less stable foldons, like loops and turns, often account for changes of functional properties by modulating the environment of the active site. In ferri-cyt c, the structural switching reaction that exchanges heme ligands at alkaline conditions seems to fall into the latter category.[67] This phenomenon will be described in greater detail in section 1.2.

1.1.5. Thermodynamic Intermediates. Information on the thermodynamic nature of the folding process can be obtained by inducing the unfolding and refolding transition through denaturation, i.e. changes in pH, temperature, ionic strength, or the addition of organic solvents (e.g. urea, guanidine hydrochloride). This information can then be utilized to deduce rate constants. It should be noted that from a thermodynamic perspective, temperature cannot induce a transition between two enthalpically equivalent states. Originally the molten globule and the unfolded state(s) were believed to be enthalpically equivalent, i.e indistinguishable thermodynamically. However, this view was challenged on experimental and theoretical (thermodynamic) grounds, and we now know that the molten globule and the unfolded state are enthalpically different.[35, 68] The enthalpy and entropy of unfolding are extremely temperature dependent, owing to the heat capacity of the unfolded state being significantly greater than the folded state.[29, 69-73] In many cases protein denaturation cannot be described by a simple two-state model, since the transition may involve several intermediates. This type of multistate model is less tractable, both experimentally and theoretically.

Different thermodynamic paths can be explained through thermodynamic cycles, which aid in analyzing the relationship between protein structure and stability.[74] The thermodynamic cycle is a series of steps that begin in one state and pass through other states, and can return to that initial state. The basic thermodynamic cycle can be written as:

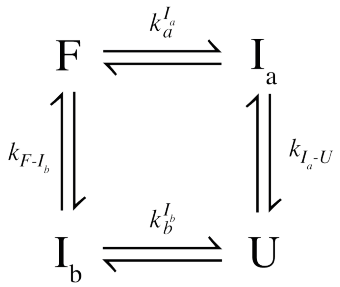

In this case, we consider the population of an intermediate, I, between the fully folded (F) and unfolded (U) state of the protein. A thermodynamic cycle can be exploited to obtain otherwise non-measurable quantities from measurable quantities in the cycle. The basic thermodynamic cycle is built on the principle that the sum around a complete cycle must equal zero (the first law of thermodynamics). As a consequence, the paths $F \rightarrow I_a \rightarrow U$ and $U \rightarrow I_b \rightarrow F$ must be thermodynamically equivalent. The technique then allows the investigator to selectively obtain physical information using any experimentally accessible path. The dissociation constants, k_a and k_b ($k_{F\text{-}Ib} = [F]/[I_b]$; *and* $k_{Ia\text{-}U} = [I_a]/[U]$), for the protonation of I_a and I_b, respectively, can then be manipulated to reflect the conservation of Gibbs energy for any route. The stability of a protein is closely connected with the problem of protein denaturation, since the stability can only be judged by breaking the fully folded structure. Thermal unfolding is often used experimentally. Thermal unfolding increases the molecular fluctuations; H-bonds are transiently broken and brought into contact with solvent. The result of this process is a change in the intrinsic property of the protein, such as a change in charge, size, or compactness of the structure.

Nonrandom thermally unfolded structures have been reported in a number of proteins, including cytochrome c, apomyoglobin, lysozyme, ribonuclease, and α-lactalbumin.[52, 73, 75, 76] Cyt c was one of the first observed examples of a thermally activated intermediate with properties of the molten globular state, i.e large amounts of secondary and some tertiary structures.[77-79] Cyt c was chosen as a model protein because its native structure is well known and structural features under a variety of different conditions are available. [73, 80, 81] In the thermal transition from molten globular state to the denatured state at a low pH with a high concentration of KCl, circular dichroism (CD) and ultraviolet circular dichroism (UVCD)

measurements revealed an acid molten globular state, with an increase in disorder of the tertiary packing but similar secondary structure.[78] Molten globule states of cytochrome c were also reported at alkaline pH and high salt concentration.[82, 83] The thermal stability of cyt c depends highly on the redox state of the heme iron, and thermal unfolding causes a decrease in the overall redox potential[84, 85] (discussed in greater detail in section 1.2).

1.1.6 Folding Route Navigation from Energy Landscapes to Folding Funnels. To account for the added complications of the multistate folding pathway a "new view" of protein folding kinetics emerged, replacing the concept of a single folding pathway with multiple energetically downhill paths on a funnel shaped energy landscape (Figure 1.4).[86-91] This conceptualization allows proteins to quickly collapse to native-like topologies, while structures that collapse to non-native topologies fold less rapidly. The funnel-shaped energy landscape can be represented by the three-dimensional surface as shown in Figure 1.4, where the vertical axis represents the free energy of a given conformation, and the horizontal axis represents the conformational degrees of freedom (entropy) of the polypeptide chain.

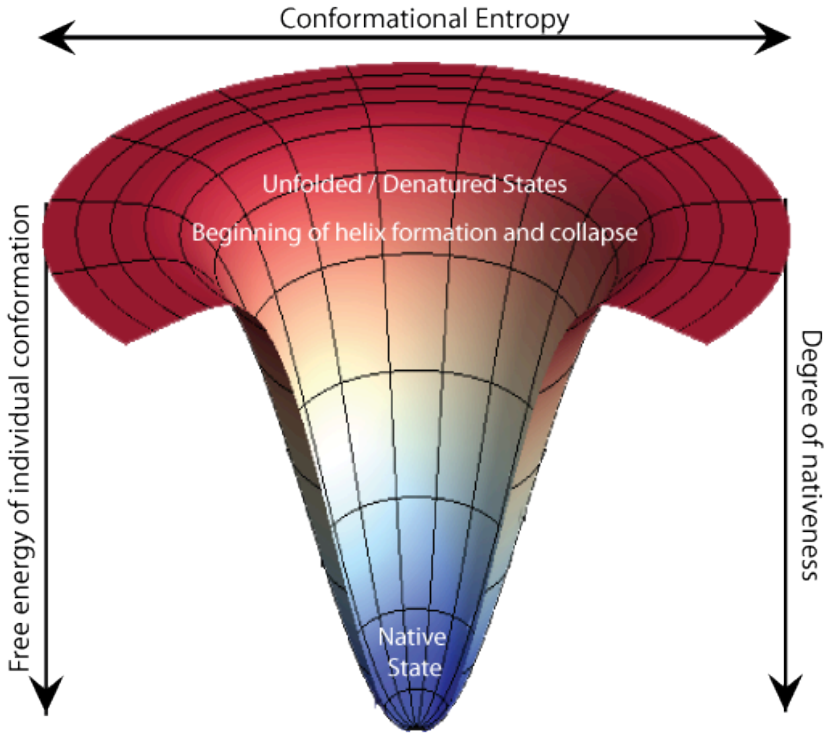

Figure 1.4. A funneled energy landscape. The vertical axis of which represents the free energy, with the funnel width representing a proteins conformational freedom. The top represents all non-native states, where conformational entropy maximal, as you move down the funnel more native characteristic is gained until it reaches the fully folded state. [17, 92]

The very simple folding funnel in Figure 1.4 provides a simple pathway in which the polypeptide chain gains more native-like characteristics as the free energy decreases, until it reaches the preferred global minimum corresponding to the fully folded state. The area at the top of the funnel is wide, owing to the larger conformational entropy of the unfolded (denatured) conformations. Proteins start in their unfolded state and follow the energy gradient down the slope, forming secondary structures, such as α-helices and β-sheets. This process is then followed by a rapid hydrophobic collapse.[93, 94] As the protein proceeds energetically downhill, the funnel narrows representing the decrease of conformational entropy, i.e. more compact conformations and fewer degrees of conformational freedom until the protein reaches its fully folded state at the energy minimum of the funnel. As a consequence the protein folding rate and the folding mechanism are largely determined by the native state

topology, changing the shape of the funnel.[95] In most real proteins, most interactions that occur are mutually supportive and cooperatively gain speed through favorable transitions to the global free energy minimum, i.e. the fully folded structure.

In reality, the folding landscape of a protein is never a perfectly smooth surface, but is rugged or bumpy in nature with several local minima. The exact structure of these minima will influence the details of the folding mechanism.[88, 96, 97] Thus, the funnel picture of the Gibbs energy landscape also illustrates how a protein may get trapped at some crevice along its folding path. Depending on the depth of the trap, it might take some time for the protein to overcome its barrier and resume its downhill motion along the folding coordinate. An idealization of this rugged energy landscape is shown in Figure 1.5. While there are many conformations sampled along multiple pathways, this model still contains some obligatory steps, or transition state ensembles, along the folding reaction path and others that the protein will pass rapidly over before arriving at the fully folded conformation.

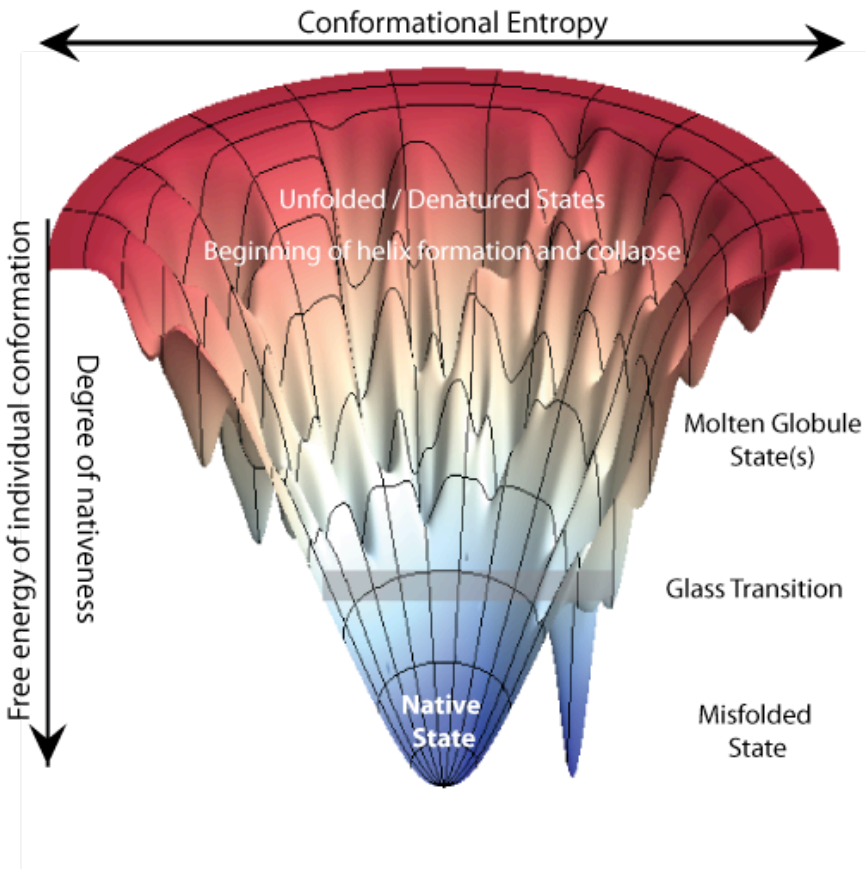

Figure 1.5. A simplified schematic of a frustrated rugged landscape. This representation shows a multitude of intermediates, around the middle of the folding funnel, and a frustrated minima similar in energy to the native state.[17, 92]

Usually, the topology of a folding funnel guarantees different segments of a protein chain will interact, but this process does not provide any guarantee that the many resulting individual interactions will not mutually conflict.[88] The protein thus attempts to minimize the non-native interactions along the folding pathway, or, restated, few conformations are energetically accessible. This concept is referred to as the "principle of minimal frustration".[89] A departure from this behavior can yield transient trapping in minima associated with non-native conformations, slowing the exploration of folding routes towards the fully folded structure. A protein caught in such a trap is often in a so-called "misfolded" state, from which it often undergoes irreversible aggregation into, e.g. amyloid fibrils.[98, 99] Forcing one of many structures to remain fixed and unable to reconfigure to the lowest energy crystalline state is

physically reminiscent of liquid being cooled to a glass state.[88, 100] Schrödinger actually referred to proteins as "aperiodic" crystals. [101] At temperatures above this glass transition the landscape can easily be sampled.[102] Below this temperature, however, the search for the absolute free energy minimum of many glassy states proceeds very slowly.

1.2 - BASIC STRUCTURE AND FUNCTION OF CYTOCHROME C

Cytochrome c (cyt c) is a relatively small (~12.4 kDa) protein that mediates the electron transfer from cyt c reductase (complex *III*) to cyt c oxidase (complex *IV*) in the electron transport chain (ETC).[103] It is located in the intermembrane space of the mitochondron (light pink in Figure 1.6, indicated with the red arrow). In the conventional sense, cyt c is not an enzyme, but is more appropriately described as a cofactor for the proteins with which it interacts. Cyt c acts as a key mediator in the production of ATP, the high-energy chemical intermediate of living cells.[104] Electron transfer is one of the most crucial reactions in biochemistry present in almost all enzymatic cycles. Cyt c is involved in the mitochondrial ETC, in which electrons are removed from an electron donor (NADH) and then passed to a terminal electron acceptor (O_2) via a series of redox reactions. These reactions are coupled to the creation of a proton gradient (ΔpH) across the mitochondrial inner membrane. The proton movement across the membrane is shown schematically in Figure 1.6, with the resulting transmembrane proton gradient used for the production of ATP from ADP via Complex *V*. In this ETC, electrons travel down the energetic chain, with cyt c mediating the passage of a single electron from the membrane bound complex *III* to complex *IV* (Figure 1.6).

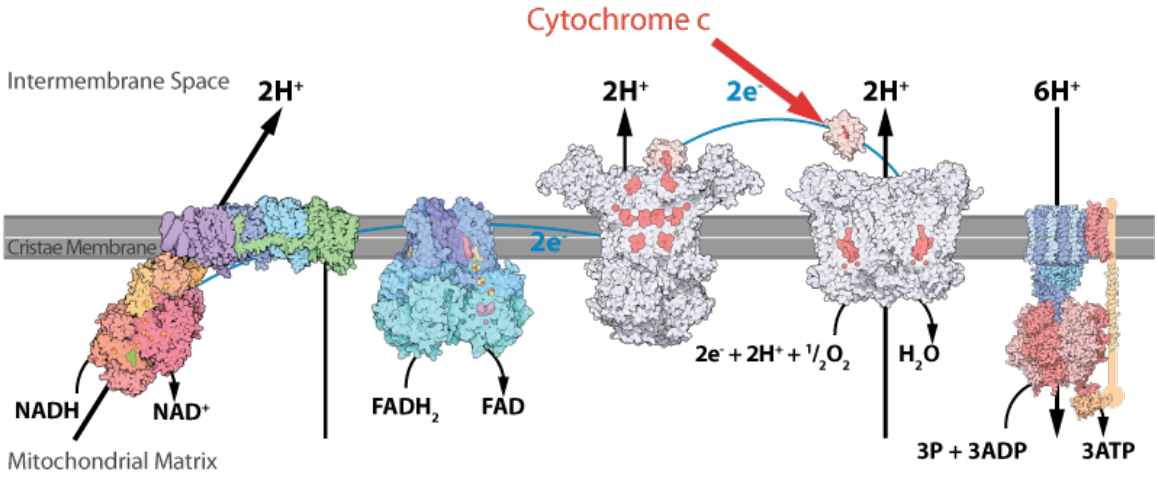

Figure 1.6. A simplified representation of the electron transport chain, found in the inner membrane space of the mitochondria, where cytochrome c acts as a key mediator. The chain is made up of five complexes starting from the left to right. Complex I is NADH-ubiquinone oxidoreductase (PDB: 3M9S),[105] complex II is succinate-ubiquinone oxidoreductase (PDB: 1NEK),[106] complex III is ubiquinone-cytochrome c oxidoreductase (PDB: 1KYO),[107] complex IV is cytochrome c oxidase (PDB: 1OCO)[108] followed by ATP synthase (PDB: 1C17, 1E79, 2E74, 1L2P).[109-111] This figure shows the heme groups in a light red. Cyt c, the main focus of this work is the small mediator protein designated with the red arrow.[17, 28]

1.2.1 The multiple functions of Cytochrome c. Cyt c's role is not limited to the production of ATP (oxidative phosphorylation); it additionally acts in a variety of roles linked to cellular life or death decisions (Figure 1.7). This small heme protein was also found to be essential for canonical intrinsic apoptosis (type II),[4, 112-115] where it was also found to bind to Apaf-1 triggering caspase activation (in the cytosol).[116] Cyt c was also found to oxidize cardiolipin,[117] a component of inner mitochondrial membrane. Cyt c was found to complex with cardiolipin[118] triggering pore formation in cardiolipin containing membranes.[119] Cyt c additionally acts as an antioxidant, scavenging reactive oxygen species (ROS).[120] During apoptosis, this role shifts, with cyt c producing ROS via increased mitochondrial membrane potentials or the $p66^{Sch}$ pathway.[121] The role of cyt c in regulating respiration and cell death has renewed experimental interest in this model protein, providing a new relevance to human disease (i.e. neurodegenerative, cardiovascular and autoimmune diseases, cancer, and sepsis).

[115, 118, 122-124] In all cases, the partial unfolding of cyt c seems to be a critical factor in the disease mechanism.

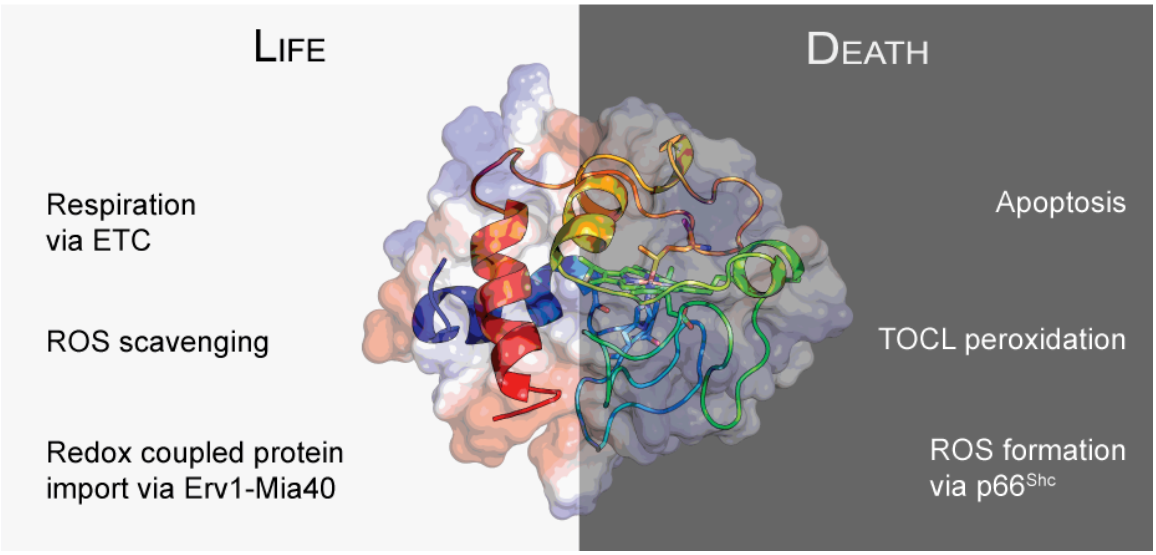

Figure 1.7. Overview of the life sustaining (left) and cellular death (right) functions of cyt c (PDB: 1AKK in the center with calculated surface electrostatic potential shown). [17, 27, 28, 115]

The role of cyt c in apoptosis. Over the last ten years, cyt c research has refocused on movement from the inner mitochondrial membrane and subsequent apoptosis. In association with lipid vesicles, cyt c binds a monoclonal antibody recognizing an unfolded region around residue Pro44, and observed in apoptotic and necrotic cells.[125] Mutation of Gly-41 to Ser was shown to alter the mobility of the 40's Ω-loops and enhanced the apoptotic activity of cyt c without altering its role in respiration.[126] Prior to becoming involved in the apoptotic process, cyt c is also transferred from the intermembrane space to the cytosol, where it can initiate the apoptotic pathway.[113, 116, 127, 128] The release of cyt c is not an irreversible step; a certain threshold of released cyt c must be reached before a cell commits to apoptosis.[129] Once in the cytosol, cyt c can interact with the inositol phosphate receptor, type 3 (IP3R) in the endoplasmic reticulum. This causes a release of calcium, calpain activation, and apoptosis-

inducing factor (AIF) into the cytosol. In the cytosol, a non-native form of cyt c binds to the apoptotic protease-activating factor 1 (Apaf-1),[130] resulting in an increased affinity of the complex to dATP.[131] This interaction triggers a massive release of cyt c from the mitochondria into the cytoplasm through modified cristae junction. When this occurs, cyt c undergoes a conformational change, tightly binding to the apoptotic protease activating factor 1 (APAF-1).[132] This Apaf-1-Cyt c complex then acts as the key factor in this multistage reaction.[116] In the presence of ATP this complex induces the formation of the apoptosome, a heptameric machine (Figure 1.8), which in turn activates caspase 9 (Casp-9), the "death protease". Casp-9 bound to the apoptosome acts as a cleavage factor of Casp-3, which is considered the major enzyme in the irreversible commitment to apoptosis (Figure 1.8).[128, 132, 133]

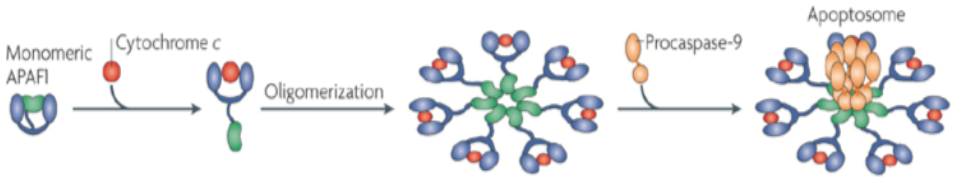

Figure 1.8. Structure of the apoptosome (left) with a proposed model for the activation dimerization of caspase-9 and location of cytochrome c in red. Modified from Shi and Ow.[25, 133]

Cyt c interactions with anionic phospholipids and peroxidase activity. The strong interaction between cyt c (polycationic; net molecular charge +9e at pH 7.4) and cardiolipin (anionic, with possibly -2e) plays an important role in both respiration and apoptosis.[134] In eukaryotic cells cardiolipin (CL) is a lipid unique to the mitochondria, where it is believed to be synthesized.[135] CL accounts for around 20% of total mitochondrial lipid, 80% of which is found on the inner membrane of the mitochondria in healthy cells.[136] On the inner membrane of the mitochondrion, about 15–20% of cyt c is bound to CL, as compared to 4% bound to cyt c found on the outer membrane of the mitochondria.[137] During apoptosis there is a transmembrane migration of CL, facilitating its interactions with membrane bound cyt c

and causing the formation of a cyt c-cardiolipin complex, in the intermembrane space of the mitochondria.[5, 138, 139] Its involvement in this process requires the acquisition of peroxidase activity and the subsequent dissociation from the surface of the innermitochondrion membrane. In this process, 40% of the CL on the inner membrane, relocates to the outer membrane ultimately creating a pore that releases cyt c into the cytosol.

Cyt c can bind to CL through three binding sites termed the A-, C- and L-sites (Figure 1.9).[140-142] There is a loose and reversible electrostatic binding to the A site, which is thought to participate in the electron transfer and radical scavenging functions of cyt c.[140-142] This site is also believed to be important for the recognition and binding of cyt c reductase and oxidase. The binding to the A-site involves the interaction of residues K72 and K73, this interaction is electrostatic and depends on pH and ionic strength.[143, 144] The C binding site involves N52 binding through hydrophobic interactions mainly by means of hydrogen bonding.[140, 141] A stabilizing mechanism to the C site was proposed to form in association with the hydrophobic cavity on the surface of cyt c via extended lipid anchorage (bordered by F10 and Y97),[142] where one of the hydrocarbon tails of CL is thought to become inserted into the structure of cyt c, thus augmenting its electrostatic association through additional hydrophobic interaction.[145] An alternative channel was proposed closer to K72, K73, K86 and M80,[146] with further suggestion of penetration by two acyl chains.[147] Nevertheless, any anchoring through this type of extensive hydrophobic interaction would likely be a substantial impediment to the dissociation of cyt c. Binding to the C site under acidic conditions dramatically influences the CD spectrum ,in that it changes the sign of the couple. However, such a change has not yet been observed in solution, nor has a physical explanation for this phenomenon been put forth. An additional electrostatic binding site was proposed adjacent to the A-site, termed the L site, which involved three lysine residues (L22, L25 and L27) and H33.[148, 149] The L site has been

shown to promote vesicle fusion in mitochondrial-mimetic vesicles with heart cardiolipin content, suggesting that an interaction at this site triggers a detachment from the mitochondrial membrane.[149] Additionally, cyt c bound to cardiolipin (cyt c-CL) was shown to form pores large enough to penetrate into the interior of a liposome.[119] This is consistent with what occurs on the outer membrane of the mitochondrion, where the cyt c-CL complexes produces a pore that facilitates the release of cyt c and other pro-apoptotic factors into the cytosol.[115]

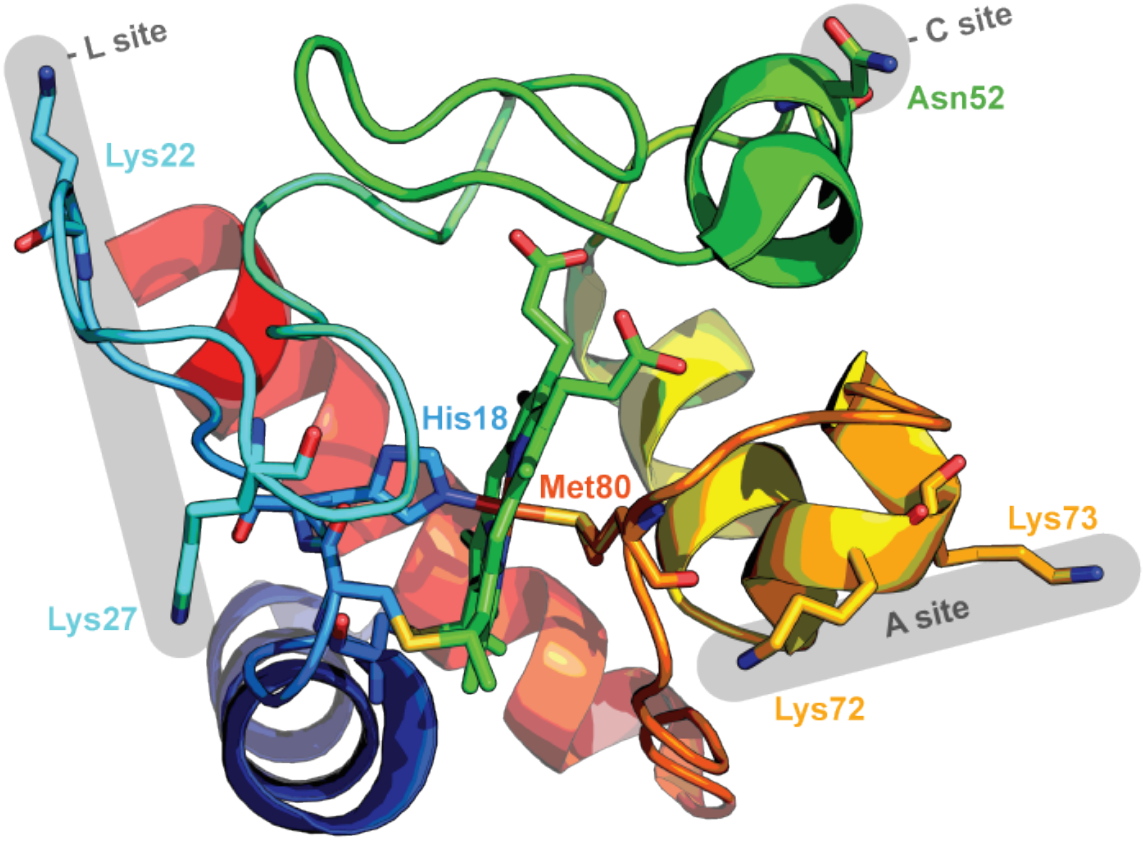

Figure 1.9. Proposed bindings sites (shown in gray) on the surface of cyt c, illustrating the A-site, L-site or the C site as described in the text (PDB: 1AKK).[17, 27, 28]

Cyt c the free radical scavenger. Reactive oxygen species (ROS) are generated in the mitochondrion as a result of the nature of electron transport. These species are highly reactive and can damage DNA and other structures within the cell. If free cyt c remains within the inner-membrane space of the mitochondrion, it can act as a free radical scavenger through the removal of the unpaired electron from superoxide, thus regenerating O_2.[120, 150] This can subsequently be used in energy production, transferring the extracted electron to cytochrome c oxidase (CcO), thereby regenerating the oxidized form of Cyt c. Cyt c has also been experimentally shown to operate as a hydrogen peroxide scavenger. [151] This conversion of hydrogen peroxide can occur in both the reduced and oxidized states of cyt c. Since cyt c constantly undergoes redox cycles during cell respiration, both detoxification reactions can take place, making it an ideal cell antioxidant.

Role of cyt c in neurodegenerative diseases. As the equilibrium shifts towards the production of ROS, major disturbances in cell function and viability occur. Such perturbations are seen in an increasing number of human diseases. Multiple neurodegenerative diseases (i.e. Alzheimer's and Parkinson's Disease) are characterized by loss of specific neuron populations due to apoptosis. In addition to apoptosis, the formation of cyt c-CL oligomers may also be of particular relevance to the co-oxidation of other proteins that have anionic lipid binding sites, such as α-synuclein. α-synuclein is a major component in aggregate forming amyloid-like fibrils in accumulations of poorly digestible cross-linked aggregates in neurodegenerative disease that oxidative stress reaction may contribute to the abnormal aggregation of this molecule, and may be significantly enhanced by iron-catalyzed oxidative reactions.[152] It is in this context that cyt c is believed to be a possible source of iron and increased oxidative stress in the cytosol which may ultimately stimulate the aggregation of α-synuclein.[152-154] The

mechanism of this aggregation process is still poorly understood. Interestingly, both cyt c and α-synuclein are abundant components of Lewy bodies, which accumulate in the brain of patients with Parkinson disease.

1.2.2 Structure of Cytochrome c. Oxidized cyt c was one of the first proteins to be fully characterized by x-ray crystallography.[80, 155] Cyt c is a roughly spherical, globular protein with diameter of 34 Å in its fully folded state, consisting of a single polypeptide chain of 104 amino acid residues packed around a covalently attached heme prosthetic group (Figure 1.10).[27, 80, 156] Cyt c is highly soluble in water (up to 200 mg/ml, pH 7), with an isoelectric point ranging from 10.0 - 10.5 depending on ionic conditions, and a net charge of +8e at neutral pH. [157, 158] Cyt c is also a highly evolutionarily conserved protein, with 36% amino acid identity in all eukaryotes (Appendix A.4).[112] The most highly conserved region of the protein encompasses residues 67-87.[159] Overall, cyt c has 19 positively charged lysine (K) residues, and two positively charged arginines (R), with only 12 acidic residues (aspartic or glutamic acids).

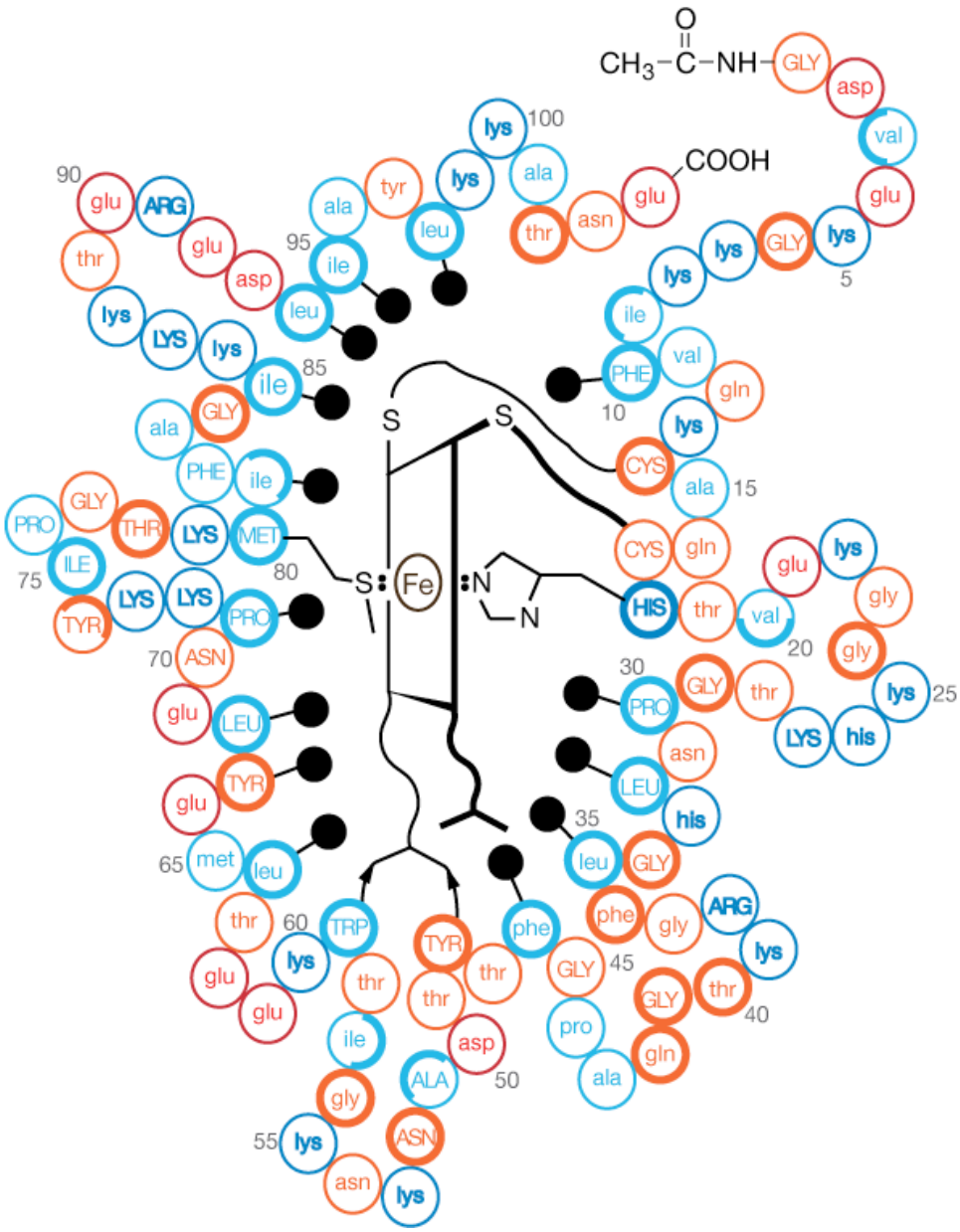

Figure 1.10. A diagram of the packing of cytochrome c about the heme. The bold circles indicate side chains buried in the interior, black dots mark residues whose side chains pack against the heme. Light circles indicate side chains on the outside of the molecule, and dark half-circles show groups that are half buried at the surface. Arrows from W59 and Y48 to the buried propionic acid group represent hydrogen bonds. The coloring shows the residues characteristic, basic, hydrophobic (nonpolar), polar (uncharged) and acidic. Residues designated by capital letters are totally invariant among cyt c species.*(17, 160)*

The secondary structure for cyt c is primarily composed of three major and two minor helical elements (~45% helix), a very short two-stranded anti-parallel β-sheet (res 37-40 and 57-59; ~7%), two type III β-turns (~8%) and four type II β-turns (~14%).[80, 155] A plot of the main chain torsional angles (Φ, φ) for horse heart cyt c in its oxidized form is shown in a Ramachandran plot Figure 1.11.[161] In this plot, there is a clustering of residues with the α-helical conformation, (-57°, -47) and to a smaller extent in the polyproline II (PPII) (-55°, 138) and β-strand conformations (-110°, 140°).

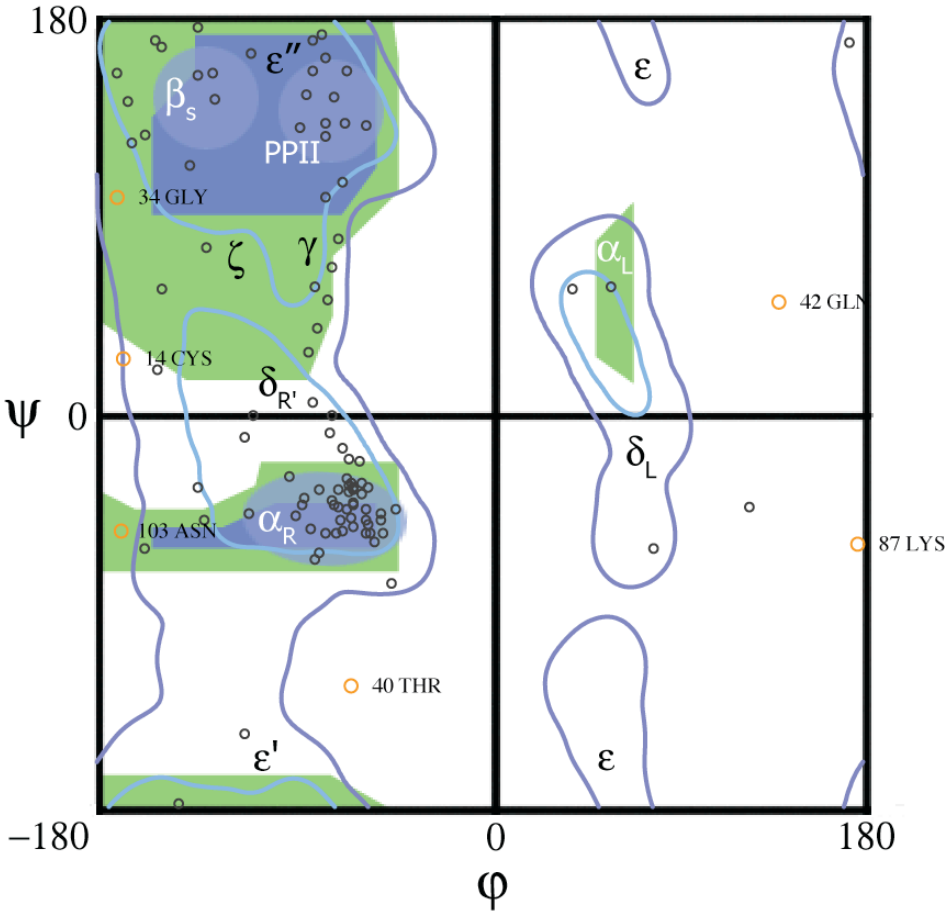

Figure 1.11. Ramachandran plot of the theoretically allowed conformational dihedral angles of the polypeptide backbone of cyt c with common structures identified in the blue shaded region. This map is overlaid with experimental results for cyt c in its F state. The black open circles show the residues within the allowed regions while the orange circles show the residues outside the allowed regions (residues C14, G34, T40, G42, K87, and N103).(PDB: 1AKK)[17, 28, 162]

The heme prosthetic group. The heme active site (heme c), a protoporphyrin *IX* derivative with a central iron atom (Figure 1.12), is coordinated proximally to a histidine (H18) and distally to a methionine (M80). H18 and M80 are a common ligand set for c type hemes, i.e. cyt c, photosynthetic reaction centers, diheme cytochrome c peroxidases, and several dehydrogenases.[163] At the center of the heme, an iron atom (Fe) serves as an acceptor and donor for electrons from and to the above mentioned reaction partners (complex *III* and *IV*) in the inner membrane of the mitochondrion.[164] The two vinyl substituents of the heme group form thioether bonds involving the two cysteine residues (C14 and C17) in the conserved C-x-x-C-H heme binding motif commonly found in the heme environment of c type cytochromes (Figure 1.12). The heme group within the protein is not planar; the principle observed deformation is an out-of-plane ruffling resulting from the covalent attachment to the heme as well as the axial ligands associated with the heme Fe.[112, 165] The heme ruffling deformation plays a role in tuning the electronic coupling,[166] causing an overall decrease in the reduction potential of the heme.[167] It has been shown in microperoxidase (MP-11) that strengthened hydrogen bonding within the CxxCH segment enhances heme ruffling.[168] Any modification in the magnitude of the heme ruffling by the protein environment naturally alters the rate of electron transfer between the heme and redox partners, by modulation of the metal ligand bond strength.[169] Another significant determinant in the electron potential is the encapsulation of the heme within the protein's hydrophobic interior, this environment favors the ferrous over the ferric state.[169, 170]

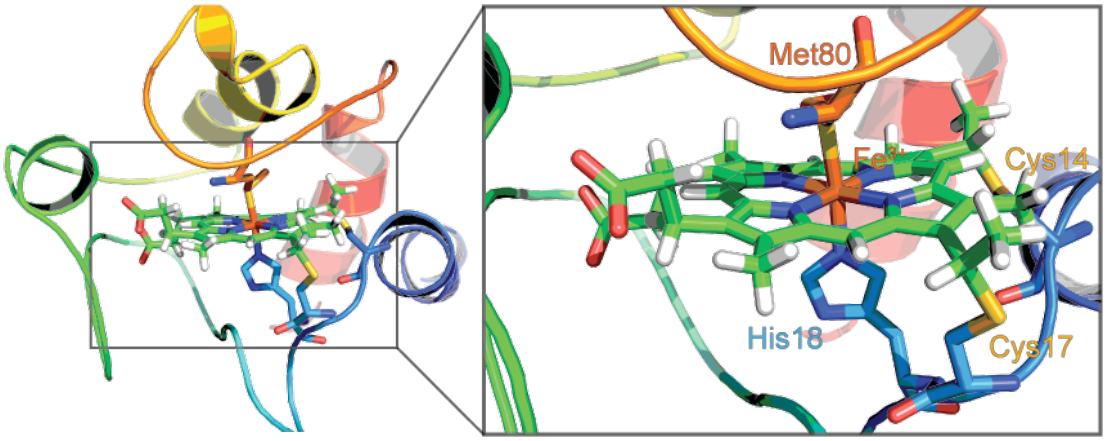

Figure 1.12. Cartoon representation of horse heart cyt c, focused on the heme prosthetic group.(PDB: 1AKK[27]) With the central heme iron (brown) and C14, C17, H18, and M80 residues showing the heme attachment via the CxxCH motif.[17, 28]

The nonplanar heme group is buried within a hydrophobic pocket formed by the polypeptide chain. In horse heart cyt c around 7 % of the heme's surface is exposed to the solvent on the front edge.[171] This arrangement is evident in the space filled diagram (Figure 1.13). The interaction of the heme prosthetic group and its surrounding protein matrix, i.e. side chains of the residues around the heme cavity, have been linked to functional properties of the protein.

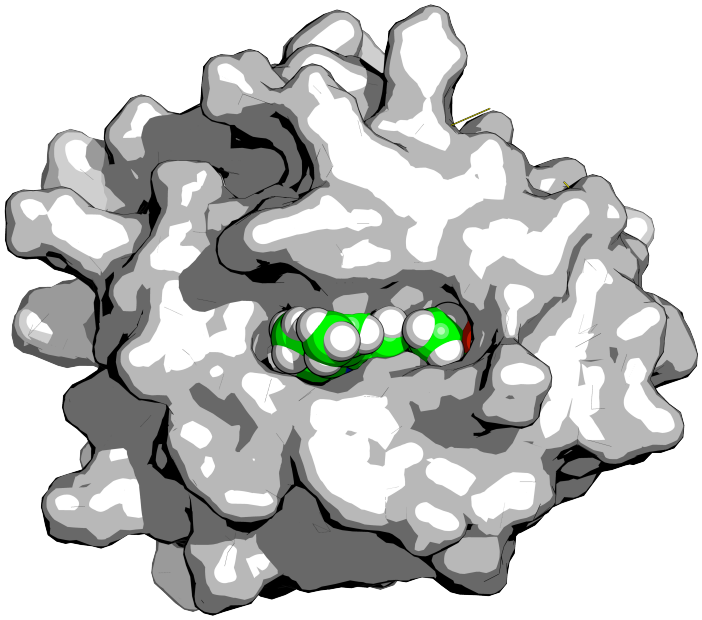

Figure 1.13. Space filled representation of cyt c (equine), with solvent exposed heme edge shown in green.[27, 28]

Cyt c oxidation state - coupled conformational changes. Cyt c exists in two physiologically important oxidation states. There are only minor conformational differences between the fully-folded oxidized and reduced states (< 1 Å RMSD), occurring in the vicinity of propionic side chains of the heme (propionate-7).[172] There are also some hydrogen bonding changes upon reduction of the heme iron (notably K13 to E90), making the protein interior slightly less solvent accessible (Figure 1.14). Despite this, there are substantial differences in the stability of the reduced and oxidized states; the former is by far more stable than the latter at acidic and alkaline pH and at high temperature (~100°C), owing to a weaker Fe-M80 bond in the oxidized form.[173] The fully-folded state of the oxidized form of the protein is well characterized (pH 7).[112, 174, 175] However, it is increasingly unclear if the fully folded state is the physiologically relevant form, owing to a conformational change upon its complexation with cyt c oxidase (CcO) as well as upon binding to the inner mitochondrial membrane.[176-178]

Figure 1.14. Ribbon diagram of ■ oxidized and ■ reduced horse heart cyt c, yellow lines illustrate structural alignment, connecting identical residues of the amino acid sequence (PDB: 1AKK,[27] 2GIW[156]).[28]

Complete unfolding by denaturing agents. Chemical agents can directly induce the unfolding of the polypeptide chain, causing the protein to adopt a largely disordered structure. Cyt c reversibly unfolds in the presence of strong denaturants, i.e. guanidinium chloride (GmCl, typically 6 M) or urea (typically around 8 M), as introduced in section 1.1.2. Guanidinium and urea destabilize proteins via different mechanisms, although the results are structurally similar (Figure 1.15). Urea acts to destabilize proteins by forming hydrogen bonds to the peptide NH and likely CO groups, while guanidinium acts without the formation of a hydrogen bond by a still unknown mechanism.[179] Following a two-state folding mechanism (section 1.1.3), however, the physical properties of the resulting unfolded states are indistinguishable: cyt c under denaturing conditions adopts a statistical coil.[180] Under mild denaturing conditions (4-4.5 M urea), proximal H18 remains bound to the heme iron and distal M80 dissociates. M80 is then readily replaced by other side chain residues, forming a flexible compact denatured protein with significant native-like secondary structure and disordered tertiary structure.[181-184] In concentrated urea or GmCl at neutral pH, the M80 ligand is replaced by a histidine (H26, H33 or H39) at the sixth coordination site.[181, 182, 185, 186] Through site-directed mutagenesis, the denatured state was determined to be predominantly populated with H33 as the sixth ligand to the heme iron, with a high spin iron.[187]

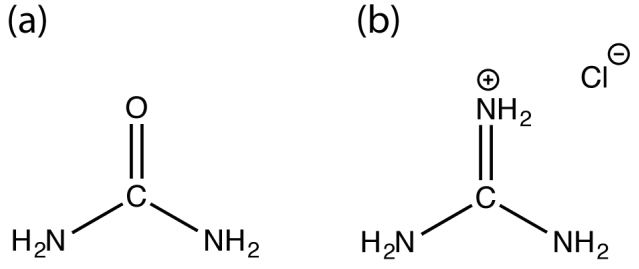

Figure 1.15. Chemical structure of denaturing agents (a) urea (MW: 60.06 g mol^{-1}) and (b) guanidinium chloride (MW: 95.53 g mol^{-1})

The cooperative units within cyt c. The foldon units (**section 1.1.4**) of cyt c were originally observed by Englander and colleagues using hydrogen–deuterium exchange (HX).[55, 64, 188] During this process, the foldon formation is guided by pre-existing structure through a sequential stabilization process by native-like interactions progressively acting to assemble the fully folded protein.[63] Cyt c consists of five cooperative foldon units, with each unit showing approximately the same kinetic and thermodynamic behavior (Figure 1.16).[9, 64, 67, 189] In the order of decreasing stabilities, these foldons are: the blue unit consisting of the N-helix (res 1-16), the C-helix (res 88-104), the green foldon containing the 60s helix (res 61-70) and loop (res 17-37), the yellow unit containing the short two-stranded anti-parallel β-sheet (res. 38-40 and 58-60), the red foldon containing an Ω-loop (res 71-87), and the infrared foldon (gray) containing a nested loop (res 41-57). The red/infrared foldon is the first to unfold, but these foldons were not seperately measured in the experiment performed.[190] This idea of sequential stabilization building the fully folded structure in a step-like manner is a more familiar observation than one might expect. For example in domain swapped dimers, the segments of one protein are induced to conform with the complementary structure of an additional protein.[191, 192] Or from the perspective of amyloidosis (a type of protein aggregate that is linked to neurodegenerative disease), proteins can be induced to join a preformed amyloid fiber by adopting a closely complementary structure.[193, 194]

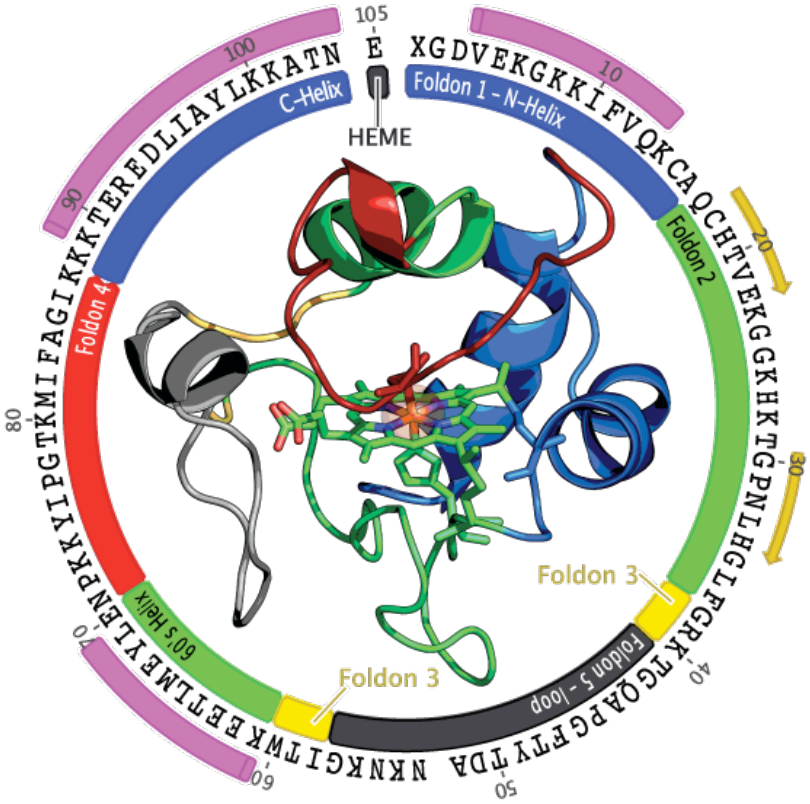

Figure 1.16. Cartoon representation of horse heart cyt c (center) illustrating its three major α-helices, three major Ω- loops. The outside ring shows amino acid letter code of cyt c's 104 residues, and its five cooperative foldon units shown in colors matching the illustration. The foldons are namely the N- and C-helix (blue), the 60s helix and loop (green), the short two-stranded anti-parallel β-sheet (yellow), and two Ω-loops (red and infrared). Also shown are the M80 ligand and H18 which are axially ligated to the heme in the fully folded state.[17, 27, 28]

Early folding of cytochrome c. The folding mechanism of oxidized cyt c consists of two kinetically distinct phases. The first phase, or nascent phase, occurs within 100 μs after initiation of folding,[195] and consists of the collapse of the backbone structure (Figure 1.17).[45, 196, 197] In the folding experiments of Yeh et al., on cyt c this phase was found to consist of an approximate 50% conversion of a pentacoordinated structure to a His-water conformation,[198] with H18 ligation occurring faster than the deadtime of the instrument due to steric constraints imposed by the thioether bonds attaching the heme to the protein through C14/17. Akiyma et al. found that this phase consisted of a small hydrophobic cluster with

around 20% helical content after the initial collapse, and further suggested a second intermediate with α-helical content resembling a molten globule state.[199] This was verified by fluorescent quenching of tryptophan located near the heme group (chapter 2).[45, 200] This stepwise formation of helical structures appears to be consistent with the foldon model, in which several cooperative units are guided by a sequential stabilization mechanism (section 1.1.4).[64]

The subsequent heme-ligand exchange phase of folding is slightly more complex. The formation of the fully folded structure begins to populate from the collapsed state. This occurs at a much slower rate, dependent upon the refolding conditions (Figure 1.17). Yeh et al. performed time-dependent resonance Raman experiments (GmCl; pH 3.6-5.0) and found clear evidence of a switch from high spin to low spin heme, correlating to four possible heme coordination states: a pentacoordinated high spin (5C), a His-water (HW), bis-His (HH), and the folded Met-His (HM) ligation (Figure 1.18). In the presence of GmCl (4.4 M) at neutral pH, cyt c adopts a random-coil-like structure in which the native H18 ligand is retained with H33 replacing the native sixth axial heme ligand, M80.[45, 198] This off-pathway intermediate was verified by site directed mutagenesis of histidines.[187] This conformational change inserts a deep barrier that imposes three-state kinetic folding and allows for the accumulation of an intermediate at the blue foldon since both peripheral histidines are found on the green foldon (Figure 1.16). This acts to block the folding process after the N and C helix formation (blue foldon), because the green loop is required to fold next, but it is held out of place by the HH misligation (Figure 1.17a). HH was found to slowly convert to the HW ,which subsequently decays to the folded HM state.[198]

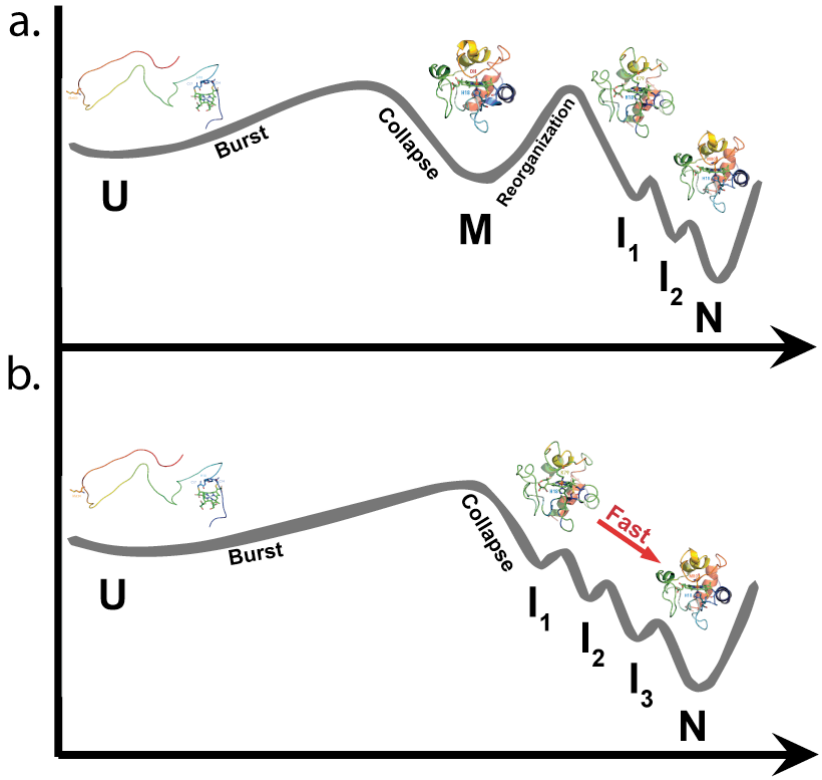

Figure 1.17. Schematic illustration of the free energy surface of cyt c during folding. The course of folding in this illustration starts in the unfolded state, U, where a burst is encountered, illustrating secondary structure formation. This is followed by a large chain collapse where common ligands, or intermediates (I) are sampled in the sequence to the fully folded state, N. (**a.**) shows the events with a folding error, causing a misfolded state, M. To overcome this off pathway state the protein must reorganize its itself to allow the proper contacts to fully fold. This reorganization causes a slowing down of the overall folding process. [17, 27, 28] (**b.**) shows the fast two state folding, with respect to conformational changes of the polypeptide chain.

Under conditions that disfavor the coordination of H33 (i.e. pH <5 when H33 is protonated, [186, 201] the presence of exogenous imidazole,[45] or His mutants[202]) the native structure is reached within a few milliseconds, folding rapidly in a two-state manner. Any intermediates are obligatorily present, stable, and on-pathway, as are subsequent intermediates, but they do not block and accumulate during the folding process (Figure 1.17b). The change in heme coordination indicates a significant amount of structural flexibility, with folding following a thermodynamic equilibrium.[198] This result is consistent with the hypothesis that the secondary structural elements formed early in the reaction are only loosely packed and are localized in a few specific polypeptide segments,[203] with any modulation in the coordination

of the heme imposing a minimal effect. Thus allowing the entire population to fold through the same more populated intermediates, which can be described though sequential stabilization as dictated by cyt c's foldons.[57] Here, the unblocked two-state case rapidly folds, in contrast to the nearly identical folding of its three-state folding analogue that accumulates intermediates, with slowed folding due to the misfolding error described above. This optional misligation and the kinetic behavior provides a general model for folding.

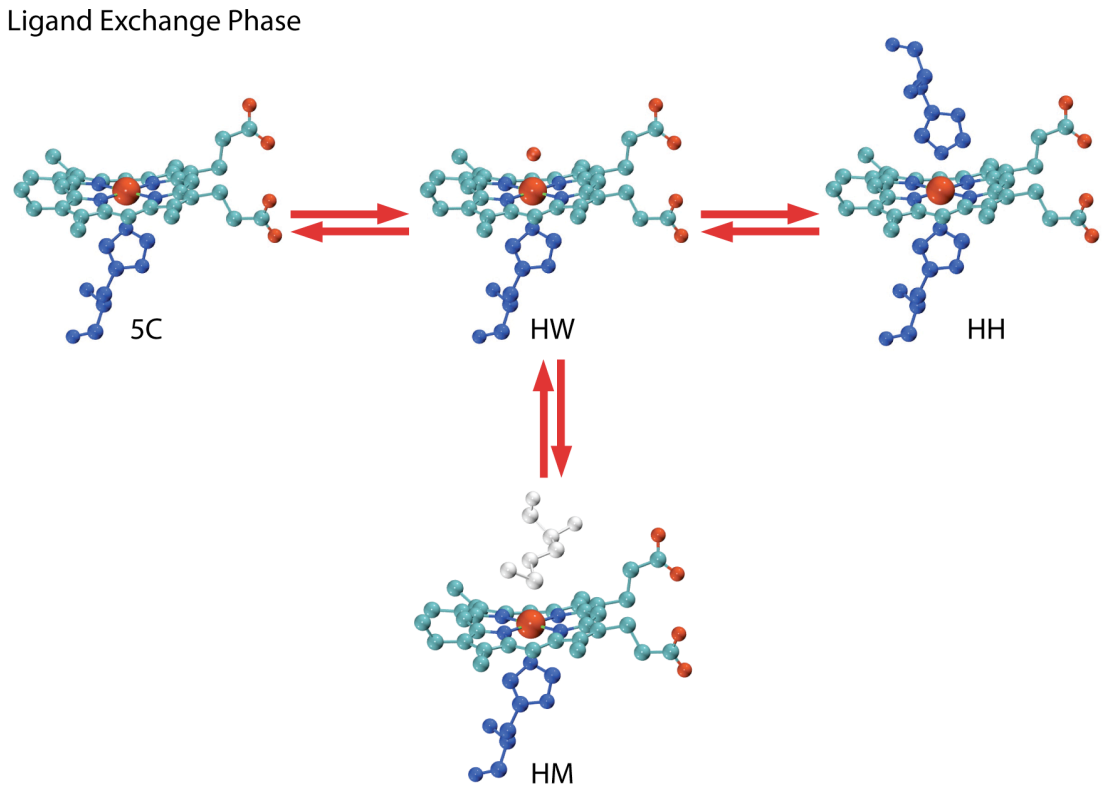

Figure 1.18. Schematic illustration of the folding dynamics of cyt c, showing the ligand exchange phase of folding. The populations of the three heme coordination states, HH, HW, and 5C, are controlled by a fast equilibrium, a slower change in the population of these heme ligation states takes place, ultimately leading to the native state (HM), as described in the text.[16, 198]

1.2.3 Cytochrome c's formation of non-native states in solution

Unfolding of cytochrome c at acidic and alkaline pH. The different protonation states of oxidized cyt c discussed here are built upon the Theorell and Åkesson state model, focusing on the structural flexibility of the oxidized state, rather than the stable reduced form of cyt c. [157, 204-206] The Theorell-Åkesson state model considers five distinct states, termed I to V, which are populated at different pH (1-12). These states are populated without the addition of denaturing reagents, i.e. without urea and Gdn-Cl. The overall reaction scheme for oxidized cyt c can be written as follows

$$I \underset{}{\overset{pK^{eff}_{I\to II}}{\rightleftharpoons}} II_{A,b} + n_1H^+ \underset{}{\overset{pK^{eff}_{II\to III}}{\rightleftharpoons}} III + n_2H^+ \underset{}{\overset{pK^{eff}_{III\to IV}}{\rightleftharpoons}} IV_{a,b,c} + n_4H^+ \underset{}{\overset{pK^{eff}_{IV\to V}}{\rightleftharpoons}} V_{a,b} + n_5H^+ \qquad [\mathrm{I}]$$

where n_j (j = 1, 2, . . .) denote the number of released protons. All pK-values of this scheme are likely to be effective values, representing multiple, cooperative deprotonation steps.[157, 205] Both, pK and n values depend on ionic strength and temperature.[157, 207]

To get a better sense of the changes occurring, I developed a purely speculative structure using a combination of molecular modeling techniques. Starting with the NMR resolved structure (PDB: 1AKK)[27] the Fe-S_{M80} bond was broken and a new bond connection was made between the experimentally-suggested axial ligations. The partially folded protein with diameter ~40Å[80, 205] was then solvated using modified periodic boundary conditions for each state with a boundary set at twice the dimension of the protein.[18, 208] The system was then allowed to minimize energy using the Bio+ (CHARMM) force field, which is a molecular mechanics force field optimized for macromolecules.[209] The minimized structures were then validated using ProCheck (Appendix 8.3),[210] and visualized with the Pymol molecular graphics system.[28] The ProCheck analysis of the modeled structures showed well preserved secondary structure elements (Appendix 8.3b), comprised of five helical elements, with the

length of individual helices varying from one modeled structure to the other.

State I is populated below pH 2 and encompasses two different species, the mole fractions of which depend on solution conditions.[180, 184, 211] Between pH 0.9 to 1.9, two states are predominantly observed, referred to as the U- state and the A-state. The U state is an unfolded state of the protein populated at low ionic strength (Figure 1.19).[195, 212] As the ionic concentration of the solution is increased, the protein population shifts from a statistical coil to a molten globule like state, termed the A state.[184] The A state is an acidic partially unfolded state populated at high ionic strength.[195, 212] Similar species have been detected by Yeh and Rousseau through kinetic studies of cyt c unfolding under denaturing conditions, i.e. with Gdn-Cl at several pH values.[213]

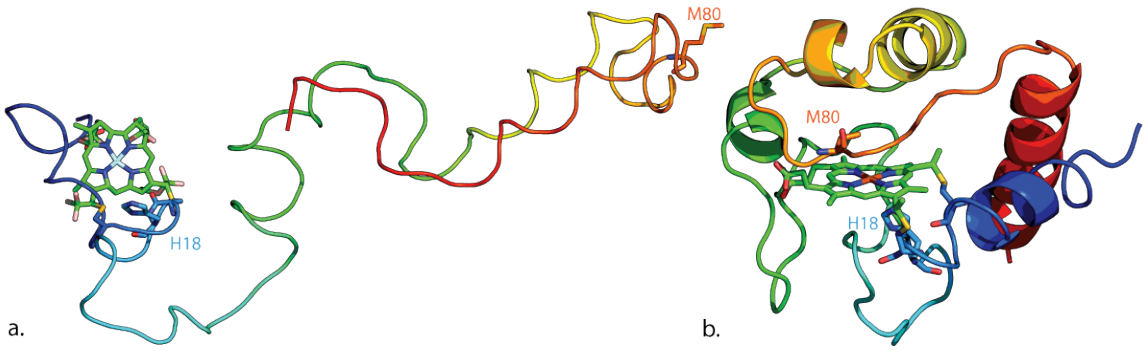

Figure 1.19. Ribbon representation of an (a.) extended unfolded state (U) of cyt c and (b.) a more compact partially unfolded state with no heme axial ligation. The Fe axial ligands of the fully folded state H18, and M80 are shown in stick form, as described in the text.[18, 214]

State II is a partially folded structure populated between pH 2.0 and 3.0, in which at least three different ligation and spin substates have been found to coexist.[184, 215] In this state, the most dominant form is a hexa-coordinated low spin species (hcls) attributed to having bis-imidazolate coordination with axial ligands H18 (as in the fully folded state), and H33 being the likely additional ligand (Figure 1.20a).[187, 195, 213] Additionally, a hexa-coordinated high spin (hchs) state becomes populated with water as the likely ligand with H18 (Figure 1.20b). The sixth coordination site may also remain vacant, producing a penta-coordinated high spin (pchs) state with axial ligand H18 remaining intact.

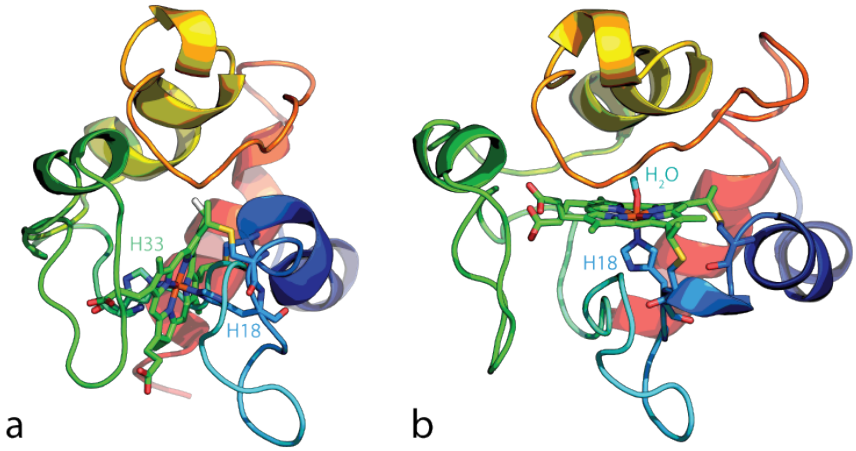

Figure 1.20. Ribbon representation of the cyt c in state II, illustrating the (a) low spin bis-histidine complex (H18 and H33) and (b) high spin complex with H18 and water as the axial ligands.[27, 28]

State III, the fully folded state is populated between pH 4.0 through 8.0 and exhibits a low spin heme iron.[157] The heme Fe of state *III* is hexa-coordinated low spin (hcls), proximally coordinated to H18 and distally ligated to M80 (Figure 1.21). This proximal histidine coordination is common to heme proteins (i.e., myoglobin and hemoglobin), although cyt c is different in that its central Fe is coordinated at both axial sites by amino acids of the protein backbone.

Recent work in our group has observed the existence of a thermodynamic intermediate of the transition between state *III* ⇌ *IV*, which is more populated at low than at high ionic strength.[216, 217] This additional transitional intermediate state, denoted as *III**, was shown to exhibit an intact, though weakened, Fe-M80 linkage.[217] State *III* begins to undergo the transition into the *III** intermediate state between pH 8.0 and 9.0 (pK_{eff} = 8.5).[217] This state escaped earlier investigations into the alkaline transition because it is less populated at the higher ionic strength at which these studies were carried out and was thus obscured.[216, 217] Bowler and coworkers assigned the state to the deprotonation of one of the propionic acid substituents of the heme group, which is known to exhibit a very high pK value.[218] Weinkam et al. also observed a similar, though not identical, intermediate at high ionic strength, termed state 3.5, in which the M80 ligation is broken but is not yet ligated to the lysine (K), found in state *IV* at slightly higher pH.[219]

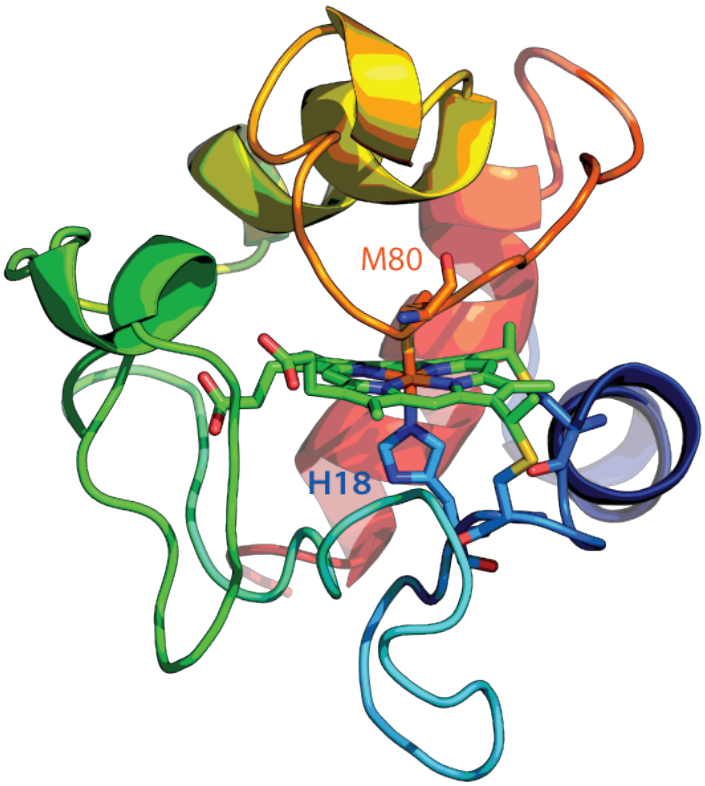

Figure 1.21. Ribbon representation of the fully folded state of cyt c in state III, with Fe axial ligands H18 and M80 shown in stick form. [17, 27, 28]

State IV is populated at pH >9.0 (pK_{eff} = 9.23); this is referred to as the first alkaline transition. This state encompasses at least thee different substates termed $IV_a/IV_b/IV_c$.[220-224] Mauk and Hildebrandt and colleagues showed through site directed mutagenesis of yeast cyt c and resonance Raman (RR) spectroscopy that the $III \rightarrow IV$ transition involves, in fact, two parallel transitions with very similar pK-values, which lead to the replacements of the distal ligand M80 by K79, K73, or K72.[222-224] The corresponding sub-states states are termed IV_a and IV_b in horse heart cyt c. As mentioned earlier K73 and K79 are found on the surface of the fully folded state of cyt c where they facilitate the interaction with several redox partners (Figure 1.22 a,b). Blouin et al. showed an even more complex transition into state IV for horse heart cyt c, involving three IV states.[225] Two of these correspond to states IV_a and IV_b, separated from the third one by a rather high energy barrier. A third transition was found in the bacterially expressed yeast iso-1 form, termed IV_c, which is of lesser stability, in which K72 becomes axially ligated (Figure 1.22c).[225, 226] This conformation showed no significant rearrangements within the protein other than the iron ligand replacement.[224, 227] The misligation by K72 in the yeast protein is precluded by post-translational trimethylation, which does not occur when the protein is bacterially prepared in *Escherichia coli*. This allows the lysine side chain to become a viable ligand once deprotonated under alkaline conditions (pK'=8.7).[224] The misligation with K72 forms a very stable conformation in yeast, however recent mutational studies of horse heart cyt c suggests that the unmodified K72 does not contribute to misligation and that ligated K79 is the most stable conformation.[228] Nevertheless, animal cells do not perform this trimethylation modification.[112]

Overall, the alkaline transition is generally thought of as yielding a more open heme crevice in which the loop (res. 70–85; red foldon) is shifted considerably with respect to the heme group.[222-224] Results from a resonance Raman study suggest that this structural change reduces

heme perturbations thus switching it to a more relaxed planar state, and thereby reducing the reduction potential.[176] This view is corroborated by a recent resonance Raman study of Alessi et al. who showed that the alkaline transition involves a decrease of symmetric A_{1g}-deformation of the heme, which could well reflect the reduction of non-planar (ruffling) deformations.[167]

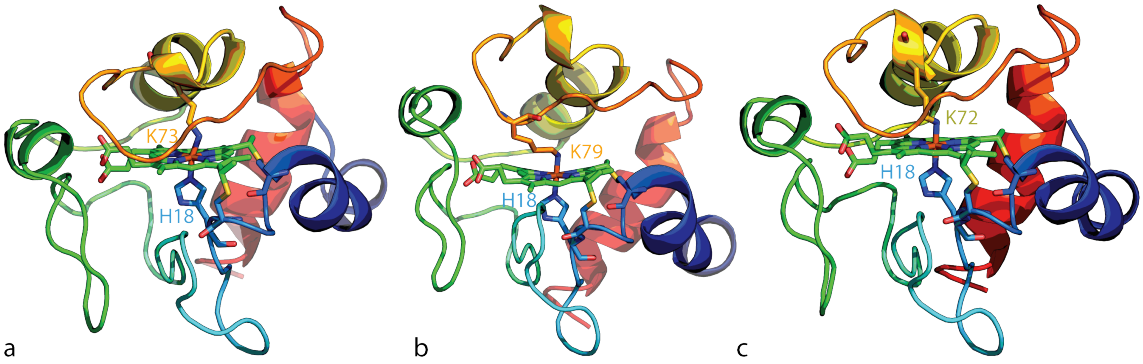

Figure 1.22. Ribbon representation of the fully folded state of cyt c in state IV. , illustrating the replacement of M80 of state III being replace with a lysine, (a) lysine 73 (K73) (b) lysine 79 (K79 or (c) lysine 72 (K72) as the distal ligand. In all cases the proximal H18 remains intact.[17, 27, 28]

State V . Döpner et al. showed that two state *V*'s are formed upon increasing the pH further, above pH 11.[220, 229] Termed states V_a and V_b, here the K ligands are replaced by another ligand, likely a hydroxide ion or L68 (Figure 1.23).[220, 229] This transition can be manipulated by replacing Y67 and K73 with a histidine residue.[230] This second alkaline transition causes a substantial decrease in the redox potential.[220, 229] Generally, this state is considered to be mostly molten globule, with intact secondary and perturbed tertiary structures. Whether a denatured molten globule state that is adopted at even more alkaline pH values (>12) is different from *V* remains to be clarified.[82]

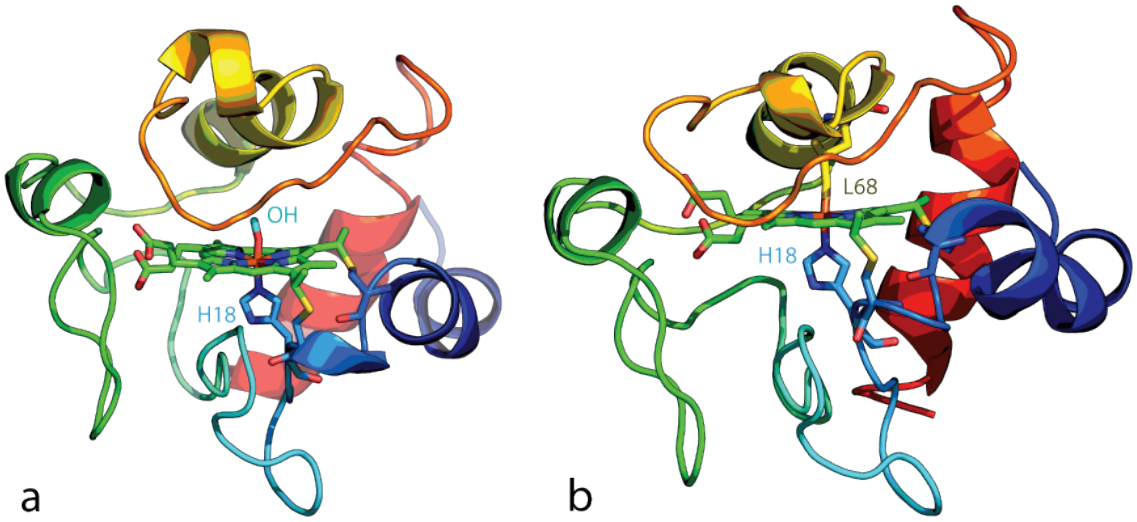

Figure 1.23. Ribbon representation of the fully folded state of cyt c in state V, illustrating the lysine of state IV being replaced with either (a) a hydroxide (OH^-) or (b) a leucine (L68) as the distal ligand. In both cases the proximal H18 remains intact. [17, 27, 28]

The role of temperature on folding. The thermal stability of cyt c and the conservation of its high redox potential depends significantly on the stability of the M80-Fe linkage. For the oxidized state of the protein, thermal unfolding starts around 40 °C (313 K, pH 7), whereas the reduced state of cyt c requires much higher temperatures to initiate unfolding (temperatures above 100 °C, 373 K, pH 7).[75, 231, 232] The thermal transitions of cyt c involve the population of a thermodynamic intermediates across the pH range as temperature is increased above 50 °C (323 K). We again follow the notation of the Theorell-Åkesson state model and additionally denote thermal intermediates with the subscript *i*. At higher temperatures the protein further unfolds entering a thermally unfolded state denoted with the subscript U. The minimal thermodynamic scheme for thermal unfolding of cyt c across the pH range is shown in Figure 1.24.

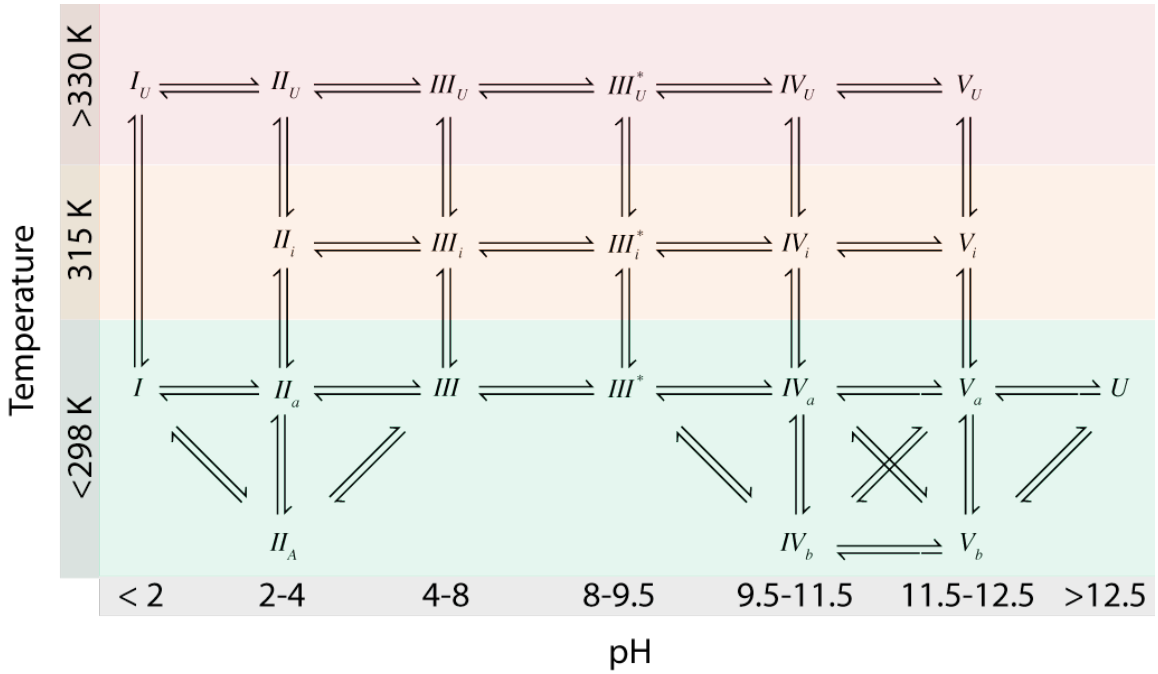

Figure 1.24. Proposed thermodynamic landscape of horse heart ferri-cyt c across the pH range (x-axis) and as a function of temperature (y-axis). Constructed based upon the original notation of the Theorell-Åkesson state model, as described in the text.[17]

Thermal unfolding of state III/III*. The oxidized fully folded state of cyt c (*III*) begins the unfolding process at a considerably lower temperatures in the range of 40 °C (313 K) to 70 °C (343 K). At a temperature above 50 °C (323 K), a thermodynamic intermediate becomes populated, termed state III_i. This thermal unfolding causes a decrease in the redox potential, and the M80 coordination was suggested to be replaced by another residue upon population of the thermal intermediate, based on the observation of a disappearing 695 nm charge transfer band.[84, 85] Recent work by Hagarman et al. suggests the existence of a unique neutral state at high temperature (> 50 °C) that was neither identical with state *IV* nor with state *III*[233] with III_i maintaining a low-spin heme iron.[234] This is also true for the aforementioned *III** state under increased temperature and its respective $III^* \rightarrow III^*_i$ transition.[207]

Thermal unfolding of state IV. The population of a thermal intermediate and unfolded state for state *IV* begins at temperatures above 75 °C (348 K); these states are termed IV_i and IV_U.[233] Analysis of this region is often very complicated, owing to the possible coexistence of multiple alkaline isomers, lysine protonation (cyt c has 19 K res), and the dissociation of M80, all thermodynamically distinct processes.[235]

Thermal unfolding of state V. The population of thermal intermediates and the thermally unfolded state of state *V* begin to populate at temperatures above 45 °C (320 K). The work of Hagarman et al. reveals the melting of state *V* into at least two thermal intermediates, termed V_{i1} and V_{i2}, before occupying a thermally unfolded state above 77 °C (350 K), termed V_U.

Role of ion concentration on cyt c. Many of the studies aimed at explaining the relationship between the structure and function of cyt c have been performed using different solution conditions. Most studies utilize an array of buffers, at various concentrations and variable salt content. Moreover, there are various stabilizing and destabilizing agents utilized throughout these studies. Cyt c is a highly charged protein (+8) at neutral pH values, making it highly susceptible to electrostatic interactions with ions present in solution. It has been shown through electrochemical studies by Sola et al. that ions, i.e., Cl^-, HPO_4^{2-}, HCO_3, NO_3^-, SO_4^{2-}, bind to the positive patches on the surface of the protein (Figure 1.25).[236] This binding occurs in the concentration regime chosen for phosphate buffers and NaCl additions in the majority of studies on cytochrome c. Binding of the respective anions create a mixture of thermodynamic states, thus complicating any thermodynamic analysis aimed at obtaining physically meaningful parameter values.[84, 236] It is often argued that the binding of anions to positively charged lysine residues has a negligible effect on the structure of the protein.[220, 229] However, this view has been questioned based on various lines of experimental evidence. ^{1}H-

NMR studies have revealed salt dependent changes of chemical shifts assignable to residues in the 83-89 region (red foldon).[219, 237-239] The distance between F82 and the heme decreases upon the increase of ionic strength.[237] Earlier work in our group provided strong evidence on how small structural changes, caused by differences in ionic strength and anion binding to the protein surface, involve substantial structural variations of the Fe(III)-M80 bond, which is one of the key determinants of the redox potential.[240] Small angle x-ray scattering (SAXS) studies of oxidized and reduced cyt c have shown an overall protein expansion under conditions of low ionic strength and compression at higher ionic strength.[175] Raman studies have also shown Tyr48 and Trp59 to be altered with changing ionic strength, reflecting an increased radius of gyration at low ionic strength and the collapses to a more compact arrangement at high ionic strength (as seen in the crystal structure).[241] Therefore, in order to obtain the basic thermodynamic parameters of cyt c unfolding due to changes in pH and temperature, experimental studies have to be performed under low ionic strength. The term "basic thermodynamic parameters" means that these experiments study 'pure' states and do not depend on pH and ion concentrations. This is of particular relevance due to the fact that low ion concentration is necessary for, e.g. the complex formation with Apaf-1 and anionic lipids as mentioned previously.[242, 243] Altogether this provides the basis for a reference system that can be used to quantitatively understand the role of ion binding, pH and temperature, as well as the influence that these parameters play with respect to cyt c folding.

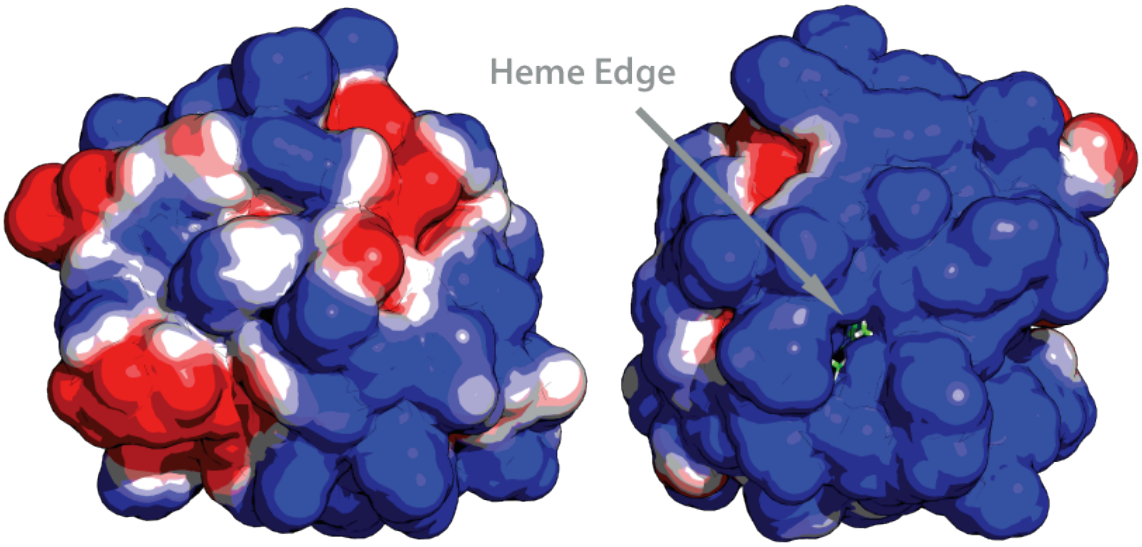

Figure 1.25. Visualization of the electrostatic surface[244] of oxidized horse heart cyt c, ● indicates a positive potential and ● indicates a negative potential (PDB: 1AKK[27]). The edge of the heme which is solvent exposed is indicated with the grey arrow.[17, 28]

1.2.4 Cyt c dimerization and higher order oligomerization. For nearly half a century, it has been known that cyt c forms polymers when heated in the presence of denaturants, i.e. upon incubation with ethanol or trichloroacetic acid (TCA).[245] Dimerization and aggregation typically can occur at higher protein concentrations. The formation of dimers and oligomeric complexes of proteins, particularly with respect to membrane proteins, frequently involves one domain of each subunit replaced by the identical domain from another subunit. The swapped "domain" can be as large as an entire tertiary globular domain or as small as an α-helix or strand of a β-sheet. It has been recently shown that polymerization of cyt c occurs by the successive domain swapping of its C-terminal α-helix (Figure 1.26).[191, 192] This creates a population of partially folded misfolded structures where the M80-heme coordination is significantly perturbed, causing higher peroxidase activity in the dimer than monomer.[192, 246]

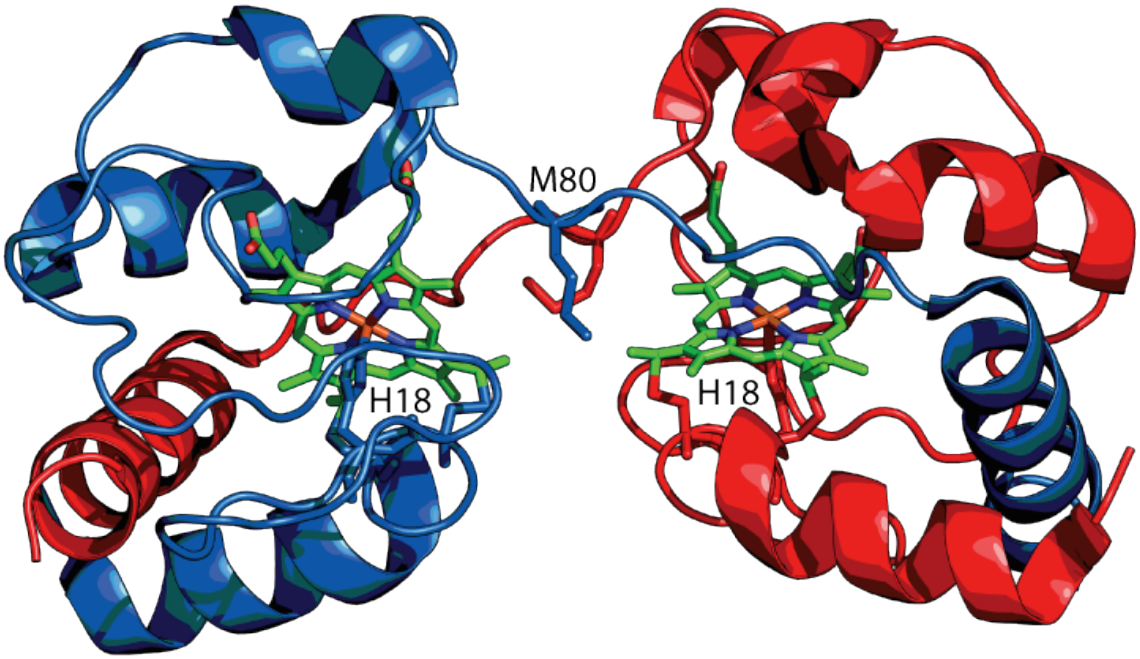

Figure 1.26. Ribbon representation for the domain swapped dimer of cyt c (PDB 3NBS[192]).[17, 28]

Unregulated domain swapping can further develop to form clusters, leading to protein precipitates and even abnormal aggregates and fibrils. Cyt c (bovine) has been shown to follow this alternate route of aggregation, forming amyloid fibrils when heated at 75 °C for 12 h under mildly alkaline conditions.[247] Amyloid fibrils are insoluble, highly-ordered aggregate structures with similar morphologies (long, unbranched with often twisted structures a few nm in diameter) and a characteristic "cross-beta" X-ray fiber diffraction pattern.[248, 249] This conversion of fully-folded proteins into well-ordered aggregates can occur during the folding process of a protein. If a protein fails to fold correctly or remain folded it will likely not be able to perform its function. This enhanced amyloid propensity was found in the case of lysozyme, in which a single point mutation is involved in hereditary systemic amyloidosis, and is associated with the deposit of fibers in several tissues.[250] Once formed, this unique type of aggregate can persist for very long periods, ultimately building up and depositing in human tissues (e.g. amyloid-β, α-synuclein). These aggregation diseases are becoming increasingly evident when discussing a wide range of various debilitating human pathologies (i.e. Alzheimer's, Parkinson's, Huntington's etc.).[251, 252] This mechanism is still poorly understood, although understanding these non-native forms and ways to inhibit them is necessary to develop a therapeutic approach to various amyloid pathogenicities.[253]

Recently, the funneled energy landscape concept of protein folding (section 1.1.6) has been extended to include protein oligomerization and fibril formation, which is now considered a generic feature of all proteins and peptides. Figure 1.27 shows the extension of the free energy landscape to include the conformational states available between multiple monomers leading to oligomerization and aggregation.

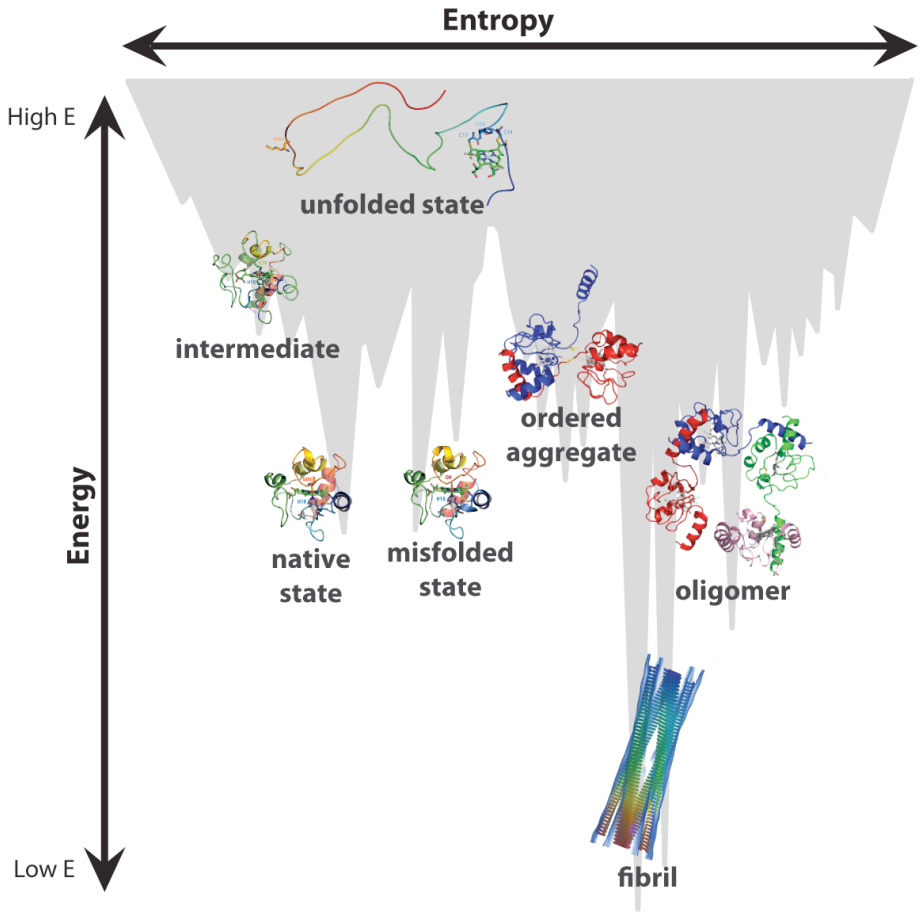

Figure 1.27. An extended energy landscape combining the protein folding perspective with aggregation. The gray surface illustrates the roughness of the energy landscape of a protein showing multiple conformational states available to a polypeptide chain (PDB: 1AKK).[27, 192, 194] While simple folding funnels can describe the conformational changes to a functional monomer, the ruggedness of the landscape can increase as intermolecular protein association occurs.[17, 28]

In this thesis, two issues related to the folding and unfolding of cyt c will be addressed. First, the thermal transition of all six protonation states of oxidized cyt c are probed by CD and absorption spectroscopy (Chapter 2). The data was analyzed in terms of a three-state model which considers the existence of a single thermodynamic intermediate (Chapter 4). Second, the surprising discovery and characterization of a novel misfolded state, created at alkaline pH that remains stable at neutral pH (Chapter 5). In this chapter it is shown that the energy landscape of cyt c is more frustrated than previously documented. Chapter 3 describes the methods to reach these conclusions.

CHAPTER 2: THEORETICAL BACKGROUND ON SPECTROSCOPIC STUDIES

Over the last 60 years cyt c has been investigated through a large variety of experimental approaches including multiple spectroscopic techniques utilizing a broad range of the optical spectrum. The application of these often complementary techniques has provided valuable and comprehensive information about the protein's structure and function, and functionally relevant heme-protein interactions. In this chapter we briefly describe the spectroscopic techniques used for experiments described in this thesis. Details of the underlying theories have been reported elsewhere and are only briefly outlined here to facilitate the readability of this thesis. To explore the secondary and tertiary structure of cyt c at a variety of solution conditions we employed optical absorption in conjunction with UV and visible circular dichroism (CD). The latter provides specific information about the symmetry lowering perturbation that the protein environment imposes on the functional heme group structure. Resonance Raman (RR) scattering was employed to determine the oxidation, ligation and spin state of the heme iron as well as the symmetry lowering deformations of the heme macrocycle. Tryptophan (W) fluorescence was exploited to probe the degree of protein unfolding.

2.1 Absorption Spectroscopy. The basic theory of absorption spectroscopy is textbook knowledge. More details about the quantum mechanical background have been provided in numerous more specialized books and articles.[207, 254, 255] The Beer-Lambert law can be applied to explain absorbance $A(\tilde{\nu})$, at a given wavenumber, $\tilde{\nu}$, which is written as

$$A(\tilde{\nu}) = \varepsilon(\tilde{\nu}) lc \qquad [2.1]$$

where l is the path length in which light travels through a medium, c is the concentration of a substance in solution, and ε is the molar extinction coefficient. ε, which is generally expressed in units of M^{-1} cm^{-1}, and reflects the interaction capability of the medium with an electromagnetic radiation field. For a manifold of electronically allowed transitions, an absorption spectrum $\varepsilon(\tilde{\nu})$ can be described, generally, as a superposition of Voigtian profiles

$$\varepsilon(\tilde{\nu}) = \sum_l \frac{A_\varepsilon \tilde{\nu} f_l \Gamma_l}{\sigma_l \sqrt{2\pi}} \int_{-\infty}^{\infty} \frac{e^{-\left(\tilde{\nu}-\tilde{\nu}_l'\right)^2 / 2\sigma_l^2}}{\left(\tilde{\nu}-\tilde{\nu}_l'\right)^2 + \Gamma_l^2} d\tilde{\nu}' \qquad [2.2]$$

where f_l is the oscillator strength of the transition associated with the electronic transition dipole moment $\vec{\mu}_l$ induced by the oscillating electromagnetic field of radiation (A_ε = 108.92 D^{-1} M^{-1} cm^{-1}). f_l can be described as

$$f_l = \left| \left\langle l \left| \vec{\mu} \right| g \right\rangle \right|^2 = \left| \int_{-\infty}^{\infty} \psi_l^* \vec{\mu} \psi_g d_r^3 \right|^2 \qquad [2.3]$$

where ψ_g and ψ_l are the electronic wavefunctions of the ground, ($|g\rangle$) and the excited ($|l\rangle$) states, respectively. Γ_l and σ_l are the half-widths at half maximum of the Lorentzian and Gaussian contributions to the corresponding Voigtian profile. The half-width of a Lorentzian

profile, Γ_l, reflects the natural lifetime as well as the dephasing of the excited state.[207] The Gaussian distribution contains a static term due to inhomogeneous broadening, and a dynamic contribution that reflects the coupling of a bath of low frequency modes to the respective electronic transition. [256, 257] The bath of low frequency modes coupled to electronic transitions of the heme group involves protein motions, described in greater detail in section 2.1.3. The electronic dipole transition moment couples the ground state ($|g\rangle$) with excited states ($|l\rangle$) states through the absorption of a photon from the radiation field. $\tilde{\nu}_l$ is the wavenumber corresponding to the energy difference between the $|g\rangle$ and $|l\rangle$ states. This summation runs over all excited vibronic states accessible by electronic dipole transitions. The electronic dipole transition moment is defined as

$$\vec{\mu} = \sum_i e\vec{r}_i \qquad [2.4]$$

where e is the elementary charge and $\vec{r}$ is the position vector operator, i.e. the coordinate of the i^{th} electron with respect to an arbitrary reference point.

2.1.1 Ultraviolet absorption. The near ultra-violet (250 - 300 nm) and far ultra-violet (UV) (< 250 nm) absorption spectra of proteins are dominated by bands assignable to transitions of the polypeptide backbone of the protein (190 - 240 nm), and to contributions from $\pi \rightarrow \pi^*$ transitions in aromatic amino acid residues. The amide backbone $\pi \rightarrow \pi^*$ and $n \rightarrow \pi^*$ electronic transitions give rise to far UV-bands at wavelengths shorter than 230 nm.

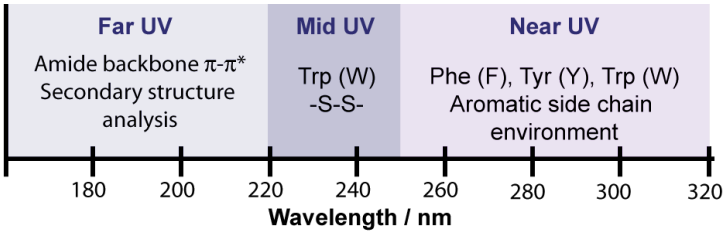

Aromatic transitions. The spectra of aromatic side chains, phenylalanine (F), tyrosine (Y) and tryptophan (W), all exhibit absorption bands corresponding to $\pi \rightarrow \pi^*$ transitions in the near UV region. The indole ring of W contributes two or more transitions in the 240 - 290 nm region with a maximum around 279 nm, Y exhibits one band around 274 nm, and F depicts a band at 258 nm and at 200 nm.[258] Overall, W has the most intense band in the 280 nm region. In most proteins the number of W residues are limited, so W-bands do not typically dominate the spectrum. Cyt c contains only a single W, four Y and four F residues. The fluorescence of the single W residue can be used to probe changes of the protein's tertiary structure, as explained in section 2.4.

2.1.2 Visible absorption.

Heme transitions. The heme prosthetic group, a Fe-protoporphyrin-IX molecule (Figure 2.1) exhibits additional transitions in the UV/visible region of the spectrum. The visible transitions can be exploited to investigate interactions of the heme with its local $\pi \rightarrow \pi^*$ environment. Electronic transitions in the heme prosthetic group dominates the visible and near-UV absorption spectrum.

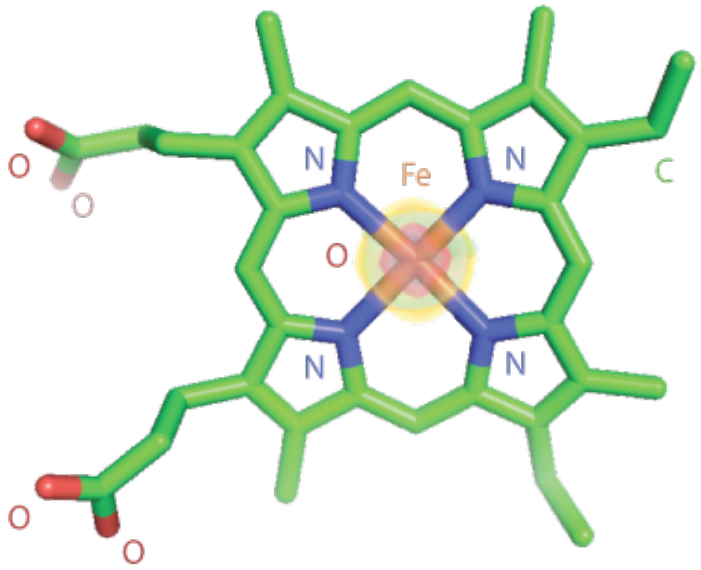

Figure 2.1. Structure of the heme, an Fe-protoporphyin IX, which occurs in cytochrome c.[17, 18, 28]

The visible absorption spectra of the reduced (Fe^{2+}) and oxidized (Fe^{3+}) cyt c are shown in Figure 2.2. In both oxidation states a strong ligand field (axial ligands H18 and M80) imposes a low-spin configuration.[7] The spectrum of ferro-cyt c depicts three bands termed *B* (408 nm), Q_v (530 nm), and Q_0 (565 nm). Q_v is assignable to transitions into the first vibrational states of heme oscillators in the excited *Q* state. This Q_0-band intensity results mostly from the $0 \rightarrow 0$ pure electronic transition (the electronic transition to and from the lowest vibrational

state) into the *Q* state. In ferricytochrome c, only one band appears in the *Q*-band region, which can be decomposed into a broad Q_0 and multiple Q_v contributions.[207, 259] The same notion generally applies to the *B*-band, which is just a superposition of the 0→0 transition into the B state combined with various vibronic contributions. The *B*-band (Soret) intensity is dominated by transitions into the first vibrational states of A_{1g}, totally symmetric mode, while Herzberg-Teller coupling involving A_{2g} type antisymmetric mode is responsible for most of the Q_v-band's oscillator strength.[260, 261] All bands in the visible absorption spectra (400 - 600 nm) can be assigned to $\pi \rightarrow \pi^*$ transitions of the heme macrocycle, owing to the four orbital model (see next section). Ferricytochrome c shows additional CT absorption maxima at 695 nm (sharp), and 655 nm, visible only in highly concentrated solutions.[205]

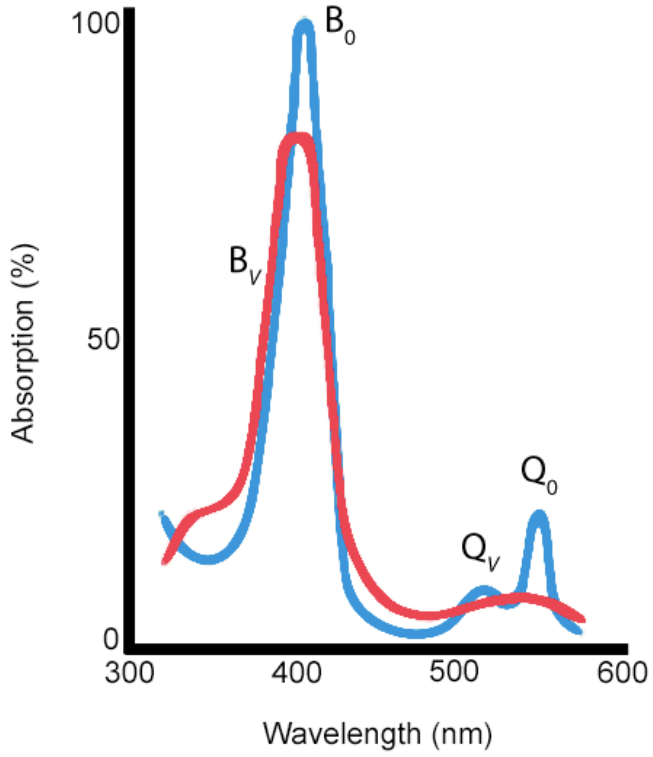

Figure 2.2. Absorption spectrum of ● oxidized and ● reduced cyt c (equine), illustrating the dominant *B*- (Soret) and *Q*-bands.[17]

The four-orbital model. The absorption spectra of metal porphyrins can be explained through the four orbital model.[262, 263] The visible absorption spectrum of cyt c (Figure 2.2) is reminiscent of the canonical absorption spectrum of metal porphyrins, in that it shows a very intense band at 415 nm and one broad or two narrower, less intense bands at 520 and 550 nm (termed *B*- and *Q*-bands respectively).[264] According to this theory, the absorption bands in a porphyrin system arise from the transitions between two of the highest occupied molecular orbitals (HOMO) and two, two-fold degenerate lowest unoccupied molecular orbitals (LUMO). The electronic state of the Fe-metal center as well as peripheral substituents affect the relative energies and intensities of these transitions.

Gouterman's four orbital model theory assumes the porphyrin to be of D_{4h} symmetry.[262, 263] Thus, the symmetry-lowering perturbations caused by the peripheral substituents, different axial ligands and the protein environment are neglected. The electronic ground state transforms like A_{1g}, and the symmetries of the excited states are E_u (*B*- and *Q*-bands), indicative of a two-fold degeneracy. The lower excited state is termed *Q*- while the higher lying one is the *B*-state. Electronic transitions are allowed only if there is a change of the parity, i.e. *g* (*gerade*)→ *u* (*ungerade*) or vice versa. Hence, transitions into $|Q\rangle$ and $|B\rangle$ are electronically allowed from a group theoretical point of view. However, since they arise from the configurational interaction between two nearly accidentally degenerate HOMO → LUMO transitions, the B-band gains intensity at the expense of the *Q* band. If the mixing of the two molecular orbital (MO) transitions is 50:50, the *Q* state transition (i.e. 0 → 0) carries practically no electronic oscillator strength (eq. 2.3). The separation of energy between the two coupled electronic states along the coordinates can be defined as

$$\Delta E = E_B^0 - E_Q^0 = \delta \qquad [2.5]$$

In contrast to the assumed ideal state, the energies of the two HOMOs are not accidentally degenerate. Thus, the two electronic transitions are not 50:50 mixed, and as a consequence the probability of a transition into the Q_0-state is non-zero. The degree of unmixing is described by the parameter v. In the presence of unmixing perturbations of the electronic state, vectors are written as

$$\begin{aligned} \left|Q_\sigma\right\rangle &= \cos(v)\left|Q_\sigma^0\right\rangle - \sin(v)\left|B_\sigma^0\right\rangle \\ \left|B_\sigma\right\rangle &= \sin(v)\left|Q_\sigma^0\right\rangle - \cos(v)\left|B_\sigma^0\right\rangle \end{aligned} \qquad [2.6]$$

where $|Q^0\sigma\rangle$ and $|B^0\sigma\rangle$ denote the electronic eigenstates emerging from complete mixing (50:50); for convenience these vectors are used as a reference system.[265, 266] The σ indicates the x or y direction of the two transition dipole moments of the E_u twofold degenerate transitions. v can be written as

$$v = \arctan\left(\frac{\delta_{A_{1g}}}{E_B^0 - E_Q^0}\right) \qquad [2.7]$$

where δ_{A1g} denotes an electronic symmetric perturbation of the heme, which yields an expansion or contraction of the heme core with respect to a macrocycle structure in which the two HOMOs are indeed degenerate. This perturbation causes a further separation between the B_0 and the Q_0 band and redistributes intensity from B_0 to Q_0 transitions. Values of this unmixing factor generally lie between 0.05 and 0.15.[267] v can be determined from the transition dipole moments found from the absorption spectrum so that

$$v = arctan(R_Q/R_B) \quad [2.8]$$

where R_Q and R_B are the matrix elements associated with the transitions into $|Q^0\rangle$ and $|B^0\rangle$, respectively. We assume here that the entire dipole strength of the unperturbed state results from unmixing of the 50:50 states, thus ignoring the small intrinsic oscillator strength of the transition into Q_0.[268] These values can be easily obtained from the integrated intensities of the *B*- and *Q*- bands, using MultiFit deconvolution software.[269]

Vibronic side bands. A vibronic approach is necessary to explain the existence of B_v and Q_v. Vibronic coupling between vibrations and electronic transitions causes displacements of excited states along the normal coordinates. The vibronic contributions are denoted with a subscript *v*. The vibronic mixing between Q_v and B_0 states can be accounted for by the adiabatic Herzberg-Teller approximation

$$\left|Q_{v,k}\right\rangle = \left|Q^0_{v,k}\right\rangle + \sum_{j=1}^{N-6} \frac{\left\langle B^0_{0,l} \left| \frac{\partial \hat{H}_{el}(Q,q)}{\partial Q^{\Gamma}_j} Q_j \right| Q^0_{v_j,k} \right\rangle}{E^0_{B_l} - E^0_{Q_k} + \Omega^Q_j} \quad [2.9]$$

where $H_{el}(q,Q_j)$ is the electronic Hamiltonian, which depends on the electronic coordinate q and the nuclear coordinates Q_j.[270] Ω_j is the wavenumber of the j^{th} vibration contributing to the vibronic side band of the Q state transition. Group theory therefore dictates for the vibronic coupling matrix element in eq. 2.9, that its symmetry is one of the irreducible representations into which the direct product representation $E_u \otimes E_u$ can be decomposed:

$$E_u \otimes E_u = A_{1g} + A_{2g} + B_{1g} + B_{2g} \quad [2.10]$$

Thus, the A_{1g}, B_{1g}, B_{2g}, and A_{2g} modes can in principle contribute to Q_v absorption (interstate coupling). Vibronic coupling between the *B*- and *Q*-states pumps intensity into the Q_v absorption band. The Q_v band profile is then dominated by vibronic coupling contributions of antisymmetric A_{2g}-type modes, since they exhibit the strongest vibronic coupling strength.[271]

For reasons of symmetry, Herzberg-Teller coupling should also contribute to B_v absorption. However, the respective contributions are weak since they are proportional to the oscillator strength of the Q_0 transition. The strong transition dipole moment of the *B*-state transitions then facilitates contributions from intrastate coupling to B_v, which is dominated by Franck-Condon coupling involving totally symmetric A_{1g}-modes. Some minor contributions emerge from Jahn-Teller coupling involving B_{1g}-modes.[260, 272] Since the displacements of the excited *B*-state potentials with respect to the ground state geometry are generally small, the effective dipole moment for transitions into B_v-states can be expressed by using Rayleigh-Schrödinger time independent perturbation theory. This yields:

$$\vec{\mu}^{B}_{\sigma,1_{A_{1g}}} = \frac{\left\langle B^{0}_{1,\sigma} \left| \frac{\partial H_{el,0}}{\partial q_i^{\Gamma_i}} q_i^{\Gamma_i} \right| B^{0}_{0,\sigma} \right\rangle}{\Omega^{B}_{j}} \vec{\mu}^{B'}_{\sigma,0_{A_{1g}}} \qquad [2.11]$$

This equation accounts for both Franck-Condon and Jahn-Teller coupling. It is generally assumed that only A_{1g}- (Franck-Condon) and B_{1g}-type (Jahn-Teller) intrastate coupling affects the *B*-band (Soret). Coupling involving B_{2g}-modes, which would mix B_x and B_y components of the excited state, is generally weak.[273-275]

Thus far we have followed Gouterman and others by assuming a D_{4h}-symmetry for the heme macrocycle. However, this is not completely realistic owing to symmetry lowering forces exerted by the protein and the peripheral substituents.[267] Asymmetric heme perturbations lift the degeneracy of the excited *Q* and *B*-states, thus giving rise to band splitting. The influence of B_{1g} type perturbations is likely to be the largest contributor to this type of splitting.[271, 276] Owing to the relative large bandwidths of *B* and *Q*-bands, band splitting is generally not detectable by absorption measurements at room temperature, whereas circular dichrosim (CD) spectroscopy can provide the necessary resolution.[277] Therefore, *B*-band splitting will be further described in the CD section below.

Bath modes. The absorption of energy of an isolated molecule going from a ground state to a first excited state occurs at a single, well defined frequency. A considerable fraction of the variance of the lineshapes of the *B*- (Soret) and *Q*-band comes from broadening due to the coupling of the electronic transitions with a bath of low-frequency modes. This yields a temperature dependent Gaussian broadening of the respective bands. The observed line shape is therefore describable as a Voigtian profile

$$V_{j,\rho}\left(\tilde{\nu}\right) = \underbrace{\frac{1}{\pi}\frac{I_{j,\rho}\Gamma}{\left(\tilde{\nu}-\tilde{\nu}_{j,\rho}\right)^2+\Gamma^2}}_{\text{Lorentzian Profile}} \otimes \underbrace{\frac{1}{\sigma\sqrt{2\pi}}e^{-\frac{\tilde{\nu}^2}{2\sigma^2}}}_{\text{Gaussian Profile}} \qquad [2.12]$$

where σ and Γ are the widths of the Gaussian and Lorentzian contributions to the convoluted band profile, respectively. The Lorentzian contribution reflects the natural (homogeneous) width of the electronic transition along with its high frequency mode coupling. The broadening of the *B*-band can then be used to derive the mean square fluctuation of the Fe atom relative to the center of mass of the heme.[257, 278] This allows the B-band (Soret) to

directly probe the local heme-iron, which is important in the development of the physical description of the protein.

2.1.3 Charge Transfer absorption. The absorption spectrum of the ferricytochrome c additionally contains some weak bands in the red and near IR region above 650 nm, which are assignable to charge transfer (CT) processes.[279, 280] One of these bands, the so-called 695 nm band, is a prominent spectral marker frequently used to probe the integrity of the Fe-M80 ligation. Theorell and Åkesson first described this band, and later detailed its disappearance at *pH* values < 2.5 and > 9.35.[281] This band was originally assigned by Eaton and Hochstrasser as an $A_{2u}(porphyrin) \rightarrow A_{1g}(d_z^2)Fe$ CT transition.[279, 280] However, more recently this band has been attributed to a $S(p_z) \rightarrow Fe^{3+}(d_{xy})$ CT transition.[282] This interpretation is in line with its disappearance in spectra of non-native cyt c, in which M80 is replaced by another ligand. Since this band is diagnostic of the fully folded native state, it has frequently been used to monitor conformational transitions into non-native states, e.g. the alkaline transition from state *III* into the partially unfolded state *IV*. Work in our group and the Cupane group showed that this band can be subdivided into three sub-bands, assignable to sub-conformations of the Fe^{3+}-S(M80) linkage.[240, 283-285] The presence of $H_2PO_4^-$ and Cl^- ions can cause a dramatic increase in this band's oscillator strength, indicative of a strengthening of the Fe^{3+}-S(M80) linkage due to anion binding to the positively charged patches of cyt c.[84, 216, 286] Ion binding, in contrast to the current belief, has shown that structural variations occurring in the heme pocket are most likely of functional significance.[240]

2.2 Circular Dichroism. The basic phenomenon of circular dichroism (CD) spectroscopy is well known and has been described in great detail elsewhere.(277) CD is defined by the difference in absorption, *A*, of left (*L*) and right (*R*) circularly polarized light (CPL). It can also be described in absolute terms as the difference between molar extinction coefficients:

$$CD = \Delta A(\tilde{\nu}) = A_L(\tilde{\nu}) - A_R(\tilde{\nu}) = \left[\varepsilon_L(\tilde{\nu}) - \varepsilon_R(\tilde{\nu})\right] lc = \varepsilon lc \qquad [2.13]$$

For the purposes of this thesis the difference in absorption will be expressed in terms of $\Delta\varepsilon$.

The occurrence of CD requires the presence of a magnetic transition dipole moment $\vec{m}$ coupling ground and excited states involved in the electronic transition of the corresponding absorption band. The corresponding operator can be written as

$$\vec{m} = \frac{e}{2m_e}\sum_i \hat{l}_i = -i\left(\frac{e\hbar}{2m_e}\right)\sum_j \left(\vec{r}_j \times \vec{\nabla}_j\right) \qquad [2.14]$$

where m_e is the mass of a resting electron, e is an elementary charge, $\hat{l}_i$ is the operator associated with the angular momentum of the i^{th}-electron, and $\vec{\nabla}_j$ the corresponding Nabla-operator. If one considers contributions from both the electronic and the magnetic transition dipole moment, the effective oscillator strength, is written as

$$f_l^{L,R} = \left(\langle l|\vec{\mu}|g\rangle + \mathrm{Im}\langle l|\vec{m}|g\rangle\right)\left(\langle l|\vec{\mu}|g\rangle - \mathrm{Im}\langle l|\vec{m}|g\rangle\right) = f_l + G_l \pm 2R_l \qquad [2.15]$$

or the combined oscillator strength of the electric and magnetic dipole transition. This expression contains the imaginary part of the scalar product of these two moments. Because the angular momentum operator is imaginary, so too is the magnetic moment operator in the complex space. The rotational strength, *R*, of the transition is therefore dependent upon both

the electronic dipole transition moment and the magnetic dipole transition moment and is analogous to the dipole strength of normal absorption, where the area under the CD related to rotational strength. Rotational strength is denoted as R_l and can be written as:

$$R_l = \mathrm{Im}\langle l|\vec{\mu}|g\rangle\langle l|\vec{m}|g\rangle \qquad [2.16]$$

The magnetic dipole moment exhibits rotational symmetry so that the respective transition requires circular polarized light. Substituting f_l in eq 2.3 with $f_i^{L,R}$ yields the extinction profiles for left and right handed CPL. The difference of these two profiles also can be written as the superposition of Voigtian profiles

$$\Delta\varepsilon(\tilde{\nu}) = \sum_l \frac{A_{\Delta\varepsilon} R_l \Gamma_l \tilde{\nu}}{\sigma\sqrt{(2\pi)_l^3}} \int_{-\infty}^{\infty} \frac{e^{-\left((\tilde{\nu}_l - \tilde{\nu}_l')^2/2\sigma_l^2\right)}}{\left(\tilde{\nu}_l' - \tilde{\nu}\right)^2 + \Gamma_l^2} d\tilde{\nu}' \qquad [2.17]$$

where the prefactor $A_{\Delta\varepsilon}$ is now 4.03 DBM^{-1} M^{-1} cm^{-1}.[287] CD reflects the simultaneous occurrence of a transfer of charges, giving rise to an electronic dipole transition moment, or the net linear displacement of charge, and a circular motion of charges, which gives rise to a magnetic dipole transition moment. For a chiral molecule electron rearrangements during a transition require that the electronic and magnetic dipole moments are not perpendicular onto each other, and can therefore produce a CD spectrum without an external perturbation. Achiral molecules can acquire CD activity through extrinsic (asymmetric) interactions, inducing chirality by lowering the symmetry of the heme group. The physical basis of this observation is that transition dipole moments associated with electronic transitions of the protein can induce a magnetic dipole moment at the heme.[288, 289] The total magnetic dipole moment can then be obtained by adding the induced magnetic dipole moment to its intrinsic magnetic dipole moment

$$\vec{m}_{Total} = \sum_{j} \left(\vec{m}_0 + i\pi \vec{R}_{jj} \times \frac{\vec{\mu}_j}{\lambda_j} \right) \quad [2.18]$$

where μ_j is the dipole moment of the j^{th} group, λ_j is the wavelength of the j^{th} electronic transitions, and R_j is the distance vector from the heme to his group.[254] When this perturbation produces a magnetic dipole vector that is not perpendicular to the heme, rotational strength is induced into the heme electronic transition. This allows the CD spectra to be highly sensitive to a number of factors (i.e. protein rigidity, environment, polarizability). These interactions can significantly alter CD spectra, especially if the distance between them is less than 10 Å.[290]

If the considered transitions are well separated, i.e. the respective band profiles do not overlap, the shapes of the corresponding absorption and CD bands are identical. The CD band can of course be positive or negative. However, if two optical active transitions of a chromophore are in close proximity, the envelope of the overlapping CD band can be quite different from that of the overlapping absorption band, because the respective rotational strengths do not necessarily scale with the corresponding absorption bands. In the case where two transitions are nearly degenerate and exhibit rotational strengths of opposite sign one obtains a couplet, i.e. a superposition of a negative and a positive Cotton band.[287] This produces a crossover energy coinciding with the peak of the absorption band illustrated by the red line in Figure 2.3. Alternatively, in the case of two overlapping transitions with comparable oscillator strength and different (both positive or negative) rotational strengths, the peaks of CD and absorption band do not coincide. This is exactly the case for the native state of deoxymyoglobin.

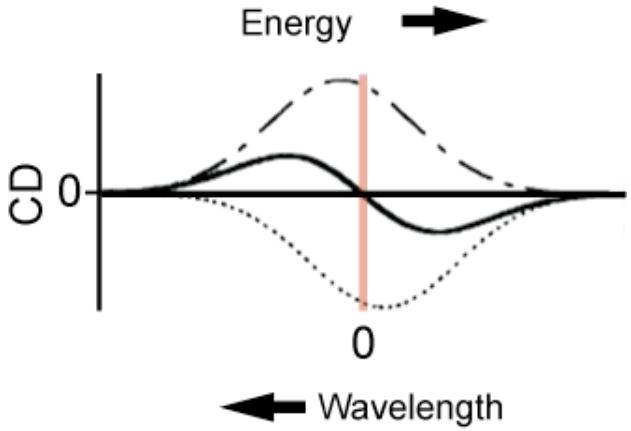

Figure 2.3. CD resulting from the coupling of a transition between two degenerate chromophores. This overlapping positive and negative band results in an overall cancellation of an excitonic spectrum.

2.2.1 Ultraviolet circular dichroism. The amide backbone $\pi \rightarrow \pi^*$ and $n \rightarrow \pi^*$ electronic transitions give rise to far UV-bands below 230 nm. They exhibit strong CD, which reflects the chirality of secondary structures. Shape and intensity of CD signals are to a major extent determined by excitonic dipole coupling between $\pi \rightarrow \pi^*$ as well as $\pi \rightarrow \pi^*$ and $n \rightarrow \pi^*$ transitions in different peptide groups of the polypeptide chain.[291] This coupling depends on the dihedral angles (Figure 1.1) so that different secondary structures yield significantly different CD spectra.[292] It has recently been shown that polarization effects can contribute as well, i.e. higher order side chain ($\sigma \rightarrow \sigma^*$) transitions contribute to the UVCD signal.[293] Proteins containing large fractions of α-helices yield UV-CD spectrum with negative maxima at 222 and 208 nm and an intense positive maximum at 192 nm. Proteins containing a substantial amount of β-sheet exhibit UV-CD spectra with minima at 210 nm and maxima at 190 nm, the relative intensities of which are less than those of the bands in spectra of α-helices. The helical content of a protein can be roughly estimated from the dichroism at 222 nm.[258, 294] The respective spectrum of a unfolded statistical coil exhibits a negative band around 197 nm,

which results from the polyproline II fraction of the conformational ensemble.[258, 277] A protein with substantial fractions of both α-helices and β-sheets yields a UV-CD spectrum characteristic of a superposition of the respective spectra.

A more quantitative analysis of secondary structure composition can be carried out using prediction software, such as the neural network analysis (K2D),[295-297] rigid regression (Contin program),[298] variable selection (VARSLC program),[299] and the self-consistent method (SELCON program).[292, 300, 301] CD spectra obtained below 200 nm are often limited for conventional instruments, due to the constraint of the Xenon arc lamp light source, which loses a significant amount of intensity below 190 nm in the so-called vacuum ultraviolet region (VUV), due to strong oxygen absorption. This limitation results in higher variability in the quantitative analysis of secondary structure composition.[302] Valuable information is gained by extending the spectra into the VUV region (<190 nm) through the use of a short pathlength quartz cell. The comprehensive secondary structure analysis routine, Dichroweb, can be used with many of the most popular structural determination algorithms and several reference sets encompassing a wide range of wavelengths to obtain secondary structure fractions.[303-305] A goodness-of-fit is also provided to allow the judgement of the reliability of the analysis.

More qualitative information about the state of a protein's tertiary structure can be obtained by using the results of a statistical analysis of the UVCD spectra of a large number of rather different proteins. Uversky recently showed from the reported CD spectra of ~100 proteins that the molar ellipticity [θ] at values of 200 nm and 222 nm could be graphically represented in a two-dimensional plot. Different regions of the plot can be related to different types of protein structure. [306] However, we prefer to use the physically easier to interpret Δε notation

as opposed to [θ]. Figure 2.4 shows this so-called "double-wavelength plot" of $\Delta\varepsilon_{222}$ versus $\Delta\varepsilon_{200}$, which can be utilized to further characterize the state of proteins in terms of structurally distinct groups.[306] The type of ordered structure in a sample can be identified depending on where its coordinates lie on the "double-wavelength plot". As shown in Figure 2.4, different regions of the plot are associated with different types of protein structure, such as coil-like, pre-molten globule (preMG), molten globule (MG), and globular (G).

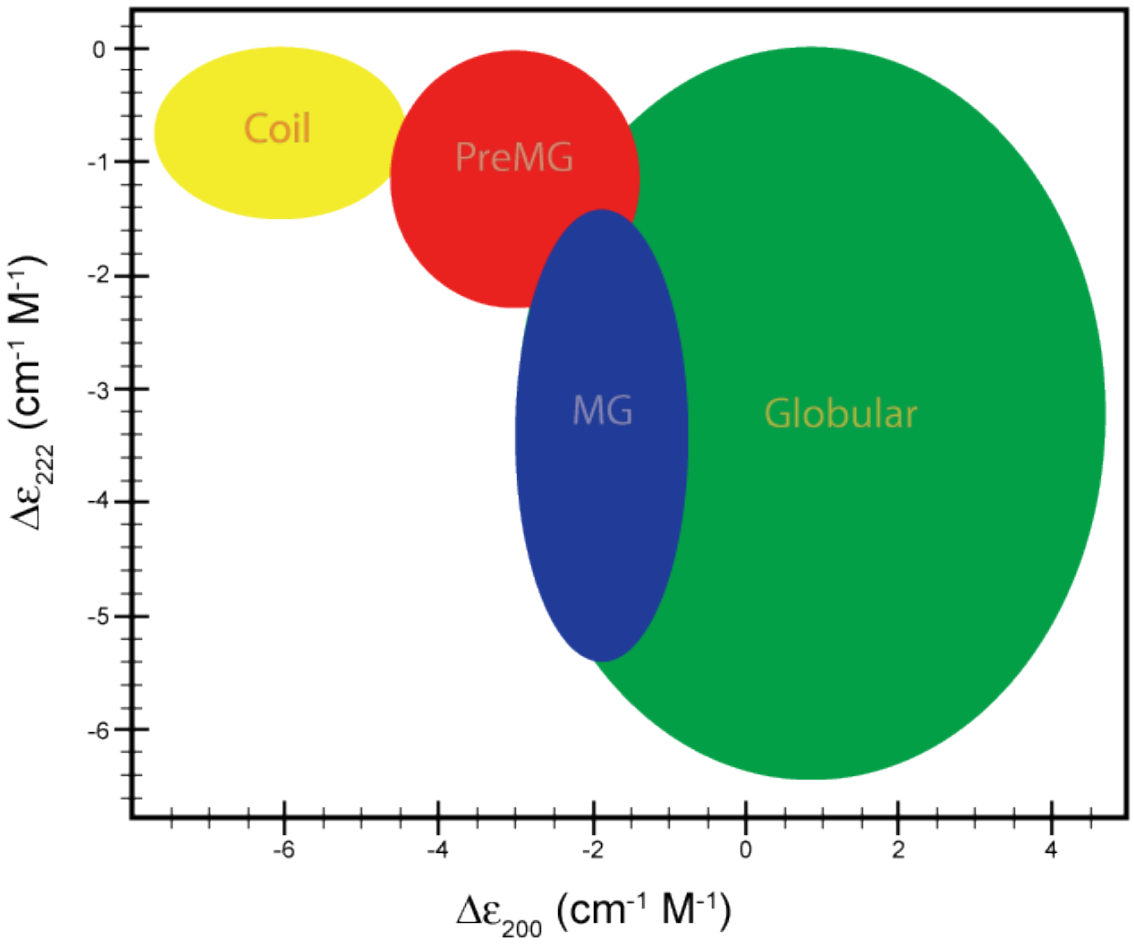

Figure 2.4. The so-called "double-wavelength plot", $\Delta\varepsilon_{222}$ vs $\Delta\varepsilon_{200}$, as introduced by Uversky showing coordinate regions of ● coil, ● pre-molten globule (preMG), ● molten globule (MG), and ● globular structural conformations.[17, 306]

2.2.2 Circular dichroism of the heme chromophore. It's well established that heme-protein interactions can modulate the function of heme proteins.[7, 24, 115, 249, 307, 308] In the case of an ideal porphyrin environment, the effective point group of the heme would exhibit D_{4h} symmetry, which is achiral. Hence, one would expect that heme electronic transitions would show no or very weak CD activity. Yet the visible CD spectrum for the oxidized state (Figure 2.5) of cyt c (pH 7) shows a very pronounced B-band couplet arising from two overlapping individual transitions having opposite rotational strength and a splitting of the excited states due to symmetry lowering perturbations induced by the protein environment.[267]

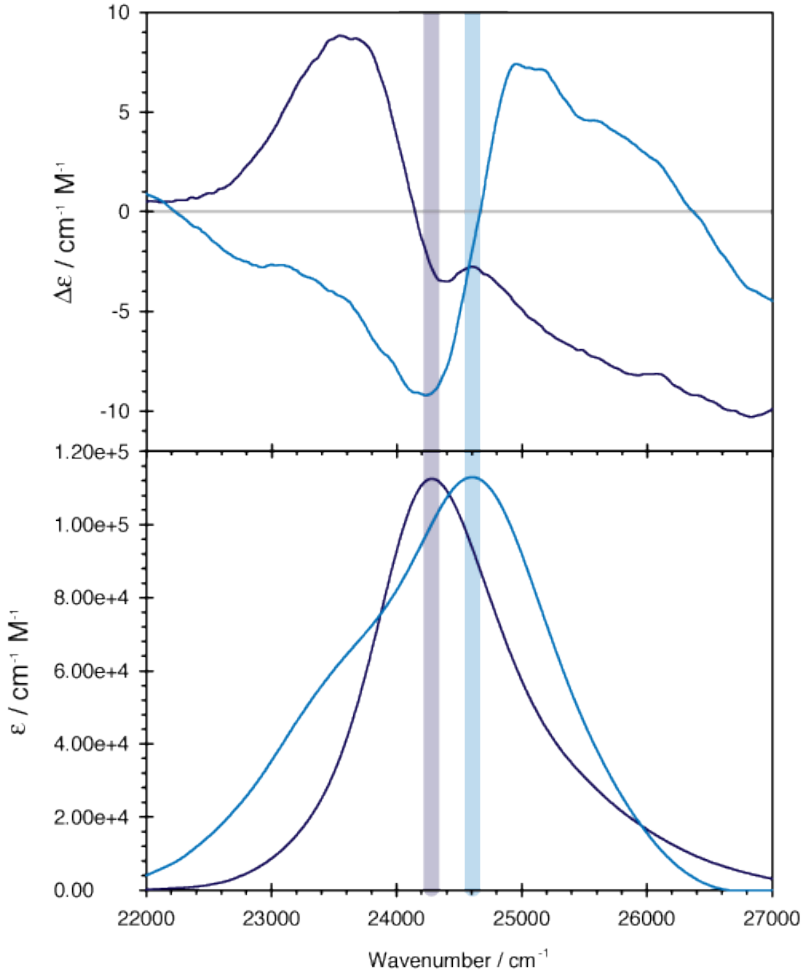

Figure 2.5. CD (top) and the baseline corrected [370] absorption (bottom) spectra of the B-band (Soret) region for ■ ferro- and ■ ferricytochrome c at pH 7. Each spectrum corresponds to the average of five accumulations.

The B-band splitting is changed by conformational transitions involving alterations of the Fe spin state, temperature, and pH. Figure 2.5 shows the significantly different B-band couplet of oxidized (blue) and reduced cytochrome c (violet). The shapes and positions of the CD (top) and the corresponding absorption bands (bottom) do not coincide. This observed non-coincidence indicates a splitting of the excited B state due to heme-protein interactions. This splitting is not large enough to be resolved in the absorption spectrum and has been found to disappear at higher temperatures.[283] The splitting of the *B* band reflects contributions from electronic splitting owing to the quadratic Stark effect.

The shapes of the two Cotton bands of the couplet are not identical owing to contributions from vibronic transitions into the first excited vibrational states, which differ for B_0 and B_v due to the influence of vibronic B_{1g}-type deformations on vibronic coupling matrix elements.[275, 309] This electronic perturbation has two sources. The first and dominant one is a quadratic Stark effect induced by the internal electric field in the heme pocket. A second, minor contribution can be assigned to the influence of numerous non-bonding interactions between the heme and the protein.

The first theoretical approach to understanding the rotational strength of the heme described the Cotton effect of the B-band in terms of a coupled oscillator model that considers transition dipole coupling between $\pi \rightarrow \pi^*$ transitions of the heme and of nearby aromatic side chains.[289, 310] Later, the CD B-Band of different oxidation and ligation states of the Heme undecapeptide of cyt c heme and ferrimyoglobin were simulated, revealing that out-of-plane deformations of the heme macrocycle eliminate the heme's inversion center, and contribute substantially to the rotational strength of the respective transition.[288] Moreover, this study found that dipole coupling between the $\pi \rightarrow \pi^*$ transitions of the heme and the protein backbone can

substantially contribute to the rotational strength of the Soret band, in spite of the large energy difference of the respective electronic transitions. Even higher lying peptide transitions, classically modeled by polarizabilities, were found to contribute to the B-band (Soret) CD.[283, 288, 289, 311-313]

The heme environment interacts directly with the heme and induces both in- plane and out-of-plane deformations of the heme macrocycle.[272, 314, 315] The crystal structure of cyt c has been shown to exhibit larger nonplanar heme deformations than other heme proteins, i.e myoglobin and hemoglobin, mainly due to the additional covalent bonds between the heme and the protein.[174, 316] The nonplanarity of the heme, or out of plane heme deformations (OOP), can be described in terms of the static normal coordinate deformation, often referred to as the normal coordinate structural deformation, which is classified by the irreducible representations in the D_{4h} point group.[314, 317] The basic theory of OOP deformations has been published in earlier work.[265, 318-320] The normal heme deformations are: propellering (A_{1g}), doming (A_{2g}), ruffling (B_{1g}), saddling (B_{2g}), and waving (E_u). B_{1g} and B_{2g} type vibrations induce an asymmetric in-plane deformation of the porphyrin and lower the symmetry from four to two-fold, i.e. $D_{4h} \rightarrow C_{2v}$. A_{2g} type vibrations induce an antisymmetric in-plane deformation of the macrocycle and can be considered as a combination of clockwise and anti-clockwise rotation, which preserves the four-fold symmetry but lowers it from $D_{4h} \rightarrow C_{4h}$. These symmetry modes are involved in different types of vibronic coupling. For horse heart cyt c, the B_{1g} deformation is the most prevalent. A linear combination of these distortions can be used to classify and quantify heme distortions.[321]

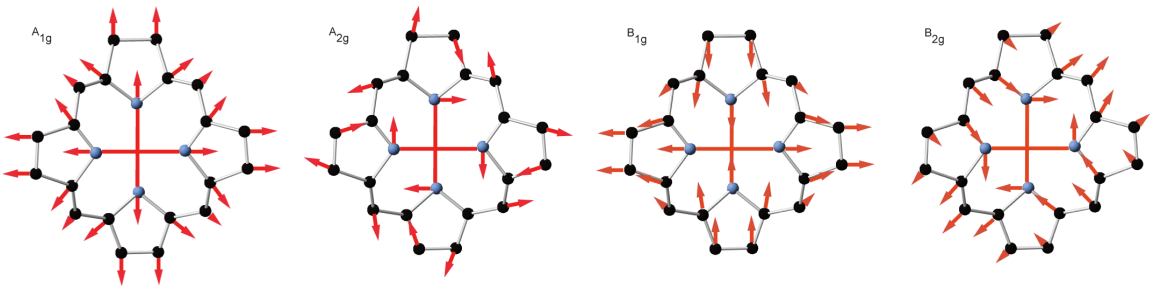

Figure 2.6. A_{1g}, A_{2g}, B_{1g} and B_{2g} type deformations of the heme macrocycle.

2.2.3 Visible circular dichroism. Visible CD has frequently been used as a tool to probe the intactness of the heme environment in heme proteins, and is particularly prominent in protein folding studies of cyt c.[322, 323] With respect to cyt c studies, CD measurements focused on the *B*-band region (between 350-450 nm) because of its superior intensity.[148, 324-326] This intensity allows for this region to serve as an ideal probe of heme-protein interactions and thus of the tertiary structure changes involving the heme pocket. For the oxidized state, a very pronounced couplet is obtained at the positions of the *B*-band (Soret), and the couplet of the reduced protein is substantially different from that of the oxidized species (Figure 2.5; top). Additionally, the CD spectra of the folded and partially unfolded states of ferri-cyt c differ significantly. The former shows a very pronounced couplet, whereas the latter all exhibit positive Cotton bands, which appear to coincide with the position of the respective absorption bands.[327] The apparent coincidence between absorption and CD suggest that band splitting is small. The total band splitting values arise from a combination of electronic and vibronic perturbations.[328] Interestingly, the CD bands exhibit a narrower profile than the corresponding absorption bands. In the case of non-coincidence the CD band is assignable to a single component of the *B*-state transition (B_0 and B_v). These non-native partially unfolded conformations will be the subject of chapter 4.

2.3 Raman Spectroscopy. Raman and resonance Raman (RR) scattering theory is well established and have been described in great detail elsewhere.[329] Briefly, the theory of resonance Raman scattering at metal porphyrins can be described as the spontaneous Raman scattering that results in first order from an electric dipole moment, $\vec{\mu}$, induced by the electric field component $\vec{E}$ of an electromagnetic field

$$\vec{\mu} = \hat{\alpha}\vec{E} \qquad [2.19]$$

where $\hat{\alpha}$ is the molecular polarizability tensor. If the frequency of an exciting laser beam coincides with an electronic transition between molecular eigenstate, i.e. it lies within the wavenumber range of an optical absorption band, the Raman bands of vibrational modes vibronically coupled to this transition become resonance enhanced.

Resonance Raman scattering involving heme vibrations therefore requires excitation in the *B*- or *Q*-band region of the optical spectrum of cyt c. The polarizability tensor for resonance Raman (and resonance Rayleigh) scattering processes is generally calculated using the Kramers-Heisenberg-Dirac (KHD) equation

$$\alpha_{\rho,\sigma} = \sum_i \underbrace{\frac{\langle f|R_\rho|i\rangle\langle i|R_\sigma|g\rangle}{E_i - E_g - \Omega_L - i\Gamma_i}}_{\text{Resonance Term}} + \underbrace{\frac{\langle f|R_\sigma|i\rangle\langle i|R_\rho|g\rangle}{E_i + E_g - \Omega_L - i\Gamma_i}}_{\text{Non-Resonance Term}} \qquad [2.20]$$

where σ denotes the components of an arbitrary molecular coordinate system (*x*, *y*, *z*); $|g\rangle$ and $|f\rangle$ denotes the total wavefunctions of the initial and final state of the scattering process; Ω_L is the wavenumber of the exciting radiation; $|i\rangle$ is an intermediate energy state E_i ; and Γ_i is the

damping constant associated with the excitation of this state. The first term of this equation describes the resonance enhancement for excitation wavenumbers approaching the transition energy, and the second term is the so-called non-resonance term. The numerator of the KHD expression describes two consecutive electronic dipole transitions involving the initial, intermediate and final states. If the excitation frequency lies within the bandwidth of the absorption band, the non-resonance term should be neglected. Contributions from nearby excited states can interfere constructively or destructively. However, because of the timescale differences in the electronic and vibrational components of the total wavefunction, these are usually separated using the Born-Oppenheimer approach, as a way to simplify the complicated Schrödinger equation for a molecule

$$\psi_{e,v} = \theta_e(q,Q)\varphi_{e,v}(Q) \qquad [2.21]$$

where $\Psi_{e,v}$ is the total vibronic wavefunction, $\theta_e(r,Q)$ is the electronic wavefunction for a fixed set of nuclear coordinates Q, and $\varphi(Q)$ is the vibrational wavefunction of the electronic state $|e\rangle$. The latter represents the electronic state and Q denotes the nuclear coordinates.

This approach can be used for porphyrins, in which vibrational modes coupled to the macrocycle appear as strong bands when the excitation frequency is tuned to the resonance frequency of the porphyrin absorption bands. Based on the assumption that the excited-state displacements are small compared with vibrational amplitude (weak coupling limit), the Raman tensor for a porphyrin can solely be accounted for by single mode contributions.[330] This can be accounted for by expanding the vibronic wave functions to third order, which yields a somewhat lengthy expression for the Raman tensor in porphyrins:

$$\alpha_{\rho\sigma} = \sum_{l,m} \frac{R^{\rho}_{gl} H^{r}_{lm} R^{\sigma}_{mg} Q^{j}_{0,1}}{\left(E^{l,j,\lambda}_{0,0} - \Omega_L - i\Gamma^{l,j,\lambda}_{0,0}\right)\left(E^{l,j,\lambda}_{0,0} - E^{m,j,\lambda}_{0,1}\right)} + \sum_{l,m} \frac{R^{\sigma}_{gl} H^{j}_{lm} R^{\rho}_{mg} Q^{j}_{0,1}}{\left(E^{l,j,\lambda}_{1,0} - \Omega_L - i\Gamma^{l,j,\lambda}_{1,0}\right)\left(E^{l,j,\lambda}_{1,0} - E^{m,j,\lambda}_{0,1}\right)} \quad [2.22]$$

Where resonance Raman (RR) activity is dependent upon vibronic coupling matrix elements

$$c^{\Gamma_r}_{lm} = H^{j}_{lm} Q^{j}_{0,1} = \left\langle l \left| \frac{\partial H_{el}(Q,q)}{\partial Q^{\Gamma}_{j}} \right| m \right\rangle \left\langle 1 \left| Q_j \right| 0 \right\rangle \quad [2.23]$$

where Γ_r is the symmetry of the Raman active vibration in the D_{4h} point group, Q, and q represents the nuclear and electronic coordinates.

Selection Rules for Raman Spectra. As any non-linear molecule, porphyrins have 3N-6 net vibrational degrees of freedom. To determine whether these vibrations are Raman active, selection rules must be applied to each normal vibration. The selection rules define the transition probability from one eigenstate to another. A vibration is considered Raman-active if the polarizability, α, is changed during the vibration (eq. 2.15), i.e. $\partial\alpha / \partial Q \neq 0$.

The high symmetry of the heme porphyrin greatly facilitates vibrational analysis. Within D_{4h} symmetry the in-plane and out-of-plane modes can be distinguished.[331-334] Since the transition dipoles lie in the porphyrin plane, resonance enhancement is only expected for the *gerade* in plane modes. The entire set of in-plane modes can be subdivided into 9 A_{1g}, 8 A_{2g}, 9 B_{1g}, and 9 B_{2g} modes (Table A.3). The non-degenerate in-plane modes are Raman-active, whereas the 19 degenerate E_u modes are IR-active. This scattering mechanism holds for modes

that belong to the irreducible representations obtained by the direct product of the electronic transitions involved, i.e. $E_u \otimes E_u$ for the vibronic coupling matrix element in eq 2.22. From the third order approach, vibronic coupling must therefore be of A_{1g}, A_{2g}, B_{1g}, B_{2g} symmetries. Depending on excitation, there is a stronger enhancement of the totally symmetric (A_{1g}), or the non-totally symmetric (B_{1g}, A_{2g}, B_{2g}) modes. The Raman spectra obtained with excitation lines within B-band absorption contain predominantly vibrational bands originating from the totally symmetric A_{1g} modes, among which the most prominent ones are found between 1300 and 1700 cm^{-1}, which mainly include the stretching coordinates of the tetrapyrroles macrocycle.[333]

2.3.1 Resonance Raman scattering of porphyrins. Cyt c was one of the first heme proteins for which a strong enhancement of Raman scattering assignable to heme vibrations was obtained with B-band excitation.[164, 335-337] Excitation in the B-band region selectively enhances predominantly totally symmetric A_{1g} modes. Contrary to conventional belief,[332] A_{1g} modes can also induce interstate (HT) vibronic coupling, which allows for the detection of the respective Raman bands if the heme group is excited in the region between Q_v and B_0-transitions.[337] The Jahn-Teller (JT) effect is associated with an excited state distortion, which occurs along the Raman normal coordinate, with opposite sign for the *x* and *y* components of a twofold degenerate state. Vibronic coupling due to B_{1g}- and B_{2g} modes is intra- and interstate (JT and HT), whereas A_{2g} modes can induce only interstate HT coupling.

2.3.2 Electronic and Vibronic Perturbations of the porphyrin macrocycle. Changes in electronic and vibronic perturbations in the vicinity of the heme macrocycle are significant and should not be neglected. The pure electronic wave functions of the porphyrin electronic states involved in resonance Raman scattering results from *B*- and *Q*-band excitation owing to Gouterman's four orbital model, as described in sect. 2.1.2.[266] A distinction should be made between a perturbation and a deformation, as these cause very different effects.[338, 339] A perturbation of the heme in proteins is an external potential produced by covalent contacts (in cytochrone c), axial ligands, hydrogen bonding, enumerable van der Waals contacts between heme and protein cavity and the external electric field. Such a perturbing potential moves the nuclei of the chromophore in the ground and excited states, thus causing a heme deformation. Electronic perturbations of B_{1g}-symmetry unrelated to the quadratic Stark effect can mix the *B*- and *Q*-states and cause a splitting of the optical spectra. The matrix elements of the asymmetric perturbations B_{1g}, B_{2g} and A_{2g} are small compared with the respective energy difference between *Q* and *B*. The vibronic perturbation reflects the variation of the perturbing potential by vibrating nuclei. They affect the eigenenergies of the vibronic *B* and *Q*-states.[338-341] In the presence of an asymmetric deformation Γ, the vibronic coupling matrix elements (eq. 2.23) can be written as

$$c_{lm}^{\Gamma} = \left\langle l \left| \frac{\partial H_{el,0}}{\partial q_i^{\Gamma_i}} + \sum_{\Gamma_j} \frac{\partial V^{\Gamma_j}}{\partial q_i^{\Gamma_i}} \right| m \right\rangle \left\langle 1 \left| q_i^{\Gamma_i} \right| 0 \right\rangle \qquad [2.24]$$

in which the first term transforms as Γ_i and the second term transforms like the product representation Γ_i (first term) $\otimes$ Γ_j (second term), with $\Gamma_i = A_{1g}, B_{1g}, B_{2g}, A_{2g}$. The B_{1g} modes are likely to provide the strongest contribution to band splitting. $c_{QQ}^{A_{1g}}$ and $c_{BB}^{A_{1g}}$ reflect intrastate Frank-Condon (FC) coupling in the *Q* and *B*-state. c_{QB}^{Γ}, accounts for interstate Herzberg-

Teller coupling between B and Q. If Γ = B_{1g}, B_{2g}. c_{QQ}^{Γ} and c_{BB}^{Γ} reflects intrastate Jahn-Teller (JT) coupling within B and Q.[272, 342]

For D_{4h}-symmetry (i.e. the second term in 2.20 is zero), the Raman tensors for the resonance Raman active modes can be expressed in terms of the McClain tensor[343]

$$A_1(l,m)=\begin{pmatrix} c_{l,m}^{A_{1g}} & 0 \\ 0 & c_{l,m}^{A_{1g}} \end{pmatrix} \qquad A_2(l,m)=\begin{pmatrix} 0 & c_{l,m}^{A_{2g}} \\ -c_{l,m}^{A_{2g}} & 0 \end{pmatrix}$$
$$A_1(l,m)=\begin{pmatrix} c_{l,m}^{B_{1g}} & 0 \\ 0 & -c_{l,m}^{B_{1g}} \end{pmatrix} \qquad B_2(l,m)=\begin{pmatrix} 0 & c_{l,m}^{B_{2g}} \\ c_{l,m}^{B_{2g}} & 0 \end{pmatrix} \qquad [2.25]$$

where the tensors *z*-components are zero since electronic dipole transitions perpendicular to the porphyrin plane do not contribute to the optical spectrum in the wavelength region investigated. When the porphyrin is in low symmetry, admixtures of all deformation types occur (i.e. A_{1g}, B_{1g}, B_{2g}, and A_{2g}) and thus all McClain tensors contribute to the Raman tensor.

The vibronic coupling operator of a Raman active porphyrin vibration , $Q^{\Gamma'_r}$, from eq. 2.25 is expanded in a Taylor series to yield

$$c_{lm}^{\Gamma}=\frac{\partial \hat{H}_{el,0}(q,Q)}{\partial Q_r^{\Gamma'_r}}+\sum_{\Gamma_i}\sum_{i}\frac{\partial^2 \hat{H}_{el,0}(q,Q)}{\partial Q_r^{\Gamma_r}\,\partial Q_i^{\Gamma_i}}\partial Q_i^{\Gamma_i} \qquad [2.26]$$

where Γ'*r* is the lowered symmetry group representation with respect to the normal coordinates of the induced distortions, classified in terms of irreducible representations of the D_{4h} point group. The Raman tensor, for first order contribution, can be written as a sum of the McClain

tensors of the same symmetry type $\Gamma(Q_r)$ weighted with the corresponding frequency (found in the denominator) and electronic transition dipole matrix elements. Deviations can be rationalized in terms of an admixture of contributions from terms other than A_{1g} in the second term on the right side of eq. 2.26. The symmetry of the heme is lowered via symmetry-lowering perturbation by peripheral substituents and heme-protein interactions. The polarizability for the lowest possible symmetry can then be written as a two-dimensional McClain tensor

$$\hat{\alpha} = \begin{bmatrix} a_{1g}(\tilde{\nu}_l) + b_{1g}(\tilde{\nu}_l) & b_{2g}(\tilde{\nu}_l) + a_{2g}(\tilde{\nu}_l) \\ b_{1g}(\tilde{\nu}_l) - a_{1g}(\tilde{\nu}_l) & a_{1g}(\tilde{\nu}_l) - b_{2g}(\tilde{\nu}_l) \end{bmatrix} \quad [2.27]$$

where the tensor elements can be calculated as the superposition of all scattering amplitudes brought about by Herzberg-Teller and Franck-Condon/Jahn-Teller coupling within the *B*- and *Q*- states.[260, 272]

2.3.3 Structure sensitive heme vibrations

Heme normal modes. The heme of cyt c can take on a variety of oxidation states (namely Fe(*II*), *Fe(III)*), spin states (high, low and intermediate) and coordination numbers (four, five, and six) dependent on experimental conditions. This makes it important to find the spectroscopic bands that are sensitive to these parameters. The heme modes of oxidized and reduced cyt c and their wavenumber positions are listed in Appendix A.4 using the notation of Abe et al.[344]

Oxidation, spin state, and core size markers. The normal modes of oxidation and spin marker bands appear in the higher frequency range (1300-1700 cm^{-1}) and originate predominantly from highly coupled C=C and C-N stretching vibrations of the heme. *(344-346)* RR frequencies of the marker bands that are characteristic of oxidation state, spin state and iron-ligand interactions are listed in Table 2.1 for ferri- and ferro-cyt c.*(273, 347-349)*

Table 2.1. Resonance Raman Bands (cm^{-1}) of Cytochrome c Sensitive to Oxidation and or Spin State[4]

		Oxidation State Markers		Spin State Markers		Oxidation and Spin State Markers	
Oxidation State	**Species**	ν_4	ν_{11}	ν_2	ν_{19}	ν_3	ν_{10}
Fe(III)	6cLS	1373	1562	1584	1582	1502	1635
		1374		1588		1506	1640
	5cHS	1371		1577		1497	1623
	6cHS	1370		1570		1485	
Fe(II)	6cLS	1361	1548	1591	1585	1491	1621
		1360		1592		1494	
	6cHS						
	5cHS	1354	1547	1572		1470	1606

The ν_4 RR mode, exhibiting A_{1g} symmetry in D_{4h} is predominantly a pyrrole half-ring symmetric stretch (Figure 2.7a). This band is most intense with *B*-band excitation, and is generally used as an oxidation state marker. For cyt c, the reduction of *Fe(III)* to *Fe(II)* downshifts this band by 12 cm^{-1} (Table 2.1).*(345)* This has been interpreted as being caused by an increase in electron back donation from the *Fe(II)* to π^* antibonding porphyrin orbitals upon Fe reduction. This effect has been shown to be enhanced by electron rich axial ligands, as in the thiolate of cytochrome P-450 (1350 cm^{-1}), making the ν_4 mode an unambiguous oxidation state marker.*(350)*

ν_{10} is the most prominent B_{1g}-type mode. Its normal mode pattern is shown schematically in Figure 2.7b. The band's wavenumber position depends on the spin and the ligation state of the heme iron (Table 2.1). In the high spin ferri-state, the band appears at 1622 cm^{-1}, whereas the

spectrum of the corresponding low spin hexacoordinated *Fe(III)* state exhibits this band at 1638 cm^{-1}.[345] Non-planar deformations, like macrocycle ruffling, cause this band to shift to lower wavenumber positions.[351] To a lesser extent this is also true for the A_{2g} ν_{19} and the B_{1g} ν_{11} mode.

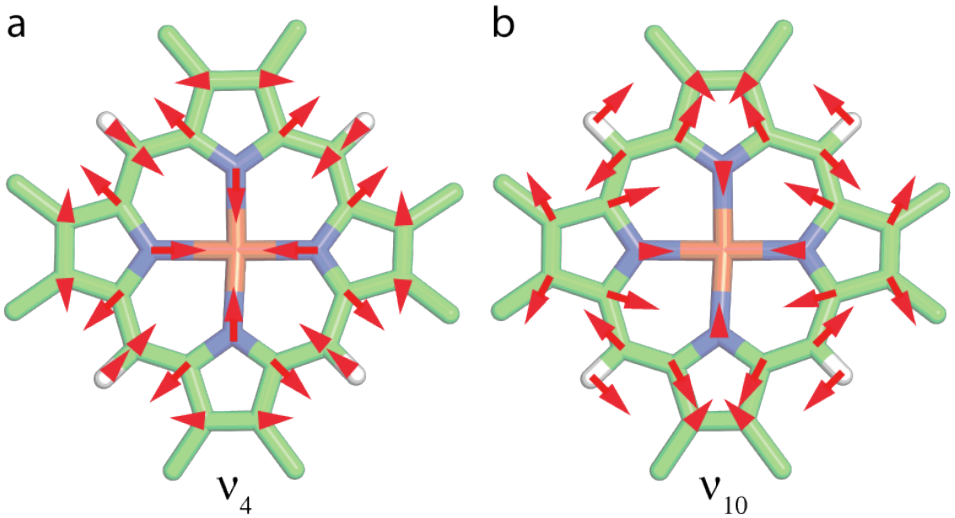

Figure 2.7. Normal mode pattern of the oxidation and spin marker, for (a) ν_4 and (b) ν_{10}, heme deformations.[17, 28]

The heme macrocycle is quite flexible, and its structure is influenced by the iron-nitrogen distance (core size) and by substituent steric interactions. [352, 353] The ν_2, ν_3, ν_{10}, ν_{11}, and ν_{19} are core-size sensitive marker bands, the wavenumber position of which serves as an indicator of the degree of heme macrocycle nonplanarity.[352, 353] The core size increases with decreasing nonplanarity. For example an increase in the iron core size upon oxidation would result in a flattening of the porphyrin.[354] The CxxC segment of the protein moiety is primarily responsible for inducing the ruffling of the heme in both horse heart and yeast cyt c. This interaction suggests a role for the core size and its environment in linking the heme active site directly to the protein. Pentacoordinated high spin iron systems generally have doming macrocycles as the dominant non-planar heme distortion, e.g. deoxyhemoglobin/myoglobin. [355]

Depolarization Ratio. The different resonance Raman active modes reveal unique polarization properties, which can be readily understood by classical treatment of the Raman scattering tensor.[349] The depolarization ratio of a Raman band is defined as the ratio of integrated intensities of radiation scattered perpendicular and parallel to the polarization of the exciting laser beam ($\rho = I_{\perp}/I_{\parallel}$). In ideal D_{4h} symmetry, a heme molecule with a symmetric in-plane arrangement would have a depolarization ratio (DPR) of the A_{1g}, A_{2g}, B_{1g} and B_{2g} modes independent of the excitation frequency. [349] The A_{1g} band is totally polarized ($\rho = 0.125$), A_{2g} is inverse polarized ($\rho = \infty$), and the B_{1g}, and B_{2g} both produce depolarized scattering ($\rho = 0.750$). In reality the DPR reflects the influence of asymmetric distortions on the porphyrin. Deviations from these values reflect admixtures of tensor elements $\alpha_{\rho\sigma}$ (eq. 2.22) describable by invariants of the isotropic, anisotropic, and antisymmetric components (Γ) into the Raman tensor for the lowest possible symmetry:

$$\rho = \frac{3}{4}\left(\frac{a_{1g}^2(\tilde{\nu}) + 5a_{2g}^2(\tilde{\nu}) + 2\left[b_{1g}^2(\tilde{\nu}) + b_{2g}^2(\tilde{\nu}) \right]}{6a_{1g}^2(\tilde{\nu}) + 2\left[b_{1g}^2(\tilde{\nu}) + b_{2g}^2(\tilde{\nu}) \right]} \right) \qquad [2.28]$$

Table 2.2 shows the relationship between the symmetries of in-plane heme deformations and symmetries of admixtures to the Raman tensor as described by the second term in eq. [2.25] for the different D_{4h}-symmetries of Raman allowed heme vibrations. To help illustrate this, we consider a mode of B_{1g} symmetry. If the deformation is of B_{1g} symmetry, the corresponding vibronic coupling operator would have A_{1g} symmetry, which would in turn lower the DPR from 0.75. Admixtures of B_{1g} and B_{2g} due to A_{1g} and A_{2g}-type deformation do not change the DPR, while B_{2g} deformations would increase the DPR by admixing A_{2g}-contributions to the

Raman tensor. In-plane heme deformations are generally smaller than out-of-plane distortions and lie in the range between 0.02 and 0.2 Å.[331] In-plane and out-of-plane deformations proceed along the normal modes, which by definition are independent in the harmonic approach. Even though it is not clear from elementary theory, non-planar deformations can make out-of-plane modes of the heme Raman active.

Table 2.2. Correlation between the symmetry of a Raman vibration (Γ_i, first row), deformation (Γ_j, first column), and the symmetry of vibronic coupling admixture to the Raman tensor

	A_{1g}	B_{1g}	B_{2g}	A_{2g}
A_{1g}	A_{1g}	B_{1g}	B_{2g}	A_{2g}
B_{1g}	B_{1g}	A_{1g}	A_{2g}	B_{2g}
B_{2g}	B_{2g}	A_{2g}	A_{1g}	B_{1g}
A_{2g}	A_{2g}	B_{2g}	B_{1g}	A_{1g}

2.4 Fluorescence. The basic theory of fluorescence spectroscopy and features of protein fluorescence is well known and has been described in several reviews.[356-359] Intrinsic protein fluorescence can often be utilized for biochemical application owing to the three aromatic amino acids (F, Y, W) or the heme porphyrin. As previously mentioned, these three amino acids are relatively rare in proteins. Fluorescence emission is observed if the emission process has a lifetime that is faster than the nonradiative loss of excitation energy.

2.4.1 Resonance Energy transfer. Förster resonance energy transfer (FRET) is a phenomenon in which nonradiative transfer of energy occurs between a donor (D) and acceptor (A) molecule in close proximity. The theory of energy transfer is based on the concept of a fluorophore acting as an oscillating dipole, which can exchange energy with another oscillating dipole with a similar resonance frequency over a long range between a D to an A fluorophore. The energy transfer efficiency is strongly dependent on the distance between D and A. Any changes in the fluorescence lifetimes represent changes in the efficiency of energy transfer and thus the distance between D and A. The energy transfer rate, $k_T(r)$, from donor to an acceptor is given by

$$k_T(r) = \frac{1}{\tau_D}\left(\frac{R_0}{r}\right)^6 \qquad [2.29]$$

where τ_D is the decay time of D in the absence of the A, R_0 is the Förster distance, and r is the distance between D and A. The $k_T(r)$ is equal to the decay rate of D ($1/\tau_D$) when r is equal to R_0 and the transfer efficiency is 50%.[359] The $1/R^6$ dependence of $k_T(r)$ makes FRET very sensitive to even small changes in the vicinity of R_0.

2.4.2 Tryptophan 59 fluorescence. FRET can be used to probe the energy transfer in Cyt c between the heme chromophore and the single tryptophan (W59). Unfolding with mild denaturing conditions results in a strong increase in tryptophan fluorescence as the distance between the heme and W59 increases. These changes in fluorescence efficiency during protein unfolding are often very large. The fluorescence of the W residue can be measured selectively by excitation at wavelengths shorter than 295 nm, where Y does not absorb. W in this case serves as the FRET D and the heme cofactor serves as the A, located within 10 Å of the heme iron in its folded state III.[27, 156, 183] When the protein is folded, energy is transferred from the excited W to the heme group, resulting in the quenched W fluorescence (pH 7). As unfolding occurs the distance between the D and A increases, thus decreasing efficiency of energy transfer and resulting in an increase in fluorescence signal. A substantial increase in W59 fluorescence is therefore indicative of a more extended protein conformation with an average Trp-heme distance larger than 35 Å. [45, 183] Since the heme is covalently linked to the protein backbone FRET can be used as a direct probe to study tertiary structural changes in cyt c conformation associated with the folding or unfolding process (Figure 2.8). [183, 360]

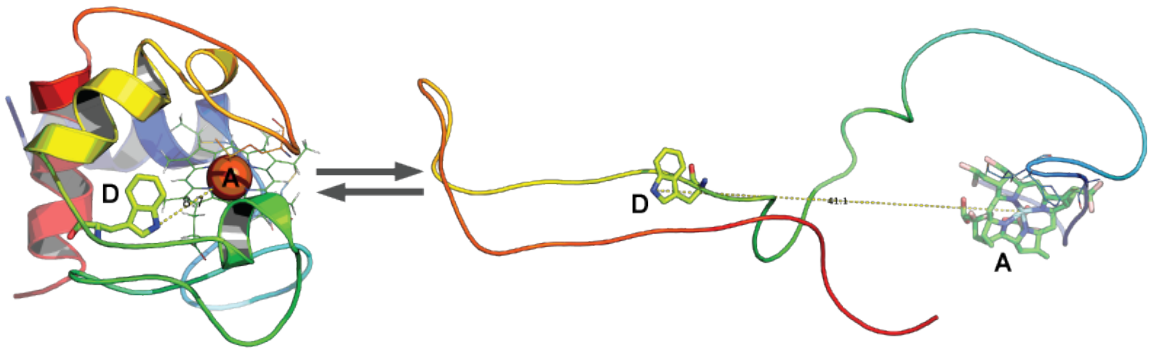

Figure 2.8. Cartoon representation of fully folded to an unfolded state of cyt c, (PDB: 1AKK [27]) illustrating the increasing distance between the Trp59 (D) to the heme (A) giving rise to FRET. Example shows D to A distance increasing from 8.7 Å in the F state to 41.1 Å in the U state.[17, 18, 28]

CHAPTER 3. MATERIALS AND METHODS

Oxidized Protein Preparation. Cytochrome c (Cyt c) from equine was purchased from Sigma-Aldrich (St Louis, MO), with >95 % purity. The crystalized form used was precipitated from acetic acid (AcOH - C7752). However, additional Cyt c crystals precipitated from trichloroacetic acid (TCA - C2506) were additionally used where specified. The protein was dissolved at concentrations of 0.05 mM, 0.5 mM and 5.0 mM in a 0.1 mM monobasic potassium phosphate buffer (pH 7.2) (Sigma-Aldrich). The low molarity of the buffer ensured that the anion concentration was always below the region in which small anions can bind to the protein (~50 mM).[162, 240, 361] Complete oxidation of the protein was achieved by adding around 2 μM potassium ferricyanide ($K[Fe(CN)_6]$) (Fisher Scientific, Pittsburgh, PA) to the sample. In a second step, a PD MidiTrap G-25 column (GE Healthcare, Mickleton, NJ) was pretreated with a solution of potassium ferricyanide to compensate for the nonspecific interactions, i.e. reducing nature, of the Sephadex gel when using buffers with ionic strength outside of the 0.15 M to 1.5 M range.[362, 363] The protein solution was then passed over the column, at pH 7.2, removing excess oxidizing agent or other impurities.[364] The pH of the eluted samples was measured using an Accumet AR50 benchtop meter with Accumet micro size glass combination electrode (Fisher Scientific, Pittsburgh, PA) and subsequently titrated to various pH values between 1 and 14 using small aliquots of 0.1 M HCl or 0.1 M NaOH. The electrode response was measured using a two-point standardization, with an efficiency >95%, indicating that the error is less than ±0.05 pH per pH unit. Absorption and CD spectra were immediately recorded after each titration. The final concentration of cytochrome c was verified by measuring Soret band absorption at 410 nm (ε_{ox}= 1.06 x 10^5 M^{-1} cm^{-1}; pH 7).[158]

Reduced Protein Preparation. Equine ferricytochrome c, precipitated from AcOH, was obtained from Sigma-Aldrich and dissolved at a protein concentrations of 5.0 mM, 0.5 mM or 0.05 mM in a 0.1 mM monobasic potassium phosphate buffer, KH_2PO_4. A small amount of sodium dithionite ($Na_2S_2O_4$) was added to the solution to reduce the protein. The pH of the eluted samples was changed using small aliquots of 0.1 M HCl or 0.1 M NaOH and immediately measured using a Fisher Scientific Accumet AR50 benchtop meter with Accumet micro size glass combination electrode and subsequently titrated to various pH, following the calibration method mentioned above.

Denatured Protein Preparation. Equine ferricytochrome c, from AcOH, was obtained from Sigma-Aldrich and dissolved at a protein concentration of 0.5 mM in a 0.1 mM monobasic potassium phosphate buffer following the method described above. Urea, from Sigma-Aldrich, was added to the solution to make a 9M urea solution. The pH of the eluted samples was changed using small aliquots of 0.1 M HCl or 0.1 M NaOH and immediately measured using an Accumet AR50 benchtop meter with Accumet micro size glass combination electrode (Fisher Scientific) and subsequently titrated to various pH, following the calibration method mentioned above.

Misfolded Protein Preparation. Equine ferricytochrome c, from AcOH, was obtained from Sigma-Aldrich and dissolved at protein concentrations of 0.5 mM or 0.05 mM in a 0.1 mM monobasic potassium phosphate buffer. We employed a sample preparation similar to a protocol previously developed by Alessi et al., which avoids photo-reduction of the sample in resonance Raman experiments after its oxidation with around 2μM potassium ferricyanide ($K[Fe(CN)_6]$).[365] First, the pH of the sample was adjusted to 11.5 to neutralize the positive

patches on the protein surface. Several lines of experimental evidence suggest that the protein adopts a partially unfolded state *V* at this condition.[157, 205, 206, 225, 233] In a second step, the protein was allowed to stay at this pH for varying time periods at 5 °C. A PD MidiTrap G-25 (GE Healthcare) or Sephadex G-75 (Pharmacia Fine Chemicals, Inc., Piscataway, NJ) column was pretreated with a solution of potassium ferricyanide to compensate for the reducing nature of the Sephadex gel. The protein solution was then passed over the column. This treatment removes any excess oxidizing agent or other impurities.[364] Finally, the pH of the eluted samples was titrated from 11.5 down to various values between 11.5 and 4.0 using small aliquots of 0.1 M HCl. The low molarity of the buffer used ensured that the anion concentration was always below the region in which small anions can bind to the protein. [162, 240, 361] The final concentration of cytochrome c was verified by measuring Soret band absorption.

Protein Hydrolysis. Complete protein hydrolysis was achieved by producing a 3 M NaOH sample solution degassed with N_2 and heated for 8 hours at 100 °C. After cooling, the alkali solution was neutralized with an equivalent amount of 1 M HCl prior to adjusting the sample to the pH of interest.[366]

Size Exclusion Gel Chromatography. The sample was passed over a Sephadex G-75 column (Pharmacia Fine Chemicals Inc.) at room temperature. The column was pretreated with potassium ferricyanide to compensate for the nonspecific interactions, i.e. reducing nature, of the G-75 Sephadex gel when using buffers with ionic strength outside of the 0.15 M to 1.5 M range. Aliquots were removed in regular intervals for electronic circular dichroism (ECD) and absorption measurements.

Gel Electrophoresis. Proteins were separated using a precast 4-20% polyacrylamide gel (Thermo Scientific) with Tris/Glycine running buffer under non-denaturing conditions. Each well was loaded with 5 μL of the aqueous cytochrome c samples and electrophoresed using a Mini-PROTEAN Tetra Cell (Bio-Rad, Hercules, CA) with FB1000 power supply (Fisher Scientific), with a constant voltage (200 V; 20-50 mA) for ca. 30 min per gel. Protein molecular weight distribution was assessed with 5 μL of SeeBlue Plus2 Prestained Standard (Invitrogen, Grand Island, NY). The gels were then stained using ProteoSilver Plus Silver stain (Sigma-Aldrich). Following staining, the gels were photographed with a 5-megapixel HDR digital iSight camera (Apple Inc., Cupertino, CA) and analyzed using ImageJ.[367]

Absorption Spectroscopy. A Perkin-Elmer Lambda 35 UV/Vis spectrometer (Shelton, CT) was used to measure the spectra of the charge transfer (CT) region between 550 and 750 nm, with a data pitch of 0.1 nm, a continuous scanning speed of 480 nm/min, a response time of 1.0 s, and a bandwidth of 2 nm. A 10 mm quartz cell (Helma, Müllheim, DE) was used as the pathlength for the measurement of each sample.

Absorption and Circular Dichroism Spectroscopy. A Jasco J-810 spectropolarimeter continuously purged with N_2 was used to obtain visible and far UV circular dichroism spectra (CD) concurrently with the absorption spectra. The charge transfer (CT) region was recorded between 650 and 800 nm using a 10 mm quartz cell (Helma), and protein concentrations of 5.0 mM and 0.5 mM. Spectra of the Soret band (B) and Q-band region were measured between 350 and 650 nm using a 1 mm quartz cell (Helma) with protein concentration of 0.5 mM. The UV region was measured between 180 and 350 nm using a 0.05 mm quartz silica

demountable cell (International Crystal Labs). The spectra were all acquired using a data pitch of 0.05 nm, and at a continuous scan speed of 200 nm/min, with response time of 0.5 s, and bandwidth of 5 nm. A minimum of 5 accumulations for each pH were averaged at a temperature range of 5 to 80 °C (±1.0 °C; 278-363K). The temperature was controlled by a Peltier heating and cooling system at a rate of 0.5 °C/min. The pH was monitored before and after each measurement. For the final analysis, the background spectra, taken with identical parameters, was subtracted with MultiFit.[368, 369]

Fourier Transformed Infrared Spectroscopy. A Chiral IR Fourier Transform VCD spectrometer from BioTools (Jupiter, Fl) was used to measure the FTIR and VCD spectra. The sample was placed into a CaF_2 BioCell (Jupiter, Fl) with a pathlength of 100 μm. The instrument was continuously purged with N_2 at 8 cm^{-1} resolution to obtain a spectrum of the protein at 0.5 mM concentration in D_2O in the amide region (1200-1700 cm^{-1}).

Fluorescence Spectroscopy. Fluorescence measurements were carried out at room temperature (20 °C) on a Perkin-Elmer model LS-55 fluorescence spectrometer. The excitation wavelength was set to 293 nm and the emission was set to scan between 300 - 500 nm. The spectra were all acquired with a scanning speed of 200 nm/min, and an excitation and emission slit of 5.0 and 2.5 nm, respectively. A 10 mm quartz cell (Helma) was used to monitor tryptophan fluorescence (Trp59) with protein concentration of 0.05 mM.

Resonance Raman Spectroscopy. Polarized resonance Raman spectra were obtained using a RM-1000 Ramascope (Renishaw, Hoffman Estates, IL), with a BH-2 confocal Raman microscope (Olympus, Tokyo, JP) equipped with a back-thinned CCD camera, a 2400 lines

per mm grating and a 50× microscope objective. Soret band resonance Raman spectra were collected using a HeCd laser (Kimmon, Centennial, CO) with an excitation wavelength of 441.6 nm. The 488.0, 514.5, 530.9, and 568.2 nm excitation wavelengths were recorded by using a mixed gas Stabilite 2018RM Ar/Kr laser (Spectra Physics, Santa Clara, CA). Aqueous cytochrome c samples were placed into a hanging drop microscope slide (Fisher Scientific) for acquisition. Spectra were collected with polarizations parallel (x) and perpendicular (y) to the polarization of the excitation laser beam. A minimum of five accumulations were collected for each spectrum at 20 °C and averaged to increase the signal to noise ratio. MultiFit[370] spectral decomposition software, was used to complete the spectral analysis.[368, 369] Depolarization ratios (ρ) were calculated using the intensity ratio of the parallel and perpendicular polarizations, i.e. $\rho = I_y/I_x$.

Data subjected to error analysis is described in the text

CHAPTER 4:
THE CONFORMATIONAL CHANGES OF CYTOCHROME C INDUCED BY pH AND TEMPERATURE

4.1 Introduction.

Cytochrome c (cyt c) has been a subject of biophysical research since it began.[1-3] It was one of the first three proteins for which a crystal structure was resolved[6] and since then has continuously served as a model system for the fundamentals of electron transfer between proteins[7] and for protein folding.[8, 9] Its more recently discovered role as mediator in the mitochondria-dependent apoptotic pathway[371] prompted studies of its conformational and functional properties on different types of anionic liposomes used as substitute for the more complex environment of the inner mitochondrial membrane.[115]

With respect to folding and unfolding, cyt c is a peculiar protein in many respects. First, there is a substantial difference between its fully folded reduced and oxidized state: the former is by far more stable than the latter at acidic and alkaline pH and at high temperature. At pH 7, for instance, oxidized cyt c seems to unfold at temperatures around 70° C, whereas the melting temperature of the reduced form lies well above 100° C.[372, 373] With regard to pH, oxidized cyt c can adopt at least six protonation states between pH 1 and 12,[157] whereas the fully folded reduced state stays stable between pH 3 and 12.[374, 375] These differences are most likely due to the weaker coordination of the axial M80 ligand in the oxidized form, since it is this ligation that keeps the protein in its fully folded state and adjusts the heme iron's redox potential.[376]

Several lines of evidence suggest that the states that oxidized cyt c adopts at acidic and alkaline pH are only partially unfolded, maintaining a substantial fraction of the protein's

secondary structure, which is a mixture of helical segments and loops.[84, 85] It is therefore not surprising that further conformational changes are observed upon increasing the temperature towards the thermal unfolding regime of the fully folded state III.[85] Recent work by Hagarman et al. suggests that the thermally unfolded states of the individual protonation states differ in terms of their heme environments.[233] Pielak and coworkers used CD spectroscopy to study the thermal unfolding of a large number of yeast cyt c mutants. However, they interpreted all their data in terms of a classical two-state model.[377] Thus far, a complete and consistent thermodynamic and structural characterization of the thermal transitions of all protonation states of oxidized cyt c has not been undertaken. This is the goal of the present study, which focuses on horse heart cyt c. Thermodynamic characterization means that we obtained the enthalpic and entropic differences between different conformations populated when oxidized cyt c in a certain titration state is heated from 5° to 90° C. We probed tertiary structure changes by measuring visible circular dichroism (CD) and absorption spectra and secondary structure changes by UVCD. In order to obtain physically meaningful thermodynamic parameters we tried to keep the anion concentration in the solution low to avoid the binding of anions like, Cl^-, PO_4^{3-}, etc., to the positively charged patches on the surface of the protein. [236] Such anion binding is known to induce minor structural changes involving changes of the Fe^{3+}-M80 coordination, which can also affect pK-values and thus the population of titration states.[84, 216, 286, 378] Our results confirm that oxidized cyt c can adopt a plethora of different conformations with very similar secondary structures. Thermal transitions can be rationalized with a two-step mechanism, three-state model. Corresponding thermodynamic values exhibit a statistically significant enthalpy-entropy compensation that points to common physical processes affecting all of the investigated protonation states in a similar way.

4.2 Proposed thermodynamic scheme. The oxidized state of cyt c is pH dependent in that it adopts five non-native states over the pH range 1-14 in addition to the native folded state (different nomenclature is used in the literature; here we used the classical nomenclature of Theorell and Åkessen updated to include the *III** state as discovered by our group).[157, 204-206] The overall reaction scheme for oxidized cyt c can be written as follows

$$I \underset{}{\overset{pK^{eff}_{I\rightarrow II}}{\rightleftharpoons}} II_{A,b} + n_1H^+ \underset{}{\overset{pK^{eff}_{II\rightarrow III}}{\rightleftharpoons}} III + n_2H^+ \underset{}{\overset{pK^{eff}_{III\rightarrow III^*}}{\rightleftharpoons}} III^* + n_3H^+ \underset{}{\overset{pK^{eff}_{III^*\rightarrow IV}}{\rightleftharpoons}} IV_{a,b,c} + n_4H^+ \underset{}{\overset{pK^{eff}_{IV\rightarrow V}}{\rightleftharpoons}} V_{a,b} + n_5H^+$$

[I]

where all pK-values of this scheme are likely to be effective values, representing multiple, cooperative deprotonation steps.[157, 205] The term n_j (j = 1, 2, . . .) denotes the number of released protons. Both pK and *n* values depend on ionic strength and temperature as described in the text.[157, 207]

The oxidized states of cyt c undergo a series of transitions if the temperature is changed from 298 K (5 ° C) to 363 K (90 ° C). Previous work in our group has shown the fully folded state *III* to thermally unfold via the two-step mechanism

$$III \underset{}{\overset{K_{III_1}}{\rightleftharpoons}} III_i \underset{}{\overset{K_{III_2}}{\rightleftharpoons}} III_u \qquad \text{[II]}$$

where III_i is a thermodynamic intermediate and III_u is the thermally unfolded state. Several lines of evidence previously suggested that III_i should be identified with the alkaline state *IV,* which becomes populated at high temperatures because the effective pK-value of the alkaline transition shifts down with increasing temperature.[85, 286] However, Hagarman et al. observed this intermediate by means of analyzing the temperature dependence of absorption and CD in the Soret band region.[233] Tris HCl (0.1 M) was used in this study to lower the pH to a mildly acidic value as the temperature increased, shifting out of the range of any pK of the alkaline

transition, thus suggesting the population of an intermediate state around 338 K (65° C) that could not be identified with the alkaline state *IV*. Moreover, the CD and absorption data of Hagarman et al. revealed similar two-step mechanism of protein unfolding for the already partially unfolded states *IV* and *V*. While these results revealed some interesting insights about the manifold of partially unfolded states of oxidized cyt c, the data are not so well suited for a thermodynamic analysis since all experiments were carried out with rather high anion concentrations. In the current study, we investigate the manifold of cyt c states at low anion concentrations and extend thermal denaturation experiments to the acidic region in order to probe the further unfolding of states I and II. The entire set of data can then be subjected to a proper thermodynamic analysis.

In this study, we explored the heterogeneity of oxidized cyt c with regard to the partially unfolded states adopted over the pH range 1-14 and temperature range 278-353 K. The anion concentration was kept as low as experimentally possible to minimize the binding to the positive patches on the surface of the protein. For pH values >2 the [Cl-] remains below the critical binding concentration (~50mM). However, for low pH, <2, and at high pH, >13, high ionic strengths become unavoidable. However, this is problematic primarily for the acidic region where the Cl^- concentration is high enough to allow for binding to positively charged groups of the protein. By measuring and analyzing the pH and temperature dependence of the visible and UV absorption and circular dichroism (CD) a rather complete manifold of the pH and temperature induced unfolding was obtained, which complement the plethora of data on cyt c unfolding by urea and guanidinium chloride (GmCl).*(195, 198, 379-382)*

4.3 Method Validation. To obtain thermodynamic parameters assignable to the thermal folding/unfolding of states *I* through *V* (including *III**), we selected pH values for our spectroscopic measurements at which one of these protonation states is nearly exclusively populated at all temperatures investigated. In order to obtain these pH values we performed an optical titration (i.e. measuring optical spectra as a function of pH) over a very broad pH range from 1-13. To this end, 0.5 mM cyt c was dissolved in a 0.1 mM 3-(N-morpholino)propanesulfonic acid buffer (MOPS; MW 209.26 g/mol) to ensure that the aforementioned requirements, i.e. low anion concentration and temperature insensitive pH, were met. MOPS is a zwitterionic Good's buffer[383] used because of its minimal absorption in the UV/visible range. MOPS has a pK_a of 7.14 at 298 K (25 °C) that decreases to 6.98 at 310 K (37 °C). In the effective buffering range of 6.5 to 7.9 the pH value of MOPS buffer decreases by 0.006 pH units per °C increase of temperature.[383] The low ionic strength allowed for a buffering power that maintained a minimal amount of anion binding or crowding around the positive patches found on the proteins surface. The same buffer and buffer concentration were utilized across the pH range in an attempt to keep the solution conditions as similar as possible across the pH range, although this solution was not ideal. However, if different buffers were used, the solvent composition would be altered and therefore might not be comparable in monitoring the conformational transitions of cyt c. The titrations towards acidic and alkaline pH were carried out as follows. The pH of the stock protein solution was adjusted with 0.1 M NaOH or 0.1 M HCl depending on the target pH being investigated. The stock solutions were titrated with 0.2-1 μL aliquots, and 1 μL aliquots changed the pH by less than 0.15 pH units. This allowed for the fine control of pH with a negligible dilution effect of the protein (<50 μL was needed to obtain pH extremes). Additionally this technique helped to avoid overshooting the desired pH, and thus back-titrating could be avoided. Only 4.95 mmol

of NaOH were added to the system to adjust the protein-water solution to its maximal pH of 13. However, at the most acidic pH, a level of 100 mM Cl^- ions could not be avoided. Since the buffer was used at a concentration below 1 mM and across the pH range, well below the effective buffering capacity, additional experiments were necessary to check whether the pH is thermostable in the acidic and alkaline region. To ensure the stability of the solution pH even outside of the buffer capacity of the MOPS buffer pH measurements were made before and after each experiment, including at increased temperature, and overall did not show a significant change in pH.

4.4 Data visualization. The temperature dependence of spectroscopic data, (i.e. absorption and visible CD spectra) focused on in this chapter are represented as two-dimensional heat plots. This is a graphic representation of the relationship among the three variables provided in two dimensions, where the third dimension is represented as a color contour plot. Figure 4.1 shows the process by means of which the heat plots were produced for this study. The spectroscopic data (CD and absorption) were measured in the UV/visible region as a function of temperature from 298 to 363 K (5 - 90° C). Figure 4.1(a) displays the conventional representation of the circular dichroism of the B-band region at various temperatures. Figure 4.1(b) shows the same dataset, now visualized in three dimensions, where x is the wavenumber, y the temperature and z the spectroscopic data, i.e. the CD, absorption or Kuhn anisotropy. As one can infer from Figure 4.1(a) to (b), there is a significant amount of structural information lost, or hidden from the standard representation of the data as acquired by the instrument due to the number of spectra presented. However, the representation in Figure 4.1(b) is not ideal either, and can easily obfuscate the interpretation for large datasets, which often hide small spectral changes based on the angle at which the 3D plot is presented. Figure 4.1(c) shows a three dimensional visualization reduced to a 2D heat plot, where the abscissa are the wavenumber and temperature scales, while the ordinate represents the obtained spectroscopic parameter, i.e. $\Delta\varepsilon$. Figure 4.1(c) demonstrates that the changes of $\Delta\varepsilon$ are more easily identifiable in this 2D heat plot presentation. The heat plot combines the densest display of information with an intuitive depiction that makes this type of visualization ideal for displaying hundreds of rows and columns into a single meaningful figure. To relate heat plots to measured spectra, spectra are additionally shown stacked on top of all the heat plots provided in this chapter. This also allows an easy identification of the positive and negative maxima in the heat plots, as the same scale was used across the pH range, thus allowing for side-by-side comparisons. The use of suitable color maps aids in revealing spectroscopic changes, elucidating

otherwise difficult to detect patterns. Figure 4.1(d) shows the trace corresponding to Δε plotted as a function of temperature, which is used for the thermodynamic analysis explained in the next section.

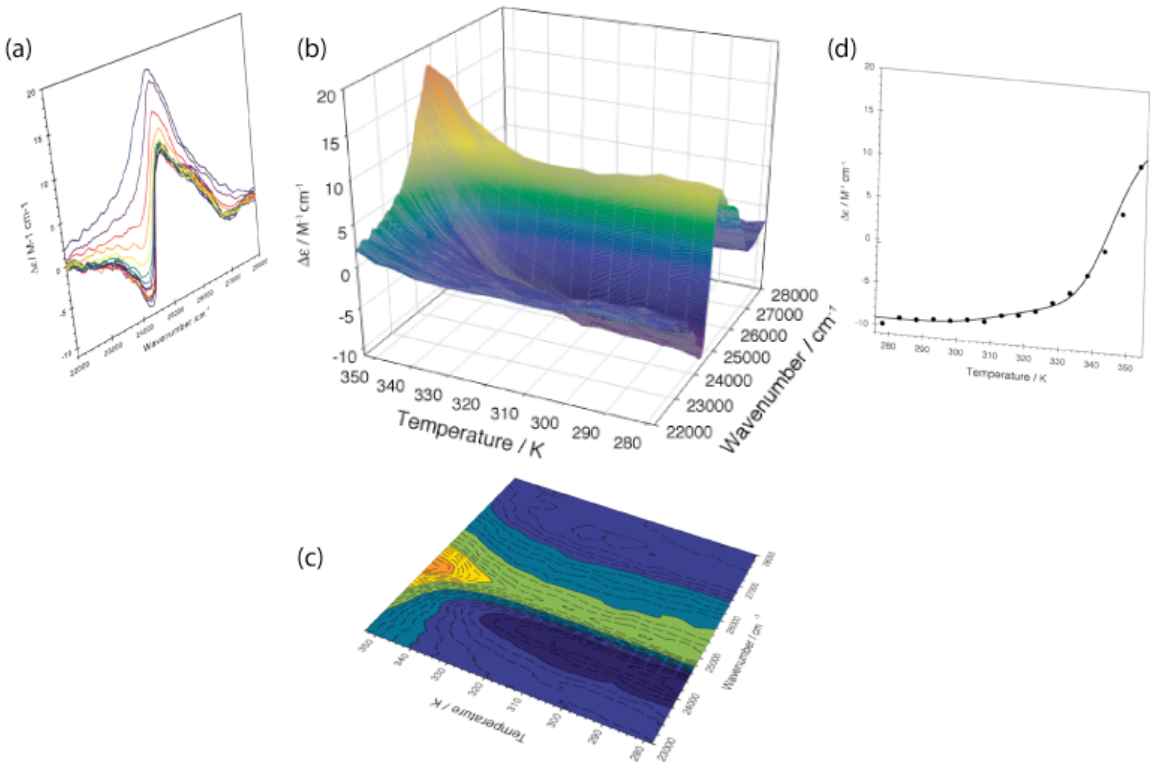

Figure 4.1. Illustration of the method used for the processing of data to arrive at the visualizations used in this chapter. (a) Spectra measured in the B-band (Soret) region of oxidized cyt c measured at pH 7.0. Spectra were measured as a function of increasing temperatures in increments of 5.0° C. (b) The dataset shown in 3D, colored to reflect the spectral intensity. (c) The same data as in (a) and (b), now flattened into a 2D contoured heat plot, the colors in this figure now correlate with the Δε intensity scale, ■ -10, ■ 0, ■ 10, ■ 20 to ■ 30 M^{-1} cm^{-1}. (d) Trace of the 3D spectrum at the position of the maxima, showing Δε a function of temperature. These data were used in the fit of the thermodynamic folding model that is described in detail in the text.[17, 384]

4.5 Results and Discussion

4.5.1 The thermal unfolding of ferricytochrome c probed by visible CD and absorption spectroscopy. The unfolding of oxidized cyt c was carried out across the pH range in increments of 0.1, and the temperature range from 5 to 90° C (278.15 to 363.15 K) as described above. A representative subset of B-band CD and absorption spectra representing each protonation state is shown in Figure 4.2 and Figure 4.3, with each state (I-V/U) identified above its respective spectrum. Figure 4.2 shows heat plots reflecting the thermal unfolding of protonation states *I* to *III*, in the acidic to neutral pH regime. Figure 4.3 shows corresponding heat plots of the alkaline transition, states *III** to the alkaline unfolded state of the protein.

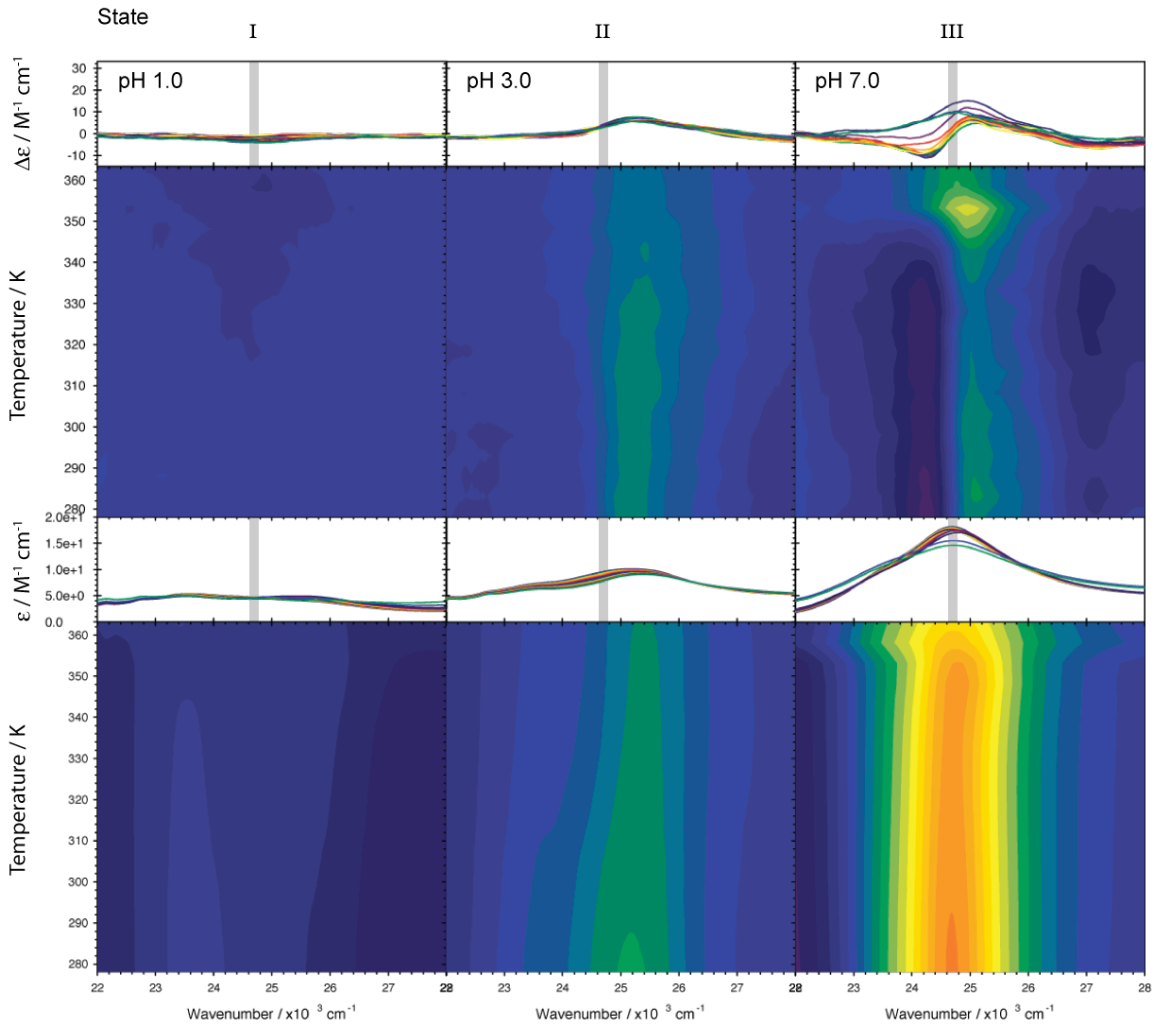

Figure 4.2. Heat plot visualizing the thermal unfolding of oxidized cyt c (0.5 mM) in 0.1 mM MOPS buffer at the indicated pH that correspond to protonation states I - III. The protonation state is shown above the respective spectra as related to the reaction scheme [I]. Original CD (top; $\Delta\varepsilon$ scale ■ -10, ■ 0, ■ 10, ■ 20 to ■ 30 $M^{-1}cm^{-1}$) and absorption spectra (middle; ε scale ■ 0, ■ $5.0x10^4$, ■ $1.0x10^5$, ■ $1.5x10^5$ to ■ $2.0x10^5$ $M^{-1}cm^{-1}$) measured at temperatures ranging from 5 to 90 °C are shown on top of corresponding heat plots. All scales are identical so that one can compare the plots simply by visual inspection.*(17, 384)*

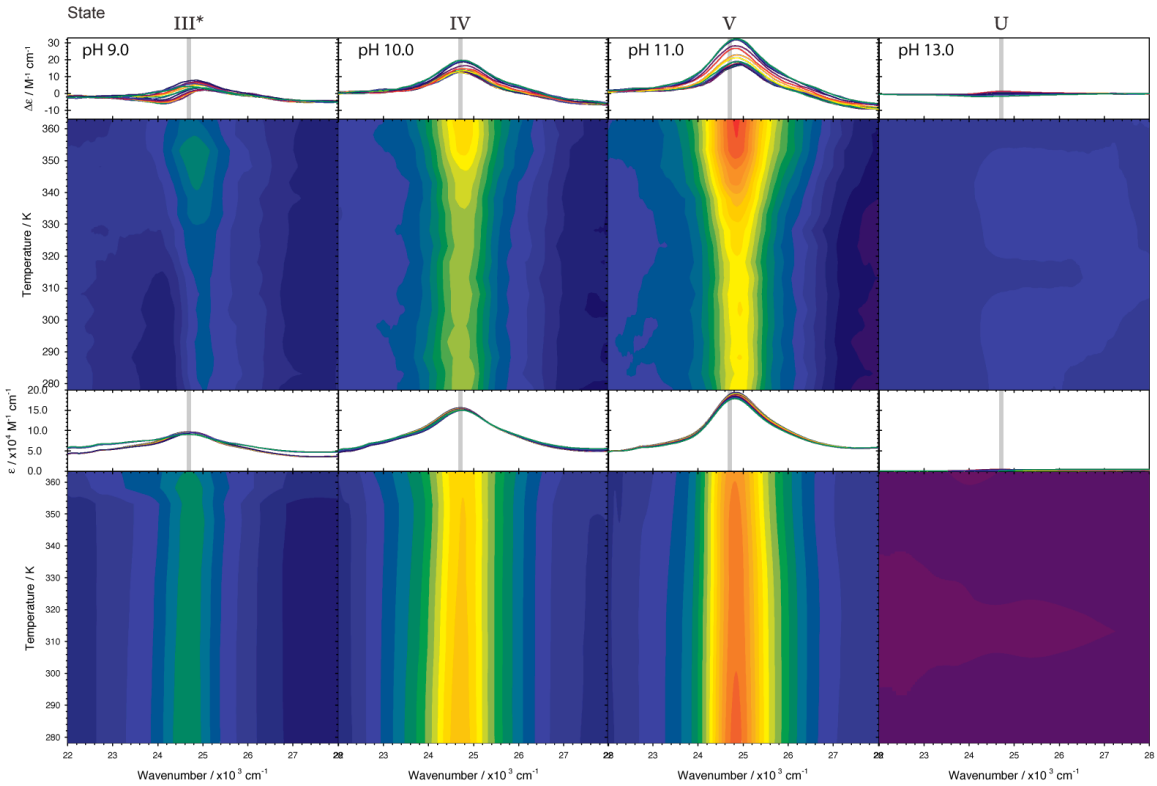

Figure 4.3. Heat plot visualizing the thermal unfolding of oxidized cyt c (0.5 mM) in 0.1 mM MOPS buffer at the indicated pH that correspond to protonation states III* - V/U. The protonation state is shown above the respective spectra as related to the reaction scheme [I]. Original CD (top; Δε scale ■ -10, ■ 0, ■ 10, ■ 20 to ■ 30 $M^{-1}cm^{-1}$) and absorption spectra (middle; ε scale ■ 0, ■ $5.0x10^4$, ■ $1.0x10^5$, ■ $1.5x10^5$ to ■ $2.0x10^5$ $M^{-1}cm^{-1}$) measured at temperatures ranging from 5 to 90 °C are shown on top of corresponding heat plots. All scales are identical so that one can compare the plots simply by visual inspection.[17, 384]

Figure 4.4 shows the combined plots of the B-band CD and absorption spectra measured at different temperatures and the above indicated pH values as well as heat plots that visualized spectral changes as a function of pH. This figure clearly indicates the heterogeneity that occurs as temperature is increased across the pH range. Between the lowest temperature 278 K (5° C) and room temperature 298 K (25° C) the spectra are very similar. Above room temperature the heat plots show distinct changes in intensity. For instance, at pH 7 (state *III*) the B-band CD spectrum exhibits a couplet at low temperatures (Figure 4.3), which gradually converts into a positive Cotton band at high temperature (Figure 4.4). This spectral changes clearly reflect a conformational transition from the low temperature state(s) into a thermally activated state.

More information about this transition is revealed by the corresponding heat plot. It shows an even purple/green coloring at low temperature reflecting the negative and positive maximum of the couplet. The intensity of the purple spot decreases with increasing temperature, as one would expect from a direct inspection of the CD spectra. Interestingly, however, the intensity of the green spot decreases as well before it substantially increases and broadens above 340 K. This clearly reflects the existence of an intermediate state, in agreement with previous data.[207, 233] Interestingly, the corresponding absorption for each respective pH shows only a slight decrease in peak intensity as temperature increases owing mainly to a slight band broadening, or aggregation. A closer inspection is necessary to infer intermediates from the heat plots of states *II*, *III**, *IV* and *V*. The biphasic character of the thermal transition can best be seen in a simultaneous inspection of the heat plots for $\Delta\varepsilon$ and ε. The former reveals a rather steep increase at high temperature, while the latter indicate a very gradual and continuous decrease with temperature until the temperature reaches the temperature at which the CD-value starts to increase. A similar though less pronounced observation can be observed from the heat plots of state *II*. The corresponding plot of state *I* is more difficult to analyze, since it does not display a lot of structure. The CD spectrum actually develops a negative Cotton band at high temperature (Figure 4.5).

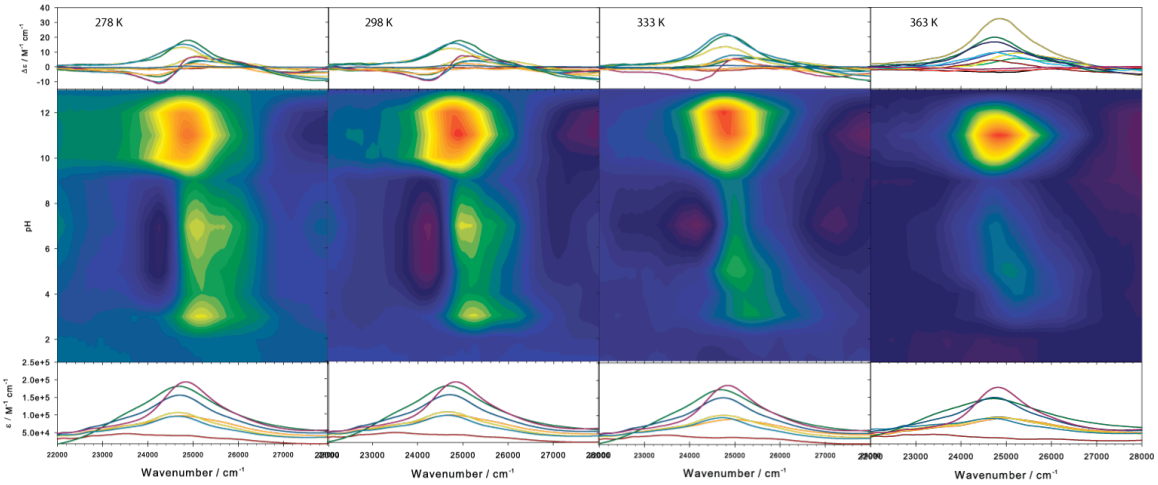

Figure 4.4. Heat plot visualizing the pH dependence of oxidized cyt c (0.5 mM) in 0.1 mM MOPS buffer at the indicated temperature. Original CD (top; Δε scale ■ -10, ■ 0, to ■ 30 $M^{-1} cm^{-1}$) and absorption spectra (bottom; ε scale 0 to $2.0x10^5$ $M^{-1} cm^{-1}$) measured at pH values ranging from 1 to 14 are shown on top of corresponding heat plots. All scales are identical so that one can compare the plots simply by visual inspection.*(17, 384)*

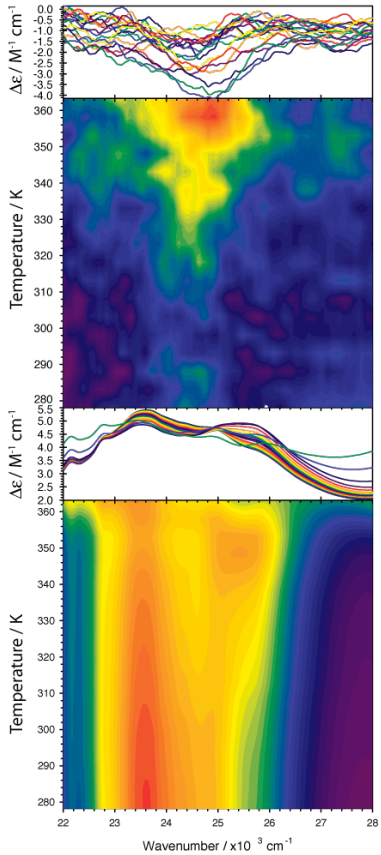

Figure 4.5. Heat plot visualizing the thermal unfolding of oxidized cyt c (0.5 mM) in 0.1 mM MOPS buffer at pH 1.0, which corresponds to the identified protonation states I. Original CD (top; Δε scale ■ 0, ■ -1, ■ -2, ■ -2.5 to ■ -4 $M^{-1}cm^{-1}$), and absorption spectra (middle; ε scale ■ 0 to ■ $5.5x10^4$ $M^{-1}cm^{-1}$) measured at temperatures ranging from 5 to 90 °C are shown on top of corresponding heat plots. Each spectrum is the average of five spectra.

The heat plots also allow a convenient identification of the peak position of the CD and absorption bands. This is shown by the gray line in Figures 4.2 and 4.3. The B-bands of states *III-V* are clearly below 25,000 cm^{-1}, indicating a hexacoordinated low spin state. For state *II*, however, the peak is above 25,000 cm^{-1} and shifts further to the blue with increasing temperature. This is indicative of a hexacoordinated high spin state (Appendix A.6). For state *I*, the heat plots are less useful when scaled the same across the pH range, owing to the B-bands' low intensity reflecting substantial precipitation due to protein aggregation. The CD-band is also very weak. Figure 4.5 shows the unscaled heat plots for state *I*. The absorption band clearly indicates two components, one at very high and the other one at very low wavenumbers (Figure 4.5). The protonation of H18 causes a dissociation of its imidazole residue from the heme iron. As a result a mixture of hexacoordinated ferric (by Cl^- or H_2O) and a pentacoordinated ferrous heme is created (Figure 4.6). The weak CD suggests that the loop region containing H18 has moved away from the heme, thus creating a very open heme environment with the heme still attached to the protein by the thioether bridges.

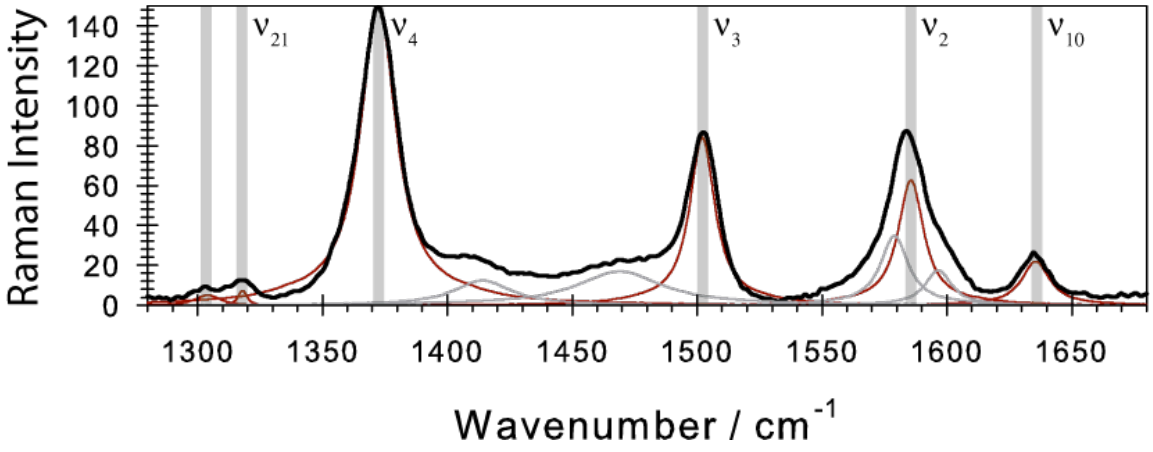

Figure 4.6. Resonance Raman spectrum (x-polarized) of horse heart cytochrome c at pH 3.0 which correspond to the identified protonation state *II*, showing the average of 5 spectra. Taken with 442 nm excitation at an integration time of 150 s.

4.5.2 **Identification of protonation states.** To obtain thermodynamic parameters assignable to the thermal folding/unfolding of states *I* through *V* (including *III**), each pH value must be selected so that one of these protonation states is predominantly populated at all temperatures investigated. To identify these states we averaged five B-band CD and absorption spectra (obtained simultaneously) and then plotted the Kuhn anisotropy spectra of ferricytochrome c measured at a λ of 405 nm (24687.50 cm^{-1}) and temperature of 298 K as a function of pH. Figure 4.7 shows the Δε/ε (Kuhn anisotropy) measured as function of pH at 298.15 K (25 °C). Individual titration states are indicated in the figure. Δε/ε is a dimensionless parameter expressing the ratio of the rotational strength to the oscillator strength of an optical transition. It has the advantage of not being affected by any errors with regard to concentration determination. From the plateaus clearly visible in the Kuhn anisotropy plot in Figure 4.7, these pH values can unambiguously be identified. Based on this plot we selected pH values of 1, 3, 7, 9, 10, 11, and 13 for investigating the thermostability of states *I*, *II*, *III*, *III**, *IV* and *V*, respectively. It is important to note in this context that state *III**,[(217)] which is difficult to detect at high anion concentration, can clearly be inferred from the data in Figure 4.3.

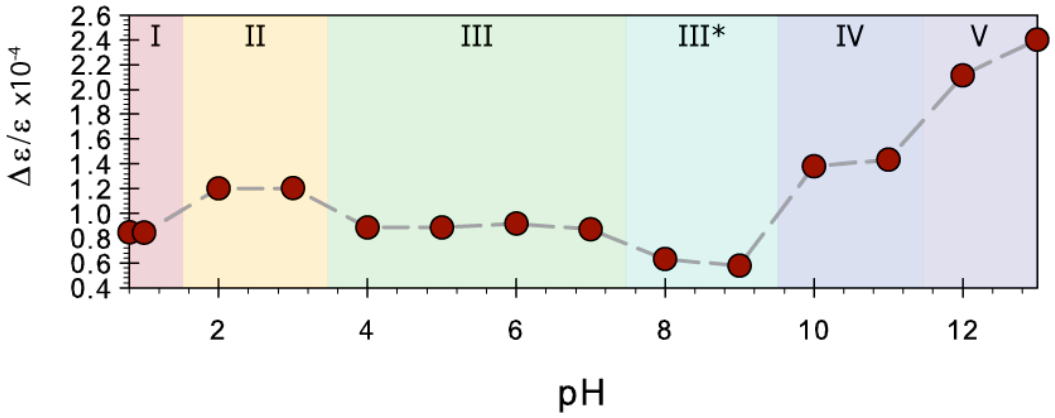

Figure 4.7. Kuhn anisotropy (Δε/ε) of 0.5 mM oxidized cyt c (equine) measured at 24691.40 cm^{-1} as a function of pH in 0.1 mM MOPS buffer at 298 K (25° C). Each datapoint corresponds to the average of five measurements.

4.5.3 Secondary Structure Analysis by UV-ECD Measurements. For the sake of completeness we measured the UV-CD spectrum of oxidized cyt c between pH 1.0 to 11.0 from 283.15 to 363.15 K (Figure 4.8). Generally, the data indicate that thermal unfolding and pH change do not substantially alter the secondary structure composition of the protein, which is predominantly helical. Spectral changes with increasing temperature are rather modest for states *III-V*. Unfortunately, the sample at pH 3.0 aggregated above 333 K (60 °C), shown by the loss of CD intensity. This observation is in agreement with recent findings of Spiro and associates.[385] Taken together with the changes in the *B*-band region (Figure 4.4) it appears that cyt c has a very limited capability to adopt a statistical coil (Figure 4.9).

Maintaining the secondary structure at high temperature underscores the suggestion of Dill and coworkers that the thermal unfolded state of proteins can still contain ordered segments, and thus depart from a statistical coil.[386] This may be further illustrated in the double wavelength plot in Figure 4.9. Uversky used this plot to relate CD values measured at 222 and 200 nm to different protein states, i.e. statistical coil, pre-molten globule, molten globule and globule.[387] Above 343 K the UVCD heat plots (Figure 4.8) show a decrease in intensity, suggesting the onset of precipitation. The varying degree of precipitation was accounted for in the double wavelength plot by estimating the amount of cyt c precipitated. This was accomplished by determining the decrease in the absorption intensity[370] at that temperature and then using that scaling factor to correct its corresponding UVCD spectrum. Without this correction the data trended towards a $\Delta\varepsilon_{222}$ and $\Delta\varepsilon_{200}$ of zero. Interestingly, the data for states *III - V* lie all in the globular region, suggesting that the loss of tertiary structure does not significantly affect the stability of the helical segments of the protein. Apparently, the changes in states *III* to *IV* solely affect the three Ω loops of the foldons introduced by Englander and

coworkers, whereas the helical foldons (N-helix, C-helix and 60's helix) maintain their structure.[8] Our results vary somewhat from those in thermal denaturation studies of English and coworkers in which IR data indicate a melting of secondary structure at 340 K.[173, 388] Their experiments were carried out at high ionic strength (high anion concentration). We conjecture that the final unfolding into a statistical coil occurs at temperatures above the investigated temperature range at the low ionic strength conditions of our experiment. However, any additional transitions into a more unfolded state are not accessible to the optical measurements used for the current study owing to the onset of aggregation at high temperatures, (actually observed by Filosa et al.[389]) but not in our experiments at neutral and alkaline pH.

The Uversky plot data for state *II* suggest that the protein moves from molten globule to pre-molten globule with increasing temperature (Figure 4.9). This observation explains the concomitant increase of protein aggregation. Only for state *I* do the data suggest a development towards a pre-molten globule state at high temperature.[390] All these data show that oxidized cyt c is exceptionally stable with regard to its secondary structure, while it is very flexible with regard to its tertiary structure. Unfolding into a statistical coil requires the addition of denaturing agents like urea or guanidinium chloride.[21] This issue will be discussed in detail below, when we introduce the results of fluorescence measurements.

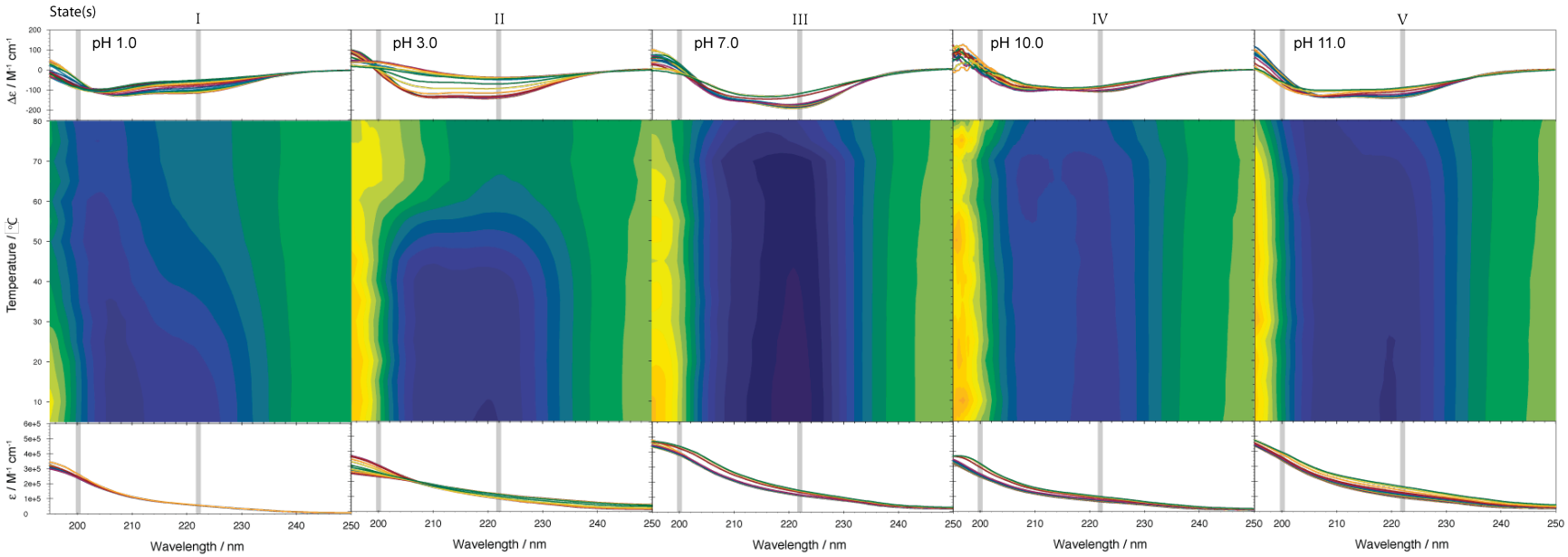

Figure 4.8. Heat plot of the UV region of oxidized cyt c (0.5 mM) for each protonation state as indicated in the figure, in 0.1 mM MOPS buffer. Original CD (top; **Δε** scale ■ -250, ■ 0, to ■ 200 $M^{-1}\,cm^{-1}$) and absorption spectra (bottom; **ε** scale 0 to $6.0x10^5$ $M^{-1}\,cm^{-1}$) measured at pH values ranging from 1 to 14 are shown on top of corresponding heat plots. All scales are identical so that one can compare the plots simply by visual inspection.[1; 2]

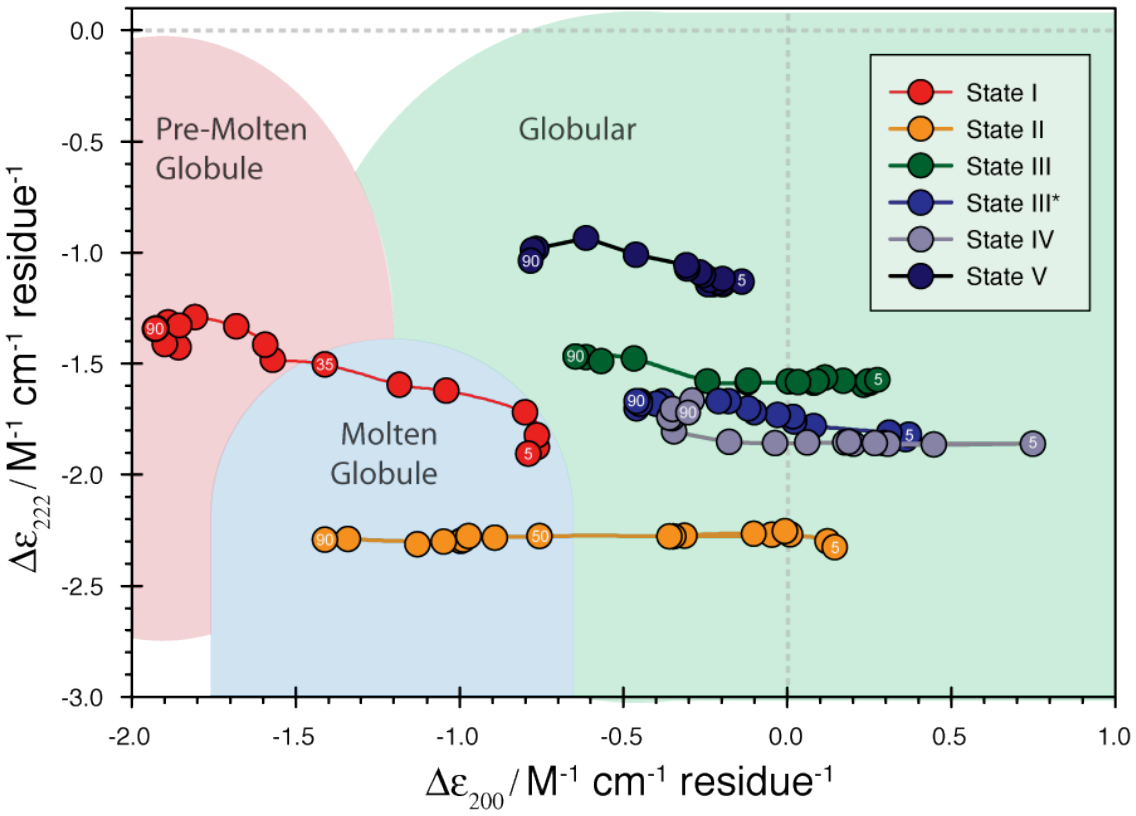

Figure 4.9. Analysis of UV circular dichroism spectra of 0.5 mM ferricyt c (equine) taken at temperatures in increments of 5° C. The pH values were selected as described in the text according to the protonation scheme I, and illustrated by means of a double-wavelength plot ($\Delta\varepsilon_{222}$ vs $\Delta\varepsilon_{200}$) as introduced by Uversky.[387] The different colored areas of the plot indicate the location of pairs of $\Delta\varepsilon_{222}$ and $\Delta\varepsilon_{200}$ associated with the pre-molten globule, molten globule, and globular structures. It should be noted that the statistical coil region is well outside the region cyt c sampled in this study; this region begins at $\Delta\varepsilon_{200}$ values lower than -3.0 M^{-1} cm^{-1} $residue^{-1}$.[17, 384]

4.5.4 Fluorescence of cyt c across the pH range. To elucidate the conformational changes taking place within the tertiary structure of the protein we measured the tryptophan (W59) fluorescence of ferri-cyt c as a function of pH. As described in section 2.4, cyt c contains a single tryptophan (W59), which can be used as a probe of the opening of the heme crevice through Förster resonance energy transfer (FRET). The occurrence of this fluorescence is indicative of (partial) protein unfolding. The fluorescence spectra across the pH range show some very interesting results[1] that have not been previously reported. Figure 4.10 shows the very intense fluorescence band (F-band) with varying peak positions between 345 and 375 nm and a rather intense band peaking in the region between 440 and 460 nm, which can be assignable to a phosphorescence emission (P-band).[391] Since phosphorescence is very sensitive to quenching, notably by dioxygen, the occurrence of the latter is somewhat surprising since we did not employ any measures to deoxygenate the sample.[391] We suspect that this observation was possible in part due to photolysis by the intense irradiation of the pulsed xenon discharge lamp of our fluorescence spectrometer (line frequency 50-60 Hz). Since this type of source reliably produces very little ozone or heat while providing enhanced sensitivity due to an intense peak intensity (>1 KW).[392-394]

[1] This fluorescence data presented was in part collected by Alicia Hoy, a work study student in our lab and Nancy Chung, a summer Maryanoff Scholar in our lab.

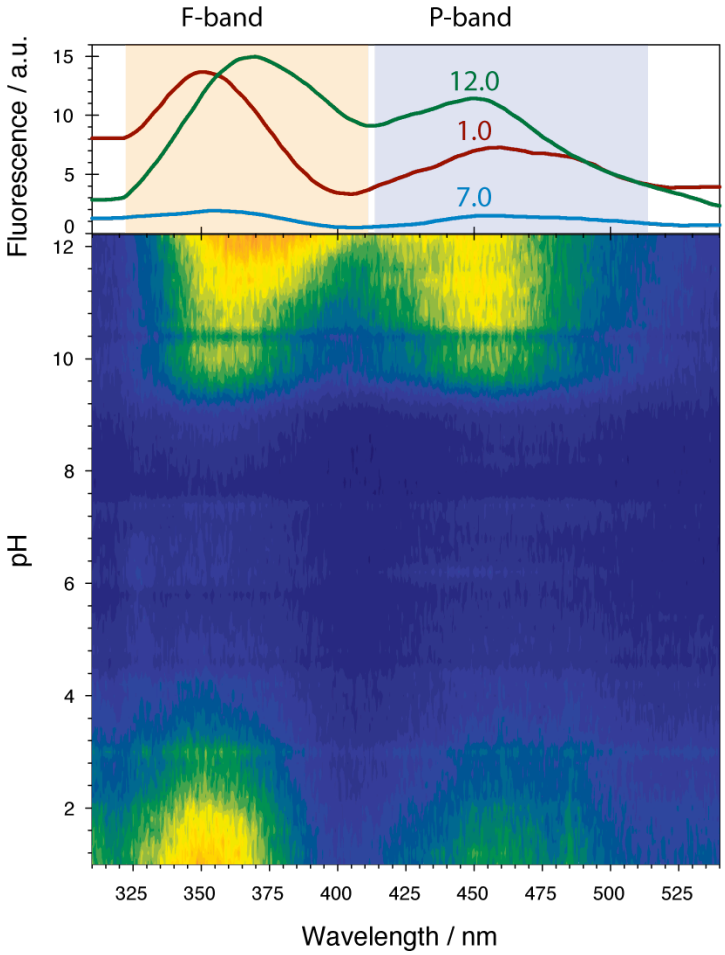

Figure 4.10. Fluorescence spectrum of 0.05 mM cyt c (equine) as a function of pH 1.0-12.2. The top shows the variation that occurs throughout the pH range with the fluorescent (F-band) and the phosphorescent (P-Band) bands at pH 1.0, 7.0 and 12.0. *(17, 384)*

Figure 4.10 shows the expected increase in tryptophan fluorescence (W59) intensity at both high and low pH, indicating the partial unfolding of cyt c in the acidic and alkaline transitions from the fully folded states (pH 7). This fluorescence is indicative of the partial unfolding of the protein, which reduces fluorescence quenching due to an increase of the distance between the heme and W59.*(395)* Under acidic conditions there is a slight blueshift, which can be seen in Figure 4.10 (top). The peak position shifts from 362 to 356 nm, which is likely due to the redistribution of substate band intensity. Under alkaline conditions there is a slight redshift, which can be seen in Figure 4.10 (top), with the peak substate band intensity (F1: 340 nm; F2:

370 nm) shifting from 362 to 373 nm. The P-band shows a similar behavior that is less intense and much more sensitive to changes under alkaline conditions (Figure 4.10) with peak position around 446 nm.

We decomposed the spectra measured between pH 1.0 to 12.2 using the MultiFit[370] program. Decomposition of the fluorescence and phosphorescence spectra was performed concurrently using four Gaussian sub-bands. Exhibiting the same band positions and halfwidths for all pH values. The shifts of both bands result from the redistribution of sub-band intensity. The integrated fluorescence intensity of the most intense F- and P-band are shown in Figure 4.12. Interestingly, the F-band at room temperature appears to follow the conformational transitions of cyt c as seen in Figure 4.3 for the CD spectrum. The P-band appears to follow the alkaline transition independently, suggesting that it is probing an alternate conformation of the protein and increasing in intensity as the protein unfolds. This further illustrates the openness of the heme crevice. The P-band at low pH also follows the conformational transitions of cyt c, although with a smaller increase in fluorescence intensity. The data indicate W59 is highly sensitive to cyt c's conformation. At the present time this change in the subband intensity is poorly understood and is under further investigation, to obtain a more consistent dataset.

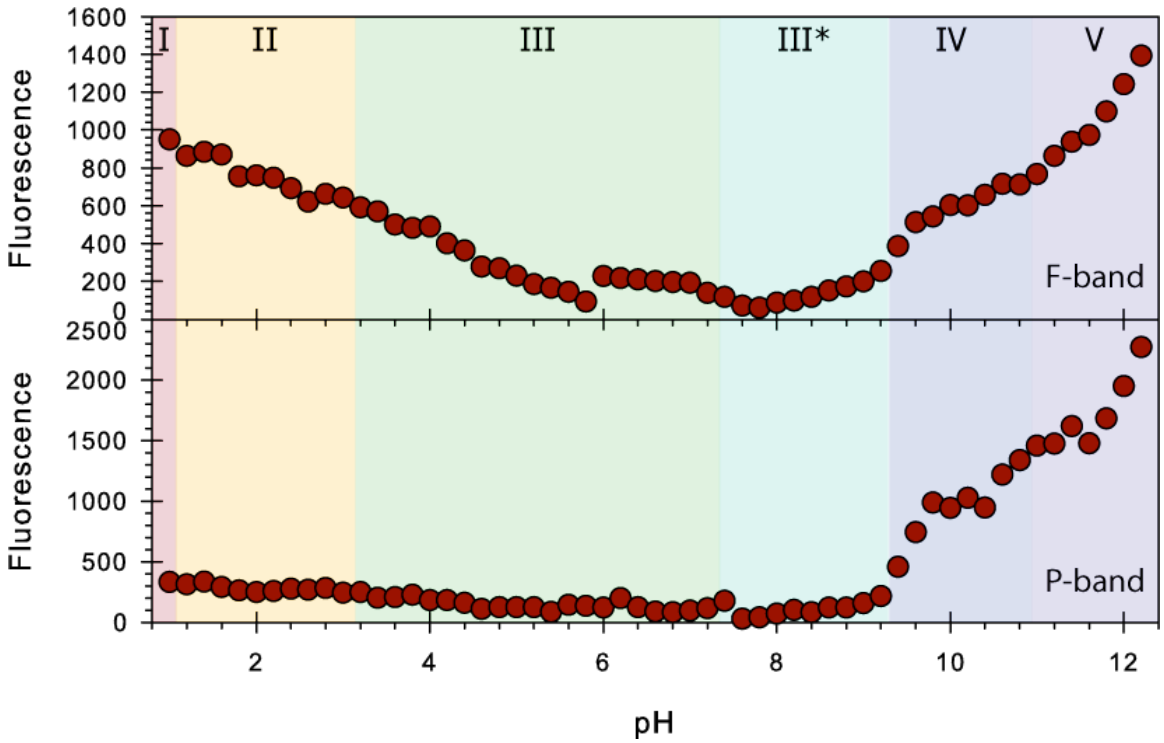

Figure 4.11. Integrated intensity of the F- and P-band for 0.05 mM cyt c as a function of pH. Overlaid is the state model as described in the text.

4.6 Thermodynamic unfolding model. From the absorption and circular dichroism (CD) spectra measured as a function of temperature at the pH values selected above, Δε at a wavelength associated with the largest spectral changes was plotted as a function of temperature (Figure 4.1d). Since the data in Figure 4.12 indicate biphasic thermal transitions, the simplest possible model for describing the temperature dependence of Δε for the different protonation states read as:

$$\Delta\varepsilon(T) = \frac{\Delta\varepsilon_n + \Delta\varepsilon_i e^{-G_i/RT} + \Delta\varepsilon_u e^{-G_u/RT}}{Z} \qquad [4.1]$$

where R is the gas constant and T the absolute temperature. G_i and G_u are the Gibbs energies of a thermal intermediate state and the thermally unfolded states relative to the state n populated at room temperature (unfolded - folded), denoted with the u and i subscript respectively. Z is the partition sum, which is written as:

$$Z = 1 + e^{-G_i/RT} + e^{-G_u/RT} \qquad [4.2]$$

If the thermal unfolding transition is non-cooperative, G_i becomes

$$G_j = H_j - TS_j \qquad [4.3]$$

where j=i,u. Enthalpy H_i and entropy S_i are related by the melting temperature

$$T_i = \frac{H_i}{S_i} \qquad [4.4]$$

However, such a simple model is generally not used for fitting thermal unfolding data, which require the consideration of a difference between the c_p-values of the folded and unfolded states. To account for the generally cooperative folding/unfolding processes, a Hill-type function could be employed to allow for the cooperativity to be empirically accounted for, i.e.

substituting $e^{-G_u/RT}$ by $e^{-nG_u/RT}$ in eqs. 4.1 and 4.2, where n is the empirical Hill coefficient. However, by considering the temperature dependence of the enthalpy in first order this somewhat heuristic parameter can be avoided.[75, 396] For the transition between states i and u, we therefore write:[75, 396]

$$H_u = H_u^0 + \delta c_p \left(T - T_u\right) \qquad [4.5]$$

where δc_p is the heat capacity difference between the two states at constant pressure and T_u is the transition temperature for the transition into the thermally unfolded state. The corresponding temperature dependence of the entropy is accordingly written in first order as:

$$S_u = S_u^0\left(T_u\right) + \delta c_p \ln\left(\frac{T}{T_u}\right) \qquad [4.6]$$

Eq. (4.5) and (4.6) can be combined to yield:

$$G_u = H_u^0 + \delta c_p\left(T - T_u\right) + T\left(S_u\left(T_u\right) + \delta c_p \ln\left(\frac{T}{T_u}\right)\right) \qquad [4.7]$$

This expression for G_u was used in the following equation to fit the data in Figure 4.12:

$$\Delta\varepsilon\left(T\right) = \frac{\Delta\varepsilon_n + \Delta\varepsilon_i e^{-G_i/RT} + \Delta\varepsilon_u e^{-G_u/RT}}{Z}$$
$$\varepsilon\left(T\right) = \frac{\varepsilon_n + \varepsilon_i e^{-G_i/RT} + \varepsilon_u e^{-G_u/RT}}{Z} \qquad [4.8]$$

where $\Delta\varepsilon_j$, ε_j are the CD and molar absorptivity values of the states n, i and u. The solid lines in the data presented below result from the consistent fit of the above formalism to the

experimental data. A consistent fit for this study means that the same thermodynamic parameters were used to fit the $\Delta\varepsilon(T)$ and $\varepsilon(T)$ measured at the same pH value. In this study H and S are defined as the difference between the unfolded and the folded states, i.e. H_u - H_f. The thermodynamic parameters used for the fits are presented in the figures and tables associated with each oxidized state of cyt c (Figure 4.12, Table 4.1).

The heat capacity difference between states i and u, δC_p, is the most uncertain parameter of the fitting procedure. δC_p for the unfolding of cyt c by calorimetric experiments has not yet reached a consensus, with reported δC_p values varying between 1.37 to 5.34 kJ K^{-1}, largely reflecting the hydration of nonpolar amino acids under various solvent conditions.[73, 397-399] The variety of conditions studied is often not reported, primarily with respect to the ionic strength of the system, thus making it difficult to compare literature values with the findings of this study. However, a consensus seems to be that the δC_p value is closer to the 1.37 kJ K^{-1} than 5.34 kJ K^{-1}. To this end, the heat capacity difference between states *i* and *u*, δC_p, was set in the fit to be 2.00 kJ mol^{-1} K^{-1}. To test the contribution of δC_p to the fit, a starting value of 2.00 kJ mol^{-1} K^{-1} was fit to the trace at pH 7.0 and then all of the variables were fixed allowing only a set increase in δC_p. Figure 4.12 clearly indicates that for values between 2.00 and 10.00 kJ mol^{-1} there is only a minimal effect. For this fit we used a common value of 2.0 kJ mol^{-1} K^{-1} which is close to the value of 2.8 kJ $mol^{-1}K^{-1}$ that Uchiyama et al obtained from calorimetric studies of horse heart cyt c.[75, 396] Pielak and coworkers obtained higher δC_p values for yeast cyt c and several mutants of this protein (around 6 kJ $mol^{-1}K^{-1}$),[398, 400] which is still inside the range of acceptable δC_p values for our thermodynamic analysis (Figure 4.12).

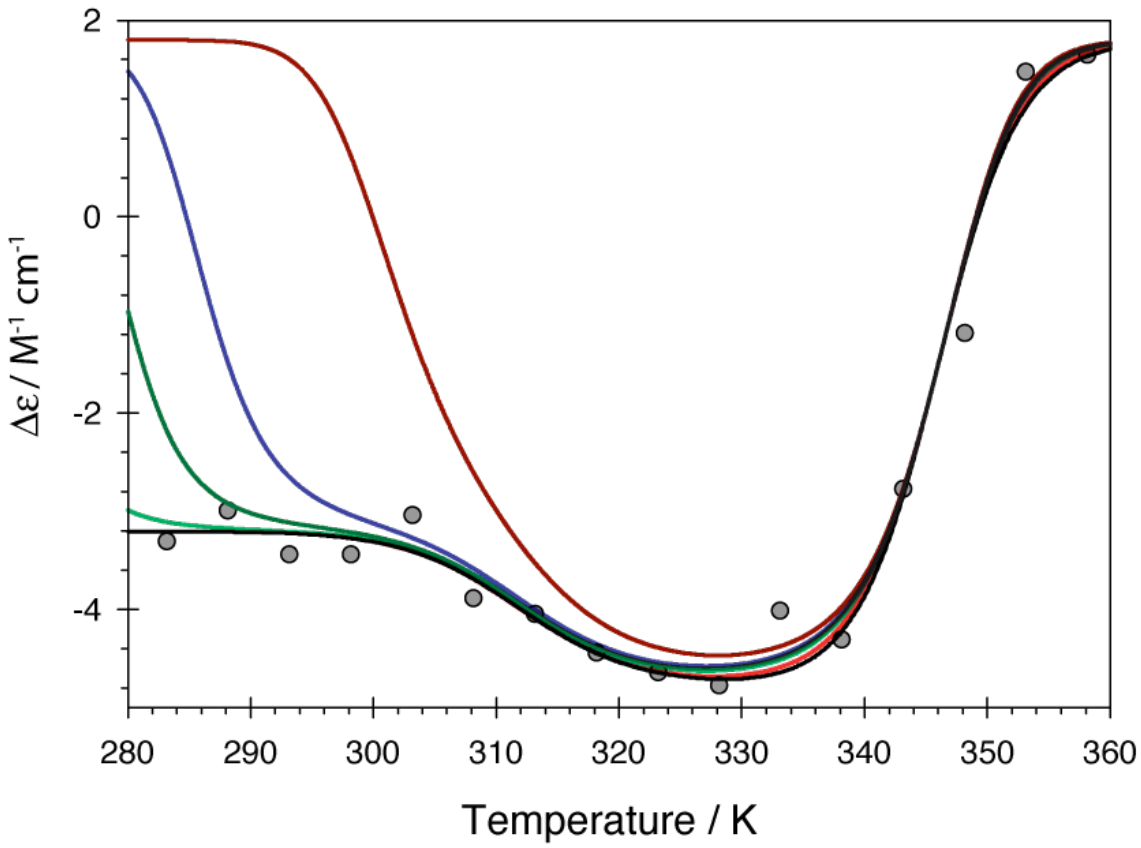

Figure 4.12. Trace from Figure 4.13 of the CD (Δε) spectrum as a function of temperature (278-363 K) of ● oxidized cyt c (0.5 mM) at pH 7.0. The solid line results from the fits described in the text, with changing C_p, ■ 2.0 kJ mol^{-1}, ■ 6.0 kJ mol^{-1}, ■ 10.0 kJ mol^{-1}, ■ 11.0 kJ mol^{-1}, ■ 12.0 kJ mol^{-1}, ■ 15.0 kJ mol^{-1}.*(17, 370, 384)*

4.6.1 Thermodynamic fit to model. Figure 4.8 exhibits the thermodynamic fits obtained from the $\Delta\varepsilon(T)$ and $\varepsilon_{max}(T)$ at 24688 cm^{-1} (405 nm) for the pH-values associated with the protein's protonation states. (Figure 4.7). This wavenumber position is additionally illustrated by the gray line in Figure 4.2 and 4.3. For all states, the data clearly indicate at least a biphasic behavior. We therefore used eqs. 4.1. and 4.2. to fit corresponding data sets consistently with our three-state model. The fits in Figure 4.13 were initially manually performed to get the $\Delta\varepsilon$ values (eq. 4.1) and an initial estimate of the entropy and transition temperature(s), before performing a more rigorous fitting routine in SigmaPlot.[384] This yielded excellent fits for a majority of the data sets as visualized by the black lines in Figure 4.13. However, the fits for state *I* (pH 1.0) and *V* (pH 11.0) data were only partially successful in that the fit could not completely reproduce all experimental data (Figure 4.13). At pH 1.0 the data indicate another transition temperature at 290.16±0.94 K, marked in blue in Figure 4.13. This might reflect a population of state *II*, owing to the shift in the pK_a at low temperates. For state *V*, the fit could not reproduce additional changes of $\Delta\varepsilon$ above 340 K.

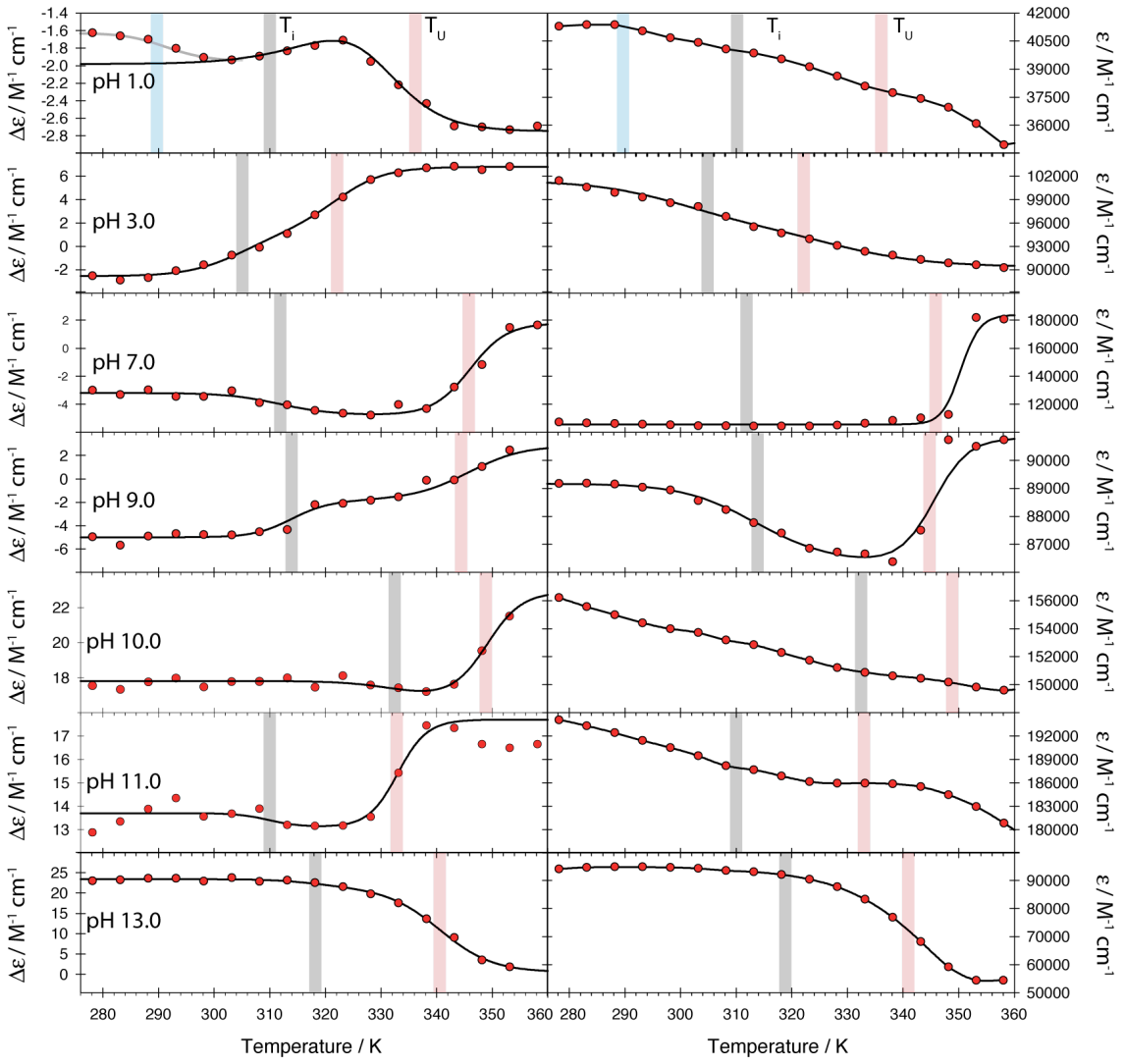

Figure 4.13. Trace from Figure 4.2 and 4.3 of the CD (Δε left) and absorption (ε right) as a function of temperature (278-363 K) of oxidized cyt c (0.5 mM) taken at 24687.50 cm^{-1}. The solid line results from the fits described in the text, with the gray line, denoting T_b, and red line denoting T_u.[17, 370, 384] The error of estimate ranged between 10-27%, with the exception of pH 11, which had an estimated fitting error of 38%.

The thermodynamic parameters obtained from these states are listed in **Table 4.1**. The enthalpy of the unfolding/folding process reported for the wild type of yeast cyt c is in good agreement with our data for the $i \leftrightharpoons u$ transition of state *III* (3.45 versus 3.0 kJ/mol), [399] whereas their transition temperature of 325.8 K lies nearly exactly between our values for T_i (312 K) and T_f(346 K). Cohen and Pielak's measurements were carried out at pH 4.9.[399] The buffer and ionic strength conditions were not specified so that a direct comparison of the data

is difficult. In another study, Cohen and Pielak investigated the folding of the C102T variant of yeast cyt c as a function of pH between pH 3 and 5, which for our experimental conditions and horse heart cyt c would cover the transition region between states *II* and *III*.[399] They found a gradual decrease of the melting temperature from ca. 327 K at pH 5 to 302 K at pH 3. A visual inspection of the respective data for states *III* and *II* suggests that this observation is inconsistent with our experimental data .

Table 4.1. Thermodynamic parameters obtained from the fitting of $\Delta\varepsilon(T)$ and $\varepsilon_{max}(T)$ as described in the text. A subset of fits as a function of pH are shown in Figure 4.8 for 0.5 mM cyt c in 0.1 mM MOPS buffer from pH 1.0 through 14.0.

pH	**1.0**	**3.0**	**7.0**	**9.0**	**10.0**	**11.0**	**13.0**
H_i *(kJ/mol)*	110.00	154.20	169.00	280.00	200.00	280.00	200.00
S_i *(kJ/mol K)*	0.35	0.51	0.54	0.89	0.60	0.90	0.63
G_i *(kJ/mol)*	5.65	2.14	8.00	14.65	21.11	11.67	12.17
H_u *(kJ/mol)*	66.30	142.30	204.30	226.30	218.30	280.30	116.30
S_u *(kJ/mol K)*	0.18	0.44	0.57	0.64	0.61	0.83	0.33
G_u *(kJ/mol)*	13.44	12.28	33.66	36.05	37.90	33.16	18.71

Figure 4.14 compares the thermodynamic parameters of each protonation state as obtained from the fitting procedure. The Gibbs energy was calculated with a temperature of 298.15 K. This analysis reveals the well-known phenomenon of partial enthalpy-entropy compensation, i.e. the enthalpic stabilization of the folded, and the entropic stabilization of the unfolded state. The compensation is significant: the enthalpic and entropic contributions to the Gibbs energies exceed, by far, their respective Gibbs energies. This effect is particularly pronounced for the $n \leftrightharpoons i$ equilibrium, for which the Gibbs energy values are just 5% of the respective enthalpy

values. It should be mentioned that variations of δC_p do not cause major changes of H_u and S_u values.

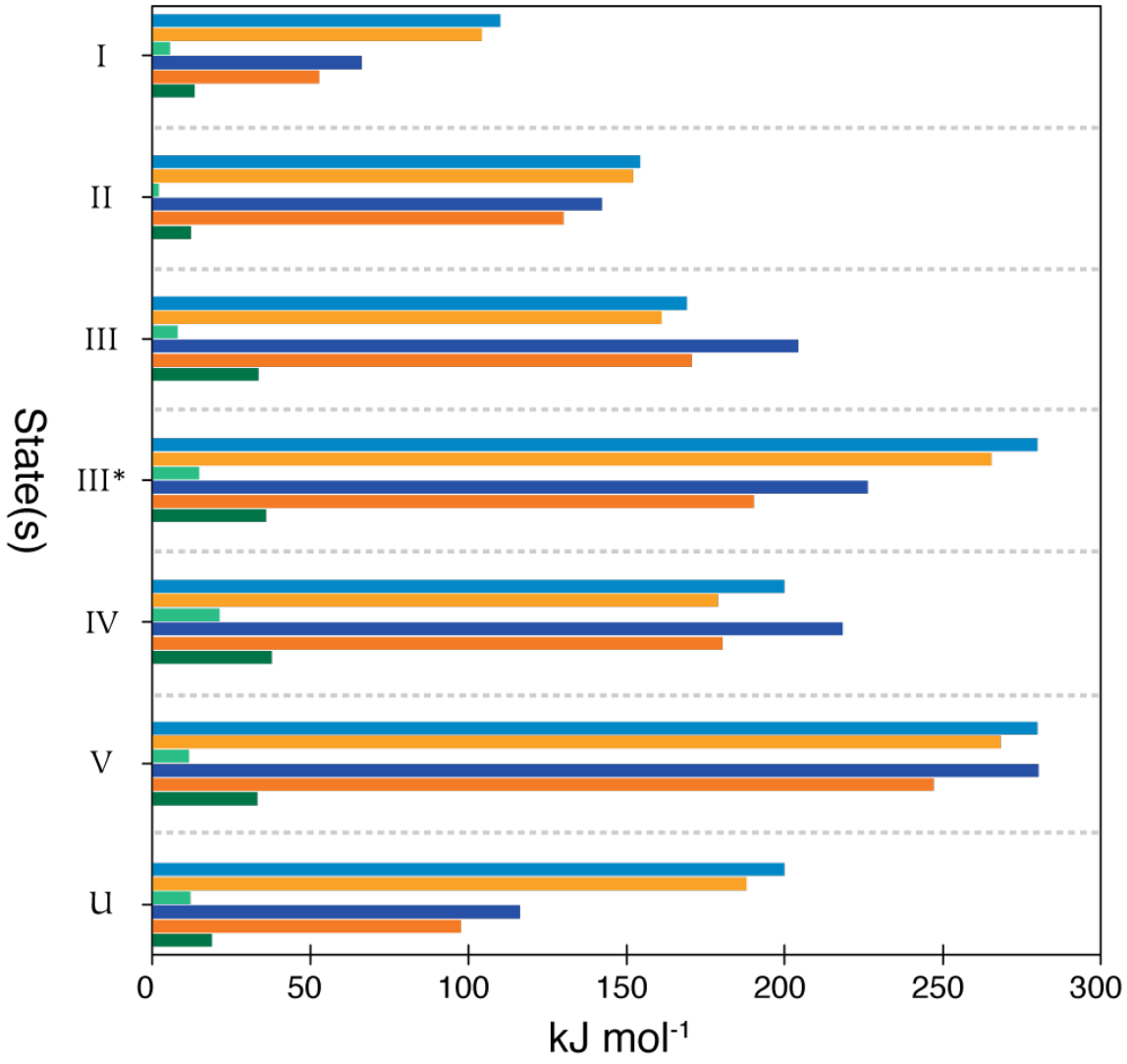

Figure 4.14. Thermodynamic profiles of each protonation state (I-V) of cyt c as determined from the fitting of $\Delta\varepsilon(T)$ as described in the text. The enthalpy, entropy and free energy are shown for the intermediate (■ H, ■ TS, ■ G) and thermally unfolded (■ H, ■ TS, ■ G) states, using a temperature of 295 K.

We wondered whether or not the above enthalpy-entropy compensations of the different unfolding/folding transitions are interrelated. If this is the case, we would expect a nearly linear relationship between entropy and enthalpy.[401, 402] As shown in Figure 4.15, *H* and *S* values of

the transitions into states *i* and *u* exhibit two different, nearly ideal linear relationships, which can be described by the equation[401]

$$S_k = S_{k_0} + T_{c_i} H_k \qquad [4.8]$$

where $k=i,u$ and T_{ci} denotes the compensation temperature. S_{k0} is the uncompensated entropy which one would obtain for $H_k=0$. T_c is the so called compensation temperature. Figure 4.15 shows two slightly different linear fits to the thermodynamic data of the n ⇆ i and i ⇆ u equilibria. The respective compensation temperatures thus obtained are T_{ci}= 316±13 K and T_{cu}=350±12 K. With respective correlation coefficients for each linear regression approximately equal to 1 (0.99), thus indicate a very strong correlation. The compensation temperatures for the two transitions are rather different indicating different mechanism for the two steps of thermal unfolding. Since the error interval for the thermal intermediate (blue) does not overlap, we interpret the difference as significant, and in the range of processes driven by protein-solvent interactions.[401] T_{cu} might reflect the weakening of hydrogen bonds, which would reduce enthalpy and increase the entropy of protein-solvent systems. In order to rule out the possibility that the obtained correlations are the product of a statistical artifact, we subjected our data to a deviation and variance analysis (built into the fitting routine, with a minimum of 200 iterations performed) determined for each experimental point followed by a LINEST error analysis for the resulting linear fit (Figure 4.15). Following the argument of Lumry and Rajender,[403] the spreading of our data cannot be explained even by correlation between statistical errors.

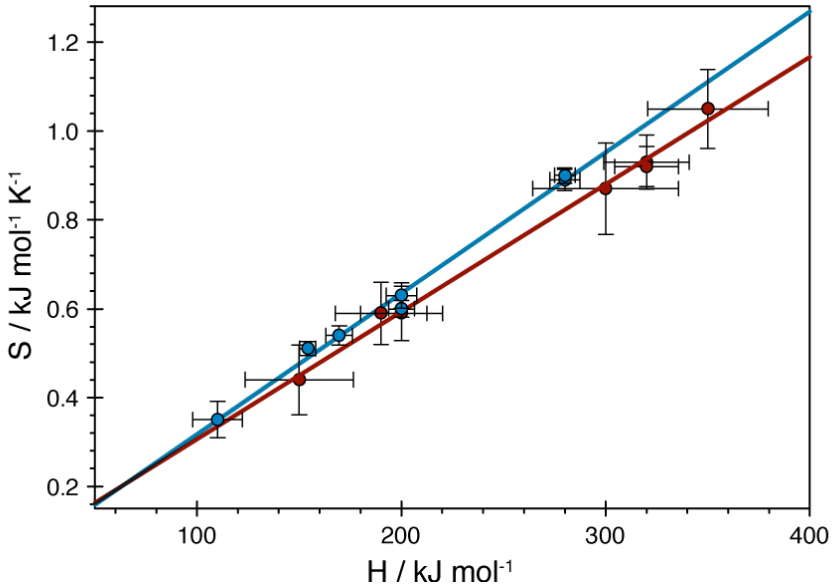

Figure 4.15. Enthalpy-entropy compensation plot of oxidized cyt c (equine) as determined by the fit to the thermodynamic model between to the ε- and Δε-plots in Figure 4.13. Thermodynamic parameters S_i, H_i (●) and S_u, H_u(●) were subjected to individual linear regression analyses.

The existence of an enthalpy-entropy compensation has been a matter of debate. As indicated above, Krug et al. showed that thermodynamic analyses based on van't Hoff and Arrhenius plots are prone to strong statistical correlation between ΔH and ΔS.[404] Beasley et al. used their criteria to critically analyze the linear relationship between the folding/unfolding enthalpies and entropies of several proteins and arrived at the conclusion that a quantitative compensation effect cannot be deduced from the data.[405] However, many papers defend the existence of enthalpy-entropy compensation on experimental and theoretical grounds.[401, 402, 406, 407] When entering this debate, one has to be careful about the definition of enthalpy-entropy compensation. Generally, this term is used just to indicate that enthalpy and entropy provide opposing contributions to the Gibbs energy. That this is the case for protein folding is textbook knowledge and again documented in this study. The real controversy is whether ΔH and ΔS values of related thermodynamic processes are linearly correlated. Examples are the

folding parameters of mutants or even different proteins, [408] the binding of different ligands to the same receptor protein[409] or the conformational equilibrium of short peptides in different solvents.[410] If a statistical linear relationship can be established, it is indicative of a temperature at which the ΔG of one or more processes that contribute to the total Gibbs energy becomes zero. At this temperature the Gibbs energies of all compared equilibria are identical. If S_0=0, the Gibbs energy difference disappears at this temperature. The existence of such isoequilibria indicate a common driving force of the compared conformational transitions. However, the detection of such isoequlibria is difficult, since in principle it requires a negligible uncertainty for ΔS and ΔH. Even small uncertainties can obfuscate the relationship between these parameters and ΔG, a frequently observed phenomenon. [402] In our case the fit exhibit a rather low scattering as documented by the correlation coefficient ≈1. However, even in this case a correlation between H_j and G_j is very weak (Figure 4.16).

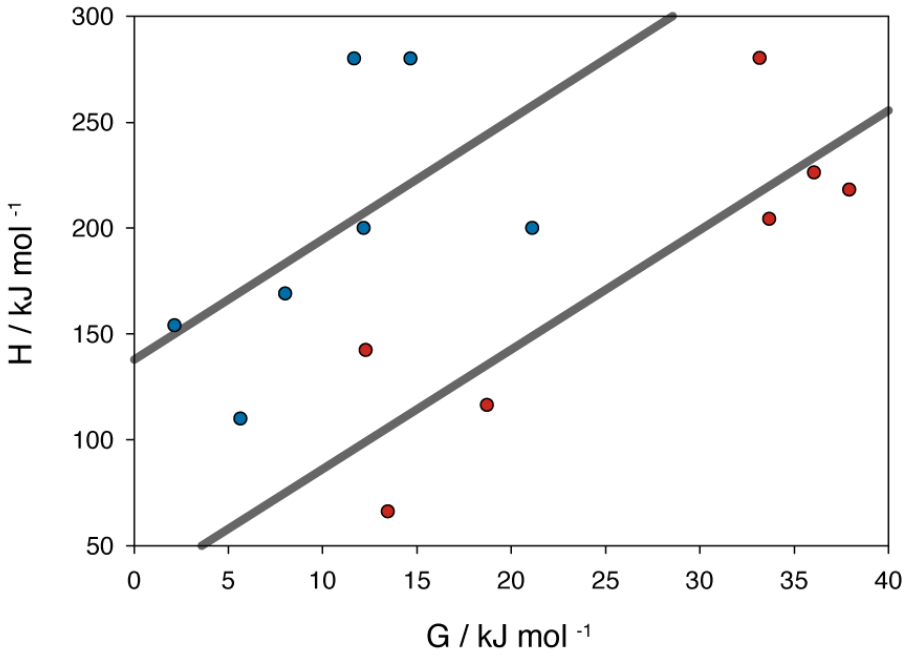

Figure 4.16. Enthalpy-entropy compensation plot (data in Figure 4.8 and Table 4.1) of 0.5 mM oxidized cyt c (equine) as determined by the fit of a thermodynamic model to the ε- and Δε-plots in Figure 4.13. Thermodynamic parameters H_i, G_i (●) and H_u, G_u(●) were subjected to individual linear regression analyses.

In this context, an earlier study of Milne et al. is noteworthy. The authors used hydrogen exchange as a site-specific probe of equilibrium between folded and unfolded cytochrome c for both the oxidized and reduced forms of equine cyt c.[411] Figure 4.17 compares a plot of enthalpy and entropy values that these authors obtained for the hydrogen exchange of a variety of cyt c residues with our data as plotted in Figure 4.17 (Milne et al. plotted TS versus H, using T=293 K). The T_c value of 293.15±15 K derived from a linear regression seems to be close to the T_{ci}-value derived from our data (the error intervals do overlap). Both values are within the range that Lumry and Rajender assigned to (aqueous) solvent-protein interactions.[401] We therefore think that hydrogen exchange should be related to the $n \leftrightharpoons i$ rather than to the i $\leftrightharpoons$ *u* equilibrium and that the former involves an increase in protein hydration, which leads to a more open conformation of the protein. The T_{cu} value might well be assignable to hydrogen bonding. Recent density functional theory (DFT) calculations have provided evidence for the notion that hydrogen bonding between amide derivatives is associated with a substantially higher compensation temperature than interactions governed by van der Waals forces.[412]

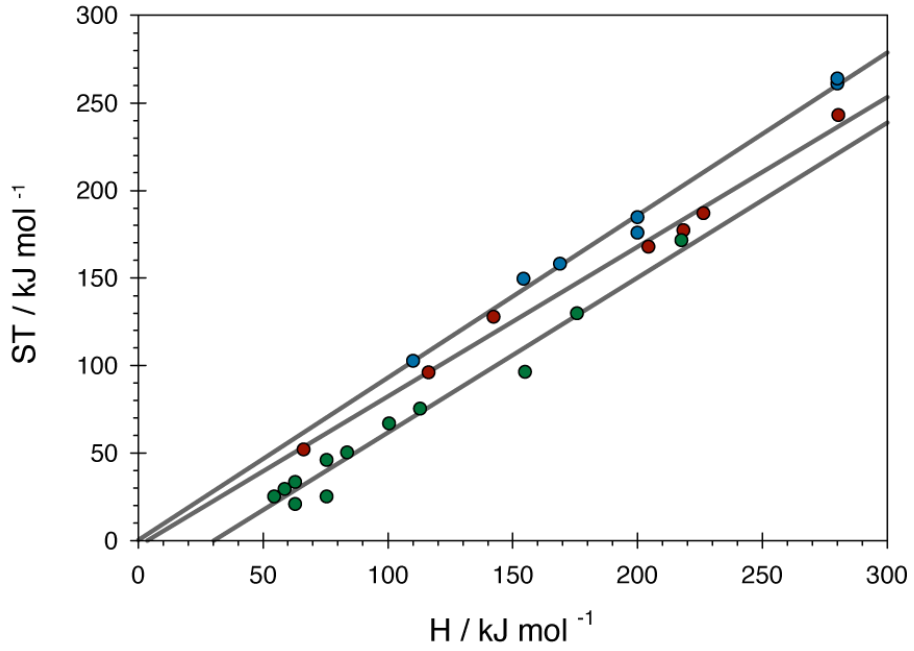

Figure 4.17. TS versus H plot derived from the entropy-enthalpy data plotted in Figure 4.15 (see the legend of Figure 4.15 for a description) compared to a TS versus H plot of hydrogen exchange processes of oxidized cyt c reported by Milne et al. (●), (m=0.89; r^2 = 0.9776).[411] A temperature of 293.15 K was used for all plots. The gray line is the result of the regression analysis.

4.7 Discussion. Our spectroscopic data clearly reveal that each of the canonical Theorell-Åkesson states and the newly discovered *III** state unfold (further) in a two-step process. While enthalpies and entropies of these processes are clearly different, differences between Gibbs enthalpies are less pronounced. G_u-values of states *III*, *III**, *IV* and *V* lie all in the region between 46 and 64 kJ/mol, with *III* being surprisingly slightly less stable than the other states. The situation is rather different on the acid side, where G_u value of states *II* and *I* are clearly lower than those of the other states. Spectroscopic evidence suggests that all *u*-states are different with respect to their secondary and tertiary structure. The UVCD spectra clearly suggest that they do not resemble statistical coils in this condition.

Krishna et al. obtained site specific information about the equilibrium between the folded and unfolded state of both oxidation states by hydrogen exchange experiments.[9] This and earlier studies from this group led to a picture in which different segments of the protein unfold consecutively. The unfolding steps of the lowest Gibbs energy are assignable to the so-called infrared and red Ω loops involving residues 40-57 and 71-85, respectively. The corresponding Gibbs energies are 15.8 and 26.14 kJ mol^{-1} at pK 5.5 and 20°C. The values are larger than what we obtained for G_i of state *III*. The next step (unfolding of two β-strand segments) requires a Gibbs energy of 30.71 kJ mol^{-1}, the first helical and loop region folding requires more than 40 kJ mol^{-1}. The latter value is close to what we obtained for G_u of state *III*. Since the measurements of Krishna et al were performed at very high ionic strength (0.5 M), the thermodynamic parameters are not directly comparable. We tentatively assign the first step to the unfolding of the Ω-loops and the second one to a somewhat combined unfolding of the β-strands and the so called green 60' helix that connects the two Ω-loops. The relevance of the Ω-

loops stems in part from the structurally pivotal hydrogen bond between H26 and E44.[413] Total unfolding can therefore be excluded from our UVCD data. The C- and N-helices may be still intact in III_u, but may become distorted in states II_u and I_u. Hence our data show that some of the steps of the foldon unfolding/folding model constitute thermodynamic intermediates. Cyt c appears as a rather stable molecule that resists total unfolding even in rather harsh conditions (extreme pH and temperatures). This shows the strength of intra-backbone hydrogen bonding as a prime determinant of helix stabilization (Figure 4.18), [168] in agreement with recent theoretical predictions from Rose and coworkers.[414]

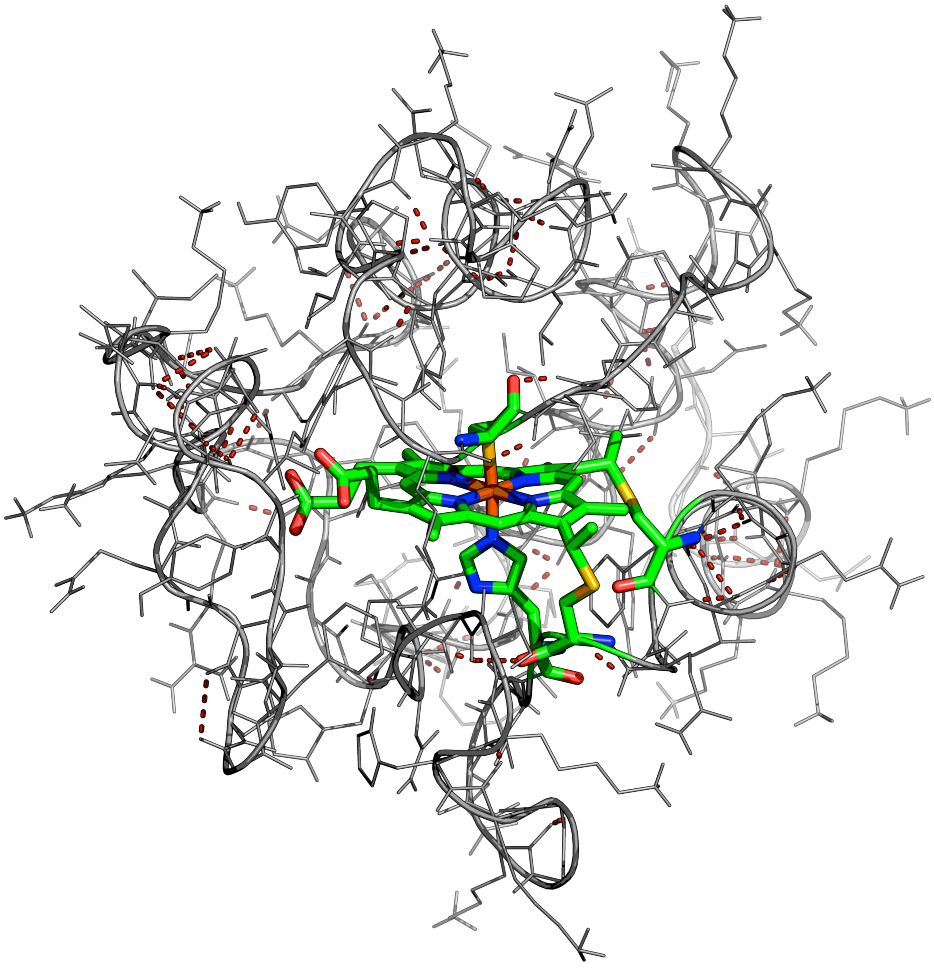

Figure 4.18. Intra-backbone hydrogen bonding, shown as the red dotted line(s), for oxidized horse heart cyt c. The colored sticks shows the heme's CxxC binding motif with M80 and H18 axially ligated to the heme iron, the fully folded conformation at physiological pH (PDB: 1AKK).[27, 28]

4.8 Acknowledgment

Submitted in part to the Biochemistry, **2013**, Soffer JB, Schweitzer-Stenner, R.

Graphical abstract (TOC) used at time of submission.

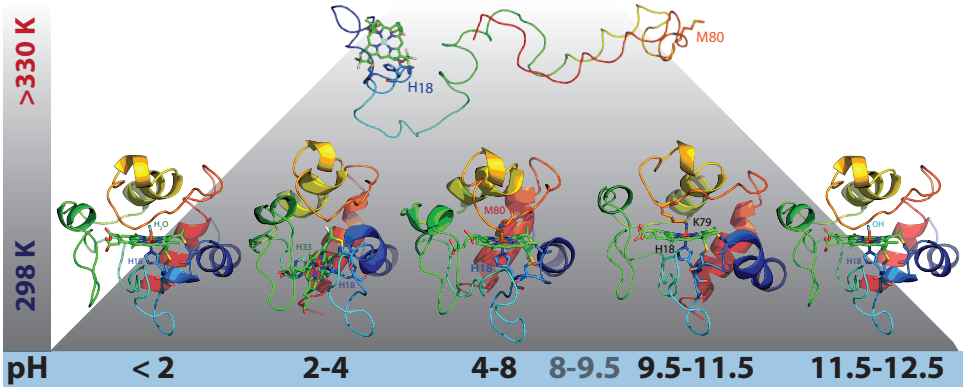

CHAPTER 5: THE OCCUPATION OF A NOVEL MISFOLDED STATE AND DOMAIN SWAPPED STATE OF CYTOCHROME C

5.1 Introduction.

Results from various kinetic experiments suggest that the folding of denatured oxidized cyt c involves the population of an off-pathway kinetic intermediate state, in which the imidazole group of H33, rather than the functionally pivotal M80, is bound axially to the heme iron.[415] This misfolded state is in equilibrium with an on-pathway state, in which the protein exhibits a hexacoordinated high spin heme iron with water as the distal ligand. The latter eventually converts into the fully folded, 'native', conformation with M80 as the proximal ligand (Figure 5.1) to complete the folding process. Recently, Tzul et al. revealed an even more complex picture for the folding pathway of ferric iso-1-cyt c, depicting a competition between intramolecular histidine loop formation and ligand mediated oligomer formation due to the binding of a histidine side chain of one molecule to the free binding site of another one.[416] Thus, the misligated kinetic intermediate can encompass monomers as well as soluble and partially folded oligomers. This finding is in line with earlier reported results from small-angle x-ray scattering (SAXS), which suggest the formation of dimers during the refolding of horse heart cyt c.[417] At equilibrium, i.e. folding (neutral pH, room temperature) or mildly unfolding conditions (high urea or guanidine hydrochloride and room temperature), ferri- and ferro-cyt c are both monomeric, but polymerization by domain swapping can be thermodynamically achieved by dissolving the protein in ethanol/water mixtures.[192]

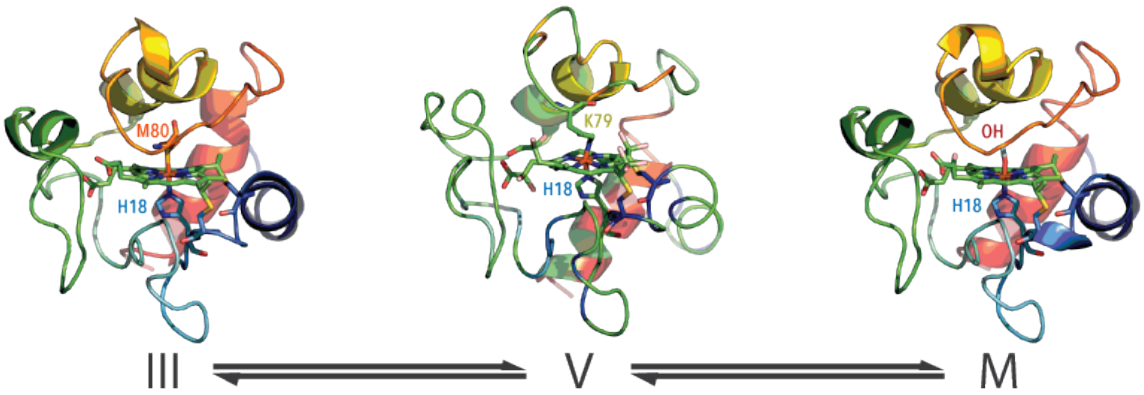

Figure 5.1. Reaction scheme showing the cartoon structure of horse heart cyt c (PDB: 1AKK)[27] of the fully folded state (III) to the alkaline state (V) populated at pH 11.5 to the proposed misfolded state (M) populated at pH 7.[17, 18, 28]

The occupation of a misfolded state is not an unusual part of the protein folding process. The energy landscape theory predicts that non-native interactions can trap proteins in kinetic intermediates along the unfolding pathway from which they can only slowly escape. However, as long as the Gibbs energy positions of such misfolded states remain above the glass transition point of the folding funnel, the barrier between the folded and misfolded state can be overcome on a sub-second timescale, thus allowing the fully folded state to become predominantly populated.[418] For some proteins the stability of the misfolded state can be increased by point mutations. The folding process of the lambda repressor fragment $\lambda_{6\text{-}85}$, for instance, shows classical fast two-state kinetics, whereas its rather thermodynamically stable mutant (λQ33Y) was found to exhibit an additional slow phase where folding proceeds only on a millisecond time scale.[419, 420] The latter reflects a slowly decaying intermediate that was found to be rich in amyloid structure due to the presence of strong hydrophobic interacting intramolecular amyloids. Such kinetic traps have been found for the folding of many proteins, but frustrated states from which a protein cannot escape on a measurable time scale are difficult to discover, since most proteins presumably evolve to avoid this possibility. Some exceptions to this rule are

serine protease inhibitors (serpins) and viral membrane fusion proteins, which remain in metastable states prior to reactions with other components of their respective environment.[421]

In this chapter we report the discovery of what we consider to be a frustrated, misfolded state of cyt c, formed after exposing the oxidized protein to alkaline conditions for an extended period of time. We show that this state is very stable even after reintroduction to physiological conditions (pH 7.0). The majority of the proteins in these samples are predominantly monomeric at 0.05 mM, but form substantial fractions of soluble dimers and higher order oligomers at 0.5 mM, most likely due to domain swapping.[192, 416] Interestingly, fractions of this ensemble switch back into the reduced native state in a pH dependent manner. Upon the addition of potassium ferricyanide to the sample, the protein is oxidized completely. Moreover, the fraction of protein in the misfolded state undergoes a very slow transition back into the fully folded state when allowed to sit at physiological conditions (pH 7.0) for an extended period of time.

5.2 Results.

5.2.1 A non-native oxidized state stabilized at neutral pH. Oxidized cyt c was prepared by using the protocol described in Chapter 3. The oxidized protein was incubated at pH 11.5 and 4 °C for two hours before passing the sample over a PD Minitrap column pretreated with potassium ferricyanide. The protein concentration of the sample was 0.5 mM. Subsequently, we incrementally lowered the pH of the solution to various values between 8.0 and 4.5 and measured the corresponding optical absorption spectrum of the protein between 12,500 and 18,200 cm^{-1}. In this spectral region one expects only a weak band at 14,388 cm^{-1}, often referred to as the 695-nm band, now attributed to a $S(M80) \rightarrow d_{\pi}(Fe^{3+})$ rather than to an $a_{2u}(heme) \rightarrow d\pi(Fe^{3+})$ charge transfer transition.[422, 423] This band, denoted as CT1, is indeed displayed in all spectra shown in Figure 5.2.

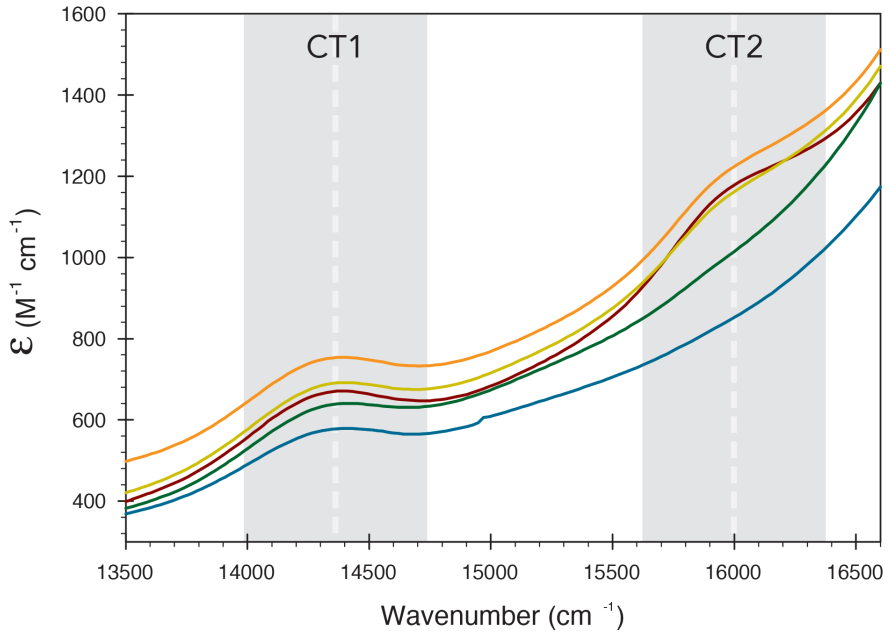

Figure 5.2. Charge transfer band region of the absorption spectrum of 0.5 mM ferricytochrome c (equine) measured between 13,500 and 17,000 cm^{-1} at ■ pH 5.0, ■ pH 5.5, ■ pH 6.0, ■ pH 7.0, ■ pH 8.0, in 0.1 mM potassium phosphate buffer. Prior to the measurement the oxidized protein was exposed to alkaline conditions (pH 11.5) for two hours. The charge transfer bands CT1 and CT2 are explained in the text.

Surprisingly, an additional weak band (CT2) appears at 16,000 cm^{-1} (625-nm) in the spectra measured below pH 6.0. Figure 5.3 shows the isolated CT1 and CT2 bands obtained after baseline subtraction (Figure 5.2). Apparently, the integrated intensity of CT1 is nearly pH independent, whereas the intensity of CT2 increases with decreasing pH. We analyzed the CT2 band using our spectral decomposition program MultiFit[424] and found that it can be fit with a single Voigtian band. Figure 5.4 shows the integrated intensity of CT2 as a function of pH.

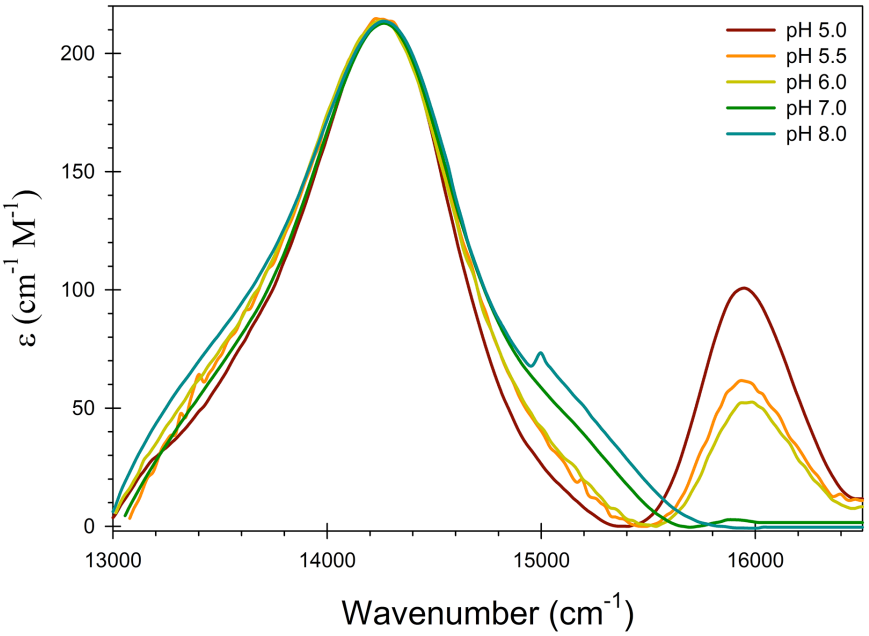

Figure 5.3. Baseline corrected absorption spectrum of horse heart ferricytochrome c measured between 13,000 and 17,000 cm^{-1} at the indicated pH. Prior to the experiment the oxidized protein was exposed to alkaline conditions (pH 11.5) for two hours.

The data clearly indicate a biphasic titration, which reflects the involvement of at least two amino acids with protonatable side chains. We fit the data using the titration model of Verbaro *et al.*,[217] which considered the influence of two different sets of interacting protonation sites

on the oscillator strength of optical transitions. For the pH dependent oscillator strength f_{CT2} this leads to the following equation:

$$f_{CT2}(pH) = \frac{f_{CT2}^{11}}{1+\left(\frac{K_1}{[H_3O^+]}\right)^{n_1}+\left(\frac{K_2}{[H_3O^+]}\right)^{n_2}+\frac{K_1^{n_1}K_2^{n_2}}{[H_3O^+]^{n_1+n_2}}} + \frac{f_{CT2}^{10}}{1+\left(\frac{K_1}{[H_3O^+]}\right)^{n_1}+\left(\frac{[H_3O^+]}{K_2}\right)^{n_2}+\frac{K_1^{n_1}}{K_2^{n_2}}} + \frac{f_{CT2}^{01}}{1+\left(\frac{K_2}{[H_3O^+]}\right)^{n_2}+\left(\frac{[H_3O^+]}{K_1}\right)^{n_1}+\frac{K_2^{n_2}}{K_1^{n_1}}} \quad [5.1]$$

This equation describes the two phases of the titration curve as cooperative processes, which involve the n_1 and n_2 protonations, respectively. The respective effective dissociation constants are K_1 and K_2. f_{CT2}^{11} is the oscillator strength of the final fully protonated state, f_{CT2}^{10} and f_{CT2}^{01} are the oscillator strengths of states in which one of the two considered groups is fully protonated. If $K_1 >> K_2$, the third term of the equation contributes only weakly to f_{CT2}. To avoid any ambiguities we assumed that $f_{CT2}^{10} = f_{CT2}^{01}$. The solid line in Figure 5.4 shows the fit to the data. The pK-values related to K_1 and K_2 are 4.70±0.07 and 6.40±0.01; for the Hill coefficients we obtained $n_1=1$ (fixed parameter) and $n_2=3.9\pm0.6$. The value of the first coefficient indicates that only a single protonation step is involved, the second number reflects a high degree of cooperativity. It should be noted that the statistical error for pK_1 was underestimated since correlations between K_1 and f_{CT2}^{11} have not been taken into account.

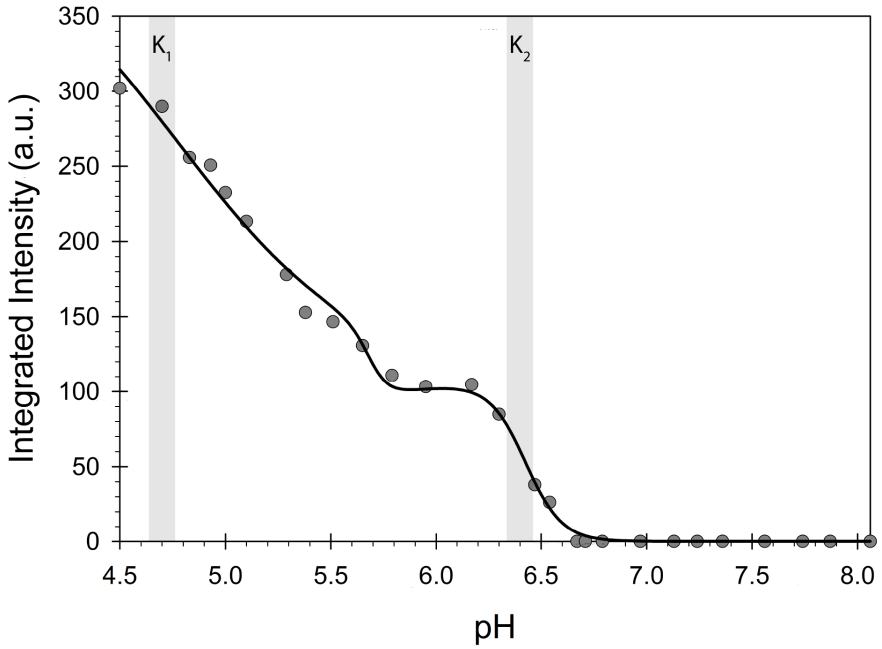

Figure 5.4: Integrated intensity of the CT2 band of horse heart ferricytochrome c incubated under oxidizing conditions at pH 11.5 for two hours plotted as a function of pH. The solid curve results from a fit explained in the text.

The above spectroscopic data suggest that our treatment of the protein caused the (weak) population of another state of cytochrome, which coexists with the native state *III* and changes upon the protonation of amino acid residues. The appearance of the CT2 band at acidic pH indicates that this state is at least partially unfolded. We designate it as M to indicate the misfolded character of the protein's state. We call the three protonation states considered in the above equation M_{11}, M_{10} and M_{01}. The deprotonated state is labeled as $M_{00.}$ The appearance of the CT2 band is generally diagnostic of a hexacoordinated high spin state (hchs).[425] However, as we will argue below, resonance Raman and optical absorption data suggest that an alternative assignment must be considered.

The simultaneous occurrence of CT1 and CT2 in spectra taken at acidic pH suggests a mixture of folded and partially unfolded proteins. The protonated M-states are formed by the

protonation of a yet undetected non-native state, $M_{00,}$ which coexists with the native state *III* at neutral pH. We wondered whether theses results might indicate a slow transition into state $M_{00.}$ In this case, we should be able to isolate this state by increasing the incubation time of the protein under alkaline conditions. Therefore, we incubated ferricytochrome c for 7 days at pH 11.5 prior to measuring its absorption spectrum between 12,500 and 18,200 cm^{-1} (550-800 nm) as a function of pH. The resulting spectra in Figure 5.5 lack the CT1 band, which clearly indicates the absence of the native state *III*. The CT2 band appears again at acidic pH. Isolated bands obtained by background subtraction are shown in Figure 5.6. We fit the above equation to the pH dependence of the integrated intensity of CT2 (Figure 5.7). The obtained pK values are 4.37±0.25 and 6.58±0.02, the Hill coefficients are $n_1 = 1$ and $n_2 = 3.9 \pm 0.7$. The oscillator strength $f_{CT\,2}^{11}$ of 2150 $M^{-1}\,cm^{-2}$ is an order of magnitude larger than the corresponding value of 194 $M^{-1}\,cm^{-2}$ obtained from data in Figure 5.4, which indicates that only a small fraction (10%) of the proteins adopt state M after a two hour incubation at alkaline pH.

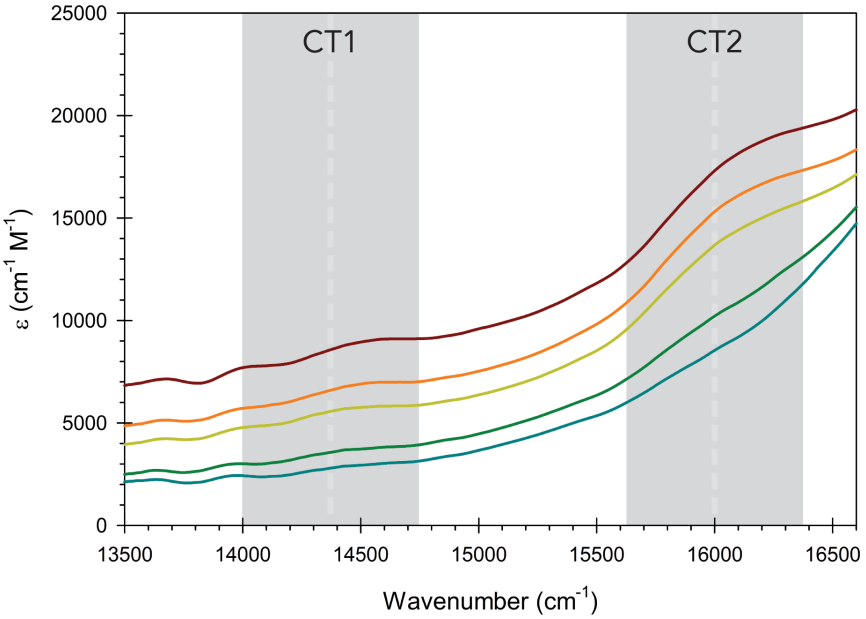

Figure 5.5. Charge transfer band region of the absorption spectrum of 0.5 mM ferricytochrome c (equine) measured between 13,500 and 17,000 cm^{-1} at ■ pH 5.0, ■ pH 5.5, ■ pH 6.0, ■ pH 7.0, ■ pH 8.0 in 0.1 mM potassium phosphate buffer. Prior to the measurement the oxidized protein was exposed to alkaline conditions (pH 11.5) for one week. The charge transfer bands CT1 and CT2 are explained in the text.

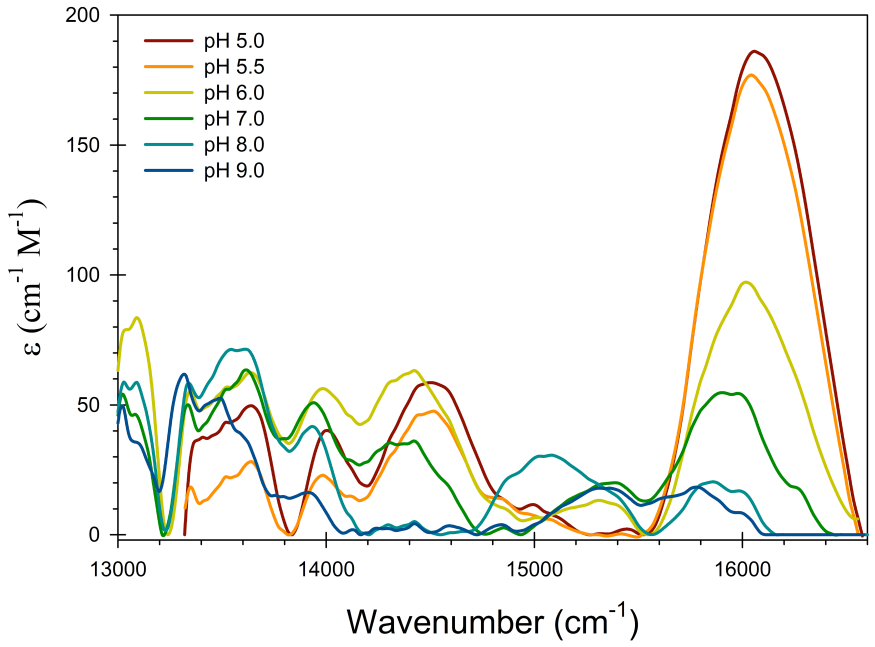

Figure 5.6. Baseline corrected absorption spectrum of horse heart ferricytochrome c measured between 13000 and 17000 cm^{-1} at ■ pH 5.0, ■ pH 5.5, ■ pH 6.0, ■ pH 7.0, ■ pH 8.0 in 0.1 mM potassium phosphate buffer. Prior to the experiment the oxidized protein was exposed to alkaline conditions (pH 11.5) for one week.

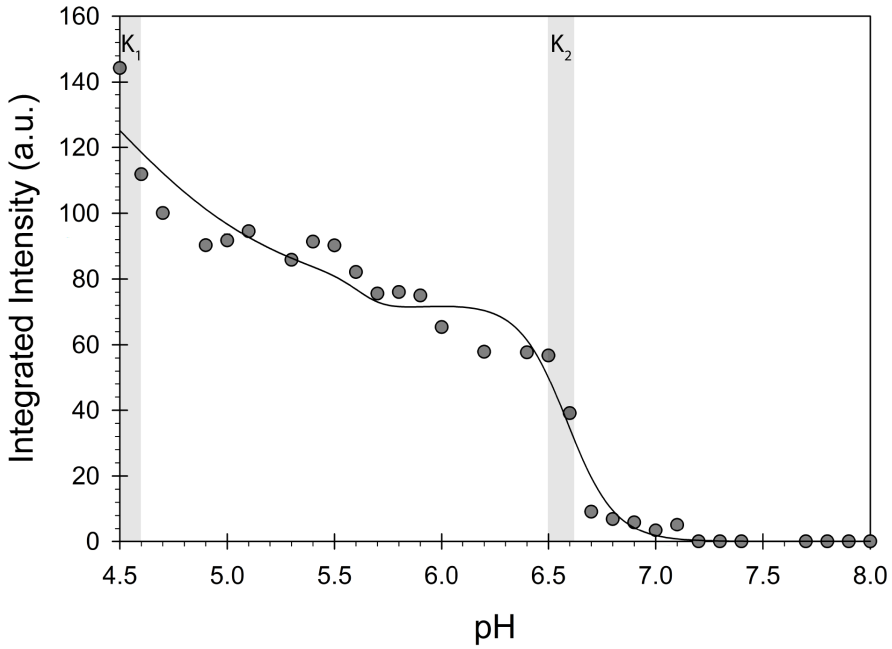

Figure 5.7. Integrated intensity of the CT2 band of horse heart ferricytochrome c incubated under oxidizing conditions at pH 11.5 for seven days plotted as a function of pH. The solid curve results from a fit explained in the text.

Figure 5.8 shows the visible CD and absorption spectra of the Soret band region, which were measured at pH 7 after exposing the oxidized protein for two hours and seven days to alkaline conditions (pH 11.5). The visible CD spectrum taken after two hours of incubation is still dominated by the classical couplet of the Soret band, which is indicative of an excited state splitting in protein state *III* due to a quadratic Stark effect induced by a very strong electric field in the heme plane.[426] The spectrum taken after one week oxidation, however, shows a positive Cotton band that nearly coincides with the absorption band. This indicates the reduced splitting typical for partially unfolded states of the protein.[427] The corresponding absorption band is broadened and upshifted. Taken together, the spectroscopic data unambiguously show that that the protein is now predominantly in one of the protonation states of M.

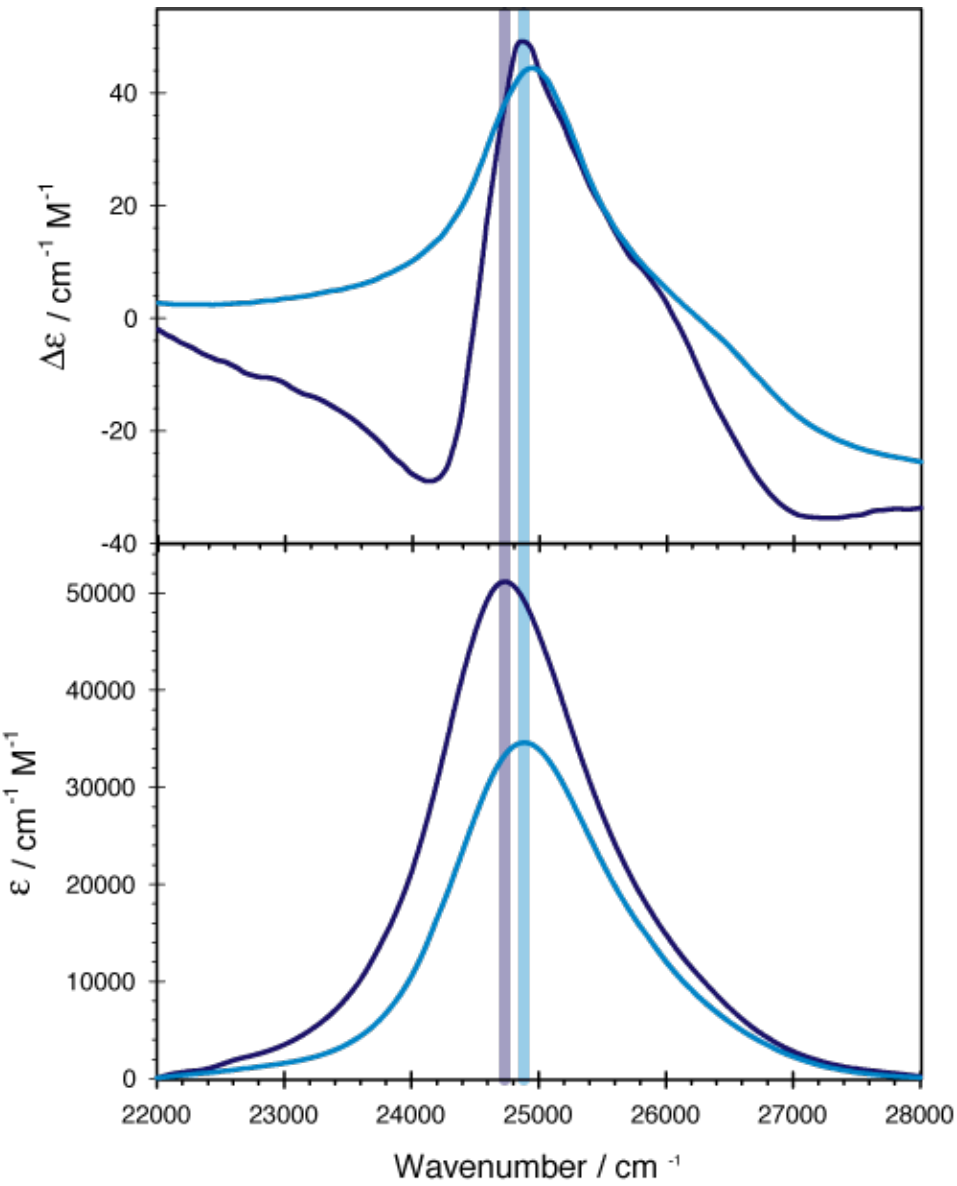

Figure 5.8. Circular dichroism (top) and absorption profile (bottom) of Soret band absorption of horse heart ferricytochrome c measured at the pH 7 after oxidation at pH 11.5 for two hours (■ purple line) and seven days (■ blue line) under refrigerated conditions (5°C).

5.2.2 Spectroscopic characterization of state M. To further characterize the different protonation states of M we measured the visible CD and absorption spectra of ferricytochrome at several pH values between 11.5 and 5 after a 7 day incubation period at pH 11.5. The protein concentration for these measurements was 0.05 mM. Figure 5.9 exhibits positive Cotton bands for all CD spectra. This confirms that non-native states are populated at all these pH-values. Interestingly, the intensities of the CD and the corresponding absorption bands are reminiscent of the respective band intensities that Hagarman et al. reported for state *V* of ferricytochrome c. This state exhibits much higher Soret band absorption and CD intensities than the alkaline state *IV* or the native state *III*.[207, 233] The CD profiles measured between pH 6 and 12 are all very similar, suggesting that the heme environment does not drastically change in this pH range. At pH 5, the CD-band profile is clearly composed of two bands, which are red- and blueshifted with respect to the position measured for the other pH values. The corresponding absorption spectrum is blueshifted, but does not coincide with the more intense sub-band of the CD profile. This could be indicative of the population of either a pentacoordinated high spin ferric (pchs) state or, as we will argue below, of a pentacoordinated quantum mixed (PcQM) state of the heme iron.[10] This conformational change at acidic pH is reminiscent of the $M_{00} \rightarrow M_{01/10} \rightarrow M_{11}$ transitions inferred from the appearance of the CT2 band in the 12,500 and 18,200 cm^{-1} region of the optical spectrum recorded with a 0.5 mM sample. It is difficult to infer the band from the spectrum of a sample with 0.05 mM concentration (Figure 5.10), since this concentration is too low for probing weak charge transfer bands.

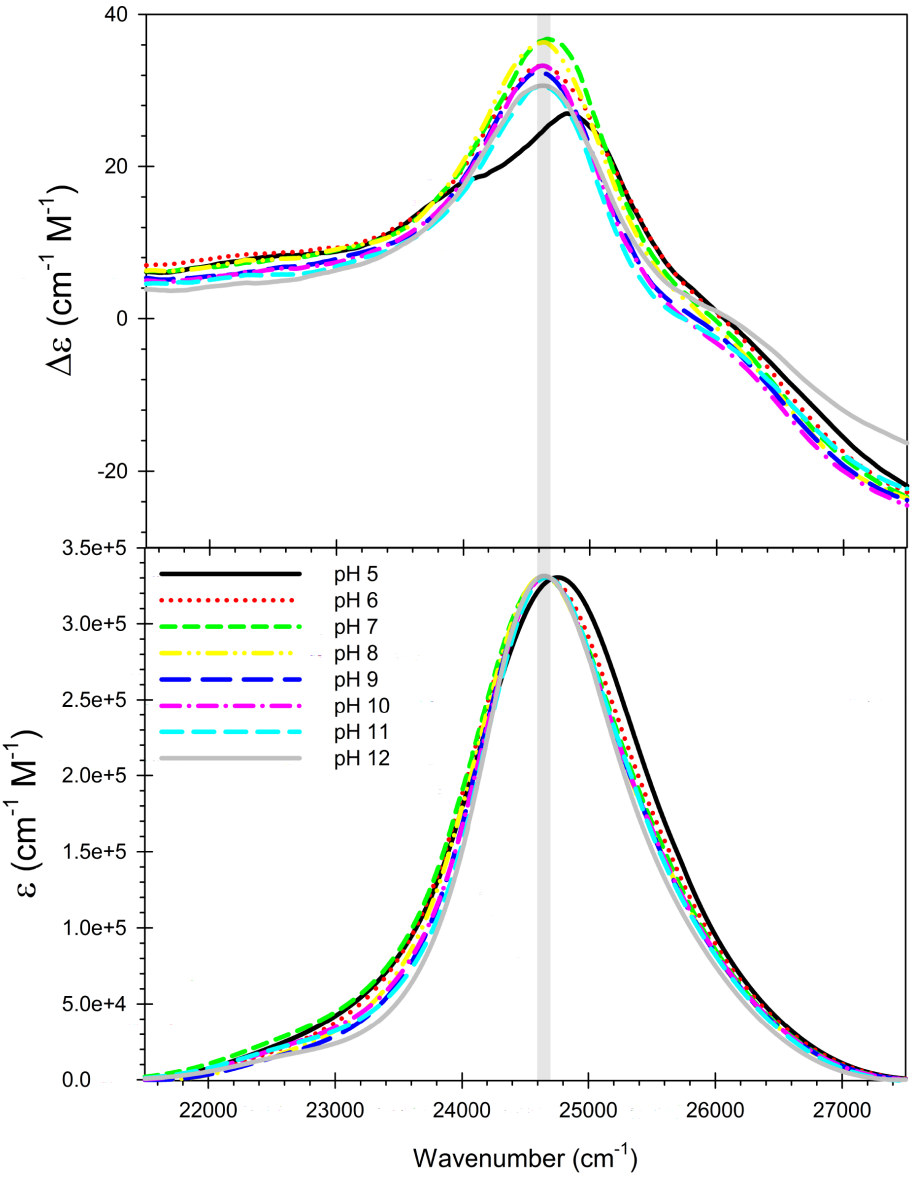

Figure 5.9. Circular dichroism (top) and absorption profile (bottom) of Soret band absorption of 0.05 mM horse heart ferricytochrome c measured at the indicated pH. Prior to the measurements, cyt c was subjected to oxidizing conditions for seven days at pH 11.5.

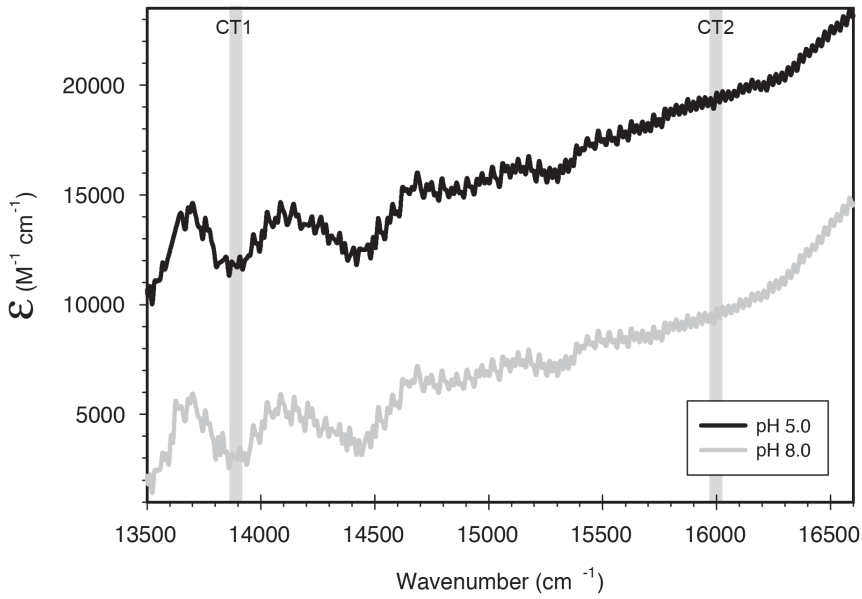

Figure 5.10. Charge transfer band region of the absorption spectrum of 0.05 mM ferricytochrome c (equine) measured between 13,500 and 16,600 cm^{-1} at ■ pH 5.0, and ■ pH 8.0 in 0.1 mM potassium phosphate buffer. Prior to the measurement the oxidized protein was exposed to alkaline conditions (pH 11.5) for one week. The charge transfer bands CT1 and CT2 are explained in the text.

The non-coincidence between absorption and CD profile indicates band splitting due to electronic perturbations.[428] The low-wavenumber component of the CD spectrum does not have a discernible counterpart in the absorption spectrum. It is suspiciously close to the positive maximum observed in the CD spectrum of intact ferrocytochrome c, which is slightly redshifted from the peak position of the respective absorption band.[426] The other absorption spectra are all slightly blueshifted from the peak position in the spectrum of native ferricytochrome c. This is consistent with a hexacoodinated low spin state.[429]

Ferricytochrome c in solution is known for its ability to adopt a variety of non-native conformations at non-physiological pH or on the surface of anionic liposomes, in which the secondary structure is predominantly maintained.[140, 176, 227, 286, 430-434] In order to probe the secondary structure of our M-states we measured the UV-CD spectra at the same pH and the

same protein concentration used for the recording of the visible CD spectra. As shown in Figure 5.11, they clearly reveal a substantial fraction of predominantly helical secondary structure. This interpretation is confirmed by a more quantitative analysis performed with DichroWeb,[435, 436] using the CDSSTR[437] method with SP175 reference set (Figure 5.12).[438] The obtained helical fraction of ca. 0.45, which is nearly pH-independent between pH 4 and 12 and drops only at pH 13, is even slightly higher than the 40% helical fraction of the native state.[439] At pH 13, the protein unfolds into statistical coil. The very weak negative maximum in the spectrum of the latter (1.9 mM cm^{-1} per residue) actually suggests a random coil state with very reduced polyproline II content.[440, 441]

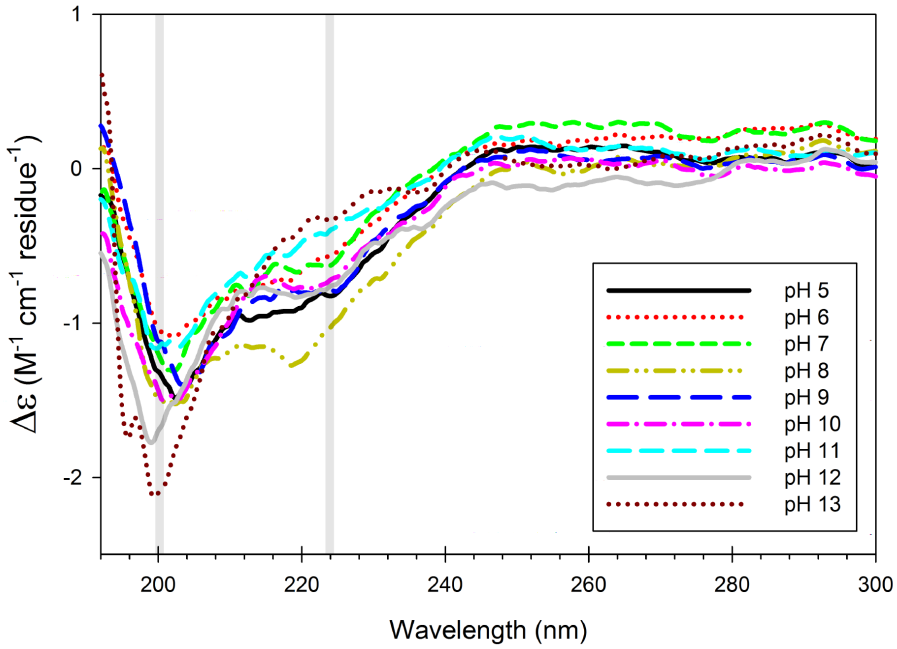

Figure 5.11. UV circular dichroism spectra 0.05 mM horse heart ferri-cyt c measured at the indicated pH. Prior to the measurements, cyt c was subjected to oxidizing conditions for seven days at pH 11.5.

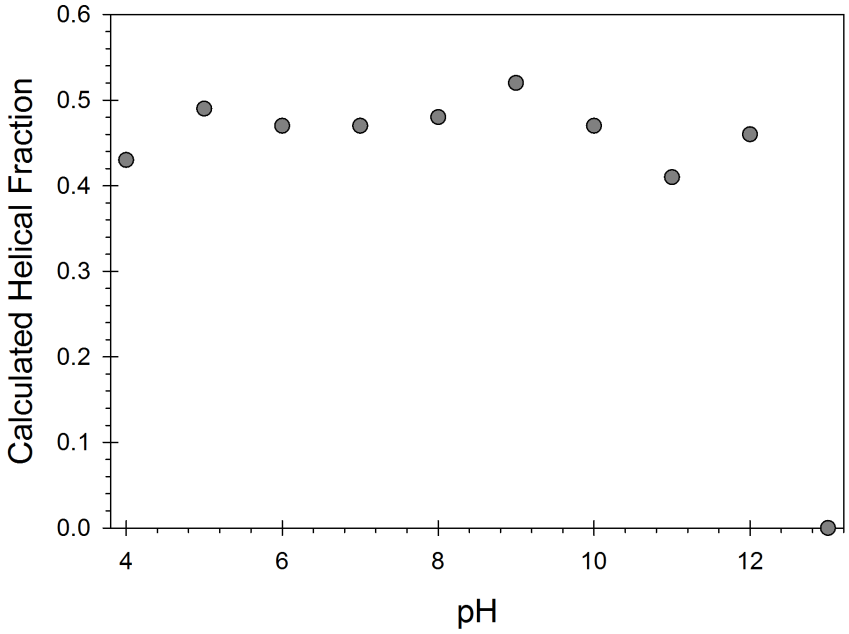

Figure 5.12. pH dependence of the α-helical content of 0.05 mM ferricytochrome c after a one week incubation at pH 11.5. This information was obtained from UV-CD spectra of the sample as described in the main manuscript.

Uversky showed that a so called "double-wavelength plot" of $\Delta\varepsilon_{222}$ versus $\Delta\varepsilon_{200}$ can be utilized to further characterize the state of proteins (the author used the molar ellipticities $[\theta]_{220}$ and $[\theta]_{200}$; we prefer the physically easier to interpret $\Delta\varepsilon$ representation).[442] The author found that the data cluster in regions that can be identified as coil-like, pre-molten globule, molten globule and globular. As shown in Figure 5.13, our data inferred from the spectra in Figure 5.11 all cluster in the transition region between the pre-molten globule and the globular region. This suggests a disordered state that lacks some of the native tertiary structure but still exhibits order on the secondary structure level, confirming again the notion that the helices of cytochrome c are very stable.

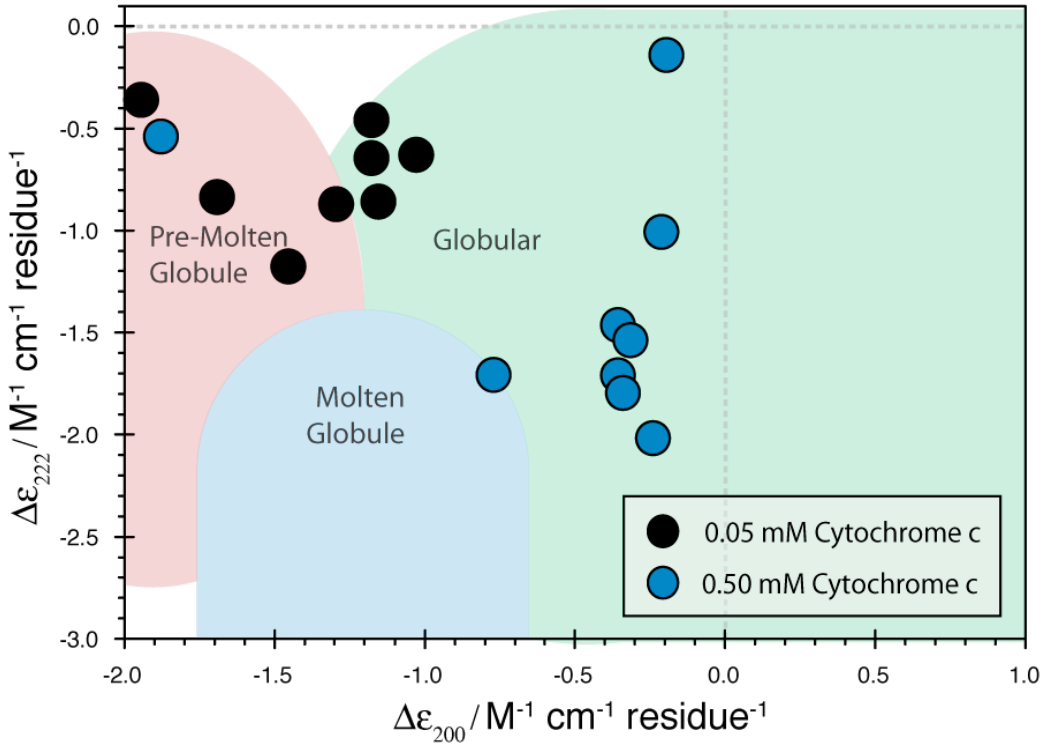

Figure 5.13: Analysis of UV circular dichroism spectra of 0.05 mM (● black) and 0.5 mM (● blue) horse heart ferricytochrome c taken at different pH by means of a double wavelength plot ($\Delta\varepsilon_{222}$ versus $\Delta\varepsilon_{200}$) as introduced by Uversky.[442] For all spectra analyzed, cyt c was subjected to oxidizing conditions at pH 11.5 for seven days. The different colored areas of the plot indicate location of $\Delta\varepsilon_{222}$, $\Delta\varepsilon_{200}$ pairs associated with pre-molten globule, molten globule, and globular structures.

We attempted to probe the resonance Raman spectrum of 0.05 mM state M ferri-cyt c at pH 5 and 7. Since our Raman microspectrometer does not allow the recording of spectra in the resonance region of the B-band (Soret) with a sufficiently good signal to noise ratio, we used the 488 and 514 nm excitation of our ArKr laser, which provides pre-resonance excitation. At 488 nm we were able to identify the peak of the ν_4-band at 1371 cm^{-1} (Figure 5.14), which indicates an oxidized state slightly upshifted with respect to the fully folded state of cyt c. The ν_{10}-band, at both 488 and 514 nm excitation was discernible at 1638 cm^{-1} (Figure 5.14 and 5.15), indicative of a low spin hexacoordinated state or possibly a quantum mixed state, which will be discussed below. The ν_2-band under 514 nm excitation was discernible at 1587 cm^{-1}

(Figure 5.15), clearly indicating a low-spin hexacoordinated state as well. The slight upshift in frequency from the fully folded state (~3 cm^{-1}) suggests a low spin hexacoordinated bis-His complex.[443] In all cases there was no trace of a high spin heme iron found.

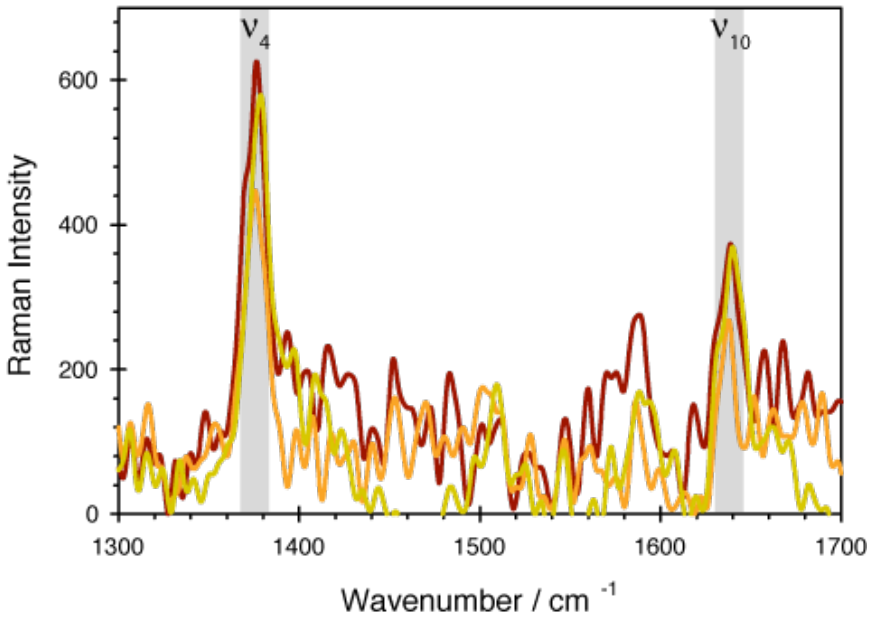

Figure 5.14. Polarized resonance Raman spectra (x-polarized) of 0.05 mM ferricytochrome c measured at pH 5.0 (■ red line), 7.0 (■ orange line) and 11.5 (■ yellow line) after the protein was subjected to oxidizing conditions at pH 11.5 for 7 days, taken with 488 nm excitation at an integration time of 150 s, showing an average of five spectra.

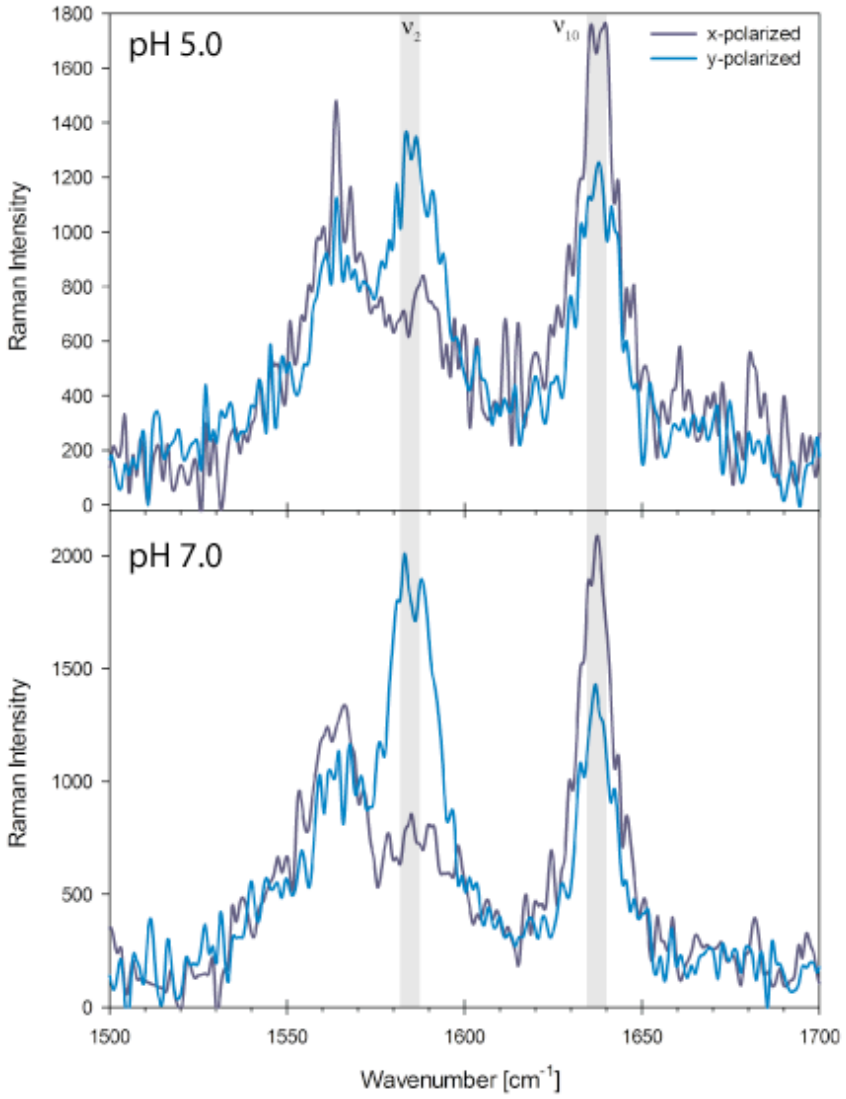

Figure 5.15. Polarized resonance Raman spectra of 0.05 mM ferricytochrome c measured at pH 5.0 and 7.0 after the protein was subjected to oxidizing conditions at pH 11.5 for 7 days, taken with 514 nm excitation with an integration time of 100 s.

5.2.3 Checking for chemical modifications. We have clearly shown that a very slow conformational transition into a stable misfolded state of the protein occurs if one allows oxidized cyt c to remain at pH 11.5 for a week. To check the stability of this transition we recorded another series of CD spectra after allowing the samples to stay for another week at their respective pH values. The CD spectra depicted in Figure 5.16 show that no significant changes had occurred. One might therefore suspect that our findings reflect irreversible unfolding due to chemical modifications of the protein rather than a conformational transition into a metastable state. It is known, for instance, that cyt c, if exposed to alkaline solutions, can form up to 15 deamidated species with conversion of asparagine and glutamine into asparaginyl and glutaminyl.[444] The most abundant deamidated species show a loss of the amides in the asparagine located at positions 52 and 54 of the protein. We checked our sample for deamination by using a cation-exchange resin at neutral pH and found no indication for deamination (this was performed as a courtesy by Dr. Carmichael Wallace, data not shown). Another possible chemical modification is hydrolyzation, which would produce protein fragmentation. If this had indeed occurred, one would expect a significant change of the secondary structure composition of our sample, since protein fragments would more likely be in a random or statistical coil state. To demonstrate this we subjected cyt c to an alkaline hydrolysis, with conditions described in Chapter 3. When the protein was allowed to fully hydrolyze, the color of the sample converted from rust-colored to a green, viscous solution, which is clearly at variance with the spectra observed after one-week oxidation at alkaline pH. In order to check whether the recorded spectra could reflect partial hydrolysis, we probed the secondary structure of the sample subjected to hydrolyzing conditions as a function of time by measuring UV-CD spectra of aliquots removed every 10 minutes (Figure 5.17). We found that even the CD spectra taken after 10 minutes strongly suggest a statistical coil-like structure.

This is in significant contrast to the UV-CD spectra of oxidized misfolded cyt c shown and discussed above (Figure 5.11).

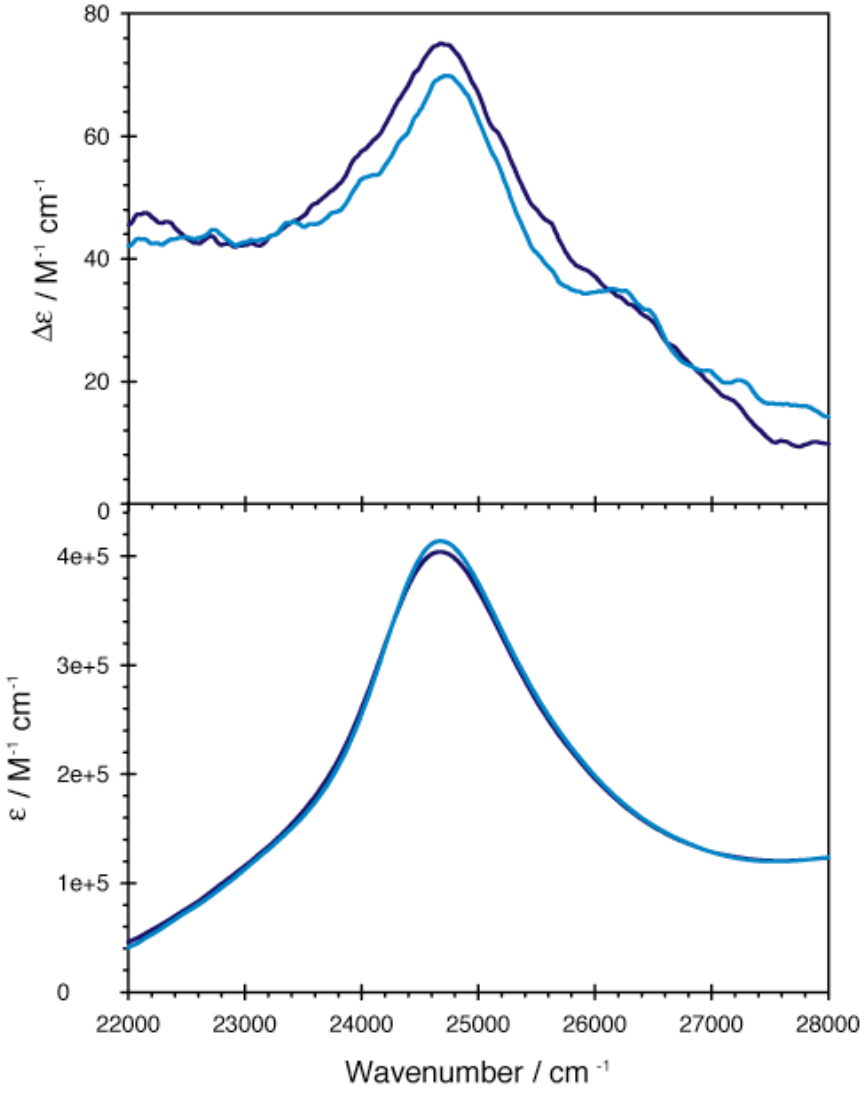

Figure 5.16. Visible CD (top) and absorption (bottom) spectra of the Soret band region of ferricytochrome c recorded at pH 7 after the protein was exposed to alkaline conditions (11.5) for one week (■ violet line) and after it was allowed to sit at pH 7 for an additional week (■ blue line).

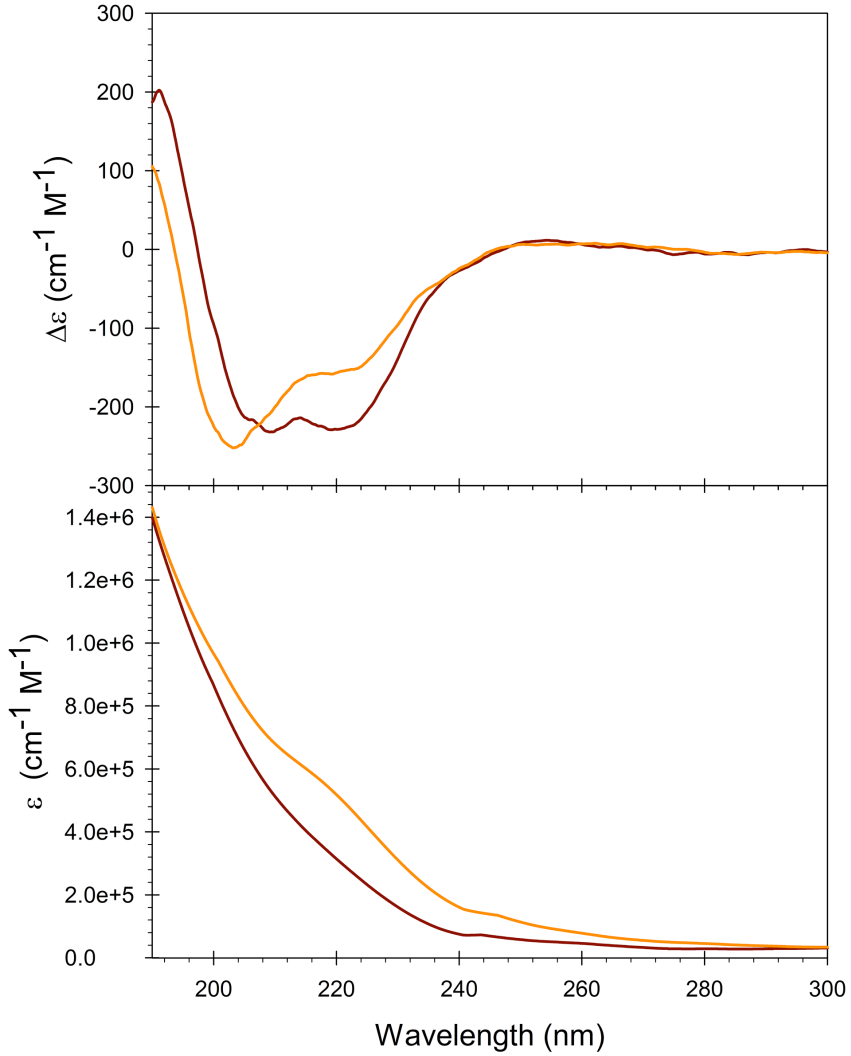

Figure 5.17. UV-CD (top) and absorption spectra (bottom) of ferricytochrome c at pH 11.5 recorded at room temperature (■ red line) and after 10min at 373K (■ orange line) under alkaline hydrolysis conditions.

To verify that our results are not caused by modifications of cyt c due to bacterial contamination of our sample, we added a drop of toluene as a bacteriocide at the start of the one-week incubation period pH 11.5. This did not lead to any significant changes of CD and absorption spectra (Figure 5.18).

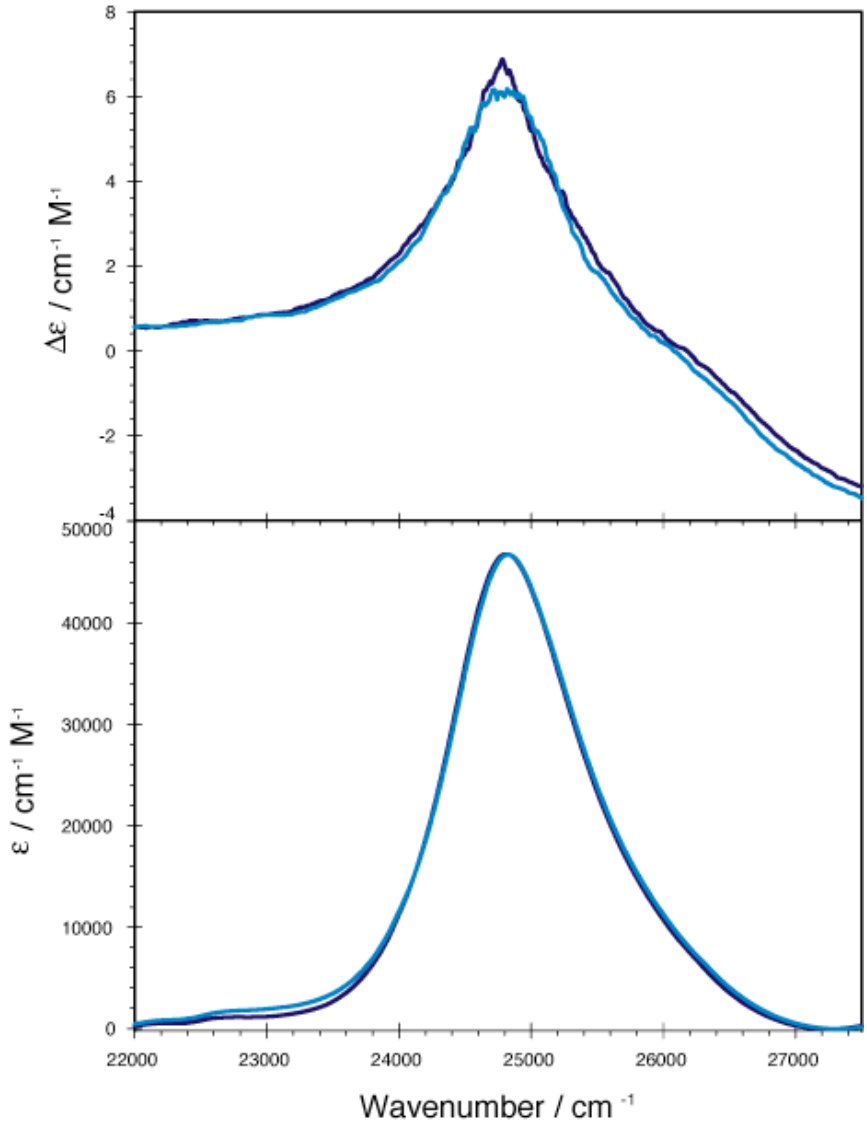

Figure 5.18. Visible CD (top) and absorption (bottom) spectra of the Soret band region of ferricytochrome c recorded at pH 11.5 after the protein was exposed to alkaline conditions (11.5) for one week (■ violet line) and with a drop of toluene (■ blue line) to determine if bacterial contamination was altering the sample.

Altogether our tests show that the conformational transition induced at alkaline pH is not due to the discussed chemical modifications of the protein. Another possible chemical change, i.e. the oxidation of the M80 ligand, is discussed below.

5.2.4 Protein aggregation. The newly discovered M_{00} state still resembles the partially unfolded alkaline state *V*.[427] As unfolded or misfolded kinetic intermediates, this state is prone to aggregation into soluble dimers and higher order oligomers.[445] Therefore the question arises whether protein oligomers are formed under our experimental conditions. One might even go a step further by invoking the idea that irreversible aggregation is the prime reason for the population of state M. In order to check for protein aggregation of our seven-day-incubation, 0.05 mM sample, we carried out native gel electrophoresis to determine the molecular weight distribution as a function of pH, shown in Figure 5.19. The samples are dominated by protein monomers at all pH values investigated. A small fraction of dimers, however, indicates that soluble oligomers are indeed formed. This result clearly shows that oligomerization cannot be the cause for the formation of M, and that its spectroscopic properties depicted in Figures 5.9 and 5.11 are assignable to the monomeric protein. Furthermore, it reaffirms the notion that the protein has not undergone fragmentation due to hydrolysis.

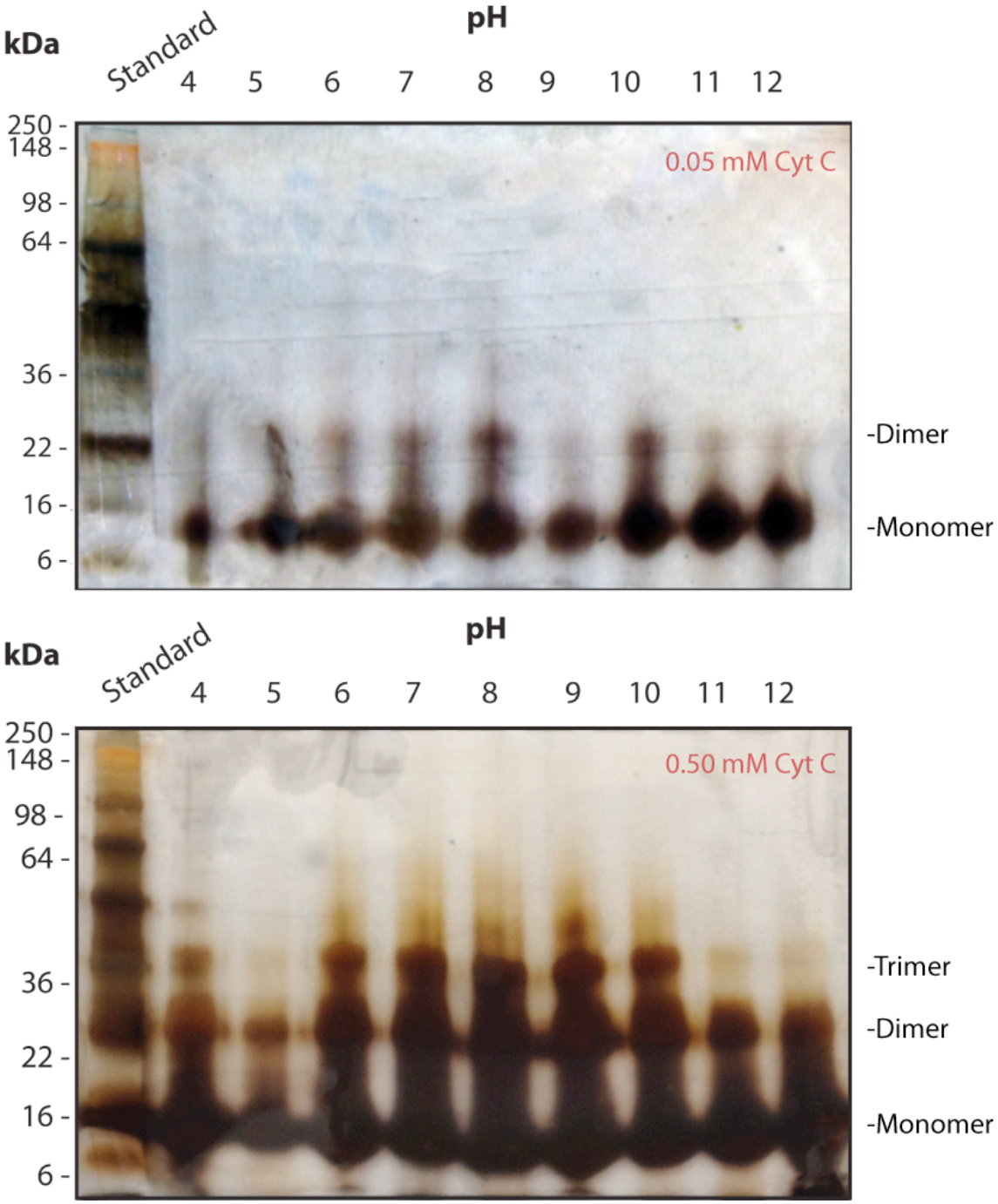

Figure 5.19. Images from gel electrophoresis of 0.05 mM (upper figure) and 0.5 mM horse heart ferricytochrome c (lower figure). The procedure was carried out after the protein was subjected to oxidizing conditions at pH 11.5 for seven days.

Protein aggregation should be concentration dependent. The low concentration of cyt c aggregates formed at 0.05 mM does not allow us to obtain the secondary structure of the observed dimers. Therefore we repeated the above set of experiments (absorption, visible and UVCD, gel electrophoresis) with a 0.5 mM solution of ferricytochrome c after a seven day incubation at pH 11.5. The result of gel electrophoresis shown in Figure 5.19 reveals a mixture of monomers, dimers and trimers. Oligomerization appears to be maximal in the pH-range between 6 and 10, whereas the monomeric form remained dominant under acidic (5) and alkaline conditions (11, 12). The corresponding UVCD spectra are shown in Figure 5.20. They are very similar to the UVCD spectrum of the native protein,[207] which is clearly indicative of nearly intact secondary structures. This is confirmed by the result of our DichroWeb analysis displayed in Figure 5.21. The $\Delta\varepsilon_{222}$, $\Delta\varepsilon_{200}$ coordinates in the Uversky plot in Figure 5.13 are now in the globular region, which corroborates the notion of very limited structural disorder in the oligomers. We can therefore conclude that the observed aggregation of cyt c does not involve the formation of β-sheet protofibrils. The interconversion of monomers and polymers in cyt c had been originally discovered by Margoliash et al. over 50 years ago.[245] More recently cyt c was found to form amyloid fibrils similar to those related in neurodegenerative diseases.[446] Due to this connection the mechanism of the protein structural change has experimentally gained a great deal of attention.[447-449] Recent work by the Hirota group reported the crystal structure of cytochrome c dimers and trimers formed by adopting the protocol of Margoliash and Lustgarten. These crystal structures revealed that cyt c polymerization occurs by successive domain swapping of the C-domain.[191, 192, 450] In view of the fact that the secondary structure of cytochrome c remains intact in the observed oligomers we propose that domain swapping is the likely mechanism leading to the formation of oligomers in our 0.5 mM samples.[192, 451]

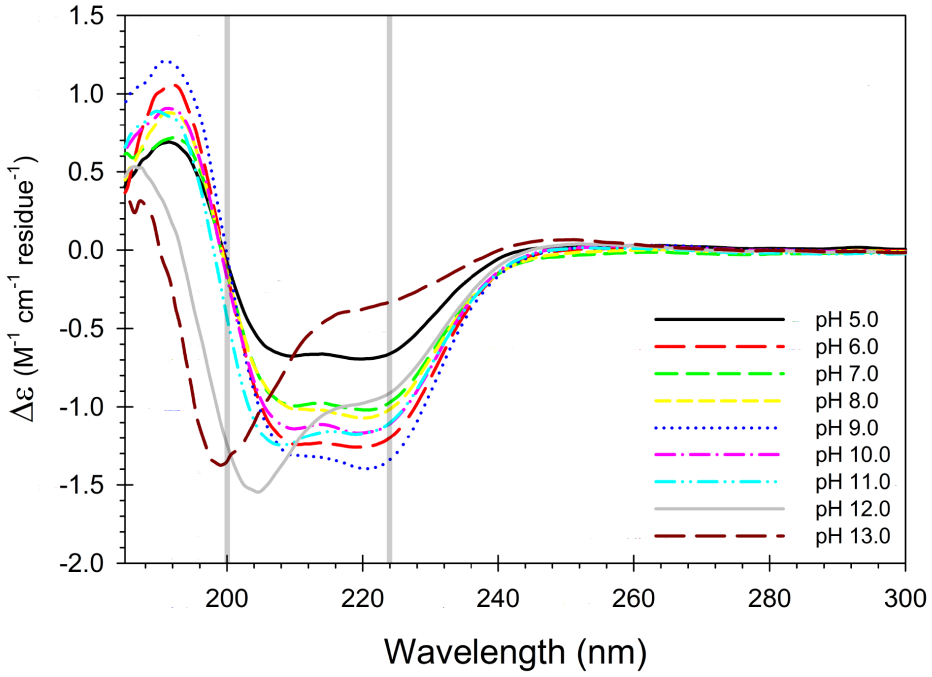

Figure 5.20. UV Circular dichroism spectra 0.5 mM horse heart ferricytochrome c measured at the indicated pH. Prior to the measurements, cyt c was subjected to oxidizing conditions for seven days at pH 11.5.

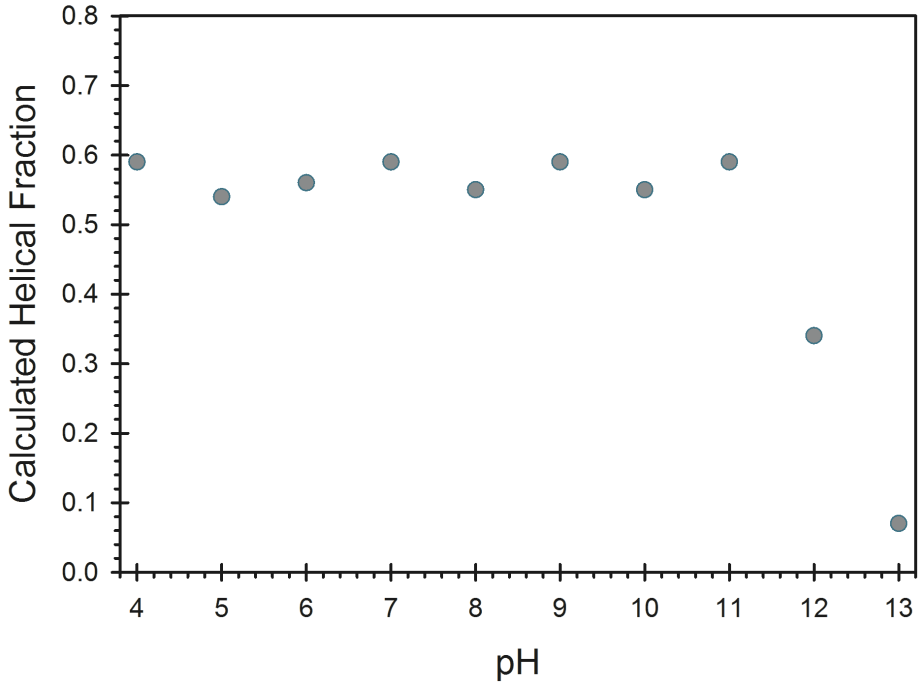

Figure 5.21. Secondary structure comparison of 0.05 mM Cyt c after being oxidized for a week at pH 4 through 13, analysis made utilizing DichroWeb[41, 42] using the CDSSTR method[43] with SP175 reference set.[44]

The visible CD and absorption spectra are rather complicated (Figure 5.22). Due to the highly pH-dependent visible Q-band spectra (Figure 5.23). The spectra taken at pH 7.0 through 10.0 all reflect a substantial amount of reduced cyt c suggesting that a fraction of proteins in our sample have switched back into the native state. However, the initial protocol had removed potassium ferricyanide by means of a Sephadex column after a short oxidation period at alkaline pH. The Q-band region of reduced cytochrome exhibits a clear separation of Q_0 and Q_v, with a higher peak intensity of the former,[452] whereas Q_0 and Q_v merge into one single band in the spectra of all ferricytochrome c species, owing to the reduced life time of the respective excited states.[423] A comparison of the spectra in Figure 5.23 and the electrophoresis result displayed in Figure 5.19 suggests a correlation between oligomer formation and reduction. We therefore subjected 0.5 mM sample of the protein to size exclusion chromatography as described in Chapter 3. The Q-band spectra of different fractions are exhibited in Figure 5.24. Apparently, the slower fractions (monomers and dimers) contain the highest fraction of reduced cyt c.

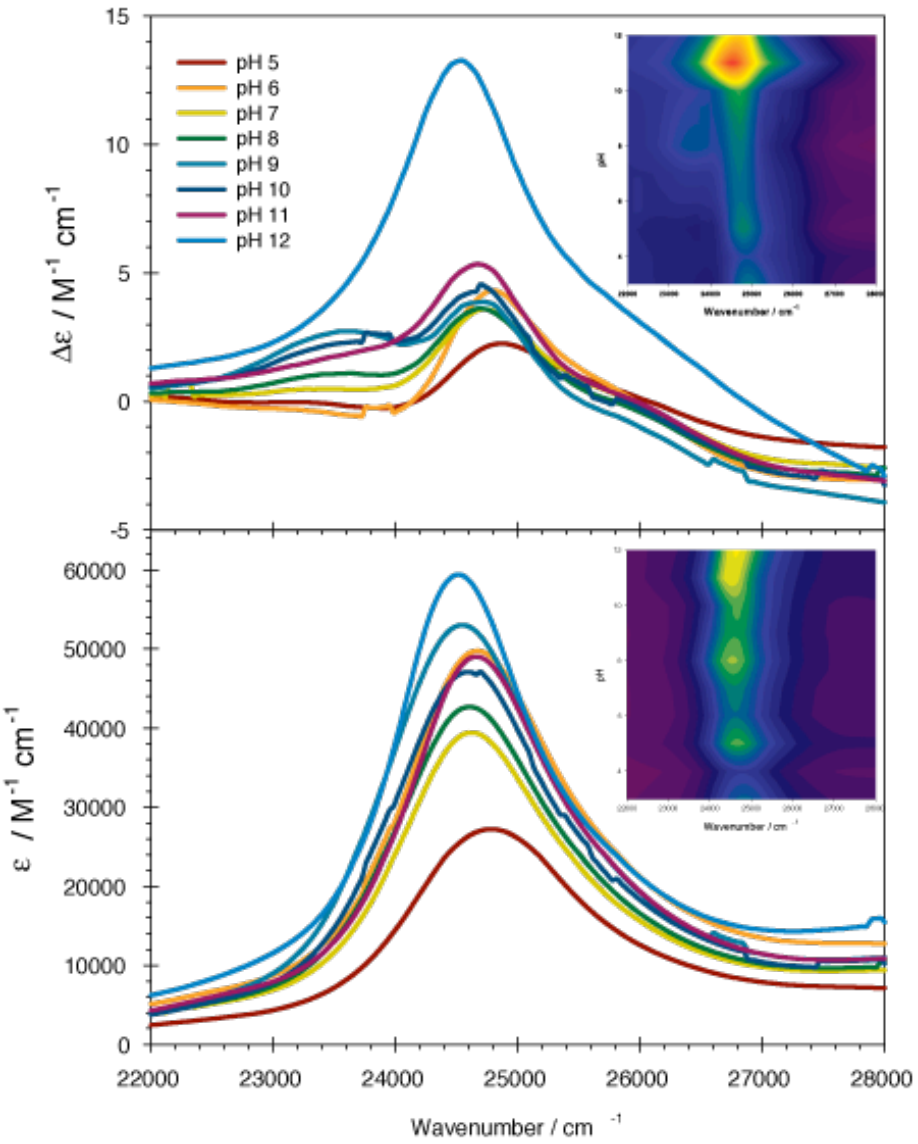

Figure 5.22. Visible CD (top) and absorption (bottom) spectra of the B-band (Soret) region of 0.5 mM ferri-cyt c measured at the indicated pH after the protein was subjected to oxidizing conditions at pH 11.5 for a week. Inset shows 2D plots of the CD and absorption spectra in the B-band region as a function of pH.

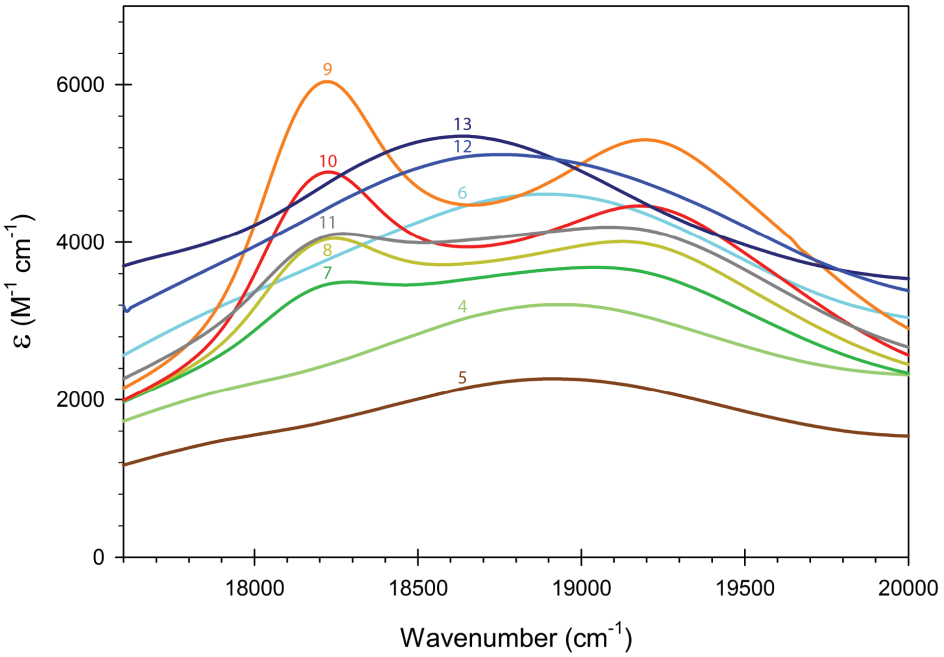

Figure 5.23. Q_0/Q_v-band spectrum of 0.5 mM ferricytochrome c measured at the indicated pH after the protein was subjected to oxidizing conditions at pH 11.5 for a week.

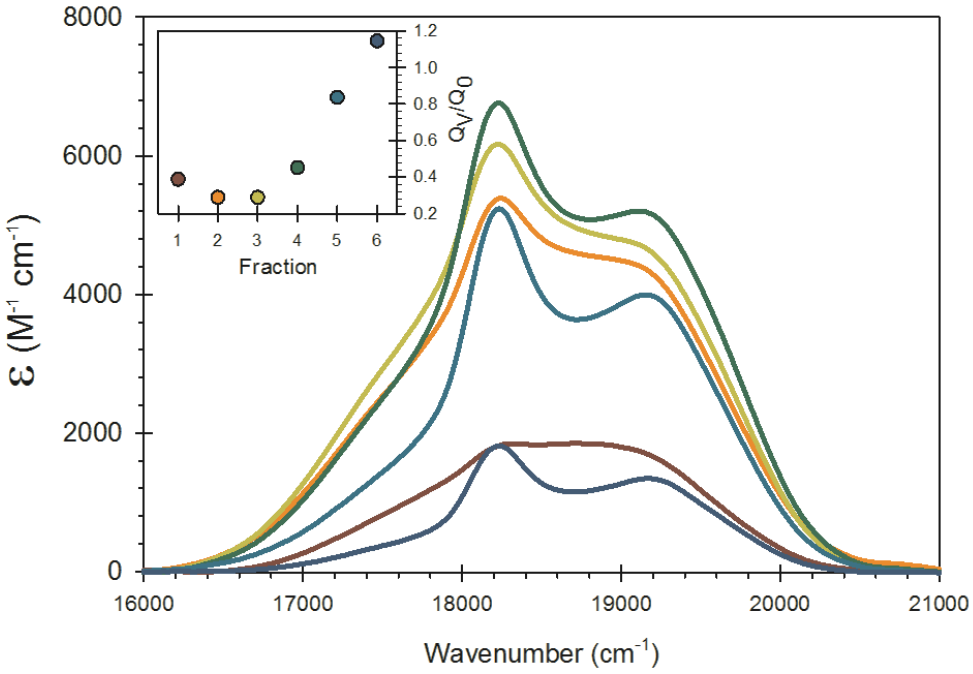

Figure 5.24. Baseline corrected absorption spectra in the Q-band region of 0.5 mM cyt c after being oxidized for a week at pH 11.5. Inset show ratio of Q_v/Q_0 for each aliquot sampled through the Sephadex column.

We measured the polarized resonance Raman spectrum of the 0.5 mM solution of ferricytochrome c after the 7-day incubation period at different pH between 5 and 12, using the 442 nm excitation of our HeCd laser which provides pre-resonance B-band excitation. Overlaid spectra of x-polarized scattering are shown in Figure 5.25. Two bands are clearly displayed in the ν_4, ν_3 and ν_{10} regions of the spectrum, which are diagnostic of a coexistence of reduced and oxidized species.[453] We normalized the spectra onto the y-component of ν_{21} at 1311 cm^{-1} and subsequently subjected all spectra to a self-consistent analysis by decomposing them into Lorentzian profiles with identical wavenumber positions and halfwidths for the same bands in different spectra. All spectra are describable as a superposition of bands from oxidized and reduced hcls-species.[453-456] The wavenumber positions of the classical marker modes of the oxidized species in Table 1 reveal a hcls-state, in agreement with what we inferred from the absorption spectra of the 0.05 mM sample. Figure 5.26 shows the relative intensity ratio of $I_{red}(\nu_4) / I_{ox}(\nu_4)$ as a function of pH. The plotted data clearly indicate that the fraction of reduced cyt c becomes maximal at pH 9.00. The reason for this pH redox coupling is not yet understood

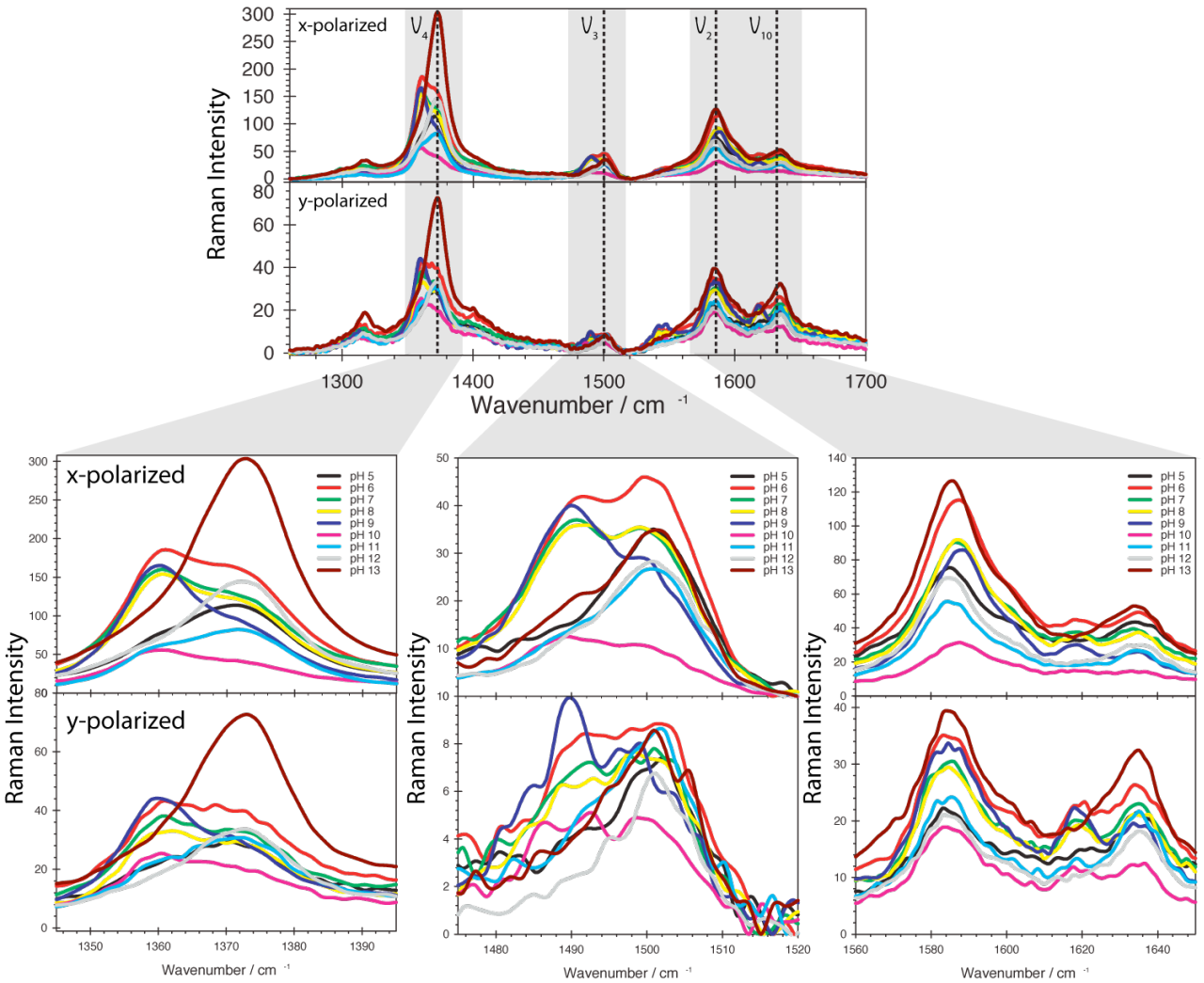

Figure 5.25. Resonance Raman spectra of 0.5 mM ferricytochrome c measured at the indicated pH after the protein was subjected to oxidizing conditions at pH 11.5 for 7 days. Shown is the average of five spectra using 442 nm excitation.

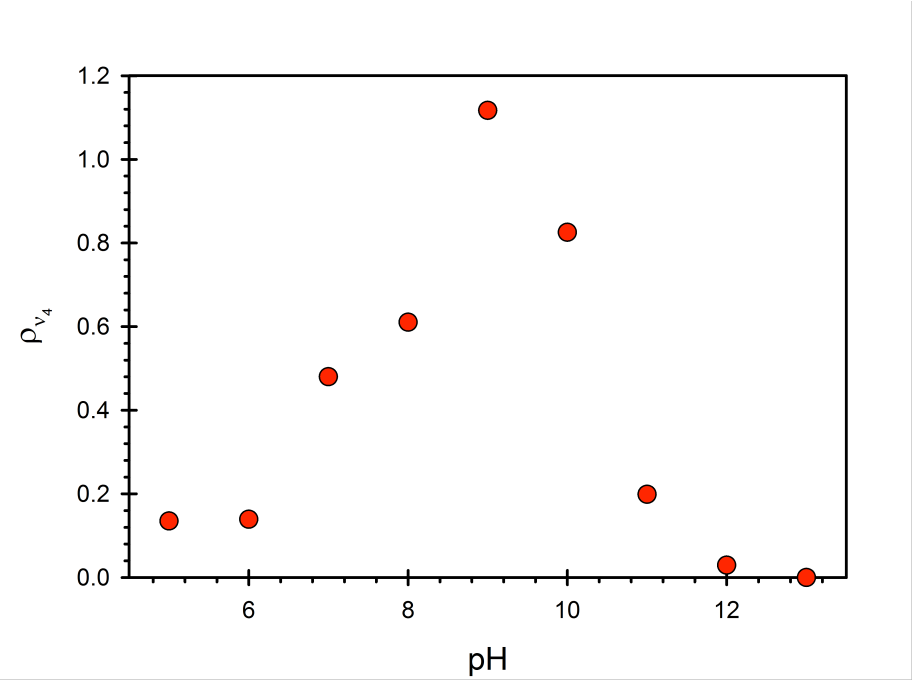

Figure 5.26. Ratio of integrated relative intensities of the reduced and oxidized ν_4 bands ($I_{\nu4(reduced)}/I_{\nu4(oxidized)}$) for the 0.5 mM sample of cyt c obtained after subjecting the proteins to oxidizing conditions at pH 11.5 for seven days. The data were obtained from a decomposition of the spectra exhibited in Figure 5.25.

Figure 5.27 shows the depolarization ratios (DPR) for the oxidized and reduced components of the ν_4 and ν_{10} bands. All DPRs of ν_4 are substantially above the D_{4h}-expectation value of 0.125, thus indicating the presence of B_{1g}/B_{2g}-type deformations. These two types of static deformations can be discriminated since they have a different impact on B_{1g}-modes. The fact that the DPRs of ν_{10} is lower than the D_{4h} expectation values of 0.75 suggests an A_{1g}-admixture to the Raman tensor and thus a B_{1g}-deformation. It has been argued earlier that a rhombic deformation of this symmetry type can be induced by a static Jahn-Teller effect involving the ground state of the ferric heme iron, which is of *E*-symmetry in hcls complexes. In high spin complexes the ground state symmetry is *A* and as a consequence, the DPRs of ν_4 are closer to 0.125.[457] Within the limits of accuracy the DPRs of ν_4 and ν_{10} are pH independent

for both oxidation states. The ν_4 DPRs of the reduced state are slightly lower than the corresponding values of the oxidized state, but somewhat higher than the values earlier obtained for the monomeric fully folded ferrocytochrome c. This might be indicative of additional B_{1g}-type deformations, but it should be mentioned that the DPR presented here are subject to substantial statistical errors owing to overlap of bands from the two redox states.

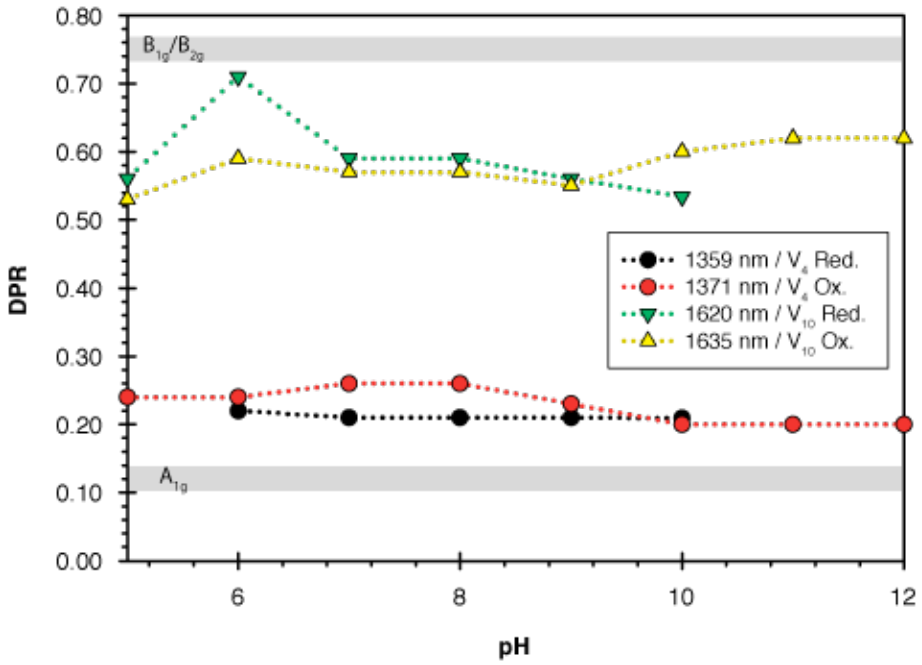

Figure 5.27. Depolarization ratio (DPR) of the ν_4 and ν_{10} bands for the 0.5 mM sample of cyt c obtained after subjecting the proteins to oxidizing conditions at pH 11.5 for seven days. The data were obtained from a MultiFit decomposition of the spectra exhibited in Figure 5.25. The DPR in an ideal D_{4h} symmetry is shown in gray.

Thus, the Raman data confirm the mixture of reduced and oxidized proteins, which we inferred from the Q-band absorption spectra. Since the reduced state of cyt c requires M80 as axial ligand, its occurrence rules out the possibility that state M is associated with the oxidation of the sulfur atom in M80. The possibility of such a modification of the M80 side chain is suggested by experiments that revealed the oxidation of the sulfur of free methionine into sulfoxide or an α-keto acid derivative at alkaline conditions.[458, 459]

5.2.5 Reversibility of the M state. The data reported thus far clearly show the very slow conformational transition that occurs if one allows oxidized cyt c to remain at pH 11.5 for a week. Figure 5.28 shows this transition at pH 7 from the native state (shown in red) to the aforementioned misfolded state (shown in orange). To determine if this was a completely irreversible state we collected an additional series of CD spectra taken at 0.5 mM but allowing the samples to stay at their respective pH values for an additional length of time under refrigerated conditions. Within the first week sitting at this pH there is a slight decrease in intensity from what is believed to be equilibrium with the soluble aggregates as previously described. This intensity decrease does not significantly change in the following weeks sitting at these conditions. The absorption maximum begins to slowly redshift 137±1 cm^{-1} (2.25 nm) over a 16 week period before returning to the native position. After 24 weeks, shown in blue, the CD spectrum clearly shows the positive Cotton band of the M state resolving to the couplet of the fully folded state (Figure 5.28). This reaffirms that both chemical modification and oligomerization are not contributing factors to the M state and that the M state is not an irreversible state along the folding pathway. The respective CD spectra measured at other pH values between 5 through 13 (data not shown) did not show any significant changes of the absorption and CD spectra. This suggest that the relaxation into the native state occurs in a very narrow pH window, a very surprising result.

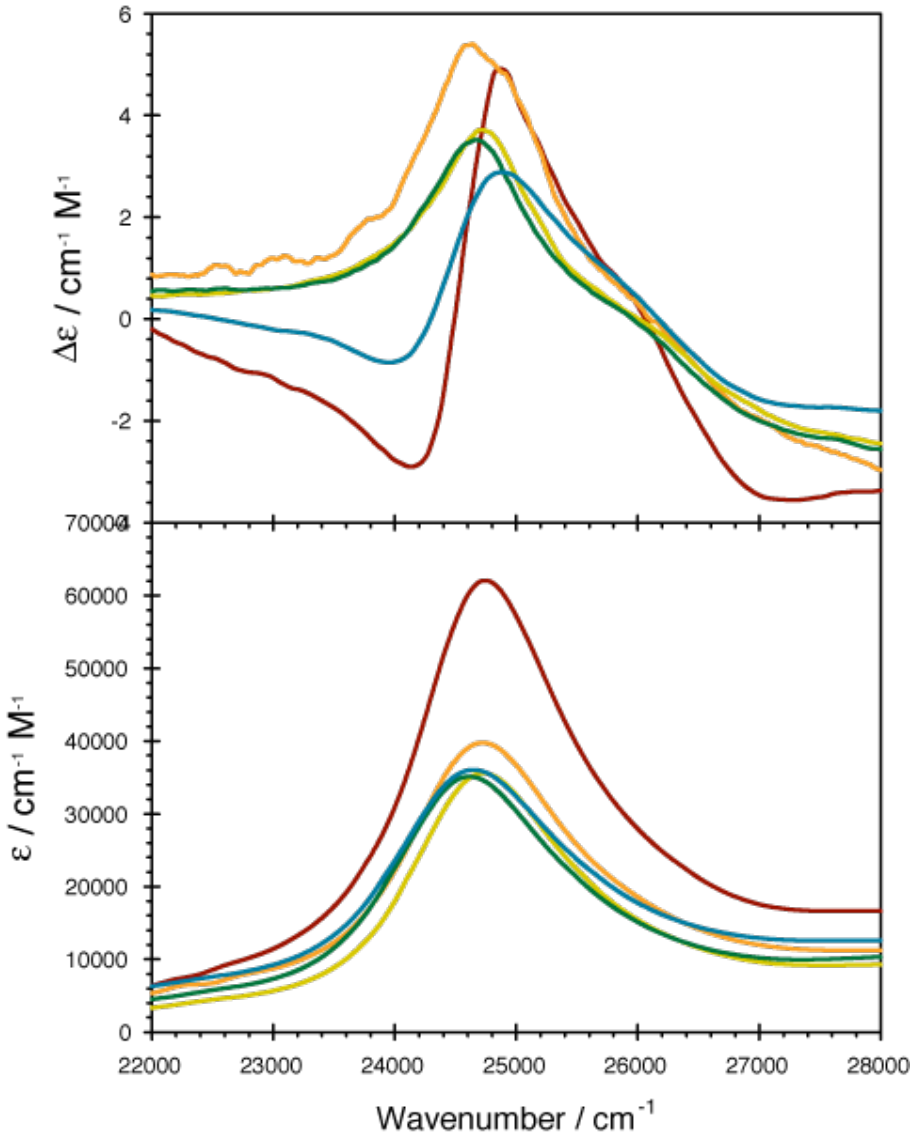

Figure 5.28. Visible CD (Top) and absorption spectrum (bottom) of ferricytochrome c at after being allowed to sit at pH 7 under refrigerated conditions for an extended period of time. The ■ red line shows the couplet of the fully folded state III, after being oxidized for 15 min. The proposed misfolded state is shown after 1 week (■ orange line), 4 weeks (■ yellow line), and 12 weeks (■ green line) illustrating the very slow transition back to the folded state after 24 weeks (■ blue line) under refrigerated conditions at pH 7.0.

5.3 Discussion. It is well known that ferricytochrome c is structurally a very flexible molecule. Seventy years ago Theorell and Åkesson identified five distinct titration states populated between pH 1 and 12 which they designated with the roman numbers *I* to *V*.[460] State *III* is the so-called native, fully folded state. State *IV* and *V* are populated under alkaline conditions. Recent spectroscopic experiments by Verbaro et al. reported the population of an intermediate state *III** at low ionic strength.[217] The complete scheme is therefore:

$$I \rightleftarrows II \rightleftarrows III \rightleftarrows III^* \rightleftarrows IV_{a,b,c} \rightleftarrows V_{a,b}$$

The subscripts *a,b* for states *IV* and *V* indicate the coexistence of different isomers.[431] In the current study we exposed the protein to alkaline conditions at pH 11.5, at which states $V_{a,b}$ are predominantly populated. We found that cyt c under these conditions undergoes a very slow conformational transition from a state *V* into a state M, which refolded only after the formation of protein aggregates. A spectroscopic comparison of the spectra of *V* and M (UV and visible CD) reveals only minor differences. This suggests that the respective secondary and tertiary structures are very similar. We can therefore propose the following scheme:

$$V \rightarrow M_{00} \rightleftarrows M_{01/10} \rightleftarrows M_{m,11}$$

The states $M_{i,j}$ ($i,j=0,1$) have been introduced above. States $M_{10/01}$ and M_{11} exhibit the CT2 band in their absorption spectra, though with different intensities. Since the measurements of the CT band spectra have been performed at a concentration of 0.5 mM, they might, to a significant extent reflect the behavior of the protein oligomers, since a dominant fraction of the monomers seems to be in the reduced state.

The resonance Raman and absorption spectra of state M_{00} indicate a low spin, hexacoordinated state (hcls) of the ferric heme iron for the predominantly monomeric 0.05 mM sample as well as for the oxidized fraction of the oligomers formed at 0.5 mM. The classical candidates for the sixth ligand of a hcls complex are lysine (K72, K73, K79)[225, 431] or histidine residues (H33 being the likely candidate).[187, 461] The position of the Soret band absorption (24,900 cm^{-1}) is close to values generally observed for bis-histidine complexes of ferricytochrome c;[429, 462] whereas the respective lysine-histidine ligation leads to band positions at 24,500 cm^{-1}.[365] However, as mentioned above, the respective CD spectra suggest that state *V* and M are very similar. As shown by Döpner et al., state *V* consists of two isomers termed V_a and V_b, which can be distinguished by means of the respective maker band frequencies in the resonance Raman spectrum.[454] A comparison of the peak positions in Table 5.1 with the corresponding values of the *V*-state isomers reported by Döpner et al. reveals that our data are close to those reported for the isomer V_b, whereas the respective bands of V_a all appear at slightly higher wavenumbers than the bands in our M-state Raman spectra. The same can be said about the marker bands in the Raman spectra of states *IV* (histidine/lysine complexes) and *B* (bis-histidine complexes).[429] The spectral analysis of Döpner et al. revealed V_b to be much less populated than V_a. We therefore propose that the $V \rightarrow$M transition is in fact a slow $V_a \rightarrow V_b$ transition.

Table 5.1. Wavenumber positions of marker bands in the resonance Raman spectrum of the oxidized fraction of cyt c incubated for one week at pH 11.5 (left column) and of the corresponding bands in the spectrum of state $V_{a/b}$ obtained by Döpner et al. (right column)[454]

Mode	$\tilde{\nu}_M\left[cm^{-1}\right]$	$\tilde{\nu}_{V_b}\left[cm^{-1}\right]$	$\tilde{\nu}_{V_a}\left[cm^{-1}\right]$
ν_4	1371	1370	1377
ν_3	1499	1501	1506
ν_2	1585	1586	1589
ν_{10}	1635	1636	1641

The work of Döpner et al. did not lead to a final identification of the sixth ligand in state *V*.[454] However, several lines of reasoning suggested a hydroxyl ion as ligand. Additional lines of evidence suggest that this is most likely the best candidate for our state M = V_b in both its monomeric and oligomeric form. First, the work of Hirota et al. provided spectroscopic evidence for OH^- as the sixth ligand in cyt c oligomers formed by domain swapping in an ethanol/water solution.[454] Second, Silkstone et al. reported OH^- to be the sixth ligand in M80A and M80S ferricytochrome c mutants even at physiological pH.[463] The conformations produced by these mutations may therefore also resemble the misfolded state M/V_b.

The appearance of the CT2 band is normally indicative of a high spin state of the metal iron, [425] but this notion is in conflict with the resonance Raman data, which still display the spin marker band close to their low spin positions. However, all our experimental data can be sufficiently explained by invoking a PcQM-state of the heme iron, which can be caused by spin-orbit coupling between a low lying high-spin and a slightly higher intermediate spin state of the heme iron.[464, 465] The absorption spectrum of such a state would appear redshifted with respect to that of all ferric hcls-states, but would have its peak still below 25,000 cm^{-1}.[10] This

is exactly what we observed (Figure 5.9). The B-band peak position of a hexacoordinated high spin state, however, lies at 25,000 cm^{-1} (400 nm).[187] The optical spectra of heme proteins with quantum mixed heme irons generally exhibit a charge transfer band in the CT2 region,[10] whereas the position of the spin marker bands in the corresponding resonance Raman spectra are close to the respective low-spin values. Quantum mixed spin states have been found in cytochromes of the c'-family and in class 3 peroxidases.[11, 464, 466, 467] A very prominent example is horseradish peroxidase.[10, 466-468] Quantum mixed states have not yet been discovered in cyt c derivatives (both native and unfolded), but one should keep in mind that cyt c on the surface of liposomes and on the inner membrane of mitochondria can acquire peroxidase activity, for which a quantum mixed state of the heme iron might be a prerequisite.[10, 11]

The formation of the proposed PcQM state is triggered by the protonation of groups with pK-values of 4.4 and 6.6. Our analysis of the CT2 titration suggest that the $M_{00} \rightarrow M_{01}$ transition exhibits a pK-value of 6.5. This lies in the region in which solvent accessible histidines protonate. In cyt c the sole candidate is H33.[469] However, the high n-numbers obtained from the fits suggest the involvement of 3 to 4 protons in the $M_{00} \rightarrow M_{10}$ transition. This indicates a network of interacting protonation sites. A possible candidate is one of the propionic acid peripheral substituents of the heme. In native cyt c, one of the respective pK-values of the two propionic acids is unusually high (>9 for the other propionic acid),[470] but it is more than likely that the respective pK-value is lower in a partially unfolded state. We hypothesize that H33 and the outer propionate, which exhibits an alkaline pK value in folded cyt c, interact with the OH^- ligand to trigger the $M_{00} \rightarrow M_{01}$ transition. We propose that the second protonation step involves the protonation of the hydroxyl ligand. For the aforementioned M80A and M80S mutants of ferricytochrome c the pK-values of this reaction were reported as 5.6 and 5.9,

which is higher than the values of 4.3 and 4.7 inferred from our titration curves in Figures 5.4 and 5.7. However, our data in the region below pH 5 must be considered as incomplete since we were not able to reach the saturation region below 4.0 owing to the onset of aggregation induced precipitation. It is possible that the data assignable to the $M_{01/10} \rightarrow M_{11}$ transition involve e.g. two protonation steps, with pK-values below 4.0 and between 5.0 and 6.0. The first could be assigned to H26,[470] and the second to the protonation of OH^-.[464]

The fact that the CT2 band is less intense in $M_{01/01}$ than in M_{11} suggests that it might in fact comprise a mixture of M_{00} and M_{11} rather than a thermodynamic intermediate between M_{00} and M_{11}. In other words: the protonation of H33, H26 and the outer propionic acid substituent change the equilibrium between two conformations with a hexacoordinated low-spin and the PcQM state, respectively. The first protonation step produces a mixture of both states, whereas the second protonation stabilizes the PcQM state.

If our assessment of the ligation state of M/V_b is correct one would expect that the protonation of the hydroxyl ligand should produce a hexacoordinated high-spin state with water as the sixth ligand. This is what the CT2 band alone would indicate. However, the PcQM state does fit into the picture as well, since a similar state in horseradish peroxidase exhibits a water molecule still close to the heme iron.[471]

The observation of a pH-dependent fraction of reduced cyt c in the 0.5 mM sample is another really surprising result. The pH-dependence itself indicates coupling with protonation/deprotonation processes, i.e. the pK-value of protonatable groups are different in the oxidized and reduced states. As shown by Hauser et al; the heme carboxylate groups as well as lysine

side chains, are likely candidates.[472] The absence of reduced species in the monomer fraction of the 0.05 mM sample under neutral and alkaline conditions suggest that the electron transfer process must occur intermolecularly in oligomeric complexes. The heme reduction switches the protein to the native state *III*. If this state is adopted in the oligomer, the M80 might actually be provided by an adjacent cytochrome, as observed for cytochrome c_{552}. The newly formed *III*-state monomers should establish a new equilibrium of reduced and oxidized proteins that reflect the corresponding redox potential.[473] A similar coupling between a protonation/deprotonation process and changes of the oxidation state have been observed for the binuclear site of cyt c oxidase. One of the groups involved in this allosteric coupling process is the carboxylate group of one of the heme's propionic acids.[474, 475]

The equilibrium between monomers and oligomers appears to stabilize within a week after sitting at their respective pH. Surprisingly, the fraction of monomers in the metastable M-state then undergoes an extremely slow transition back to the fully folded state, at neutral pH under refrigerated conditions. This observed slow transition indicates the proteins ability to anneal itself, returning on-pathway from a frustrated state to complete its folding process (at neutral pH). If this can be confirmed by further experiments, it would be the first experimental observation of the long time relaxation of a frustrated misfolded state, and as such, an impressive confirmation of the theoretical approach that treats proteins like spin glasses.[418]

Our data indicate a reversible metastable state of cyt c that can be described as an equilibrium between monomers and oligomers of pre-molten globule/globular proteins, stabilized at neutral pH. This suggests that the associated folding process has its transition region at higher energy than the glass transition of the protein.[418] If we allow the protein to undergo this very slow transition at pH 11, we change the folding landscape by lifting the glass transition above

the transition region of the folding process along the pH-coordinate. This is illustrated by the folding funnel in Figure 5.29. For unknown reasons, this ensemble of protein monomers and oligomers establishes a dynamic equilibrium that involves the formation of reduced proteins in a pH range between 6 and 10.

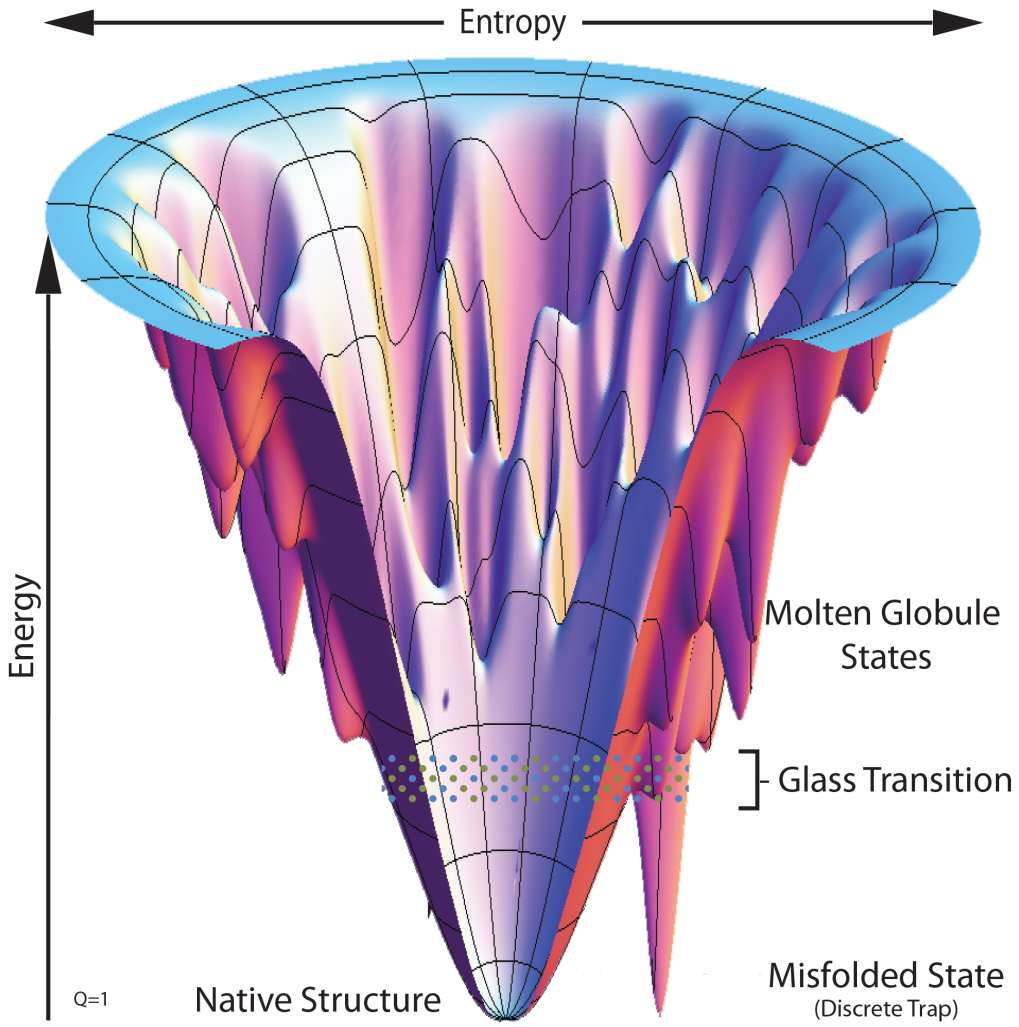

Figure 5.29. A feasible funnel-like protein folding landscape for a small helical protein. The preferred direction of flow is towards a unique native structure. When the glass transition temperature is higher than the folding temperature, the population of a frustrated misfolded state can occur over that of the native state.

5.4 Adapted From

Soffer, J. B.; Fradkin, E. K.; Pandiscia, L. A.; Schweitzer-Stenner, R. Biochemistry **2013**, 52, 1397–1408.[476] (Selected cover article for October, November and December 2013)

6.0 Summary

Cytochrome c is a multifaceted protein, tightly regulating cell respiration and cell death. In addition to mitochondrial electron transfer it was also found to bind to Apaf-1 triggering caspase activation (in the cytosol),[116] to complex with cardiolipin,[118] to trigger pore formation in cardiolipin containing membranes,[119] to act as a cardiolipin peroxidase,[477, 478] and to initiate canonical intrinsic apoptosis.[115, 117] Cyt c can also scavenge reactive oxygen species (ROS) under healthy conditions,[120] or produce ROS via increased mitochondrial membrane potentials or the $p66^{Sch}$ pathway.[121] From a human pathology perspective this links cyt c to neurodegenerative diseases,[479, 480] cardiovascular diseases,[481] cancer,[482, 483] sepsis[484, 485] and autoimmune disorders.[122, 482] These newly described functions[486] are closely associated with so-called non-native states of cyt c.[24] The structure and function relationships of these discrete non-native states are thus as important as that of the native state for elucidating the precise roles of this important protein in complex biological systems.

In contrast to the reduced state, it is the oxidized state of cyt c that has the ability to adopt a wide range of different folded and partially folded conformations, depending on solution conditions. These partially folded conformations maintain a substantial fraction of the protein's secondary structure, form early in protein folding, and are relatively stable in both thermodynamic and kinetic folding intermediates.[45, 55] This is consistent with results from rapid mixing experiments and the unfolding/folding foldon model.[487] The partial maintenance of the secondary structure allows for a more diverse pool of meta-stable conformations close to that of the fully folded state of the protein, allowing the protein to keep the same folding pattern in its diverse functional landscape. Thermodynamic principles requires a protein to continuously cycle through an equilibrium of all possible states and populate them in a Boltzmann manner. The ability to control the population of these partially

unfolded states and the characterization of these conformations is essential for understanding the folding pathway *in vivo* and ultimately in relation to disease.

As frequently as cyt c has been investigated, only a limited number of experiments have been carried out under low ionic strength, which reduces the anion induced minor structural changes involving changes of the Fe^{3+}-M80 coordination.[126, 216] Under these conditions we were able to evaluate the temperature dependence of the canonical Theorell-Åkesson states including the *III** state. Our experimental data suggest a two-step process of thermal unfolding for all protonation states with a statistically significant enthalpy-entropy compensation with different compensation temperatures (T_{ci} = 316±13 K, T_{cu} = 316±13 K) for the two consecutive thermal transitions. This further points to a common physical process which similarly affects all of the investigated protonation states. The complete unfolding of cytochrome c was not obtained in this study at rather harsh conditions (extreme pH and temperature), so it appears that complete unfolding can only be obtained through the addition of urea or guanidine hydrochloride. This result illustrates the significant stabilizing strength of the intra-backbone hydrogen bonding in cyt c.

A slight change in the folding pathway results in the population of a frustrated misfolded state, at which the foldon energy levels are close enough to rearrange.[488] This peculiar state was occupied because the glass transition preceded the folding step on the pH-coordinate. This state exhibited a predominantly hexacoordinated low-spin state under folding conditions (0.05 mM cyt c), likely with a hydroxyl ion replacing M80 as the sixth axial position of the heme iron. This misfolded state slowly resumes the fully folded state when allowed to sit under folding conditions for an extended period of time under physiological conditions. At higher protein concentrations (0.5 mM cyt c), a substantial fraction of soluble dimers and higher-order oligomers formed containing even more helical structure, likely formed as a result of

domain swapping. It has been shown by Hirota et al. that the domain-swapped form of cyt c contains locally unfolded regions containing the M80, which maintain a mostly intact secondary structure.[191, 192] Domain-swapped dimers have been shown to create an additional heme binding site which results in enhanced peroxidase activity.[450] We speculate that our misfolded state may be the prerequisite state that cyt c adopts on the surface of liposomes and on the inner mitochondrial membrane.

Protein folding is a complex problem involving complicated series of events that can be described using the funneled energy landscape theory. The adjustment of the local environment, i.e., pH, temperature, and anion concentration, can affect the shape of the energy landscape. This allows for the complete quantitative description of cyt c's conformational landscape including the misfolded state to be characterized by the funneled landscape. This theory allows for protein folding and binding to be a thermodynamically controlled process involving a large variety of driving forces, i.e. entropic effects (uptake and release of solvent molecules), enthalpic contribution (noncovalent bond formations), and the hydrophobic effect, which are driven by a decrease in total Gibbs free energy.[89] This decrease in free energy is dictated by a delicate balancing of opposing enthalpic and entropic contributions, the compensation of which dictates the conformational selection observed in the folding process.[489] The thermodynamic entropy-enthalpy compensation based on the dynamic energy landscape view can be used to help in the understanding of the forces that drive conformational variation. Eventually, understanding this will likely serve as the connection between conformational variation and function.

Overall, the comprehensive analysis of the fully folded and pH and temperature induced partially unfolded states of ferri-cyt c at low anion concentration reveals the relationship between structure and thermodynamics in solution. Our discovery of a misfolded state (M)

suggests that cyt c's energy landscape is more frustrated than previously envisioned along certain folding coordinates. It can be expected that the obtained result will provide the framework for future work aimed at characterizing the conformational changes which this protein undergoes on the surface of anionic phospholipid containing membranes. Such membranes serve as model systems for the inner membrane of the mitochondrion to which cyt c can bind in order to shuttle electrons between cyt c reductase and cyt c oxidase. Structural changes of cyt c are a prerequisite for other, non-electron transfer related functions: i.e., the acquisition of peroxidase activity, the subsequent oxidation of cardiolipin in the presence of H_2O_2, and the subsequent involvement of the protein in apoptosis. This can ultimately serve to help understand the precise functional role of this protein in complex biological systems.

References

1. Bodo, G. (1955) Crystalline Cytochrome c from the King Penguin, *Nature 176*, 829-830.
2. Keilin, D. (1930) Cytochrome and Intracellular Oxidase, *Proc R Soc London, Ser B 106*, 418-444.
3. MacMunn, C. A. (1885) Researches on Myohaematin and the Histohaematins, *Proc R Soc Lond 39*, 239-241.
4. Scott, R. A., and Mauk, A. G. (1996) *Cytochrome c: A Multidisciplinary Approach*, University Science Books, Sausalito, CA.
5. Cortese, J. D., Voglino, A. L., and Hackenbrock, C. R. (1998) Multiple conformations of physiological membrane-bound cytochrome c, *Biochemistry 37*, 6402-6409.
6. Dickerson, R. E., Kopka, M. L., Borders Jr, C. L., Varnum, J. V., and Weinzierl, J. E. (1967) A centrosymmetric projection at 4 Å of horse heart oxidized cytochrome c, *J Mol Biol 29*, 77-80.
7. Adman, E. T. (1979) A Comparison of the Structures of Electron Transfer Proteins, *Biochim Biophys Acta 549*, 107-144.
8. Englander, S. W. (2000) Protein folding intermediates and pathways studied by hydrogen exchange, *Annu Rev Biophys Biomol Struct 29*, 213-238.
9. Krishna, M. M. G., Maity, H., Rumbley, J. N., Lin, Y., and Englander, S. W. (2006) Order of steps in the cytochrome C folding pathway: evidence for a sequential stabilization mechanism, *J Mol Biol 359*, 1410-1419.
10. Huang, Q., Szigeti, V., Fidy, J., and Schweitzer-Stenner, R. (2003) Structural Disorder of Native Horseradish Peroxidase Probed by Resonance Raman and Low Temperature Optical Absorption Spectroscopy, *J. Phys. Chem. B 107*, 2822.
11. Howes, B. D., Schiødt, C. B., Welinder, K. G., Marzocchi, M. P., Ma, J.-G., Zhang, J., Shelnutt, J. A., and Smulevich, G. (1999) The quantum mixed spin heme state of barley peroxidase:a paradigm for class III peroxidases, *Biophys. J. 77*, 478-492.
12. Dill, K. A., and MacCallum, J. L. (2012) The Protein-Folding Problem, 50 Years On, *Science 338*, 1042-1046.
13. Dill, K. A., and Chan, H. S. (1997) From Levinthal to pathways to funnels, *Nat Struct Biol 4*, 10-19.
14. Anfinsen, C. B., Haber, E., Sela, M., and White, J. (1961) The Kinetics of Formation of Native Ribonuclease During Oxidation of the Reduced Polypeptide Chain, *Proc Natl Acad Sci USA 47*, 1309-1314.
15. Levinthal, C. (1969) How to Fold Graciously, In *Mossbauer Spectroscopy in Biological Systems*, pp 22 - 24, University of Illinois Press, Allerton House, Monticello, Illinois.
16. Humphrey, W., Dalke, A., and Schulten, K. (1996) VMD: Visual molecular dynamics, *J Mol Graph 14*, 33-38.
17. Adobe Illustrator CS6, 16.0.1 ed., Adobe Systems, Inc., San Jose, Ca.
18. HyperChem Professional 7.51, Hypercube, Inc., Gainesville, Fl.
19. Bennett, C. L., Larson, D., Weiland, J. L., Jarosik, N., Hinshaw, G., Odegard, N., Smith, K. M., Hill, R. S., Gold, B., Halpern, M., Komatsu, E., Nolta, M. R., Page, L., Spergel, D. N., Wollack, E., Dunkley, J., Kogut, A., Limon, M., Meyer, S. S., Tucker, G. S., and Wright, E. L. (2012) Nine-Year Wilkinson Microwave Anisotropy Probe (WMAP) Observations: Final Maps and Results, *Ap. J. S. 2*, 177.

20. Anfinsen, C. B. (1972) Studies on the Principles that Govern the Folding of Protein Chains, In *Nobel Lecture, Chemistry 1971-1980* (Frängsmyr, T., and Forsén, S., Eds.), pp 103 - 119, World Scientific Publishing Co., Singapore.
21. Tanford, C. (1968) Protein denaturation, *Adv. Protein Chem. 23*, 121-282.
22. Tanford, C. (1970) Protein Denaturation: Part C. Theoretical Models for The Mechanism of Denaturation, *Adv. Protein Chem. 24*, 1-95.
23. Privalov, P. L. (1979) Stability of Proteins: Small Globular Proteins, *Adv. Protein Chem. 33*, 167-241.
24. Lin, Y.-W., and Wang, J. (2013) Structure and function of heme proteins in non-native states: A mini-review, *J Inorg Biochem Article in Press*, 1-10.
25. Ow, Y.-L. P., Green, D. R., Hao, Z., and Mak, T. W. (2008) Cytochrome c: functions beyond respiration, *Nat Rev Mol Cell Biol 9*, 532-542.
26. Simon, M., Meuth, V. M.-L., Chevance, S., Delalande, O., and Bondon, A. (2013) Versatility of non-native forms of human cytochrome c: pH and micellar concentration dependence, *J Biol Inorg Chem 18*, 27-38.
27. Banci, L., Bertini, I., Gray, H. B., Luchinat, C., Reddig, T., Rosato, A., and Turano, P. (1997) Solution Structure of oxidized horse heart cytochrome c, *Biochemistry 36*, 9867-9877.
28. The PyMOL Molecular Graphics System, Version 1.5.0.4 ed., Schrödinger, LLC.
29. Privalov, P. L. (1989) Thermodynamic problems of protein structure, *Annu Rev Biophys Biophys Chem 18*, 1-47.
30. Bashford, D., Cohen, F. E., Karplus, M., Kuntz, I. D., and Weaver, D. L. (1988) Diffusion–collision model for the folding kinetics of myoglobin, *Proteins 4*, 211-227.
31. Nishimura, C., Prytulla, S., Dyson, J. H., and Wright, P. E. (2000) Conservation of folding pathways in evolutionarily distant globin sequences, *Nat Struct Biol* 679-686.
32. Wong, K. B., Clarke, J., Bond, C., Neira, J. L., Freund, S. M., Fersht, A. R., and Daggett, V. (2000) Towards a complete description of the structural and dynamic properties of the denatured state of barnase and the role of residual structure in folding, *J Mol Biol 296*, 1257-1282.
33. Myers, J. K., and Oas, T. G. (1999) Contribution of a buried hydrogen bond to lambda repressor folding kinetics, *Biochemistry 38*, 6761-6768.
34. Jackson, S. (1998) How do small single-domain proteins fold?, *Fold Des 3*, R81–91.
35. Creighton, T. E. (1990) Protein folding, *Biochem J 270*, 1-16.
36. Clarke, J., and Fersht, A. R. (1996) An evaluation of the use of hydrogen exchange at equilibrium to probe intermediates on the protein folding pathway, *Fold Des 1*, 243-254.
37. Clarke, J., Itzhaki, L. S., and Fersht, A. R. (1997) Hydrogen exchange at equilibrium: a short cut for analysing protein-folding pathways?, *Trends Biochem Sci 22*, 284-287.
38. Dill, K. A., Bromberg, S., Yue, K., Fiebig, K. M., Yee, D. P., Thomas, P. D., and Chan, H. S. (1995) Principles of protein folding-A perspective from simple exact models, *Protein Sci 4*, 561-602.
39. Sosnick, T. R., and Barrick, D. (2011) The folding of single domain proteins - have we reached a consensus?, *21*, 12-24.
40. Eder, J., Rheinnecker, M., and Fersht, A. R. (1993) Folding of subtilisin BPN': characterization of a folding intermediate, *Biochemistry 32*, 18-26.

41. Baker, D., Sohl, J. L., and Agard, D. A. (1992) A protein-folding reaction under kinetic control, *Nature 356*, 263-265.
42. Pande, V. S., Grosberg, A. Y., Tanaka, T., and Rokhsar, D. S. (1998) Pathways for protein folding: is a new view needed?, *Curr Opin Struct Biol 8*, 68-79.
43. Baldwin, R. L. (2008) The search for folding intermediates and the mechanism of protein folding, *Annu Rev Biophys 37*, 1-21.
44. Evans, M. S., Clarke, T. F., and Clarke, P. L. (2005) Conformations of co-translational folding intermediates, *Protein Pept Lett 12*, 189-195.
45. Chan, C.-K., Hu, Y., Takahashi, S., Rousseau, D. L., Eaton, W. A., and Hofrichter, J. (1997) Submillisecond protein folding kinetics studied by ultrarapid mixing, *Proc Natl Acad Sci USA 94*, 1779–1784.
46. Eaton, E. A., Munoz, V., Thompson, P. A., Chan, C.-K., and Hofricher, J. (1997) Submillisecond kinetics of protein folding, *Curr Opin Struct Biol 7*, 10-14.
47. Eaton, W. A., Muñoz, V., Hagen, S. J., Jas, G. S., Lapidus, L. J., Henry, E. R., and Hofrichter, J. (2000) Fast kinetics and mechanisms in protein folding, *Annu Rev Biophys Biomol Struct 29*, 327-359.
48. Roder, H., Maki, K., and Cheng, H. (2006) Early events in protein folding explored by rapid mixing methods, *Chem Rev 106*, 1836-1861.
49. Roder, H., Maki, K., Cheng, H., and Ramachandra Shastry, M. (2004) Rapid mixing methods for exploring the kinetics of protein folding, *Methods 34*, 15-27.
50. Ohgushi, M., and Wada, A. (1983) 'Molten-globule state': a compact form of globular proteins with mobile side-chains, *FEBS Lett 164*, 21-24.
51. Arai, M., and Kuwajima, K. (2000) Role of the molten globule state in protein folding, *Adv Protein Chem 53*, 209-282.
52. Jamin, M., and Baldwin, R. L. (1998) Two forms of the pH 4 folding intermediate of apomyoglobin, *J Mol Biol 276*, 491-504.
53. Heidary, D. K., Gross, L. A., Roy, M., and Jennings, P. A. (1997) Evidence for an obligatory intermediate in the folding of interleukin-1beta, *Nat Struct Biol 4*, 725-731.
54. Walkenhorst, W. F., Green, S. M., and Roder, H. (1991) Kinetic evidence for folding and unfolding intermediates in staphylococcal nuclease, *Biochemistry 36*, 5795-5805.
55. Maity, H., Maity, M., Krishna, M. M. G., Mayne, L., and Englander, S. W. (2005) Protein Folding: The Stepwise Assembly of Foldon Units, *Proc Nat Acad Sci USA 102*, 4741-4746.
56. Bai, Y., Englander, J. J., Mayne, L., Milne, J., and Englander, S. W. (1995) Thermodynamic parameters from hydrogen exchange measurements, *Meth Enzymol 259*, 344-356.
57. Englander, S. W., Mayne, L., Bai, Y., and Sosnick, T. R. (1997) Hydrogen exchange: the modern legacy of Linderstrom-Lang, *Protein Sci 6*, 1101-1109.
58. Huyghues-Despointes, B. M., Pace, C. N., Englander, S. W., and M, S. J. (2001) Measuring the conformational stabil- ity of a protein by hydrogen exchange, *Methods Mol Biol 168*, 69–92.
59. Weinkam, P., Zong, C., and Wolynes, P. G. (2005) A funneled energy landscape for cytochrome c directly predicts the sequential folding route inferred from hydrogen exchange experiments, *Proc Natl Acad Sci USA 102*, 12401-12406.
60. Skinner, J. J., Lim, W. K., Bédard, S., Black, B. E., and Englander, S. W. (2012) Protein hydrogen exchange: Testing current models, *Protein Sci 21*, 987–995.

61. Skinner, J. J., Lim, W. K., Bédard, S., Black, B. E., and Englander, S. W. (2012) Protein dynamics viewed by hydrogen exchange, *Protein Sci 21*, 996–1005.
62. Hu, W., Walters, B. T., Kana, Z.-Y., Maynea, L., Rosen, L. E., Marquseec, S., and Englander, S. W. (2013) Stepwise protein folding at near amino acid resolution by hydrogen exchange and mass spectrometry, *Proc Natl Acad Sci USA 110*, 7684-7689.
63. Panchenko, A. R., Luthey-Schulten, Z., Cole, R., and Wolynes, P. G. (1997) The Foldon Universe: A Survey of Structural Similarity and Self-recognition of Independently Folding Units, *J Mol Biol 272*, 95-105.
64. Bai, Y., Sosnick, T. R., Mayne, L. C., and Englander, S. W. (1995) Protein folding intermediates: native-state hydrogen exchange, *Science 269*, 192-197.
65. Myers, J. K., Pace, C. N., and Scholtz, J. M. (1995) Denaturant m values and heat capacity changes: relation to changes in accessible surface areas of protein un-folding, *Protein Sci 4*, 2138–2148.
66. Krishna, M. M. G., and Englander, S. W. (2007) A unified mechanism for protein folding: predetermined pathways with optional errors, *Protein Sci 16*, 449.
67. Hoang, L., Maity, H., Krishna, M. M. G., Lin, Y., and Englander, S. W. (2003) Folding units govern the cytochrome c alkaline transition, *J Mol Biol 331*, 37-43.
68. Yutani, K., Ogasahara, K., and Kuwajima, K. (1992) Absence of the thermal transition in apo-a-lactalbuminin the molten globule state, *J Mol Biol 228*, 347-350.
69. Atkins, P., and De Paula, J. (2006) *Physical Chemistry*, Oxford University Press, New York.
70. Haynie, D. T., and Freire, E. (1993) Structural energetics of the moltenglobule state, *Proteins Struct Funct Genet 16*, 115-140.
71. Haynie, D. T., and Freire, E. (1994) Thermodynamic strategies for stabilizing intermediate states of proteins, *Biopolymers 34*, 261-272.
72. Xie, D., Bhakuni, V., and Freire, E. (1993) Are the moltenglobule andthe unfolded states of apo-a-lactalbumin enthalpically equivalent?, *J Mol Biol 232*, 5-8.
73. Hagihara, Y., Tan, Y., and Gotto, Y. (1994) Comparison of the conformational stability of the molten globule and native states of cytochrome c: effects of acetylation, urea and guanidine-hydrochloride, *J Mol Biol 237*, 336-348.
74. McGee, W. A., Rosell, F. I., Liggins, J. R., Rodriguez-Ghidarpour, S., Luo, Y., Chen, J., Brayer, G. D., Mauk, A. G., and Nall, B. T. (1996) Thermodynamic Cycles as Probes of Structure in Unfolded Proteins, *Biochemistry 35*, 1995-2007.
75. Uchiyama, S., Ohshima, A., Nakamura, S., Hasegawa, J., Terui, N., Takayama, S.-i. J., Yamamoto, Y., Sambongi, Y., and Kobayashi, Y. (2004) Complete thermal-unfolding profiles of oxidized and reduced cytochromes C, *J Am Chem Soc 126*, 14684-14685.
76. Matthews, C. R. (1993) Pathways of protein folding, *Annu Rev Biochem 62*, 653-683.
77. Kataoka, M., Hagihara, Y., Mihara, K., and Goto, Y. (1993) Molten globule of cytochrome c studied by small angle X-ray scattering, *J Mol Biol 229*, 591-596.
78. Kuroda, Y., Kidokoro, S.-i., and Wada, A. (1992) Thermodynamic characterization of cytochrome c at low pH: Observation of the molten globule state and of the cold denaturation process, *J Mol Biol 223*, 1139-1153.
79. Kuwajima, K. (1989) The molten globule state as a clue for understanding the folding and cooperativity of globular-protein structure, *Proteins 6*, 87-103.

80. Dickerson, R. E., Takano, T., Eisenberg, D., Kallai, O. B., Samson, L., Cooper, A., and Margoliash, E. (1971) Ferricytochrome c. I. General features of the horse and bonito proteins at 2.8 A resolution, *J Biol Chem 246*, 1511-1535.
81. Potekhin, S., and Pfeil, W. (1989) Microcalorimetric studies of conformational transitions of ferricytochrome c in acidic solution, *Biophys Chem 34*, 55-62.
82. Kumar, R., Prabhu, N. P., Rao, D. K., and Bhuyan, A. K. (2006) The alkali molten globule state of horse ferricytochrome c: observation of cold denaturation, *J Mol Biol 364*, 483-495.
83. Bhuyan, A. K. (2010) Off-pathway status for the alkali molten globule of horse ferricytochrome c, *Biochemistry 49*, 7764-7773.
84. Battistuzzi, G., Loschi, L., Borsari, M., and Sola, M. (1999) Effects of nonspecific ion-protein interactions on the redox chemistry of cytochrome c, *J Biol Inorg Chem 4*, 601-607.
85. Taler, G., Schejter, A., Navon, G., Vig, I., and Margoliash, E. (1995) The nature of the thermal equilibrium affecting the iron coordination of ferric cytochrome c, *Biochemistry 34*, 14209-14212.
86. Chan, H. S., and Dill, K. A. (1998) Protein folding in the landscape perspective: chevron plots and non-Arrhenius kinetics, *Proteins 30*, 2-33.
87. Leopold, P. E., Montal, M., and Onuchic, J. N. (1992) Protein folding funnels: a kinetic approach to the sequence-structure relationship., *Proc Natl Acad Sci USA 89*, 8721-8725.
88. Bryngelson, J. D., Onuchic, J. N., Socci, N. D., and Wolynes, P. G. (1995) Funnels, pathways, and the energy landscape of protein folding: a synthesis, *Proteins 21*, 167-195.
89. Wolynes, P. G., Onuchic, J. N., and Thirumalai, D. (1995) Navigating the folding routes, *Science 267*, 1619-1620.
90. Plotkin, S. S., and Onuchic, J. N. (2002) Understanding protein folding with energy landscape theory. Part II: Quantitative aspects, *Q Rev Biophys 35*, 205-286.
91. Plotkin, S. S., and Onuchic, J. N. (2002) Understanding protein folding with energy landscape theory. Part I: Basic concepts, *Q Rev Biophys 35*, 111.
92. MATLAB, 8.0.0.783, The MathWorks Inc., Natick, Ma.
93. Dill, K. A. (1985) Theory for the folding and stability of globular proteins, *Biochemistry 24*, 1501-1509.
94. Daggett, V., and Fersht, A. R. (2003) Is there a unifying mechanism for protein folding?, *Trends Biochem Sci 28*, 18-25.
95. Baker, D. (2000) A surprising simplicity to protein folding, *Nature 405*, 39-42.
96. Dill, K. A. (1999) Polymer principles and protein folding, *Protein Sci 8*, 1166-1180.
97. Plotkin, S., Wang, J., and Wolynes, P. G. (1996) Correlated energy landscape model for finite, random heteropolymers, *Phys Rev E 53*, 6271-6296.
98. Capaldi, A. P., Kleanthous, C., and E, R. S. (2002) Im7 folding mechanism: misfolding on a path to the native state, *Nature Struct Biol 9*, 209–216.
99. Dobson, C. M. (2004) Principles of protein folding, misfolding and aggregation, *Semin Cell Dev Biol 15*, 3-16.
100. Bryngelson, J. D., and Wolynes, P. G. (1987) Spin glasses and the statistical mechanics of protein folding, *Proc Natl Acad Sci U S A 84*, 7524-7528.
101. Schrödinger, E. (1944) *What Is Life?*, Cambridge University Press, London.

102. Ringe, D., and Petsko, G. A. (2003) The 'glass transition' in protein dynamics: what it is, why it occurs, and how to exploit it, *Biophys Chem 105*, 667-680.
103. Nelson, D. L., and Cox, M. M. (2008) *Lehninger Principles of Biochemistry*, 5 ed., W. H. Freeman, New York.
104. Salemme, F. (1977) Structure and Function of Cytochromes C, *46*, 299-330.
105. Efremov, R. G., Baradaran, R., and Sazanov, L. A. (2010) Crystal structure of respiratory complex I from Thermus thermophilus, *Nature 465*, 441-445.
106. Yankovskaya, V., Horsefield, R., Tornroth, S., Luna-Chavez, C., Miyoshi, H., Leger, C., Byrne, B., Cecchini, G., and Iwata, S. (2003) Complex II (Succinate Dehydrogenase) From E. Coli with ubiquinone bound, *Science 299*, 700-704.
107. Lange, C., and Hunte, C. (2002) Yeast Cytochrome BC1 Complex with Bound Substrate Cytochrome c, *Proc Natl Acad Sci USA 99*, 2800-2805.
108. Yoshikawa, S., Shinzawa-Itoh, K., Nakashima, R., Yaono, R., Yamashita, E., Inoue, N., Yao, M., Fei, M. J., Libeu, C. P., Mizushima, T., Yamaguchi, H., Tomizaki, T., and Tsukihara, T. (1998) Redox-coupled crystal structural changes in bovine heart cytochrome c oxidase, *Science 280*, 1723-1729.
109. Rastogi, V. K., and Girvin, M. E. (1999) Structural changes linked to proton translocation by subunit c of the ATP synthase, *Nature 402*, 263-268.
110. Gibbons, C., Montgomery, M. G., Leslie, A. G. W., and Walker, J. E. (2000) The structure of the central stalk in bovine F(1)-ATPase at 2.4 A resolution, *Nat Struct Biol 7*, 1055.
111. Del Rizzo, P. A., Bi, Y., Dunn, S. D., and Shilton, B. H. (2002) The "second stalk" of Escherichia coli ATP synthase: structure of the isolated dimerization domain, *Biochemistry 41*, 6875-6884.
112. Moore, G., and Pettigrew, G. W. (1990) *Cytochrome c - Evolutionary, Structural and physicochemical Aspects*.
113. Brown, G. C., and Borutaite, V. (2008) Regulation of apoptosis by the redox state of cytochrome c, *Biochim Biophys Acta 1777*, 877-881.
114. Santucci, R., Sinibaldi, F., Patriarca, A., Santucci, D., and Fiorucci, L. (2010) Misfolded proteins and neurodegeneration: role of non-native cytochrome c in cell death, *Expert Rev Proteomics 7*, 507-517.
115. Hüttemann, M., Pecina, P., Rainbolt, M., Sanderson, T. H., Kagan, V. E., Samavati, L., Doan, J. W., and Lee, I. (2011) The multiple functions of cytochrome c and their regulation in life and death decisions of the mammalian cell: From respiration to apoptosis, *Mitochondria 11*, 369-381.
116. Jiang, X., and Wang, X. (2004) Cytochrome c - Mediated Apoptosis, *Annu Rev Biochem 73*, 87-106.
117. Hengartner, M. (2000) The biochemistry of apoptosis, *Nature 407*, 770-776.
118. Kagan, V. E., Bayir, H. A., Belikova, N. A., Kapralov, A. A., Tyurina, Y. Y., Tyurin, V. A., Jiang, J., Stoyanovsky, D., Wipf, P., Kochanek, P. M., Greenberger, J. S., Pitt, B., Shvedova, A. A., and Borisenko, G. (2009) Cytochrome c/cardiolipin relations in mitochondria: a kiss of death, *Free Radic Biol Med 46*, 1439-1453.
119. Bergstrom, C. L., Beales, P. A., Lv, Y., Vanderlick, T. K., and Groves, J. T. (2013) Cytochrome c causes pore formation in cardiolipin-containing membranes, *Proc Natl Acad Sci USA 110*, 6269-6274.

120. Pereverzev, M. O., Vygodina, T. V., Konstantinov, A. A., and Skulachev, V. P. (2003) Cytochrome c, an ideal antioxidant, *Biochem Soc Trans 31*, 1312-1315.
121. Giorgio, M., Migliaccio, E., Orsini, F., Paolucci, D., Moroni, M., Contursi, C., Pelliccia, G., Luzi, L., Minucci, S., Marcaccio, M., Pinton, P., Rizzuto, R., Bernardi, P., Paolucci, F., and Pelicci, P. G. (2005) Electron transfer between cytochrome c and p66Shc generates reactive oxygen species that trigger mitochondrial apoptosis, *Cell 122*, 221–233.
122. Pullerits, R., Bokarewa, M., Jonsson, I. M., Verdrengh, M., and Tarkowski, A. (2005) Extracellular cytochrome c, a mitochondrial apoptosis-related protein, induces arthritis, *Rheumatology 44*, 32-39.
123. Ascenzi, P., Santucci, R., Coletta, M., and Polticelli, F. (2010) Cytochromes: Reactivity of the "dark side" of the heme, *Biophys Chem 152*, 21-27.
124. Brookes, P. S., Levonen, A.-L., Shiva, S., Sarti, P., and Darley-Usmar, V. M. (2002) Mitochondria: regulators of signal transduction by reactive oxygen and nitrogen species, *Free Radical Biol Med 33*, 755-764.
125. Jemmerson, R., Liu, J., Hausauer, D., Lam, K.-P., Mondino, A., and Nelson, R. D. (1999) A conformational change in cytochrome c of apoptotic and necrotic cells is detected by monoclonal antibody binding and mimicked by association of the native antigen with synthetic phospholipid vesicles, *Biochemistry 38*, 3599-3609.
126. Josephs, T. M., Liptak, M. D., Hughes, G., Lo, A., Smith, R. M., Wilbanks, S. M., Bren, K. L., and Ledgerwood, E. C. (2013) Conformational change and human cytochrome c function: mutation of residue 41 modulates caspase activation and destabilizes Met-80 coordination, *J Biol Inorg Chem 18*, 289-297.
127. Yan, N., and Shi, Y. (2003) Histone H1.2 as a trigger for apoptosis, *Nat Struct Biol 10*, 983-985.
128. Green, J., and Reed, D. (1998) Mitochondria and Apoptosis, *Science 281*, 1309-1312.
129. Clayton, R., Clark, J. B., and Sharpe, M. (2005) Cytochrome c release from rat brain mitochondria is proportional to the mitochondrial functional deficit: implications for apoptosis and neurodegenerative disease, *J Neurochem 92*, 840–849.
130. Kluck, R. M., Ellerby, L. M., Ellerby, H. M., Naiem, S., Yaffe, M. P., Margoliash, E., Bredesen, D., Mauk, A. G., Sherman, F., and Newmeyer, D. D. (2000) Determinants of cytochrome c pro-apoptotic activity. The role of lysine 72 trimethylation, *J Biol Chem 275*, 16127-16133.
131. Liu, X., Kim, N., Yang, J. T., Jemmerson, R., and Wang, X. (1996) Induction of apoptotic program in cell-free extracts: requirement for dATP and cytochrome c, *Cell 86*, 147-157.
132. Wang, C., and Youle, R. J. (2009) The Role of Mitochondria in Apoptosis*, *Annu Rev Genet 43*, 95-118.
133. Shi, Y. (2002) Mechanisms of Caspase Activation and Inhibition during Apoptosis, *Mol Cell 9*, 459-470.
134. Heimburg, T., and Marsh, D. (1995) Protein surface-distribution and protein-protein interactions in the binding of peripheral proteins to charged lipid membranes., *Biophys J 68*, 536-546.
135. Kagan, V. E., Borisenko, G. G., Tyurina, Y. Y., Tyurin, V. A., Jiang, J., Potapovich, A. I., Kini, V., Amoscato, A. A., and Fujii, Y. (2004) Oxidative lipidomics of apoptosis: redox

catalytic interactions of cytochrome c with cardiolipin and phosphatidylserine, *Free Radic Biol Med 37*, 1963-1985.

136. Gomez Jr, B., and Robinson, N. C. (1999) Quantitative determination of cardiolipin in mitochondrial electron transferring complexes by silicic acid high-performance liquid chromatography, *Anal Biochem 267*, 212-216.
137. Ardail, D., Privat, J. P., Egret-Charlier, M., Levrat, C., Lerme, F., and Louisot, P. (1990) Mitochondrial contact sites. Lipid composition and dynamics., *J Biol Chem 265*, 18797-18802.
138. Balakrishnan, G., Hu, Y., Oyerinde, O. F., Su, J., Groves, J. T., and Spiro, T. G. (2007) A conformational switch to beta-sheet structure in cytochrome c leads to heme exposure. Implications for cardiolipin peroxidation and apoptosis, *J Am Chem Soc 129*, 504-505.
139. Beales, P. A., Bergstrom, C. L., Geerts, N., Groves, J. T., and Vanderlick, T. K. (2011) Single vesicle observations of the cardiolipin-cytochrome C interaction: induction of membrane morphology changes, *Langmuir 27*, 6107-6115.
140. Rytömaa, R., Mustonen, P., and Kinnunen, P. K. J. (1992) Reversible, nonionic, and pH-dependent association of cytochrome c with cardiolipin-phosphatidylcholine liposomes., *J Biol Chem 267*, 22243-22248.
141. Rytömaa, M., and Kinnunen, P. K. J. (1994) Evidence for two distinct acidic phospholipid-binding sites in cytochrome c, *J Biol Chem 269*, 1770-1774.
142. Rytömaa, M., and Kinnunen, P. K. J. (1995) Reversibility of the Binding of Cytochrome c to Liposomes, *J Biol Chem 270*, 3197-3202.
143. Nicholls, P. (1974) Cytochrome c binding to enzymes and membranes, *346*, 261-310.
144. Pelletier, H., and Kraut, J. (1992) Crystal structure of a complex between electron transfer partners, cytochrome c peroxidase and cytochrome c, *Science 258*, 1748-1755.
145. Tuominen, E. K. J., Wallace, C. J. A., and Kinnunen, P. K. J. (2002) Phospholipid-Cytochrome c Interaction, *EVIDENCE FOR THE EXTENDED LIPID ANCHORAGE J Biol Chem 277*, 8822-8826.
146. Kalanxhi, E., and Wallace, C. J. A. (2007) Cytochrome c impaled: investigation of the extended lipid anchorage of a soluble protein to mitochondrial membrane models, *Biochem J 407*, 179-187.
147. Sinibaldi, F., Howes, B. D., Piro, M. C., Polticelli, F., Bombelli, C., Ferri, T., Coletta, M., Smulevich, G., and Santucci, R. (2010) Extended cardiolipin anchorage to cytochrome c: a model for protein-mitochondrial membrane binding, *J Biol Inorg Chem 15*, 689-700.
148. Nantes, I. L., Zucchi, M. R., Nascimento, O. R., and Faljoni-Alario, A. (2001) Effect of heme iron valence state on the conformation of cytochrome c and its association with membrane interfaces. A CD and EPR investigation, *J Biol Chem 276*, 153-158.
149. Kawai, C., Pessoto, F. S., Rodrigues, T., Mugnol, K. C. U., Tórtora, V., Castro, L., Milícchio, V. A., Tersariol, I. L. S., Di Mascio, P., Radi, R., Carmona-Ribeiro, A. M., and Nantes, I. L. (2009) pH-sensitive binding of cytochrome c to the inner mitochondrial membrane. Implications for the participation of the protein in cell respiration and apoptosis, *Biochemistry 48*, 8335-8342.
150. Korshunov, S. S., Krasnikov, B. F., Pereverzev, M. O., and Skulachev, V. P. (1999) The antioxidant functions of cytochrome c, *FEBS Lett 462*, 192-198.

151. Wang, Z.-B., Li, M., Zhao, Y., and Xu, J.-X. (2003) Cytochrome C Is a Hydrogen Peroxide Scavenger In Mitochondria, *Protein Pept Lett 10*, 247-253.
152. Hashimoto, M., Hsu, L. J., Xia, Y., Takeda, A., Sisk, A., Sundsmo, M., and Masliah, E. (1999) Oxidative stress induces amyloid-like aggregate formation of NACP/alpha-synuclein in vitro, *NeuroReport 10*, 717-721.
153. Yamato, M., Egashira, T., and Utsumi, H. (2003) Application of in vivo ESR spectroscopy to measurement of cerebrovascular ROS generation in stroke, *Free Radic Biol Med 35*, 1619–1631.
154. Wang, X., Pal, R., Chen, X. W., Limpeanchob, N., Kumar, K. N., and Michaelis, E. K. (2005) High intrinsic oxidative stress may underlie selective vulnerability of the hippocampal CA1 region, *Brain Res Mol Brain Res 140*, 120–126.
155. Dickerson, R. E. (1971) The structure of cytochrome c and the rates of molecular evolution, *J Mol Evol 1*, 26-45.
156. Banci, L., Bertini, I., Huber, J. G., Spyroulias, G. A., and Turano, P. (1999) Solution structure of reduced horse heart cytochrome c, *J Biol Inorg Chem 4*, 21-31.
157. Theorell, H., and Akesson, A. (1941) Studies on Cytochrome c. III. Titration Curves, *J Am Chem Soc 63*, 1818-1820.
158. Van Gelder, B. F., and Slater, E. C. (1962) The extinction coefficient of cytochrome c, *Biochim Biophys Acta 58*, 593-595.
159. Banci, L., Bertini, I., Rosato, A., and Varani, G. (1999) Mitochondrial cytochrome c: a comparative analysis, *J Biol Inorg Chem 4*, 824-837.
160. Dickerson, R. E., Takano, T., and Eisenberg, D. (1971) Ferricytochrome c.
161. Ramachandran, G. N., and Sasisekharan, V. (1968) Conformation of Polypeptides and Proteins, *Adv Protein Chem 23*, 283-437.
162. Banci, L., Bertini, I., Reddig, T., and Turano, P. (1998) Monitoring the conformational flexibility of cytochrome c at low ionic strength by H-NMR spectroscopy, *Eur J Biochem 256*, 271-278.
163. Bowman, S. E. J., and Bren, K. L. (2008) The chemistry and biochemistry of heme c: functional bases for covalent attachment, *Nat Prod Rep 25*, 1118– 1130.
164. Cartling, B. (1988) Cytochrome c, In *Biological Applications of Raman Spectroscopy*, T.G. Spiro, ed., John Wiley, New York, vol. 3, 217-248.
165. Ma, J.-G., Zhang, J., Franco, R., Jia, S.-L., Moura, J. J. G., Kroneck, P. M. H., and Shelnutt, J. A. (1998) The Structural Origin of Nonplanar Heme Distortions in Tetraheme Ferricytochromes c_3, *Biochemistry 37*, 12431-12442.
166. Michel, L. V., Ye, T., Bowman, S. E. J., Levin, B. D., Hahn, M. A., Russell, B. S., Elliott, S. J., and Bren, K. L. (2007) Heme attachment motif mobility tunes cytochrome c redox potential, *Biochemistry 46*, 11753-11760.
167. Liptak, M. D., Wen, X., and Bren, K. L. (2010) NMR and DFT investigation of heme ruffling: functional implications for cytochrome c, *J Am Chem Soc 132*, 9753-9763.
168. Ma, J. G., Vanderkooi, J. M., Zhang, J., Jia, S. L., and Shelnutt, J. A. (1999) Resonance Raman Investigation of Nickel Microperoxidase-11, *Biochemistry 38*, 2787-2795.
169. Mao, J. J., Hauser, K., and Gunner, M. R. (2003) How cytochromes with different folds control heme redox potentials, *Biochemistry 42*, 9829-9840.
170. Tezcan, F. A., Winkler, J. R., and Gray, H. B. (1998) Effects of ligation and folding on reduction potentials of heme proteins, *J Am Chem Soc 120*, 13383-13388.

171. Connolly, M. L. (1983) Solvent-accessible surfaces of proteins and nucleic acids, *Science 221*, 709-713.
172. Takano, T., and Dickerson, R. E. (1981) Conformation change of cytochrome c, *I. Ferricytochrome c Refinement at l.8 A and Comparison with the Ferrocytochrome Structure, J Mol Biol 153*, 95-115.
173. Filosa, A., Wang, Y., Ismail, A. A., and English, A. M. (2001) Two-dimensional infrared correlation spectroscopy as a probe of sequential events in the thermal unfolding of cytochromes c, *Biochemistry 40*, 8256-8263.
174. Berghuis, A. M., and Brayer, G. D. (1992) Oxidation state-dependent conformational changes in cytochrome c, *J Mol Biol 223*, 959-976.
175. Trewhella, J., Carlson, V. A. P., Curtis, E. H., and Heidorn, D. B. (1988) Differences in the solution structures of oxidized and reduced cytochrome c measured by small-angle X-ray scattering, *Biochemistry 27*, 1121-1125.
176. Döpner, S., Hildebrandt, P., Rosell, F. I., Mauk, A. G., von Walter, M., Buse, G., and Soulimane, T. (1999) The structural and functional role of lysine residues in the binding domain of cytochrome c in the electron transfer to cytochrome c oxidase, *Eur J Biochem 261*, 379-391.
177. Garber, E. A. E., and Margoliash, E. (1994) Circular-dichroism studies of the binding of mammalian and nonmammalian cytochromes-c to cytochrome-c-oxidase, cytochrome-c peroxidase, and polyanions, *Biochim Biophys Acta 1187*, 289-295.
178. Weber, C., Michel, B., and Bosshard, H. R. (1987) Spectroscopic analysis of the cytochrome c oxidase-cytochrome c complex: circular dichroism and magnetic circular dichroism measurements reveal change of cytochrome c heme geometry imposed by complex formation, *Proc Natl Acad Sci USA 84*, 6687-6691.
179. Lim, W. K., Rosgen, J., and Englander, S. W. (2009) Urea, but not guanidinium, destabilizes proteins by forming hydrogen bonds to the peptide group, *Proc Natl Acad Sci USA 106*, 2595-2600.
180. Goto, Y., Takahashi, N., and Fink, A. L. (1990) Mechanism of acid-induced folding of proteins, *Biochemistry 29*, 3480-3488.
181. Babul, J., and Stellwagen, E. (1971) The existence of heme-protein coordinate-covalent bonds in denaturing solvents, *Biopolymers* 10, 2359-2361.
182. Babul, J., and Stellwagen, E. (1972) Participation of the protein ligands in the folding of cytochrome c, *Biochemistry 11*, 1195-1200.
183. Tsong, T. Y. (1974) The Trp-59 Fluorescence of Ferricytochrome c as a Sensitive Measure of the Over-all Protein Conformation, *J Biol Chem 249*, 1988-1990.
184. Dyson, H. J., and Beattie, J. K. (1982) Spin State and Unfolding Equilibria of Ferricytochrome c in Acidic Solutions, *J Biol Chem 257*, 2267-2273.
185. Muthukrishnan, K., and Nall, B. T. (1991) Effective concentrations of amino acid side chains in an unfolded protein, *Biochemistry 30*, 4706-4710.
186. Elove, G. A., Bhuyan, A. K., and Roder, H. (1994) Kinetic mechanism of cytochrome c folding: involvement of the heme and its ligands, *Biochemistry 33*, 6925-6935.
187. Colon, W., Wakem, L. P., Sherman, F., and Roder, H. (1997) Identification of the predominant non-native histidine ligand in unfolded cytochrome c, *Biochemistry 36*, 12535-12541.

188. Maity, H., Maity, M., and Englander, S. W. (2004) How cytochrome c folds, and why: submolecular foldon units and their stepwise sequential stabilization, *J Mol Biol 343*, 223-233.
189. Roder, H., Elove, G. A., and Englander, S. W. (1988) Structural characterization of folding intermediates in cytochrome c by H-exchange labelling and proton NMR, *Nature 335*, 700-704.
190. Hoang, L. (2002) Cytochrome c folding pathway: kinetic native-state hydrogen exchange, *Proc Natl Acad Sci USA 99*, 12173-12178.
191. Hirota, S., Ueda, M., Hayashi, Y., Nagao, S., Kamikubo, H., and Kataoka, M. (2012) Maintenance of the secondary structure of horse cytochrome c during the conversion process of monomers to oligomers by addition of ethanol, *J Biochem 152*, 521-529.
192. Hirota, S., Hattori, Y., Nagao, S., Taketa, M., Komori, H., Kamikubo, H., Wang, Z., Takahashi, I., Negi, S., Sugiura, Y., Kataoka, M., and Higuchi, Y. (2010) Cytochrome c polymerization by successive domain swapping at the C-terminal helix, *Proc Natl Acad Sci USA 107*, 12854-12859.
193. Ellis, R. J., and Pinheiro, T. (2002) Danger-misfolding proteins, *Nature 416*, 483-484.
194. Dobson, C. M. (1999) Protein misfolding, evolution and disease, *Trends Biochem Sci 24*, 329-332.
195. Takahashi, S., Yeh, S.-R., Das, T. K., Chan, C.-K., Gottfried, D. S., and Rousseau, D. L. (1997) Folding of cytochrome c initiated by submillisecond mixing, *Nat Struct Biol 4*, 44-50.
196. Shastry, M. C. R., Sauder, J., and Roder, H. (1998) Kinetic and Structural Analysis of Submillisecond Folding Events in Cytochrome c, *Acc Chem Res 31*, 717-725.
197. Pollack, L., Tate, M. W., Darnton, N. C., Knight, J. B., Gruner, S. M., Eaton, W. A., and Austin, R. H. (1999) Compactness of the denatured state of a fast-folding protein measured by submillisecond small-angle X-ray scattering, *Proc Natl Acad Sci USA 96*, 10115–10117.
198. Yeh, S.-R., Han, S., and Rousseau, D. L. (1998) Cytochrome c folding and unfolding: a biphasic mechanism, *Acc Chem Res 31*, 727-736.
199. Akiyama, S., Takahashi, A., Ishimori, K., and Morishima, I. (2000) Stepwise formation of a-helices during cytochrome c folding, *Nat Struct Mol Biol 7*, 514-520.
200. Shastry, M. C. R., and Roder, H. (1998) Evidence for barrier-limited protein folding kinetics on the microsecond time scale, *Nature Struct Biol 5*, 385-392.
201. Sosnick, T. R., Mayne, L., Hiller, R., and Englander, S. W. (1994) The barriers in protein folding, *Nat Struct Biol 1*, 149-156.
202. Panda, M., Benavides-Garcia, M. G., Pierce, M. M., and Nall, B. T. (2000) Cytochrome c folds through a smooth funnel, *Protein Sci 9*, 536-543.
203. Sauder, J., and Roder, H. (1998) Amide protection in an early folding intermediate of cytochrome c, *Fold Des 3*, 293-301.
204. Theorell, H. (1941) Studies on Cytochrome c. IV. The Magnetic Properties of Ferric and Ferrous Cytochrome c, *J Am Chem Soc 63*, 1820-1827.
205. Theorell, H., and Akesson, A. (1941) Studies on Cytochrome c. II. The Optical Properties of Pure Cytochrome c and Some of Its Derivatives, *J Am Chem Soc 63*, 1812-1818.

206. Theorell, H., and Akesson, A. (1941) Studies on Cytochrome c. I. Electrophoretic Purification of Cytochrome c and its Amino Acid Composition, *J Am Chem Soc 63*, 1804-1820.
207. Schweitzer-Stenner, R., Hagarman, A. M., Verbaro, D., and Soffer, J. B. (2009) Conformational Stability of Cytochrome c Probed by Optical Spectroscopy, *Meth Enzymol 466*, 109-153.
208. Jorgensen, W. L., Chandrasekhar, J., Madura, J. D., Impey, R. W., and Klein, M. L. (1983) Comparison of simple potential functions for simulating liquid water, *J Chem Phys 79*, 926-935.
209. Brooks, B. R., Bruccoleri, R. E., Olafson, B. D., States, D. J., Swaminathan, S., and Karplus, M. (2004) CHARMM: A program for macromolecular energy, minimization, and dynamics calculations, *J Comput Chem 4*, 187-217.
210. Laskowski, R. A., MacArthur, M. W., Moss, D. S., and M, T. J. (1993) PROCHECK - a program to check the stereochemical quality of protein structures, *J App Cryst 26*, 283-291.
211. Goto, Y., Calciano, L. J., and Fink, A. L. (1990) Acid-induced folding of proteins, *Proc Natl Acad Sci USA 87*, 573-577.
212. Jordan, T., Eads, J. C., and Spiro, T. G. (1995) Secondary and tertiary structure of the A-state of cytochrome c from resonance Raman spectroscopy, *Protein Sci 4*, 716-728.
213. Yeh, S.-R., and Rousseau, D. L. (1999) Ligand Exchange during Unfolding of Cytochrome c, *J Biol Chem 274*, 17853-17859.
214. (2013) Schrödinger Suite, V.9.4, Schrödinger, LLC, New York, NY.
215. Indiani, C., de Sanctis, G., Neri, F., Santos, H., Smulevich, G., and Coletta, M. (2000) Effect of pH on axial ligand coordination of cytochrome c" from Methylophilus methylotrophus and horse heart cytochrome c, *Biochemistry 39*, 8234-8242.
216. Shah, R., and Schweitzer-Stenner, R. (2008) Structural changes of horse heart ferricytochrome c induced by changes of ionic strength and anion binding, *Biochemistry 47*, 5250-5257.
217. Verbaro, D., Hagarman, A. M., Soffer, J. B., and Schweitzer-Stenner, R. (2009) The pH dependence of the 695 nm charge transfer band reveals the population of an intermediate state of the alkaline transition of ferricytochrome c at low ion concentrations, *Biochemistry 48*, 2990-2996.
218. Finnegan, M. L., and Bowler, B. E. (2010) Propensities of Aromatic Amino Acids versus Leucine and Proline to Induce Residual Structure in the Denatured-State Ensemble of Iso-1-cytochrome c, *J Mol Biol 403*, 459-504.
219. Weinkam, P., Zimmermann, J., Sagle, L. B., Matsuda, S., Dawson, P. E., Wolynes, P. G., and Romesberg, F. E. (2008) Characterization of alkaline transitions in ferricytochrome c using carbon-deuterium infrared probes., *Biochemistry 47*, 13470-13480.
220. Döpner, S., Hildebrandt, P., Rosell, F. I., and Mauk, A. G. (1998) Alkaline Conformational Transitions of Ferricytochrome c Studied by Resonance Raman Spectroscopy, *J Am Chem Soc 120*, 11246-11255.
221. Döpner, S., Hildebrandt, P., Heibel, G., Vanhecke, F., and Mauk, A. G. (1995) The effect of pH and hydrogen-deuterium exchange on the heme pocket structure of cytochrome c probed by resonance Raman spectroscopy, *J Mol Struct 349*, 125-128.

222. Rosell, F. I., Ferrer, J. C., and Mauk, A. G. (1998) Proton-linked protein conformational switching: definition of the alkaline conformational transition of yeast iso-l-ferricytochrome c, *J Am Chem Soc 120*, 11234-11245.
223. Ferrer, J. C., Guillemette, J. G., Bogumil, R., Inglis, S. C., Smith, M., and Mauk, A. G. (1993) Identification of Lys79 as an iron ligand in one form of alkaline yeast iso-1-ferricytochrome c, *J Am Chem Soc 115*, 7507-7508.
224. Pollock, W. B. R., Rosell, F. I., Twitchett, M. B., Dumont, M. E., and Mauk, A. G. (1998) Bacterial Expression of a Mitochondrial Cytochrome c. Trimethylation of Lys72 in Yeast iso-1-Cytochrome cand the Alkaline Conformational Transition, *Biochemistry 37*, 6124-6131.
225. Blouin, C., Guillemette, J. G., and Wallace, C. J. A. (2001) Resolving the individual components of a pH-induced conformational change, *Biophys J 81*, 2331-2338.
226. Smith, H. T., and Millett, F. (1980) Involvement of lysines -72 and -79 in the alkaline isomerization of horse heart ferricytochrome c, *Biochemistry 19*, 1117-1120.
227. Rosell, F. I., Ferrer, J. C., and Mauk, A. G. (1998) Proton-linked protein conformational switching: definition of the alkaline conformational transition of yeast iso-l-ferricytochrome c, *J Am Chem Soc 120*, 11234-11245.
228. Maity, H., Rumbley, J. N., and Englander, S. W. (2006) Functional role of a protein foldons - An omega-loop foldon controls the alkaline transition in ferricytochrome c, *Proteins 63*, 349–355.
229. Barker, P. D., and Mauk, A. G. (1992) pH-Linked conformational regulation of a metalloprotein oxidation-reduction equilibrium: electrochemical analysis of the alkaline form of cytochrome c, *Biochemistry 114*, 3619-3624.
230. Baddam, S., and Bowler, B. E. (2006) Mutation of asparagine 52 to glycine promotes the alkaline form of iso-1-cytochrome c and causes loss of cooperativity in acid unfolding, *Biochemistry 45*, 4611-4619.
231. Jones, C. M., Henry, E. R., Hu, Y., Chan, C. K., Luck, S. D., Bhuyan, A., Roder, H., Hofrichter, J., and Eaton, W. A. (1993) Fast events in protein folding initiated by nanosecond laser photolysis, *Proc Natl Acad Sci USA 90*, 11860-11864.
232. Droghetti, E., Oellerich, S., Hildebrandt, P., and Smulevich, G. (2006) Heme coordination states of unfolded ferrous cytochrome c, *Biophys J 91*, 3022-3031.
233. Hagarman, A. M., Duitch, L., and Schweitzer-Stenner, R. (2008) The conformational manifold of ferricytochrome c explored by visible and far-UV electronic circular dichroism spectroscopy, *Biochemistry 47*, 9667-9677.
234. Döpner, S., Hildebrandt, P., Rosell, F. I., and Mauk, A. G. (1998) The alkaline conformational transitions of ferricytochrome c studied by resonance Raman spectroscopy, *J Am Chem Soc 120*, 11246-11255.
235. Blouin, C., Guillemette, J. G., and Wallace, C. J. A. (2001) Resolving the individual components of a pH-induced conformational change, *Biophys J 81*, 2331-2338.
236. Battistuzzi, G., Borsari, M., Dallari, D., Lancellotti, I., and Sola, M. (1996) Anion Binding to Mitochondrial Cytochromes c Studied through Electrochemistry, *Eur J Biochem 241*, 208-214.
237. Feng, Y., and Englander, S. W. (1990) Salt dependent Structural Change and Ion Binding in Cytochromec Studied by Two-Dimensional Proton NMR, *Biochemistry 29*, 3505-3509.

238. Moench, S. J., Shi, T.-M., and Satterlee, J. D. (1991) Proton-NMR studies of the effects of ionic strength and pH on the hyperfine-shifted resonances and phenylalanine-82 environment of three species of mitochondrial ferricytochrome c, *Eur J Biochem 197*, 631-641.
239. Assfalg, M., Bertini, I., Dolfi, A., Turano, P., Mauk, A. G., Rosell, F. I., and Gray, H. B. (2003) Structural Model for an alkaline Form of Ferricytochrome c, *J Am Chem Soc 125*, 2913-2922.
240. Shah, R., and Schweitzer-Stenner, R. (2008) Structural changes of horse heart ferricytochrome c induced by changes of ionic strength and anion binding, *Biochemistry 47*, 5250-5257.
241. Liu, G. Y., Grygon, C. A., and Spiro, T. G. (1989) Ionic strength dependence of cytochrome c structure and Trp-59 hydrogen/deuterium exchange from ultraviolet resonance Raman spectroscopy, *Biochemistry 28*, 5046-5050.
242. Ruf, R. A. S., Lutz, E. A., Zigoneanu, I. G., and Pielak, G. J. (2008) α-Synuclein Conformation Affects Its Tyrosine-Dependent Oxidation Aggregation, *Biochemistry 47*, 13604-13609.
243. Belikova, N. A., Vladimirov, Y., Osipov, A. N., Kapralov, A. A., Tyurin, V. A., Potapovich, M., Basova, L. V., Peterson, J., Kurnikov, I. V., and Kagan, V. E. (2006) Peroxidase activity and structural transitions of cytochrome c bound to cardiolipin-containing membranes, *Biochemistry 45*, 4998-5009.
244. Baker, N., Sept, D., Joseph, S., Holst, M. J., and McCammon, J. A. (2001) Electrostatics of nanosystems: application to microtubules and the ribosome, *Proc Natl Acad Sci USA 98*, 10037-10041.
245. Margoliash, E., and Lustgarten, J. (1962) Interconversion of Horse Heart Cytochrome c Monomer and Polymers, *J Biol Chem 237*, 3397-3405.
246. Wang, Q., Christiansen, A., Samiotakis, A., Wittung-Stafshede, P., and Cheung, M. S. (2011) Comparison of chemical and thermal protein denaturation by combination of computational and experimental approaches. II, *J Chem Phys 135*, 175102.
247. de Groot, N. S., and Ventura, S. (2005) Amyloid fibril formation by bovine cytochrome c, *Spectroscopy 19*, 199-205.
248. Sunde, M., and Blake, C. (1997) The structure of amyloid fibrils by electron microscopy and X-ray diffraction, *Adv Protein Chem 50*, 123–159.
249. Pertinhez, T. A., Bouchard, M., Tomlinson, E. J., Wain, R., Ferguson, S. J., Dobson, C. M., and Smith, L. J. (2001) Amyloid fibril formation by a helical cytochrome, *FEBS Lett 495*, 184-186.
250. Plakoutsi, g., Bemporad, F., Calamai, M., Taddei, N., Dobson, C. M., and Chiti, F. (2005) Evidence for a Mechanism of Amyloid Formation Involving Molecular Reorganisation within Native-like Precursor Aggregates, *J Mol Biol 351*, 910-922.
251. Kelly, J. W. (1998) The Alternative Conformations of Amyloidogenic Proteins and Their Multi-Step Assembly Pathways, *Curr Opin Struct Biol 8*, 101-106.
252. Lansbury, J. P. T. (1999) Evolution of Amyloid: What Normal Protein Folding May Tell Us About Fibrillogenesis and Disease, *Proc Natl Acad Sci USA 96*, 3342-3344.
253. Aggeli, A., Nyrkova, I. A., Bell, M., Harding, R., Carrick, L., McLeish, T. C. B., Semenov, A. N., and Boden, N. (2001) Hierarchical Self-Assembly of Chiral Rod-Like

Molecules as a Model for Peptide β-Sheet Tapes, Ribbons, Fibrils, and Fibers, *Proc Natl Acad Sci USA 98*, 11857-11862.

254. van Holde, K. E., Johnson, W. C., and Ho, P. S. (2006) *Principles of physical biochemistry*, 2nd ed., Pearson/Prentice Hall Upper Saddle River, NJ.
255. Ingle, J. D., and R, C. S. (1988) *Spectrochemical Analysis*, Prentice Hall.
256. Cupane, A., Leone, M., Vitrano, E., and Cordone, L. (1995) Low temperature optical absorption spectroscopy: an approach to study the stereodynamic properties of heme proteins, *Eur Biophys J 23*, 385–398.
257. Melchers, B., Knapp, E. W., Parak, F., Cordone, L., Cupane, A., and Leone, M. (1996) Structural fluctuations of myoglobin from normal-modes, Mössbauer, Raman, and absorption spectroscopy, *Biophys J 70*, 2092-2099.
258. Rodger, A., Norden, B., and Ismail, M. (1997) *Circular Dichroism and Linear Dichroism*.
259. Dragomir, I. C., Hagarman, A. M., Wallace, C. J. A., and Schweitzer-Stenner, R. (2007) Optical band splitting and electronic perturbations of the heme chromophore in cytochrome c at room temperature probed by visible electronic circular dichroism spectroscopy, *Biophys J 92*, 989-998.
260. Schweitzer-Stenner, R. (2001) Polarized resonance Raman dispersion spectroscopy on metalporphyrins, *J Porphyrins Phthalocyanines 5*, 198-224.
261. Shelnutt, J. A., Cheung, L., Chang, R., Yu, N.-T., and Felton, R. (1977) Resonance Raman spectra of metalloporphyrins. Effects of Jahn–Teller instability and nuclear distortion on excitation profiles of Stokes fundamentalsDistortion on Excitation Profiles of Stokes Fundamentals, *J Chem Phys 66*, 3387-3398.
262. Gouterman, M. (1961) Spectra of porphyrins: Part I, J Mol *Spectros 6*, 138-163.
263. Gouterman, M., Wagnière, G. H., and Snyder, L. C. (1963) Spectra of porphyrins : Part II. Four orbital model, *J Mol Spectros 11*, 108-127.
264. Margoliash, E., and Nehamah, F. (1959) Spectrum of horse-heart cytochrome c, *Biochem J 71*, 570-572.
265. Schweitzer-Stenner, R. (1989) Allosteric linkage-induced distortions of the prosthetic group in haem proteins as derived by the theoretical interpretation of the depolarization ratio in resonance Raman scattering, *22*, 381-479.
266. Gouterman, M. (1959) Study of the Effects of Substitution on the Absorption Spectra of Porphin, *30*, 1139-1161.
267. Schweitzer-Stenner, R. (2008) Internal Electric Field in Cytochrome C Explored by Visible Electronic Circular Dichroism Spectroscopy., *Q Rev Biophys 112*, 10358-10366.
268. Unger, E., Bobinger, U., Dreybrodt, W., and Schweitzer-Stenner, R. (1993) Vibronic coupling in nickel(II) porphine derived from resonant Raman excitation profiles, *J Phys Chem B 97*, 9956-9968.
269. Schweitzer-Stenner, R., Soffer, J. B., and Verbaro, D. (2012) Structure Analysis of Unfolded Peptides I: Vibrational Circular Dichroism Spectroscopy, In *Methods in Molecular Biology*, pp 271-313, Humana Press, Totowa, NJ.
270. Schweitzer-Stenner, R., and Bigman, D. (2001) Electronic and Vibronic Contributions to the Band Splitting in Optical Spectra of Heme Proteins, *J Phys Chem B 105*, 7064–7073.

271. Levantino, M., Huang, Q., Cupane, A., Laberge, M., Hagarman, A. M., and Schweitzer-Stenner, R. (2005) The importance of vibronic perturbations in ferrocytochrome c spectra: A reevaluation of spectral properties based on low-temperature optical absorption, resonance Raman, and molecular-dynamics simulations, *J Chem Phys 123*, 054508.
272. Shelnutt, J. A., Cheung, L., Chang, R., Yu, N.-T., and Felton, R. (1977) Resonance Raman spectra of metalloporphyrins. Effects of Jahn–Teller instability and nuclear distortion on excitation profiles of Stokes fundamentals - Distortion on Excitation Profiles of Stokes Fundamentals, *J Chem Phys 66*, 3387-3398.
273. Champion, P. M., and Albrecht, A. C. (1979) Investigations of Soret excited resonance Raman excitation profiles in cytochrome c, *J Chem Phys 71*, 1110-1122.
274. Stallard, B. R., Callis, P. R., Champion, P. M., and Albrecht, A. C. (1984) Application of the transform theory to resonance Raman excitation profiles in the Soret region of cytochrome-c, *J Chem Phys 80*, 70-82.
275. Schweitzer-Stenner, R., Cupane, A., Leone, M., Lemke, C., Schott, J., and Dreybrodt, W. (2000) Anharmonic Protein Motions and Heme Deformations in Myoglobin Cyanide Probed by Absorption and Resonance Raman Spectroscopy, *J Phys Chem B 104*, 4754-4764.
276. Manas, E. S., Vanderkooi, J. M., and Sharp, K. A. (1999) The effects of protein environment on the low temperature electronic spectroscopy of cytochrome c and microperoxidase-11, *J Phys Chem B 103*, 6334-6348.
277. Woody, R. W. (1996) Theory of Circular Dichroism of Proteins, In *Circular Dichroism and the Conformational Analysis of Biomolecules* (Fasman, G. D., Ed.), pp 25-67, Plenum Press, New York.
278. Leone, M., Cupane, A., Militello, V., and Cordone, L. (1994) Thermal broadening of the Soret band in heme complexes and in heme-proteins: role of the iron dynamics, *Eur. Biophysic. J. 23*, 349-352.
279. Eaton, W. A., and Hochstrasser, R. M. (1968) Single-Crystal Spectra of Ferrimyoglobin Complexes in Polarized Light, *J Chem Phys 49*, 985-995.
280. Schejter, A., and George, P. (1964) The 695-mμ Band of Ferricytochrome c and Its Relationship to Protein Conformation, *Biochemistry 3*, 1045-1049.
281. Theorell, H., and Akesson, A. (1941) Studies on Cytochrome c. II. The Optical Properties of Pure Cytochrome c and Some of Its Derivatives, *J Am Chem Soc 63*, 1812-1818.
282. McKnight, J., Cheesman, M., Thomson, A., Miles, J., and Munro, A. (1993) Identification of charge-transfer transitions in the optical spectrum of low-spin ferric cytochrome P-450 Bacillus megaterium, *Eur J Biochem 213*, 683-687.
283. Dragomir, I. C., Hagarman, A. M., Wallace, C. J. A., and Schweitzer-Stenner, R. (2007) Optical band splitting and electronic perturbations of the heme chromophore in cytochrome c at room temperature probed by visible electronic circular dichroism spectroscopy, *Biophys J 92*, 989-998.
284. Schweitzer-Stenner, R., Shah, R., Hagarman, A. M., and Dragomir, I. C. (2007) Conformational substates of horse heart cytochrome c exhibit different thermal unfolding of the heme cavity, *J Phys Chem B 111*, 9603-9607.

285. Spilotros, A., Levantino, M., and Cupane, A. (2010) Conformational substates of ferricytochrome c revealed by combined optical absorption and electronic circular dichroism spectroscopy at cryogenic temperature., *Biophys Chem 147*, 8-12.
286. Battistuzzi, G., Borsari, M., Loschi, L., Martinelli, A., and Sola, M. (1999) Thermodynamics of the alkaline transition of cytochrome c, *Biochemistry 38*, 7900-7907.
287. Woody, R. W., and Dunker, A. K. (1996) *Aromatic and Cysteine Side Chain Circular Dichroism in Proteins*, Plenum Press, New York.
288. Blauer, G. B., Sreerama, N., and Woody, R. W. (1993) Optical activity of hemoproteins in the soret region. circular dichroism of the heme undecapeptide of cytochrome c in aqueous solution, *Biochemistry 32*, 6674-6679.
289. Hsu, M. C., and Woody, R. W. (1971) The origin of the heme cotton effects in myoglobin and hemoglobin, *J Am Chem Soc 93*, 3515–3525.
290. Kelly, S. M., and Price, N. C. (2006) Circular Dichroism to Study Protein Interactions, *Curr Prot Protein Sci 20.10*, 1-18.
291. Tinoco, I. (1962) Theoretical Aspects of Optical Activity, *Adv. Chem. Phys. 4*, 113 - 160.
292. Sreerama, N., and Woody, R. W. (1993) A Self-Consistent Method for the Analysis of Protein Secondary Structure from Circular Dichroism, *209*, 32-44.
293. Woody, R. W. (2009) Circular dichroism spectrum of peptides in the poly(Pro)II conformation, *J Mol Biol 131*, 8234-8245.
294. Greenfield, N. (1996) Methods to Estimate the Conformtation of Proteins and Polypeptides from Circular Dichroism Data, *Anal Biochem 235*, 1-10.
295. Andrade, M. A., Chacón, P., Merelo, J. J., and Morán, F. (1993) Evaluation of secondary structure of proteins from UV circular dichroism spectra using an unsupervised learning neural network, *Protein Eng Des Sel 6*, 383-390.
296. Böhm, G., Muhr, R., and Jaenicke, R. (1992) Quantitative analysis of protein far UV circular dichroism spectra by neural networks *Protein Eng Des Sel 5*, 191-195.
297. Merolo, J. J., Andrade, M. A., Prieto, A., and Moran, F. (1994) Proteinotopic feature maps, *Neurocomputing 6*, 443-454.
298. Provencher, S. W., and Glockner, J. (1981) Estimation of globular protein secondary structure from circular dichroism, *Biochemistry 20*, 33-37.
299. Manavalan, P., and Johnson, W. C., Jr. (1987) Variable selection method improves the prediction of protein secondary structure from circular dichroism spectra, *Anal Biochem 167*, 76-85.
300. Sreerama, N., and Woody, R. W. (1994) Poly(Pro)II Helixes in Globular Proteins: Identification and Circular Dichroic Analysis, *33*, 10022-10025.
301. Sreerama, N., and Woody, R. W. (1994) Protein secondary structure from circular dichroism spectroscopy - Combining variable selection principle and cluster analysis with neural network, ridge regression and self-consistent methods, *J Mol Biol 242*, 497-507.
302. Black, K. M., and Wallace, C. J. A. (2007) Probing the role of the conserved β-II turn Pro-76/Gly-77 of mitochondrial cytochrome c, *Biochem Cell Biol 85*, 366-374.
303. Lobley, A., Whitmore, L., and Wallace, B. (2002) DICHROWEB: An interactive website for the analysis of protein secondary structure from circular dichroism spectra, *Bioinformatics 18*, 211-212.

304. Whitmore, L., and Wallace, B. (2008) Protein Secondary Structure Analyses from Circular Dichroism Spectroscopy: Methods and Reference Databases, *Biopolymers 89*, 392-400.
305. Whitmore, L., and Wallace, B. (2004) DICHROWEB, an online server for protein secondary structure analyses from circular dichroism spectroscopic data, *Nucleic Acids Res 32*, W668-W673.
306. Uversky, V. N. (2002) Natively unfolded proteins: A point where biology waits for physics, *Protein Sci 11*, 739-756.
307. Lu, Y., Yeung, N., Sieracki, N., and Marshall, N. M. (2009) Review Article Design of functional metalloproteins, *Nature 460*, 855-862.
308. Lu, Y., Berry, S. M., and Pfister, T. D. (2001) Engineering Novel Metalloproteins: Design of Metal-Binding Sites into Native Protein Scaffolds, *Chem Rev 101*, 3074-3080.
309. Schweitzer-Stenner, R., Gorden, J. P., and Hagarman, A. M. (2007) Asymmetric band profile of the Soret band of deoxymyoglobin is caused by electronic and vibronic perturbations of the heme group rather than by a doming deformation, *J Chem Phys 127*, 135103.
310. Woody, R. W., and Hsu, M.-C. (1971) The Origin of the heme Cotton effects in myoglobin and hemoglobin, *Biochemistry 93*, 3515-3525.
311. Kiefl, C., Sreerama, N., Haddad, R. E., Sun, L., Jentzen, W., Lu, Y., Qiu, Y., Shelnutt, J. A., and Woody, R. W. (2002) Heme Distortions in Sperm-Whale Carbonmonoxy Myoglobin: Correlations between Rotational Strengths and Heme Distortions in MD-Generated Structures, *J Am Chem Soc 124*, 3385-3394.
312. Urry, D. W. (1965) Protein-heme interactions in heme-proteins: cytochrome c, *Proc Natl Acad Sci 54*, 640-648.
313. Urry, D. W., and Doty, P. (1965) On the conformation of horse heart ferri- and ferrocytochrome-c, *J Am Chem Soc 87*, 2756-2758.
314. Shelnutt, J. A., Song, X.-Z., Ma, J.-G., Jia, S.-L., Jentzen, W., and Medforth, C. J. (1998) Nonplanar porphyrins and their significance in proteins, *Chem Soc Rev 27*, 31-41.
315. Schweitzer-Stenner, R. (1989) Allosteric linkage-induced distortions of the prosthetic group in haem proteins as derived by the theoretical interpretation of the depolarization ratio in resonance Raman scattering, *Q Rev Biophys 22*, 381-479.
316. Hobbs, J. D., and Shelnutt, J. A. (1995) Conserved nonplanar heme distortions in cytochromes c, *J Protein Chem 14*, 19-25.
317. Jentzen, W., Simpson, M. C., Hobbs, J. D., Song, X., Ema, T., Nelson, N. Y., Medforth, C. J., Smith, K. M., and Veyrat, M. (1995) Ruffling in a Series of Nickel(II) meso-Tetrasubstituted Porphyrins as a Model for the Conserved Ruffling of the Heme of Cytochromes c, *J Am Chem Soc 117*, 11085-11097.
318. Huang, Q., Medforth, C. J., and Schweitzer-Stenner, R. (2005) Nonplanar Heme Deformations and Excited State Displacements in Nickel Porphyrins Detected by Raman Spectroscopy at Soret Excitation, *J Phys Chem A 109*, 10493–10502.
319. Schweitzer-Stenner, R. (2001) Polarized resonance Raman dispersion spectroscopy on metalporphyrins, *J Porphyrins Phthalocyanines 5*, 198-224.
320. Shelnutt, J. A. (2001) Normal-Coordinate Structural Decomposition and the Vibronic spectra of porphyrins, *J Porphyrins Phthalocyanines*, 5, 300-311.

321. Shelnutt, J. A. (2000), Vol. 7, Academic Press, San Diego.
322. Urry, D. W. (1965) Protein-heme interactions in heme-proteins: cytochrome C, *Proc Natl Acad Sci USA 54*, 640-648.
323. Urry, D. W., and Doty, P. (1965) On the conformation of horse heart ferri- and ferrocytochrome-c, *J Am Chem Soc 87*, 2756-2758.
324. Blauer, G. B., Sreerama, N., and Woody, R. W. (1993) Optical activity of hemoproteins in the Soret region. Circular dichroism of the heme undecapeptide of cytochrome c in aqueous solution, *Biochemistry 32*, 6674-6679.
325. Hsu, M. C., and Woody, R. W. (1971) The origin of the heme Cotton effects in myoglobin and hemoglobin, *J Am Chem Soc 93*, 3515–3525.
326. Pinheiro, T., Elove, G. A., Watts, A., and Roder, H. (1997) Structural and kinetic description of cytochrome c unfolding induced by the interaction with lipid vesicles, *Biochemistry 36*, 13122-13132.
327. Hagarman, A. M., Duitch, L., and Schweitzer-Stenner, R. (2008) The conformational manifold of ferricytochrome c explored by visible and far-UV electronic circular dichroism spectroscopy, *Biochemistry 47*, 9667-9677.
328. Schweitzer-Stenner, R. (2008) Internal electric field in cytochrome c explored by visible electronic circular dichroism spectroscopy, *J Phys Chem B 112*, 10358-10366.
329. Long, D. A. (2002) *The Raman Effect: A Unified Treatment of the Theory of Raman Scattering by Molecules*, John Wiley & Sons Ltd.
330. Schweitzer-Stenner, R., Stichternath, A., Dreybrodt, W., Jentzen, W., Song, X.-Z., Shelnutt, J. A., Nielson, O. F., Medforth, C. J., and Slade, K. M. (1997) Raman dispersion spectroscopy on the highly saddled nickel(II)-octaethyltetraphenylporphyrin reveals the symmetry of nonplanar distortions and the vibronic coupling strength of normal modes, *J Chem Phys 107*, 1794.
331. Jentzen, W., Song, X.-Z., and Shelnutt, J. A. (1997) Structural Characterization of Synthetic and Protein-Bound Porphyrins in Terms of the Lowest-Frequency Normal Coordinates of the Macrocycle, *J Phys Chem B 101*, 1684-1699.
332. Spiro, T. G. (1975) Biological Applications of Resonance Raman Spectroscopy: Haem Proteins, *Proc R Soc London, Ser A 345*, 89-105.
333. Spiro, T. G. (1983) In *Iron Porphyrins, Part II* (Lever, A., and Grey, H., Eds.), pp 89-160, Addison-Wesley, Reading, Mass.
334. Li, X.-Y., Czernuszewicz, R. S., Kincaid, J. R., and Spiro, T. G. (1989) Consistent porphyrin force field. 3. Out-of-plane modes in the resonance Raman spectra of planar and ruffled nickel octaethylporphyrin, *J Am Chem Soc 111*, 7012-7023.
335. Spiro, T. G., and Strekas, T. C. (1972) Resonance Raman spectra of hemoglobin and cytochrome c: inverse polarization and vibronic scattering, *Proc Natl Acad Sci USA 69*, 2622-2626.
336. Spiro, T. G., and Strekas, T. C. (1974) Resonance Raman spectra of heme proteins. Effects of oxidation and spin state, *J Am Chem Soc 96*, 338-345.
337. Strekas, T. C., and Spiro, T. G. (1972) Cytochrome c: resonance Raman spectra, *Biochim Biophys Acta 278*, 188-192.
338. Zgierski, M. Z., and Pawlikowski, M. (1979) Theory of resonance Raman scattering by doubly degenerate modes a), *J Chem Phys 71*, 2025-2043.

339. Zgierskic, M. Z., and Pawlikowski, M. (1979) Jahn–Teller, pseudo Jahn–Teller coupling, and circular dichroism spectra of (E+A) e systemsa),b), *J Chem Phys 70*, 3444-3452.
340. Bobinger, U., Schweitzer-Stenner, R., and Dreybrodt, W. (1989) Highly Resolved Depolarization Dispersion and Excitation Profiles of Raman Fundamentals of Protoporphyrin IX in a Cytochrome c Matrix, *J Raman Spectros 20*, 191-202.
341. Rush, I., Kozlowski, P. M., Piffat, C. A., Kumar, R., Zgierski, M. Z., and Spiro, T. G. (2000) Computational Modeling of Metalloporphyrin Structure and Vibrational Spectra: Porphyrin Ruffling in NiTPP, *J Phys Chem B 104*, 5020–5034.
342. Shelnutt, J. A. (1980) The Raman excitation spectra and absorption spectrum of a metalloporphyrin in an environment of low symmetry, *J Chem Phys 72*, 3948-3958.
343. McClain, W. (1971) Excited State Symmetry Assignment Through Polarized Two-Photon Absorption Studies of Fluids, *J Chem Phys 55*, 2789-2796.
344. Abe, M., Kitagawa, T., and Kyogoku, Y. (1978) Resonance Raman spectra of octaethylporphyrinato-Ni(II) and meso-deuterated and 15N substituted derivatives. II. A normal coordinate analysis, *J Chem Phys 69*, 4526-4534.
345. Hu, S., Slade, K. M., and Spiro, T. G. (1996) Assignment of Protoheme Resonance Raman Spectrum by Heme Labeling in Myoglobin, *J Am Chem Soc 118*, 12638–12646.
346. Kitagawa, T., Abe, M., and Ogoshi, H. (1978) Resonance Raman spectra of octaethylporphyrinato-Ni(II) and meso-deuterated and 15N substituted derivatives. I. Observation and assignments of nonfundamental Raman lines, *J Chm Phys 69*, 4516.
347. Ozaki, Y., Kitagawa, T., Kyogoku, Y., Shimada, H., and Iizuka, T. (1976) An Anomaly in the Resonance Raman Spectra of Cytochrome P-450cam in the Ferrous High-spin State, *J Biochem 80*, 1447-1451.
348. Spiro, T. G., and Burke, J. M. (1976) Protein control of porphyrin conformation. Comparison of resonance Raman spectra of heme proteins with mesoporphyrin IX analogs, *J Am Chem Soc 98*, 5482-5489.
349. Spiro, T. G., and Strekas, T. C. (1974) Resonance Raman spectra of heme proteins. Effects of oxidation and spin state, *J Am Chem Soc 96*, 338-345.
350. Kincaid, J. R. (2000) Resonance Raman Spectra of Heme Proteins and Model Compounds, In *The Porphyrin Handbook* (Kadish, K. M., Smith, K. M., and Guillard, R., Eds.), pp 225-292, Academic Press.
351. Tsai, H.-H., and Simpson, M. C. (2004) Isolated Impact of Ruffling on the Vibrational Spectrum of Ni Porphyrins. Diagnosing Out-of-Plane Distortions, *J Phys Chem A 108*, 1224-1232.
352. Jentzen, W., Simpson, M. C., Hobbs, J. D., Song, X., Ema, T., Nelson, N. Y., Medforth, C. J., Smith, K. M., Veyrat, M., Mazzanti, M., Ramasseul, R., Marchon, J.-C., Takeuchi, T., Goddard III, W. A., and Shelnutt, J. A. (1995) Ruffling in a Series of Nickel(II) meso-Tetrasubstituted Porphyrins as a Model for the Conserved Ruffling of the Heme of Cytochromes c, *J Am Chem Soc 117*.
353. Shelnutt, J. A., Medforth, C. J., Berber, M. D., Barkigia, K. M., and Smith, K. M. (1991) Relationships between structural parameters and Raman frequencies for some planar and nonplanar nickel(II) porphyrins, *J Am Chem Soc 113*, 4077–4087.
354. Hobbs, J. D., and Shelnutt, J. A. (1995) Conserved nonplanar heme distortions in cytochromes c, *J Protein Chem 14*, 19-25.

355. Klug, D. D., Zgierski, M. Z., Tse, J. S., Liu, Z., Kincaid, J. R., Czarnecki, K., and Hemley, R. J. (2002) Doming modes and dynamics of model heme compounds, *Proc Natl Acad Sci USA 99*, 12526-12530.
356. Kronman, M. J., and Holmes, L. G. (1971) The Fluorescence of Native, Denatured and Reduced-denatured proteins *Photochem Photobiol 14*, 113-134.
357. Longworth, J. W. (1971) Luminescence of polypeptides and proteins, In *Excited states of proteins and nucleic acids* (Steiner, R. F., and Weinryb, I., Eds.), pp 319–484, Plenum Press, New York.
358. Burstein, E. A., Abornev, S. M., and Reshetnyak, Y. K. (2001) Decomposition of Protein Tryptophan Fluorescence Spectra into Log-Normal Components. I. Decomposition Algorithms, *Biophys J 81*, 1699-1709.
359. Lakowicz, J. R. (2006) *Principles of Fluorescence Spectroscopy*, 3rd ed., Springer, New York, NY.
360. Brems, D. N., and Stellwagen, E. (1983) Manipulation of the observed kinetic phases in the refolding of denatured ferricytochromes c, *J Biol Chem 258*, 3655-3660.
361. Battistuzzi, G., Borsari, M., Loschi, L., Martinelli, A., and Sola, M. (1999) Thermodynamics of the Alkaline Transition of Cytochrome c, *Biochemistry 38*, 7900-7907.
362. Dixon, H. B. F., and Mcintosh, R. (1967) Reduction of Methaemoglobin in Haemoglobin Samples using Gel Filtration for Continuous Removal of Reaction Products, *Nature 213*, 399-400.
363. Dixon, H. B. F., and Moret, V. (1965) Removal of the N-terminal residue of a protein after transamination, *Biochem J 94*, 463-469.
364. Linder, R. E., Records, R., Barth, G., Bunnenberg, E., Djerassi, C., Hedlund, B. E., Rosenberg, A., Benson, E. S., Seamans, L., and Moscowitz, A. (1978) Partial reduction of aquomethemoglobin on a sephadex G-25 column as detected by magnetic circular dichroism spectroscopy and revised extinction coefficients for aquomethemoglobin, *Anal Biochem 90*, 474-480.
365. Alessi, M., Hagarman, A. M., Soffer, J. B., and Schweitzer-Stenner, R. (2011) In-plane deformations of the heme group in native and non-native oxidized cytochrome c probed by resonance Raman dispersion spectroscopy., *J Raman Spectros 42*, 917-925.
366. Aitken, A., and Learmonth, M. P. (2002) Quantitation of Tryptophan in Proteins, In *The Protein Protocols Handbook* (Walker, J. M., Ed.) 2nd ed., pp 41-44, Humana Press, Totowa, NJ.
367. Schneider, C. A., Rasband, W. S., and Eliceiri, K. W. (2012) NIH Image to ImageJ: 25 years of image analysis, *Nature Methods 9*, 671-675.
368. Jentzen, W., Simpson, M. C., Hobbs, J. D., Song, X., Ema, T., Nelson, N. Y., Medforth, C. J., Smith, K. M., and Veyrat, M. (1995) Ruffling in a Series of Nickel(II) meso-Tetrasubstituted Porphyrins as a Model for the Conserved Ruffling of the Heme of Cytochromes c, *Biochemistry 117*, 11085-11097.
369. Schweitzer-Stenner, R., Soffer, J. B., Toal, S., and Verbaro, D. (2012) Structural Analysis of Unfolded Peptides by Raman Spectroscopy, In *Methods in Molecular Biology*, pp 315-346, Humana Press, Totowa, NJ.
370. Karounis, G., and Unger, E. (1995) MultiFit, v. 1.32

371. Kulikov, A. V., Shilov, E. S., Mufazalov, I. A., Gogvadze, V., Nedospasov, S. A., and Zhivotovsky, B. (2012) Cytochrome c: the Achilles's heel in apoptosis, *Cell Mol Life Sci 69*, 1787-1797.
372. Cohen, D. S., and Pielak, G. J. (1995) Entropic Stabilization of Cytchrome c upon Reduction, *J. Am. Chem. Soc 117*, 1675-1677.
373. Lett, C. M., Berghuis, A. M., Frey, H. E., Lepock, J. R., and Guillemette, J. G. (1996) The Role of Conserved Water Molecule in redox-dependent Thermal Stability of Iso-1-cytochrome c, *J. Biol. Chem. 271*, 29088-29093.
374. Kubitscheck, U., Dreybrodt, W., and Schweitzer-Stenner, R. (1986) Detection of Heme-Distortions in Ferri- and Ferrocyto-Chrome C by Resonance Raman Scattering, *Spectrosc. Letts. 19*, 681-690.
375. Moore, G. R., and Williams, R. J. (1980) Nuclear-magnetic-resonance studies of errocytochrome c. pH and temperature dependence, *Eur. J. Biochem. 103*, 513-521.
376. Wackerbarth, H., and Hildebrandt, P. (2003) Redox and Conformational Equilibria and Dynamics of Cytochrome c at High Electric Fields, *Chem Phys Chem 4*, 714-724.
377. Pielak, G. J., Oikawa, K., Mauk, A. G., Smith, M., and Kay, C. (1986) Elimination of the negative soret Cotton effect of cytochrome c by replacement of the invariant phenylalanine using site-directed mutagenesis, *J Am Chem Soc 108*, 2724-2727.
378. Battistuzzi, G., Borsari, M., and Sola, M. (2001) Medium and temperature effects on the redox chemistry of cytochrome c, *Eur J Inorg Chem 2001*, 2989-3004.
379. Monari, S., Ranieri, A., Di Rocco, G., Zwan, G., Peressini, S., Tavagnacco, C., Millo, D., and Borsari, M. (2009) Redox thermodynamics of cytochromes c subjected to urea induced unfolding, *J Appl Electrochem 39*, 2181-2190.
380. Myer, Y. P. (1968) Conformation of cytochromes. III. Effect of urea, temperature, extrinsic ligands, and pH variation on the conformation of horse heart ferricytochrome c, *Biochemistry 7*, 765-776.
381. Myer, Y. P., MacDonald, L., Verma, B., and Pande, A. (1980) Urea denaturation of horse heart ferricytochrome c. Equilibrium studies and characterization of intermediate forms, *Biochemistry 19*, 199-207.
382. Yeh, S.-R., and Rousseau, D. L. (1998) Folding intermediates in cytochrome c, *Nat Struct Biol 5*, 222-228.
383. Good, N. E., Winget, G. D., Winter, W., Connolly, T. N., Izawa, S., and Singh, R. M. M. (1966) Hydrogen ion buffers for biological research, *Biochemistry 5*, 467–477.
384. Software, S. SigmaPlot, v. 12.2, Systat Software, San Jose, CA.
385. Balakrishnan, G., Hu, Y. Y., and Spiro, T. G. (2012) His26 protonation in cytochrome c triggers microsecond beta-sheet formation and heme exposure: implications for apoptosis, *J Am Chem Soc 134*, 19061-19069.
386. Dill, K. A., and Shortle, D. (1991) Denatured States of Proteins, *Annu Rev Biochem 60*, 795-825.
387. Uversky, V. N. (2002) Natively unfolded proteins: A point where biology waits for physics, *Protein Sci 11*, 739-756.
388. Filosa, A., Ismail, A. A., and English, A. M. (1999) FTIR-monitored thermal titration reveals different mechanisms for the alkaline isomerization of tuna compared to horse and bovine cytochromes c, *J Biol Inorg Chem 4*, 717-726.
389. Filosa, A., and English, A. M. (2000) Probing local thermal stabilities of bovine, horse, and tuna ferricytochromes c at pH 7, *J Biol Inorg Chem 5*, 448-454.

390. Chaffotte, A. F., Guijarro, J. I., Guillou, Y., Delepierre, M., and Goldberg, M. E. (1997) The "Pre-Molten Globule," a New Intermediate in Protein Folding, *J Protein Chem 16*, 433-439.
391. Vanderkooi, J. M., Calhoun, D. B., and Englander, S. W. (1987) On the prevalence of room-temperature protein phosphorescence, *Science 236*, 568-569
392. Gabellieri, E., and Strambini, G. B. (2001) Structural Perturbations of Azurin Deposited on Solid Matrices as Revealed by Trp Phosphorescence, *Biophysical J 80*, 2431-2438.
393. Strambini, G. B. Room-temperature phosphorescence of alcohol dehydrogenase from horse liver, *Biophys J 43*, 127-130.
394. Papp, S., and Vanderkooi, J. M. (1989) Tryptophan phospherescence at room temperature as a tool to study protein structure and dynamics, *Photochem Photobiol 49*, 775-784.
395. Tsong, T. Y. (1976) Ferricytochrome c chain folding measured by the energy transfer of tryptophan 59 to the heme group, *Biochemistry 15*, 5467-5473.
396. Uchiyama, S., Hasegawa, J., Tanimoto, Y., Moriguchi, H., Mizutani, M., Igarashi, Y., Sambongi, Y., and Kobayashi, Y. (2002) Thermodynamic characterization of variants of mesophilic cytochrome c and its thermophilic counterpart, *Protein Eng 15*, 445-461.
397. Kurodab, Y., Kidokoro, S.-i., and Wada, A. (1992) Thermodynamic characterization of cytochrome c at low pH: Observation of the molten globule state and of the cold denaturation process, *J Mol Biol 223*, 1139-1153.
398. Cohen, D. S., and Pielak, G. J. (1995) Entropic Stabilization of Cytochrome c upon Reduction, *J Am Chem Soc 117*, 1675-1677.
399. Cohen, D. S., and Pielak, G. J. (1994) Stability of yeast iso-1-ferricytochrome c as a function of pH and temperature, *Protein Sci 3*, 1253-1260.
400. Pielak, G. J., Auld, D. S., Beasley, J. R., Betz, S. F., Cohen, D. S., Doyle, D. F., Finger, S. A., Fredericks, Z. L., and Hilgen-Willis, S. (1995) Protein Thermal Denaturation, Side-Chain Models, and Evolution: Amino Acid Substitutions at a Conserved Helix-Helix Interface, *Biochemistry 34*, 3268–3276.
401. Lumry, R., and Rajender, S. (1970) Enthalpy-entropy compensation phenomena in water solutions of proteins and small molecules: a ubiquitous property of water, *Biopolymers 9*, 1125-1227.
402. Liu, L., and Guo, Q.-X. (2001) Isokinetic Relationship, Isoequilibrium Relationship, and Enthalpy–Entropy Compensation, *Chem Rev 101*, 673-695.
403. Lumry, R., and Shyamala, R. (1970) Enthalpy-Entropy Compensation Phenomena in Water Solutions of Proteins and Small M olecules: A Ubiquitous Property of Water, *Biopolymers 9*, 1125-1227.
404. Krug, R. R., Hungter, W. G., and Grieger, R. A. (1976) Statistical interpretation of enthalpy-entropy compensation, *Nature 261*, 566–567.
405. Beasley, J. R., Doyle, D. F., Chen, L., Cohen, D. S., Fine, B. R., and Pielak, G. J. (2002) Searching for Quantitative Entropy-Enthalpy Compensation among Protein Variants, *Proteins 49*, 398–402.
406. Grunwald, E., and Steel, C. (1995) Solvent reorganization and thermodynamic enthalpy-entropy compensation, *J Am Chem Soc 117*, 5687-5692.
407. Qian, H., and Hopfield, J. J. (1996) Entropy-enthalpy compensation: Perturbation and relaxation in thermodynamic systems, *J Chem Phys 105*, 9292-9298.

408. Beasley, J. R., Doyle, D. F., Cohen, D. S., Fine, B. R., and Pielak, G. J. (2002) Searching for Quantitative Entropy-Enthalpy Compensation among Protein Variants, *Proteins 49*, 398-402.
409. Chodera, J. D., and Mobley, D. L. (2013) Entropy-Enthalpy Compensation: Role and Ramifications in Biomolecular Ligand Recognition and Design, *Annu Rev Biophys 42*, 121-142.
410. Toal, S., Omidi, A., and Schweitzer-Stenner, R. (2011) Conformational Changes of Trialanine Induced by Direct Interactions between Alanine Residues and Alcohols in Binary Mixtures of Water with Glycerol and Ethanol, *J. Am. Chem. Soc. 133*, 12728.
411. Milne, J., Xu, Y., Mayne, L., and Englander, S. W. (1999) Experimental study of the protein folding landscape: Unfolding reactions in Cytochrome c, *J Mol Biol 290*, 811–822.
412. Korth, M. (2013) A quantum chemical view of enthalpy-entropy compensatiom, *MedChemComm 4*, 1025-1033.
413. Sinibaldi, F., Piro, M. C., Howes, B. D., Smulevich, G., Ascoli, F., and Santucci, R. (2003) Rupture of the hydrogen bond linking two Omega-loops induces the molten globule state at neutral pH in cytochrome c, *Biochemistry 42*, 7604-7610.
414. Rose, G. D., Fleming, P. J., Banavar, J. R., and Maritan, A. (2006) A backbone-based theory of protein folding, *Proc Natl Acad Sci USA 103*, 16623-16633.
415. Yeh, S.-R., Takahashi, S., Fan, B., and Rousseau, D. L. (1997) Ligand exchange during cytochrome c folding, *Nature Struct. Biol. 4*, 51-56.
416. Tzul, F. O., Kurchan, E., Roder, H., and Bowler, B. E. (2009) Competition between reversible aggregation and loop formation in denatured iso-1-cytochrome c, *Biochemistry 48*, 481-491.
417. Segel, D. J., Eliezer, D., Uversky, V. N., Fink, A. L., Hodgson, K., and Doniach, S. (1999) Transient Dimer in the Refolding Kinetics of Cytochrome c Characterized by Small-Angle X-ray Scattering, *Biochemistry 38*, 15352-15359.
418. Onuchic, J. N., Luthey-Schulten, Z., and Wolynes, P. G. (1997) Theory of Protein Folding: The Energy Landscape Perspective, *Ann Rev Phys Chem 48*, 545-600.
419. Liu, F., Gao, Y. G., and Gruebele, M. (2010) A Survey of λ Repressor Fragments from Two-State to Downhill Folding, *J Mol Biol 397*, 789-798.
420. Liu, F., and Gruebele, M. (2007) Tuning λ6–85 Towards Downhill Folding at its Melting Temperature, *J. Mol. Biol. 370*, 574-584.
421. Im, H., Woo, M.-S., Hwang, K. Y., and Yu, M.-H. (2002) Interactions Causing the Kinetic Trap in Serpin Protein Folding, *J Biol Chem 277*, 46347–46354.
422. McKnight, J., Cheesman, M. R., Thomson, A. J., Miles, J. S., and Munro, A. W. (1993) Identification id charge transfer transitions in the optical spectrum of low-spin ferric cytochrome -P450 *Bacillus Megaterium*., *Eur J Biochem 213*, 683-687.
423. Eaton, W. A., and Hochstrasser, R. M. (1967) Electronic Spectrum of Single Crystals of Ferricytochrome c, *J. Chem. Phys. 46*, 2533-2539.
424. Jentzen, W., Ma, J.-G., and Shelnutt, J. A. (1998) *Biophys. J. 74*, 7653.
425. Eaton, W., and Hochstrasser, R. M. (1958) Single-crystal spectra of ferrimyoglobin complexes in polarized light, *J. Chem. Phys 49*, 985-995.

426. Schweitzer-Stenner, R. (2008) The Internal Electric Field in Cytochrome C Explored by Visible Electronic Circular Dichroism Spectroscopy, *J. Phys. Chem. B 112*, 10358-10366.
427. Hagarman, A., Duitch, L., and Schweitzer-Stenner, R. (2008) The Conformational Manifold of Ferricytochromec Explored by Visible and Far-UV Electronic Circular Dichroism Spectroscopy, *Biochemistry 47*, 9667-9677.
428. Schweitzer-Stenner, R., Gorden, J. P., and Hagarman, A. (2007) The asymmetric band profile of the soret band of deoxymyoglobin is caused by electronic and vibronic perturbations of the heme group rather than by a doming deformation, *J. Chem. Phys. 127*, 135103.
429. Oellerich, S., Wackerbarth, H., and Hildebrandt, P. (2002) Spectroscopic Characterization of Nonnative Conformational States of Cytochrome c., *J. Phys. Chem. B. 106*, 6566-6580.
430. Barker, P. D., and Mauk, A. G. (1992) pH-Linked conformational regulation of a metalloprotein oxidation-reduction equilibrium: electrochemical analysis of the alkaline form of cytochrome c, *J Am Chem Soc 114*, 3619-3624.
431. Döpner, S., Hildebrandt, P., Rosell, F. I., and Mauk, A. G. (1998) Alkaline Conformational Transitions of Ferricytochrome c Studied by Resonance Raman Spectroscopy, *J Am Chem Soc 120*, 11246-11255.
432. Gorbenko, G. P., Molotkovsky, J. G., and Kinnunen, P. K. J. (2006) Cytochrome C interaction with cardiolipin/phosphatidylcholine model membranes: effect of cardiolipin protonation, *Biophys J 90*, 4093-4103.
433. Rytömaa, M., and Kinnunen, P. K. J. (1994) Evidence for two distinct acidic phospholipid-binding sites in cytochrome c, *J Biol Chem 269*, 1770-1774.
434. Kapralov, A. A., Kurnikov, I. V., Vlasova, I. I., Belikova, N. A., Tyurin, V. A., Basova, L. V., Zhao, Q., Tyurina, Y. Y., Jiang, J., Bayir, H. A., Vladimirov, Y., and Kagan, V. E. (2007) The hierarchy of structural transitions induced in cytochrome c by anionic phospholipids determines its peroxidase activation and selective peroxidation during apoptosis in cells, *Biochemistry 46*, 14232-14244.
435. Lobley, A., Whitmore, L., and Wallace, B. A. (2002) DICHROWEB: An interactive website for the analysis of protein secondary structure from circular dichroism spectra, *Bioinformatics 18*, 211-212.
436. Whitmore, L., and Wallace, B. A. (2004) DICHROWEB, an online server for protein secondary structure analyses from circular dichroism spectroscopic data, *Nucleic Acids Research 32*, W668-W673.
437. Sreerama, N., and Woody, R. W. (2000) Estimation of protein secondary structure from CD spectra: Comparison of CONTIN, SELCON, and CDSSTR methods with an expanded reference set, *Anal. Biochem. 287*, 252-260.
438. Lees, J. G., Miles, A. J., Wien, F., and Wallace, B. A. (2006) A reference database for circular dichroism spectroscopy covering fold and secondary structure space, *Bioinformatics 22*, 1955-1962.
439. Louie, G. V., and Brayer, G. D. (1990) High-resolution Refinement of Yeast Iso-1-Cytochrome c and Comparisons With Other Eukaryotic Cytochromes c, *J. Mol. Biol. 214*, 527-555.
440. Shi, Z., Woody, R. W., and Kallenbach, N. R. (2002) Is polyproline II a major backbone conformation in unfolded proteins?, *Adv. Protein Chem. 62*, 163-240.

441. Hagarman, A., Measey, T. J., Mathieu, D., Schwalbe, H., and Schweitzer-Stenner, R. (2010) Intrinsic Propensities of Amino Acid Residues in GxG Peptides Inferred from Amide I band profiles and NMR Scalar Coupling Constants, *J. Am. Chem. Soc. 132*, 540.
442. Uversky, V. N. (2002) Natively Unfolded Proteins: A point where biology waits for physics, *Science 11*, 739-756.
443. Oellerich, S., Wackerbarth, H., and Hildebrandt, P. (2002) Spectroscopic Characterization of Nonnative Conformational States of Cytochrome c, *J Phys Chem B 106*, 6566-6580.
444. Robinson, A. B., McKerrow, J. H., and Cary, P. (1970) Controlled Deamidation of Peptides and Proteins: An Experimental Hazard and a Possible Biological Timer, *Proc. Nat. Acad. Sci. 66*, 753-757.
445. Tzul, F. O., Kurchan, E., Roder, H., and Bowler, B. E. (2009) Competition between Reversible Aggregation and Loop Formation in Denatured Iso-1-cytochrome c, *Biochemistry 48*, 481-491.
446. Pertinhez, T. A., Bouchard, M., Tomlinson, E. J., Wain, R., Ferguson, S. J., Dobson, C. M., and Smith, L. J. (2001) Amyloid fibril formation by a helical cytochrome, FEBS Letters *495*, 184-186.
447. Bemporad, F., De Simone, A., Chiti, F., and Dobson, C. M. (2012) Characterizing Intermolecular Interactions That Initiate Native-Like Protein Aggregation, EMBO J *102*, 2595-2604.
448. Bennett, M. J., Sawaya, M. R., and Eisenberg, D. (2006) Deposition Diseases and 3D Domain Swapping, *Structure 14*, 811–824.
449. Bennett, M. J., Schlunegger, M. P., Eisenberg, D (1995) 3D domain swapping: a mechanism for oligomer assembly., *Protein Sci 4*, 2455.
450. Wang, Z., Matsuo, T., Nagao, S., and Hirota, S. (2011) Peroxidase activity enhancement of horse cytochrome c by dimerization, *Org Biomol Chem 9*, 4766-4769.
451. Yamasaki, M., Li, W., Johnson, D. J., and Huntington, J. (2008) Crystal structure of a stable dimer revelas the molecular basis of serpin polymerization, *Nature 455*, 1255-1258.
452. Friedman, J. M., Rousseau, D. L., and Adar, F. (1977) Excited state lifetimes in cytochromes measured from Raman scattering data: Evidence for iron-porphyrin interactions, *Proc. Natl. Acad. Sci. USA 74*, 2607-2611.
453. Hu, S., Morris, I. K., Singh, J. P., Smith, K. M., and Spiro, T. G. (1993) Complete Assignment of Cytochrome c Resonance Raman Spectra via Enzymatic Reconstitution with Isotopically Labeled Hemes, *J. Am. Chem. Soc. 115*, 12446.
454. Döpner, S., Hildebrandt, P., Rosell, F. I., and Mauk, A. G. (1998) Alkaline Conformational Transitions of Ferricytochrome c Studied by Resonance Raman Spectroscopy, *J. Am. Chem. Soc. 120*, 11246-11255.
455. Spiro, T. G. (1993) *The resonance Raman spectra of metalloporphyrins and heme proteins*, Addison-Wesley London.
456. Oellerich, S., Wackerbarth, H., and Hildebrandt, P. (2002) Spectroscopic characterization of nonnative conformational states of cytochrome c, *J. Phys. Chem. Part B. 106*, 6566–6580.

457. Huang, Q., and Schweitzer-Stenner, R. (2005) Non-planar heme deformations and excited state displacements in horseradish peroxidase detected by Raman spectroscopy at Soret excitation, *J Raman Spectrosc 36*, 363-375.
458. Sharanabasamma, K., and Tuwar, S. M. (2010) Kinetics and mechanism of oxidation of DL-mthionine by hexacyanoferrate (III) in aqueous alkaline medium, *J. Sulfur Chem. 31*, 177-187.
459. Shukla, R., and Upadhyay, S. K. (2008) Tween-80 catalysis in the oxidation of methionine and proline by alkalne hexacyanoferrate (III), *Colloides and Surfaces A 331*, 245-249.
460. Theorell, H., and Akesson, A. (1939) Absorption Spectrum of Further Purified Cytochrome c, *Science 90*, 67-67.
461. Oellerich, S., Wackerbarth, H., and Hildebrandt, P. (2002) Spectroscopic Characterization of Nonnative Conformational States of Cytochrome c, *J Phys Chem B 106*, 6566-6580.
462. Oellerich, S., Lecomte, S., Paternostre, M., Heimburg, T., and Hildebrandt, P. (2004) Peripheral and Integral Binding of Cytochrome c to Phospholipids Vesicles, *J. Phys. Chem. B. 108*, 3781-3878.
463. Silkstone, G. G., Cooper, C. E., Svistunenko, D., and Wilson, M. T. (2005) EPR and Optical Spectroscopic Studies of met80X Mutants of Yeast Ferricytochrome c. Models for Intermediates in the Alkaline Transition, *J. Am. Chem. Soc. 127*, 92-99.
464. Maltempo, M. M. (1976) Visible absorption spectra of quantum mixed-spin ferric heme proteins, *Biochim. Biophys. Acta 434*, 513–518.
465. Maltempo, M. M., and Moss, T. H. (1976) The spin 3/2 state and quantum spin mixtures in haem proteins, *Q Rev Biophys 9*, 181–215.
466. Feis, A., Howes, B. D., Indiani, C., and Smulevich, G. (1998) Resonance Raman and electronic absorption spectra of horseradish peroxidase isoenzyme A2: evidence for a quantum mix species, *J. Raman Spectrosc. 29*, 933-938.
467. Howes, B. D., Feis, A., Indiani, C., Morzocchi, M., and Smulevich, G. 2000, *J. Biol. Inorg. Chem. 276*, 40704-40711.
468. Huang, Q., Al-Azzam, W., Griebenow, K., and Schweitzer-Stenner, R. (2003) Heme Structural Perturbation of PEG-Modified Horseradish Peroxidase C in Aromatic Organic Solvents Probed by Optical Absorption and Resonance Raman Dispersion Spectroscopy, *Biophys. J. 84*, 3288-3298.
469. Balakrishnan, G., Hu, Y., and Spiro, T. G. (2012) H26 Protonation in Cytochrome c Triggers Microsecond β-Sheet Formation and Heme Exposure: Implications for Apoptosis, *J. Am. Chem. Soc. 134*, 19061–19069.
470. Bandi, S., and Bowler, B. E. (2011) Probing the Dynamics of a His73–Heme Alkaline Transition in a Destabilized Variant of Yeast Iso-1-cytochrome cwith Conformationally Gated Electron Transfer Methods, *Biochemistry 50*, 10027-10040.
471. Gajhede, M., Schuller, D. J., Heriksen, A., Smith., A. T., and Poulos, T. L. (1997) Crystal structure determination of classical horseradish peroxidase at 2.15 Å resolution, *Nat. Struct. Biol. 4*, 1032-1038.
472. Hauser, K., Mao, J., and Gunner, M. R. (2004) pH Dependence of Heme Electrochemistry in Cytochromes Investigated by Multiconformation Continuum Electrostatic Calculations, *Biopolymers 74*, 51-54.

473. Hayashi, Y., Nagao, S., Osuka, H., Komori, H., Higuchi, Y., and Hirota, S. (2012) Domain Swapping of the Heme and N-Terminal α-Helix in *Hydrogenobacter thermophilus* Cytochrome c_{552} Dimer, *Biochemistry 51*, 8608-8616.
474. Egawa, T., Lee, H. J., Ji, H., Gennis, R. B., Yeh, S.-R., and Rousseau, D. L. (2009) Identification of heme propionate vibrational modes in the resonance Raman spectra of cytochrome c oxidase, *Anal Biochem 394*, 141-143.
475. Branden, G., Branden, M., B, S., Mills, D. A., Ferguson-Miller, S., and Brzezinski, P. (2005) The protonation state of a heme propionate controls electron transfer in cytochrome c oxidase, *Biochemistry 44*, 10466-10474.
476. Soffer, J. B., Fradkin, E. K., Pandiscia, L. A., and Schweitzer-Stenner, R. (2013) The (Not Completely Irreversible) Population of a Misfolded State of Cytochrome c at Folding Conditions, *Biochemistry*, 1397-1408.
477. Everse, J., Liu, C.-J. J., and Coates, P. W. (2011) Physical and catalytic properties of a peroxidase derived from cytochrome c, *Biochim Biophys Acta 1812*, 1138-1145.
478. Belikova, N. A., Vladimirov, Y., Osipov, A. N., Kapralov, A. A., Tyurin, V. A., Potapovich, M., Basova, L. V., Peterson, J., Kurnikov, I. V., and Kagan, V. E. (2006) Peroxidase activity and structural transitions of cytochrome c bound to cardiolipin-containing membranes, *Biochemistry 45*, 4998-5009.
479. Alakoskela, J.-M., Jutila, A., Simonsen, A. C., Pirneskoski, J., Pyhäjoki, S., Turunen, R., Marttila, S., Mouritsen, O. G., Goormaghtigh, E., and Kinnunen, P. K. (2006) Characteristics of Fibers Formed by Cytochrome cand Induced by Anionic Phospholipids, *Biochemistry 45*, 13447-13453.
480. Ghosh, C., Mukherjee, S., and Dey, S. G. (2013) Direct electron transfer between cyt c and heme-Aβ relevant to Alzheimer's disease, *Chem Commun 49*, 5754-5756.
481. Narula, J., Pandey, P., Arbustini, E., Haider, N., Narula, N., Kolodgie, F. D., Dal Bello, B., Semigran, M. J., Bielsa-Masdeu, A., Dec, G. W., Israels, S., Ballester, M., Virmani, R., Saxena, S., and Kharbanda, S. (1999) Apoptosis in heart failure: release of cytochrome c from mitochondria and activation of caspase-3 in human cardiomyopathy, *Proc Natl Acad Sci USA 96*, 8144–8149.
482. Balasubramanian, K., and Schroit, A. J. (2003) Aminophospholipid asymmetry: A matter of life and death, *Annu Rev Physiol 65*, 701-734.
483. Reed, J. C. (1999) Dysregulation of Apoptosis in Cancer, *J Clin Oncol 17*, 2941-2953.
484. Piel, D. A., Deutschman, C. S., and Levy, R. J. (2008) Exogenous cytochrome C restores myocardial cytochrome oxidase activity into the late phase of sepsis, *Shock 29*, 612–616.
485. Piel, D. A., Gruber, P. J., Weinheimer, C. J., Courtois, M. R., Robertson, C. M., Coopersmith, C. M., Deutschman, C. S., and Levy, R. J. (2007) Mitochondrial resuscitation with exogenous cytochrome c in the septic heart, *Crit Care Med 35*, 2120–2127.
486. Tokuriki, N., and Tawfik, D. S. (2009) Protein Dynamism and Evolvability, *Science 324*, 203-207.
487. Bedard, S., Krishna, M. M., Mayne, L., and Englander, S. W. (2008) Protein folding: independent unrelated pathways or predetermined pathway with optional errors, *Proc Natl Acad Sci USA 105*, 7182-7187.

488. Weinkam, P., Zimmermann, J., Romesberg, F. E., and Wolynes, P. G. (2010) The folding energy landscape and free energy excitations of cytochrome c, *Acc Chem Res 43*, 652-660.
489. Yang, L.-Q., Ji, X.-L., and Liu, H.-Q. (2013) The free energy landscape of protein folding and dynamics: a global view, *J Biomol Struct Dyn 31*, 982-992.
490. Hu, S., Morris, I. K., Singh, J. P., Smith, K. M., and Spiro, T. G. (1993) Complete assignment of cytochrome c resonance Raman spectra via enzymic reconstitution with isotopically labeled hemes, *Biochemistry 115*, 12446-12458.

APPENDIX

AI. Abbreviations

ρ	depolarization ratio
A	FRET acceptor
AcOH	acetic acid
APAF-1	apoptotic protease activating factor 1
ATP	adenosine triphosphate
C	carbon atom
CD	circular dichroism
CE	Cotton effect
CI	compact intermediate sub-state of a protein
Cl-	chloride ion, the predominant negative ion in blood plasma
Complex III	cytochrome bc1 complex/ cytochrome reductase
Complex IV	cytochrome c oxidase
CPL	circularly polarized light
CT	charge transfer
cyt c	cytochrome c
D	FRET donor
D_2O	deuterium oxide
DBM	Debye-Bohr magneton
DFT	Density Functional Theory
DLS	dynamic light scattering
ECD	electronic circular dichroism
EPR	electron paramagnetic resonance
F	fully folded state of a protein, also referred to as the native state
FTIR	Fourier-transformed infrared spectroscopy

G	globular state of a protein
GdmCl	guanidinium chloride
hs	high spin iron
hchs	hexacoordinated high spin
HCl	hydrochloric acid
hcls	hexacoordinated low spin
HPO_4^{2-}	hydrogen phosphate, an ion found in blood plasma
HCO_3^-	hydrogen carbonate, the third most abundant ion in blood plasma
HOMO	highest occupied molecular orbital
I	intermediate state of a protein
I_x	Raman scattering intensity polarized parallel to incoming excitation frequency
I_y	Raman scattering intensity polarized perpendicular to excitation frequency
IUP	intrinsically unstructured protein
$K[Fe(CN)_6]$	potassium ferricyanide
KH_2PO_4	monobasic potassium phosphate buffer
KHD	Kramers-Heisenberg-Dirac relation for the polarizability tensor
LCAO	linear combination of atomic orbitals
ls	low spin iron
LUMO	lowest unoccupied molecular orbital
M	misfolded state of a protein
MD	molecular dynamics
MG	molten globular state of a protein
MOPS	3-(N-morpholino)propanesulfonic acid
N	native or fully folded state of a protein
NaOH	sodium hydroxide
$Na_2S_2O_4$	sodium dithionite
NADH	H-nicotinamide adenine dinucleotide

NMR	nuclear Magnetic Resonance
NO_3^-	nitrate, a common environmental ion, found in drinking water
ORD	optical rotatory dispersion
pcls	penta-coordinated low spin
pchs	penta-coordinated high spin
PcQM	pentacoordinated quantum mixed
PDB	protein data bank
preMG	pre-molten globular state of a protein
REDOX	Oxidation-Reduction reactions
ROA	Raman optical activity
ROS	reactive oxygen species
RR	resonance Raman
SAXS	small angle X-ray scattering
S	sulfur atom
SO_4^{2-}	sufate, a common environmental ion
TCA	trichloroacetic acid also known as trichloroethanoic acid
TFA	trifluoroacetic acid
Tris	tris(hydroxylmethyl)aminomethane
U	unfolded state of a protein
UV	ultraviolet
UVRR	ultraviolet resonance raman
VCD	vibrational circular dichroism

Appendix A.2. Amino Acid Abbreviations

Amino acid	Three letter code	One letter code
alanine	ala	A
arginine	arg	R
asparagine	asn	N
aspartic acid	asp	D
asparagine or aspartic acid	asx	B
cysteine	cys	C
glutamic acid	glu	E
glutamine	gln	Q
glutamine or glutamic acid	glx	Z
glycine	gly	G
histidine	his	H
isoleucine	ile	I
leucine	leu	L
lysine	lys	K
methionine	met	M
phenylalanine	phe	F
proline	pro	P
serine	ser	S
threonine	thr	T
tryptophan	trp	W
tyrosine	tyr	Y
valine	val	V

Appendix A.3. Amino Acid sequence comparing horse heart to yeast cytochrome c

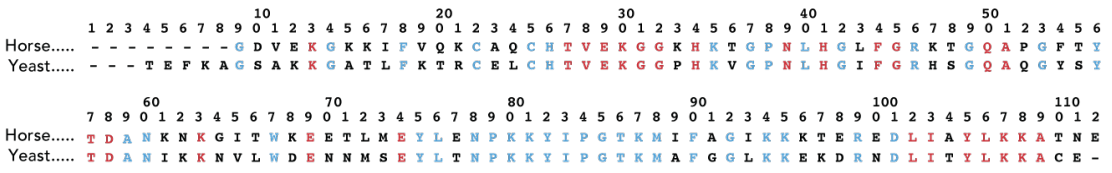

Symbols in blue represent amino acids which are consistent across all organisms, the red represents the additional amino acids similar between horse heart and yeast cytochrome c.[112]

Appendix A.4. Procheck results showing (a) Ramachandran plots and (b) secondary structure with estimated accessibility for states II to V.[210] The 104 amino acid residues are shown in black, and those in unfavorable conformations (score < -3.00) are labelled in red.

a. Ramachandran Plot(s)

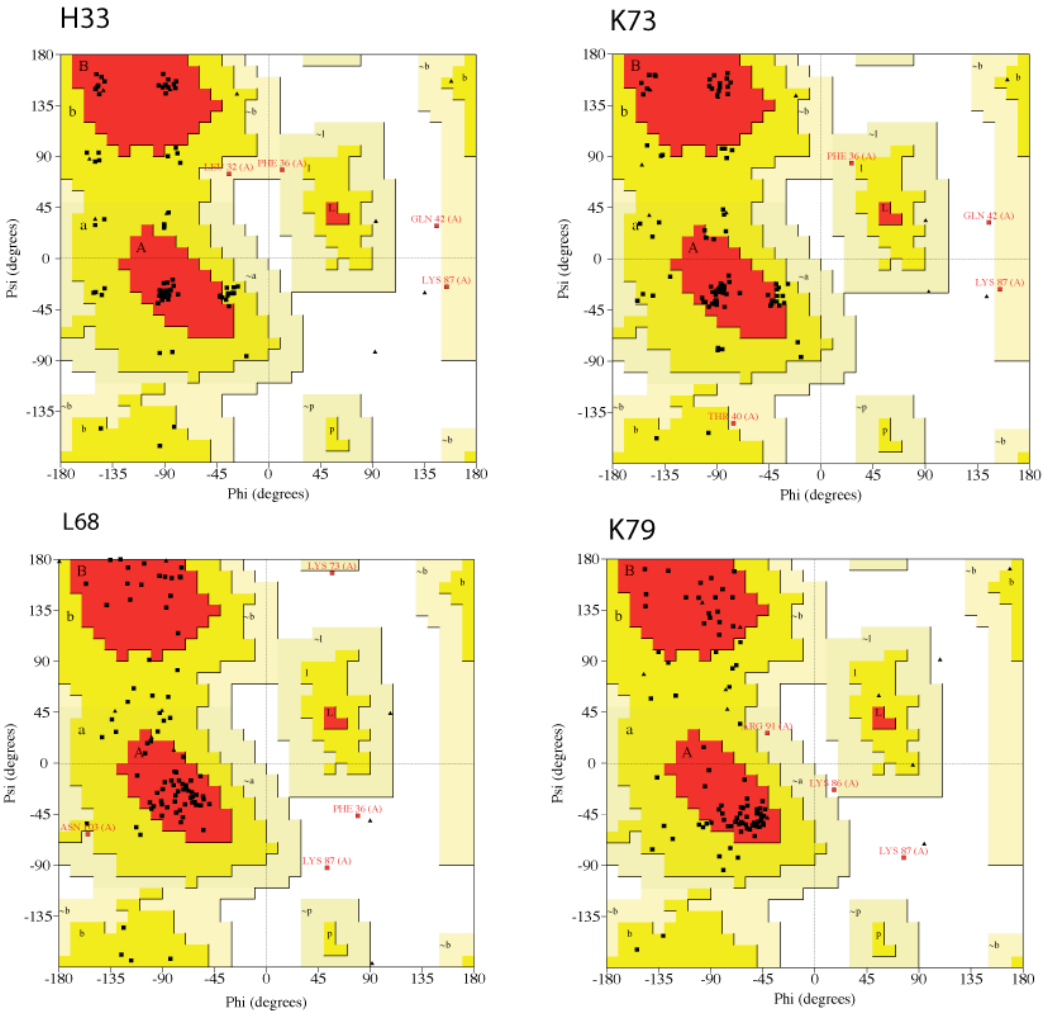

b. Secondary structure & estimated accessibility

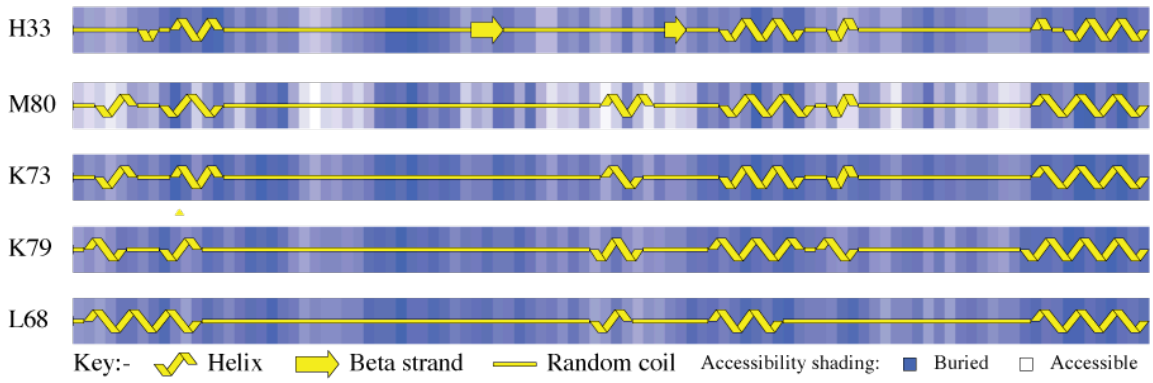

Appendix A.5. Complete assignment of cytochrome c RR Bands (cm^{-1})

Symmetry	Mode[a]	Fe(II)[b]	Fe(III)[b]
A_{1g}	ν_1	[3041]	---
	ν_2	1591 (B1 6cls); 1592 (B2 6cls); 1572 (B2 5chs)	1584 (B1 6cls); 1588 (B2 6cls); 1570 (B2 6chs); 1577 (B2 5chs)
	ν_3	1491 (B1 6cls); 1494 (B2 6cls); 1470 (B2 5chs)	1502 (B1 6cls); 1506 (B2 6cls); 1485 (B2 6chs); 1497 (B2 5chs)
	ν_4	1361 (B1 6cls); 1360 (B2 6cls); 1354 (B2 5chs)	1373 (B1 6cls); 1374 (B2 6cls); 1370 (B2 6chs); 1371 (B2 5chs)
	ν_5	1118	1124
	ν_6	796	797
	ν_7	691	701
	ν_8	347	349
	ν_9	268	274
B_{1g}	ν_{10}	1621 (B1 6cls); 1606 (B2 5chs)	1635 (B1 6cls); 1640 (B2 6cls); 1623 (B2 5chs)
	ν_{11}	1547;1577	1562
	ν_{12}	[1343]	--
	ν_{13}	1230	1232
	ν_{14}	1131	1130
	ν_{15}	750	750
	ν_{16}	746	
	ν_{17}	305	
	ν_{18}	162; 168	
A_{2g}	ν_{19}	1585; 1603	1582
	ν_{20}	1399	1401
	ν_{21}	1314; 1307	1316
	ν_{22}	1130	1134[c]
	ν_{23}	1080	
	ν_{24}	603; 597	
	ν_{25}	502; 551	
	ν_{26}	[243]	---
B_{2g}	ν_{27}	[3041]	---
	ν_{28}	1483	1426 (h.s); 1463
	ν_{29}	1402 (h.s.)	1407
	ν_{30}	1173	1166; 1177
	ν_{31}	1132; 1015	
	ν_{32}	947; 938	
	ν_{33}	479; 493	480
	ν_{34}	183; 197	206[c]
	ν_{35}	144	

[a]Mode numbering notation.[344, 346] [b] Unpublished data. [c]Frequency assignments.[164, 234, 345, 349, 443, 490] B1 6cls has Met/His axially ligated to the heme; B2 6cls His/His axially ligated to the heme; B2 6chs H_2O/His axially ligated to the heme; B2 5chs -/His axially ligated to the heme.[461,442]

Appendix A.6. High/Low Spin Heme Iron assignment for Oxidized Cyt c as a function of pH.

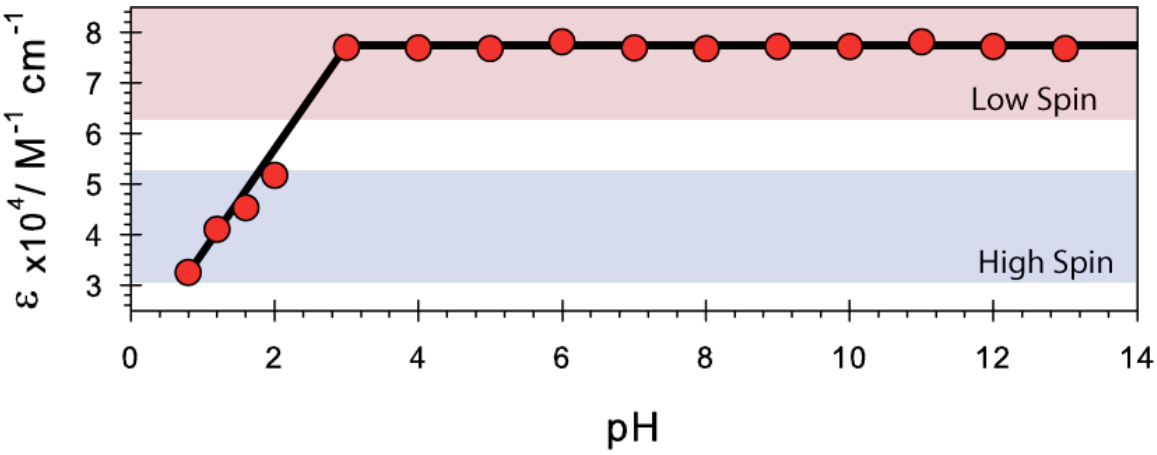

Vita

Jonathan Barrot Soffer was born in Philadelphia, PA. His interest in science began at a very early age, staining microscope slides aside his uncle in a research lab at Ohio State University. He developed an interest in music at a young age, and took up various instruments, including guitar, bass, piano and drums. Jonathan received his first guitar as a gift, at the age of 6, and began taking lessons. He was also very interested in nature and joined the Boy Scouts (troop 708) while in middle school. At the age of 13 he became one of the youngest scouts at that time to be awarded with the rank of Eagle scout. His interest in science and medicine continued throughout his youth. While in High School he joined the medical explorers, and volunteered in Hospitals, and worked in the neighborhood pharmacy. He was medically knowledgeable and found himself soon shadowing and assisting physicians within the hospital system. He additionally continued to pursue music at this time, and to the present day. Playing in the orchestra, string ensembles, jazz band, as well as playing in bands with friends, and performing at various events around the country. While working for a local hospice pharmacy, excelleRx, he began to taking chemistry courses at Drexel University, obtaining a BS. This is where he met Prof. Reinhard Schweitzer-Stenner who offered a project working on histone peptide fragments. After completion of this project, Jonathan was asked if he was interested in pursuing a higher degree in the Schweitzer-Stenner Biospectroscopy group. During his graduate student career he is coauthor on six peer reviewed journal articles and four book chapters, and participated at many national and international conferences. His first author publication in Biochemistry was selected as the journal cover for October-December, 2013. He additionally served as the secretary and president of the Graduate Student Association. In this capacity he served on many university committees and was invited graduate representative at the inauguration of President Fry, Drexel's 14th president. He was a founding member of the Chemistry Graduate Student Association at Drexel, where he served as president in its inaugural year. Jonathan obtained his Ph.D in Physical Chemistry in 2013, from Drexel University.

Publications Contributing to this Thesis

J. B. Soffer, and R. Schweitzer-Stenner. (2013) Enthalpy-Entropy Compensation Governs the Thermal Unfolding of Protonation States of Oxidized Cytochrome c. Biochemistry, Submitted.

J. B. Soffer, E. Fradkin, L. Pandiscia, and R. Schweitzer-Stenner. (**2013**) The (not completely irreversible) population of a misfolded state of cytochrome c under folding conditions. Biochemistry, 52,1397-408. DOI: 10.1021/bi301586e

R. Schweitzer Stenner, J. B. Soffer, S. Toal and D. Verbaro. (**2012**) Chapter 19: Structure Analysis of Unfolded Peptides by Raman Spectroscopy. Methods Mol. Biol. 895, 315. DOI: 10.1007/978-1-61779-927-3_19

R. Schweitzer-Stenner, J. B. Soffer and D. Verbaro. (**2012**) Chapter 18: Structure Analysis of Unfolded Peptides by Vibrational Circular Dichroism Spectroscopy. Methods Mol. Biol. 895, 271. DOI: 10.1007/978-1-61779-927-3_18

R. Schweitzer-Stenner and Soffer, J. B. (**2012**) Other spectroscopy - UV-Vis, CD, Raman, vibrational CD applied in biophysical research. Elsevier, In *Comprehensive Biophysics*, Ed. E. Egelman Elsevier. ISBN: 978-0-12-374820-8

M. Alessi, A.M. Hagarman, J. B. Soffer, R. Schweitzer-Stenner. (**2010**) In-plane deformations of the heme group in native and nonnative oxidized cytochrome c probed by resonance Raman dispersion spectroscopy. J. Raman. Spectrosc., 42, 917-925. DOI: 10.1002/jrs.2796

R. Schweitzer-Stenner, A. Hagarman, D. Verbaro and J. B. Soffer. (**2009**) Chapter Six - Conformational Stability of Cytochrome c Probed by Optical Spectroscopy, Meth. Enzymol., 466, 109-153. DOI:10.1016/S0076-6879(09)66006-7

D. Verbaro, A. Hagarman, J. B. Soffer, and R. Schweitzer-Stenner. (**2009**) The pH Dependence of the 695 nm Charge Transfer Band Reveals the Population of an Intermediate State of the Alkaline Transition of Ferricytochrome c at Low Ion Concentrations. Biochemistry, 48 (13) 2990-2996. DOI: 10.1021/bi802208f.

(page intentionally left blank)